Design, construction and commissioning of a packed bed reactor system for methane to methanol conversion

Thesis presented for the degree of Master of Science in Engineering in Chemical Engineering

In the Department of Chemical Engineering

University of Cape Town

October 2018

By:

Junfeng Guo

Supervisor:

Professor Eric van Steen

This page is intentionally left blank

Declaration

I know the meaning of plagiarism and declare that all the work in the document, save for that which is properly acknowledged, is my own. This thesis/dissertation has been submitted to the Turnitin module (or equivalent similarity and originality checking software) and I confirm that my supervisor has seen my report and any concerns revealed by such have been resolved with my supervisor.

Signed by candidate

Junfeng Guo

2018/10/04

This page is intentionally left blank

Synopsis

The direct conversion of methane to methanol can have great economic implications and have been under extensive research for the past century. It is speculated that platinum-based catalysts may achieve this due to its ability to adsorb molecular oxygen as reactive surface oxygen species that may react with methane to form methanol. The selective conversion to methanol over such a catalyst might be possible through site blocking action with in presence of steam and/or high oxygen partial pressures as well as the presence of a promoter.

Thus, a packed bed reactor system capable of safely operating under high pressures (< 50 bar) is designed and constructed to investigate the performance of platinum-based catalysts in the direct oxidative conversion of methane to methanol whilst co-feeding steam. The design procedure is carried out from flowsheet development to the detailed design of individual units of the reactor system. The constructed reactor system is built around a quartz lined microreactor 200 mm long and 2.4 mm in diameter to minimize risks associated with the flammability of methane and oxygen mixtures. A method for complete product analysis of all carbon containing reaction products using gas chromatography with flame ionization detector in conjunction with an oxidizer-methanizer microreactor is developed which is capable of quantifying minor carbon containing reaction products formed at low conversions with yields greater than 10 µmol/mol. Flow, pressure and temperature controls are also developed for the reactor system to ensure steady state operation.

Exploratory experiments on the autocatalytic conversion of methane to methanol as well as the catalytic conversion of methane to methanol using promoted platinum catalyst, Pt_3Mo and Pt_3Bi catalysts were carried out in the constructed reactor system. The catalysts were prepared in-house. The reactor system was shown to generate reproducible quantitative results (methane conversions and product selectivities) at steady state conditions, provided the experiments were properly carried out. The autocatalytic conversion of methane to methanol reached a maximum methanol yield of 1.2 C-% (at a methane conversion of 5 % and a methanol selectivity of 23 C-%; selectivity defined as: $\frac{Yield_{desired\ product}}{Yield_{all\ products}}$) at 495 °C and 40 bar with similar reactor productivity of 282 $\frac{mol_{CH4\ converted}}{min.m^3_{rctr\ volume}}$ compared to 97 $\frac{mol_{CH4\ converted}}{min.m^3_{rctr\ volume}}$ obtained by Zhang et al. [1] at 450 °C and 40 bar.

The two catalysts were not able to selectively convert methane to methanol. The Pt_3Mo catalyst selectively converted methane to an unidentified compound with a TOF of 8.2 h^{-1} when liquid water is present in the reactor and converted methane to CO_2 with a TOF of 20.5 h^{-1} in the presence of steam. Both experiments on Pt_3Mo were carried out under low methane conversion (<1 %), intermediate temperatures (100 °C – 300 °C), high steam partial pressure (approximately 10 bar) and oxygen partial pressure of approximately 1 bar. The Pt_3Bi catalyst deactivated at high oxygen partial pressures (28 bar) but could be reactivated using a lower oxygen partial pressure of a 3.6 bar while co-feeding 0.8 bar of steam. The reactivated Pt_3Bi converted methane to only CO_2 with a TOF of 149 h^{-1} at 400 °C. These TOFs are agreeable within an order of magnitude to the homogenous Pt catalysed conversion of methane to methanol of 36 h^{-1} obtained by Periana et al. [2]. The constructed reactor system should be used in more catalyst screening experiments to identify more suitable catalysts for the possible direct conversion of methane to methanol, such as pure Pt, Ag, Au, Pd and their alloys.

Acknowledgement

I would like to acknowledge the following individuals and institutions who were instrumental to this research, without their effect, this research would not have been possible.

I would like to express my most sincere gratitude to my supervisor and the head of department of Chemical Engineering, Professor Eric van Steen for the guidance provided during this research project. Professor Eric van Steen have remained a mentor for me throughout this research project, through his patience, presence and knowledge. I would like to thank Professor Eric van Steen for motivating me through the bad times, without which I would have never be able to complete this work. Our interactions and discussions have not only made me passionate about this research but have also cultivated me into a better person. As the days turns into weeks and weeks into years from now, Professor Eric van Steen will always remain as my most venerable teacher.

I would like to thank my friends and co-worker in our research group, Dr Gerald Leteba, Ms Chelsea Tucker, Mr Thobani Gambu and Mr Sandeeran Govender, for all the support, discussions and friendship throughout this project and for being my friend. Confucius once said: “In a party of three, there must be my teachers; select their good qualities and follow them.” With so many good people like you around me, I have learnt many lessons over the course of this work.

I would also like to thank the technical staff in the Centre of Catalysis Research, Mr Waldo Koorts, Mr Gideon Kaufmann, Ms Rachel Cupido and Ms Portia Johnston, at the Department of Chemical Engineering for always being available to offer assistance and expertise, as well as always having a stockpile of spare parts when needed.

I would also like to thank Mr Jacobus van Der Merwe and the IKEY workshop for their expertise and loan of spare parts throughout this project.

I would like to thank NRF for funding this research.

As for my family, without their love and support, this research project would certainly not be possible.

Lastly, I would like to acknowledge the Department of Chemical Engineering at UCT for teaching me the foundations of chemical engineering throughout my undergraduate years and providing me the opportunity to continue my study by working on this research project. I would like to thank the department for all the facilities used during this research project.

Table of Contents

List of Figures

List of tables

Abbreviation

DFT:	Density Functional Theory
DMTM:	Direct Methane to Methanol Conversion
FID:	Flame Ionization Detector
GC:	Gas Chromatography
HETP:	Height Equivalent of Theoretical Plate
HPLC:	High Pressure Liquid Chromatography
ID:	Inner Diameter
L:	Length
LFL:	Lower Flammability Limit
LNG:	Liquidfied Natural Gas
MeOH:	Methanol
MeOOH:	Methyl hydroperoxide
MeF:	Methyl Formate
MS:	Mass Secptrometer
NPT:	National Pipe Thread
OD:	Outer Diameter
RTD:	Resistance Temperature Detectors
TCD:	Thermal Conductivity Detector
TNT:	Trinitrotoluene
TOF:	Turn Over Frequncy
TOS:	Time on Stream
UFL:	Upper Flammability Limit
WT:	Wall Thickness

Glossary

Autoclave:	Pressurized and heated vessel, usually used as batch reactor
Cracking pressure:	The pressure needed to start flow in an one way valve
Dead weight tonnage:	Weight of a ship without cargo
Decibel:	A factor of $10^{0.1}$, A multiplication factor of ×1.26
Dynamic range:	The range in which a variable varies, expressed in Decibel
Grounded:	An electrical connection into the earth, the ground is defined as having the same electrical potential regardless of current sourced or sunk into it
Lewis-Randall rule:	A model of an ideal solution where the fugacity (equivalent to pressure for an ideal gas) of a component is directly proportional to its mole fraction
Methanizer:	A small reactor added before a FID in a GC-FID to convert carbon containing compounds eluting out of GC into methane
Nichrome:	An alloy of nickel, chromium and sometimes iron used as resistance wires
Noise floor:	The average magnitude of noise in a signal
Port connector:	Small tubing with female nuts on either side to join together male fittings
Reynold number:	A dimensionless number describing the ratio of inertial to viscous forces, defined as $\frac{\rho u D}{\mu}$
Schmidt number:	A dimensionless number describing the ratio of viscous diffusion to molecular diffusion, defined as $\frac{\mu}{\rho D_{AB}}$, D_{AB} is the mass diffusivity
superficial fluid velocity:	The average fluid velocity obtained by the ratio of volumetric flow rate and the flow's cross-sectional area
Synthesis gas:	A mixture of CO and H_2
Transducer:	A device that turns one form of energy into another, usually used in instrumentation, e.g. a thermocouple that turns thermal energy into electrical energy

1. Introduction

1.1 The natural gas market

Natural gas, a type of fossil fuel mainly consisting of methane, is an abundant source of energy and accounted for 23.9 % of the global energy consumption in 2015. This together with the consumption of other two types of fossil fuels: oil at 32.9 % and coal at 29.2 %, indicates the world's energy supply is still highly dependent on fossil fuels as it makes up 86 % of the global energy supply [3], [4]. Currently (June 2018), natural gas makes up 27.2 % of the fossil fuel use worldwide [4]. It is expected that in the near future natural gas usage will continue to grow as the increase in natural gas consumption last year (2017) was the fastest since 2010 at 3 % [4].

Natural gas has been priced at about two-thirds of the price of oil on a heat equivalent basis, as shown by regression analysis looking at historic data since 1993 [5]. Oil has been trading at a premium compared to natural gas because unlike natural gas, oil is a globally traded commodity with many inexpensive options for transportation and storage; its price broadly follows the global supply and demand cycles [5]. Natural gas with its much lower density cannot be readily transported and stored in the same way as oil. Unlike the global market of oil, the natural gas market is made up of regional markets of gas suppliers and consumers interconnected with long distance pipe lines or liquidified natural gas (LNG) shipping lanes [5]. Both methods of transportation are expensive in terms of capital investments. Gas pipe lines requires compressor stations along the pipe line to recompress natural gas and its transport is highly dependent on the geo-political stability of the regions the pipe lines pass through. The liquification of natural gas and thereafter its transportation requires extensive refrigeration as the boiling point of methane is -164 °C [6].

The difficulties in the transportation of natural gas compared with oil can easily be seen by reviewing the total tonnage of the global oil tanker fleet and the global liquid gas tanker fleet. At the beginning of 2016, the global oil tanker fleet consists of 12269 ships with a total dead weight tonnage of 545.7 million tons. In contrast, at the same time the global liquid gas tanker fleet is approximately 10 times smaller at 1770 ships with a total dead weight tonnage of 54.5 million tons [7]. The high-risk investment required for natural gas transportation hinders the wide-spread use of natural gas at the centres of consumption.

1.2 Conversion of methane to methanol

Given the difficulties in transporting natural gas in its raw form, conversion of methane in natural gas into an easily transportable liquid such as liquid hydrocarbons using the Fischer-Tropsch synthesis or methanol has been under intensive industrial and scientific research over the last century [8]. It can be used as a fuel directly or converted into dimethyl ether, olefins, gasoline and biodiesel [9]. Methanol is a versatile feedstock that can also be converted into other chemicals products such as formaldehyde, acetic acid, methyl chloride, methyl tert-butyl ether (MTBE), dimethyl terephthalate and methyl methacrylate. The annual global demand of methanol was 40 million tons in 2007 and is predicted to increase due to the increased demand from the energy sector [9]. It has also been estimated that the demand of methanol can grow

by as much as 75 million tons per year initially if it achieves a 10 % penetration into the US automotive fuel markets [6].

1.3 Difficulties in conversion of methane to methanol

The conversion of methane to methanol requires the activation of the strong C-H bond in methane and is often regarded as the dream reaction in catalytic chemistry [8]. This is in part due to the high H_3C-H bond energy (439 kJ/mol), which is one of the strongest C-H bond encountered in saturated hydrocarbon compounds (see Table 1.1).

Table 1.1: Bond dissociation enthalpy ($\Delta_{dis}\underline{H}$) in alkanes [10]

	$\Delta_{dis}\underline{H}°$ (298 K) (kJ/mol)
$H_3C – H$	439
$H_3CH_2C – H$	423
$(CH_3)_2HC – H$	413
$(CH_3)_3C – H$	404

Thus, to activate the strong C-H bond in methane, a highly active catalyst and/or high temperatures is required. Using molecular oxygen as an oxidant and purely under thermodynamic control the conversion of methane to methanol will most likely yield more stable deep oxidation products such as formaldehyde, carbon monoxide and carbon dioxide as can be seen from the increase in Gibbs free energy as methane is progressively oxidized (see Table 1.2). The same motif is observed from the C-H bond dissociation energy as methane is progressively oxidized (see Table 1.3), leading to a scenario where the C-H bond in the successive oxidation products being more readily activated than the C-H bond in methane.

Table 1.2: Standard Gibbs free energy change in gas phase methane oxidation reactions [11]

Reaction	$\Delta_{rxn}\underline{G}°$ (298 K) (kJ/mol)
$CH_4 + 0.5\ O_2 \rightarrow CH_3OH$	-111
$CH_4 + O_2 \rightarrow HCHO + H_2O$	-291
$CH_4 + 1.5\ O_2 \rightarrow CO + 2\ H_2O$	-544
$CH_4 + 2\ O_2 \rightarrow CO_2 + 2\ H_2O$	-801

Table 1.3: Bond dissociation energy in methane and C_1 oxygenates [10]

	$\Delta_{dis}\underline{H}°$ (298 K) (kJ/mol)
$H_3C – H$	439
$H – CH_2OH$	402
$H – CHO$	369

1.4 Multi-step conversion of methane to methanol

1.4.1 Conversion of methane to methanol via synthesis gas

Commercially, the difficulties in converting methane to methanol is solved with a two-step process. Methane processed from raw natural gas free of non-methane components in particular sulphur containing compounds such as mercaptans is first reformed into synthesis gas – a mixture of hydrogen and carbon monoxide. The energy needed for the highly endothermic reforming reaction is usually provided through the combustion of a portion of methane by co-feeding oxygen in the reforming reactor, a process known as auto-thermal reforming.

$$CH_{4\,(g)} + H_2O_{\,(g)} \rightarrow CO_{\,(g)} + 3\,H_{2\,(g)} \qquad \Delta\underline{H}^\circ\,(298\ K) = 206\ kJ/mol$$

$$CH_{4\,(g)} + 2\,O_{2\,(g)} \rightarrow CO_{2\,(g)} + 2\,H_2O_{\,(g)} \qquad \Delta\underline{H}^\circ\,(298\ K) = -802\ kJ/mol$$

This versatile mixture of carbon monoxide and hydrogen gas can then be converted directly in an equilibrium limited reaction to methanol using a catalyst or converted into liquid hydrocarbons using the Fischer-Tropsch process [12].

The reforming process is energy intensive and special reactor materials are required to withstand the high temperatures of the reforming reaction due to its highly endothermic nature. Thus, 60 – 70 % of the cost of the indirect methane to methanol conversion process is associated with the production of synthesis gas [6]. This makes the two-step process expensive and only 0.5 % of the average daily global natural gas consumption in 2016, at 9.5 billion cubic metres per day [13] were reformed into synthesis gas to produce methanol or Fischer-Tropsch products.

1.4.2 Acid assisted conversion of methane to a methanol derivative

Inspired by the success of Hg(II) as a catalyst in the activation of the Ar-H bonds in aromatic compounds, Periana et al. [14] first reported the successful activation of methane using mercury bisulphate as a catalyst in concentrated sulphuric acid at 180 °C, where methyl bisulphate and sulphur dioxide was produced from methane with a conversion of 50 % and a selectivity of 85 %. The methyl bisulphate can be hydrolysed yielding methanol; the catalytic cycle subsequently closed by re-oxidizing the co-product sulphur dioxide with atmospheric oxygen in another reactor to regenerate the sulphuric acid consumed in the reaction. This reaction scheme was confirmed in the same study using isotopically marked $^{13}CH_4$ and $^{2}H_2SO_4$ and is shown below [14]:

$$CH_4 + 2\,H_2SO_4 \xrightarrow{Hg^{2+}} CH_3OSO_3H + 2\,H_2O + SO_2$$

$$CH_3OSO_3H + H_2O \rightarrow CH_3OH + H_2SO_4$$

$$SO_2 + 0.5\,O_2 \rightarrow H_2SO_4$$

Besides Hg(II), Au(II), Pd(II) and Pt(II) are also capable of catalysing this reaction [2], [15], [16]. However, it should be noted, that the acid assisted conversion of methane to a methanol derivative uses a homogenous catalyst, based on toxic or precious metals, requiring complex separation steps post reaction to recover the catalyst in solution. Although this problem can be overcome by depositing the metal catalysts on supports such as covalent triazine-based network (CTF) [17] or pyrolyzed lobster exoskeleton [18]. The use of strong acids as a reaction medium still requires corrosion resistant equipment and complex product separation steps, making the

industrialization of these processes an expensive endeavour, limiting this process currently to laboratory scale experiments only.

1.5 Single-reactor conversion of methane to methanol / direct methane to methanol conversion (DMTM)

The conversion of methane to methanol via synthesis gas and the acid assisted conversion of methane to methanol are both multi-step processes requiring different reactor units. A single step process or a multi-step process that can be carried out in a single reactor unit for the conversion of methane to methanol can have far reaching economic implications. This would not only render methane transportable in a less expensive manner but also allows it to be converted to more valuable chemical products with increasing demands. In fact, more than a century of research has been conducted on the topic of direct methane to methanol conversion (DMTM) since its possibility was discovered by Newitt and Haffner [19] by reacting methane and molecular oxygen using a batch reactor at a pressure of 100 bar and temperatures of approximately 350 °C [19]. An overview of the obtained results for the direct conversion of methane to methanol is given in Table 1.4.

1.5.1 Autocatalytic direct methane to methanol conversion

The simplest process for the direct conversion of methane to methanol (DMTM) is the gas phase partial oxidation of methane with oxygen in a single reactor. The combustion of methane is prevented by feeding large excess of methane in relation to oxygen, making oxygen the limiting reagent. Since, the autocatalytic partial oxidation of methane in the gas phase follows a branched chain mechanism involving free radicals [6], it is inherently difficult to control by adjusting the operating parameters of the reaction and the overall yield of methanol remains low (see Table 1.4. and Figure 1.1). The autocatalytic nature of the reaction is substantiated by the fact it does not proceed until a certain temperature (~400 °C) is reached, and then proceed sharply to completion over a short temperature range [1], [20], [8], which is characteristic for reactions proceeding via radicals [1], [20], [8]. However, high pressures are essential to produce methanol from the auto-catalytic partial oxidation of methane to methanol under these conditions [1], [21], [22], [8], [6], [23].

1.5.2 Heterogeneously catalysed conversion methane to methanol using molecular oxygen

In order to improve the autocatalytic direct conversion of methane to methanol, many solids have been tested for their catalytic ability in this reaction using oxygen as the oxidant. At high pressures and temperatures (> 30 bar and > 400 °C), the autocatalytic conversion of methane to methanol is significant and the presence of a heterogeneous catalyst does not have any positive effect on the selectivity of methanol [39]. For example, the use of MoO_3-ZrO_2 catalyst at 400 °C and 50 bar resulted in the production of formaldehyde rather than methanol [40] . The use of $FePO_4$-SiO_2 catalyst [28] or highly dispersed NiO-CeO_2/ZrO_2 [29] at ambient pressure and 600 °C did produce methanol as a product only if water is co-fed with oxygen. Ethanol is then also produced as a major product in the second case. Interestingly, using single atom dispersed Rh-ZrO_2 catalysts the reaction between methane and molecular oxygen produced

ethane as the major product at ambient pressure and 260 °C [33], however no measures were taken to analysis any carbon oxide products.

Table 1.4: Overview of direct methane to methanol (DMTM) processes

System	Catalyst	Oxidant	T (°C)	P (bar)	TOF (h^{-1})	X_{CH_4} (%)	S_{MeOH} (C-%)	Reference
Autocatalytic	n.a.	O_2	430	34	n.a.	7	54	[24]
		O_2	370	50	n.a.	1.7	64	[24]
		O_2	500	50	n.a.	5	30	[25]
		O_2	375	50	n.a.	0.13	55	[25]
		O_2	401	30	n.a.	3.1	47	[26]
		O_2	405	15	n.a.	7.7	18	[26]
		O_2	455	34	n.a.	7.5	60	[27]
		O_2	456	65.4	n.a.	11	67	[27]
Heterogenous – O_2	Mo-V-Cr-Bi-oxide/ SiO_2	O_2	430	50	n.i.	1.6[a]	10	[23]
	$FePO_4/SiO_2$[b]	O_2	600	1	n.i.	2	65	[28]
	NiO/CeO_2-ZrO_2[c]	O_2	450	1	50	14	19	[29]
	Cu - S3	O_2	200[d]	1	3.6×10^{-3}	n.a.	76[e]	[30]
	CuO-SBA-15	O_2	200[d]	1	0.08	n.a.	90	[31]
	Cu-SSZ-13	O_2	200[d]	1	0.343[f]	n.a.	90	[32]
Heterogenous – H_2O_2	Rh/ ZrO_2	H_2O_2	70	30	1.75	n.i.	71[g]	[33]
	AuPd/ TiO_2	H_2/O_2[h]	70	30	0.16	n.i.	79[g]	[34]
	ZSM-5[i]	H_2O_2	50	10	5.6	0.91	12[j]	[35]
	Cu-ZSM-5	H_2O_2	50	30.5	2113	0.3	83[k]	[36]
Novel	Plasma	O_2	[l]	1	n.a.	15.4	35.4	[37]
	Photoinduced Cl·	O_2	25	1	n.i.	99	14	[38]

a: Conversion estimated assuming CO_2 as the only other product
b: 3% steam co-fed
c: Water cofed; ethanol also observed as a major product
d: Catalyst activation at 500°C with oxygen; reaction at 200°C with methane; and extraction of methanol with steam at <135°C
e: Assuming methanol and CO_x as the only products
f: Assuming every Cu atom is an active site
g: MeOOH and CO_2 as other product
h: H_2O_2 generated in-situ
i: Gas bag for analysis
j: Formic acid and formaldehyde also observed
k: Formic acid and peroxide
l: Heating via plasma discharge only

1.5.3 Heterogeneously catalysed conversion of methane to methanol using hydrogen peroxide

Instead of molecular oxygen, hydrogen peroxide can be used as the oxidant in the conversion of methane into methanol. The presence of a catalyst such as AuPd-TiO_2 [34], single atom dispersed Rh-ZrO_2 [33], Cu-ZSM-5 [36] and ZSM-5 [35] may facilitate the reaction at much lower temperatures (<100 °C). These reactions were carried out in batch reactors (autoclaves) with an aqueous phase containing hydrogen peroxide and a gas phase containing methane at elevated pressure (>10 bar). It is assumed that the primary product formed in these systems is MeOOH with methanol being produced from the subsequent hydrolysis of MeOOH [36]. Formaldehyde and formic acid are also formed with methanol and MeOOH as the oxygenated products from these reactions. Interestingly, it has been claimed, that the required hydrogen peroxide for the activation of methane can be generated in-situ from H_2 and O_2 [36]. The selectivity for methanol in these systems can be as high as 83 % albeit at very low methane conversions of 0.3 % [36].

1.5.4 Biocatalytic conversion of methane to methanol

Methanotrophic bacteria, whose sole source of energy is methane, has an enzyme named methane monooxygenase, capable of selectively oxidising methane to methanol at ambient conditions using oxygen [41]. Biocatalytic processes based on the raw bacteria culture, isolated methane monooxygenase or genetic modified organisms with such enzyme can convert methane into methanol selectively [42]. These systems can be challenging due to the need for fast gas-liquid mass transfer. A methanol productivity of 4.2 $\frac{mmol}{g_{dry\ cell}\ h}$ can be achieved with immobilised *Methylosinus trichosporium* cells in a batch reactor [43].

1.5.5 Heterogeneously catalysed step-wise conversion of methane to methanol

The structure of methane monooxygenase contains either a diiron centre or a dicopper centre bridged by oxygen as its active site [41]. The same motif can be achieved using zeolites. Zeolites such as ZSM-5 usually contains trace amounts of iron impurity which forms similar structures as the enzyme's diiron centre in the zeolite matrix [35], whereas the dicopper centre can be introduced into zeolites artificially [32]. These zeolite-based catalysts are able to convert methane to methanol in a single reactor, albeit via a stepwise process where the active sites in the zeolite is first activated in oxygen at temperatures above 450 °C. Methane is then introduced over the activated catalyst at a lower temperature of ~200 °C to form a surface methanol intermediate, finally methanol is extracted from the catalyst with steam or water at an even lower temperature below 135 °C [32], [31], [30]. The methanol selectivity of these systems can reach as high as 90 % [32], [31]. However, the yield of methanol is very small and only trace amounts (measured at µmol/mol levels) of methanol have been obtained for Cu-SSZ-13 catalyst [44]. Carrying all three steps isothermally at 200 °C (and omitting the heating / cooling cycle), a 10-fold decrease in methanol yield can be observed for Cu-MOR catalyst [45].

1.5.6 Novel processes for direct methane to methanol conversion

On top of the above mentioned direct methane to methanol processes, some very novel processes have been developed for the direct conversion of methane to methanol. Plasma discharge was used by Chawdhury et al. [37] to obtain a methane conversion of 15 % and a methanol selectivity of 35 % using oxygen as the oxidant under ambient conditions (although the reaction mixture will be heated by the plasma discharge). This was accomplished by creating a large potential difference between a metal mesh surrounding the outside of a quartz reactor and an internal electrode in the centre of the reactor. Light induced Cl radical can also catalyse the conversion of methane to methanol in a biphasic reactor under ambient conditions [38]. The oxygen required for the reaction is dissolved in the aqueous phase which also contains the source of the Cl radical ($NaClO_2$ in acid) whilst the methane is dissolved in an organic phase of perfluorinated solvent. This system can essentially fully convert (99 % conversion) the dissolved methane into methanol (14 % selectivity) and formic acid.

1.6 Summary of current direct methane to methanol processes

Figure 1.1 summarizes the relationship between methane conversion and methanol selectivity for a selected number of direct methane to methanol conversion processes mentioned previously. It is clear that the methanol selectivity drops significantly upon increasing the methane conversion indicating that the consecutive oxidation of the intermediate product methanol is highly favoured under the studied reaction conditions. The state of the art in the direct methane to methanol conversion renders this process currently as unattractive, since the methanol selectivity must be greater than 80 % with a methane conversion greater than 10 % in order for the process to become industrially attractive [46].

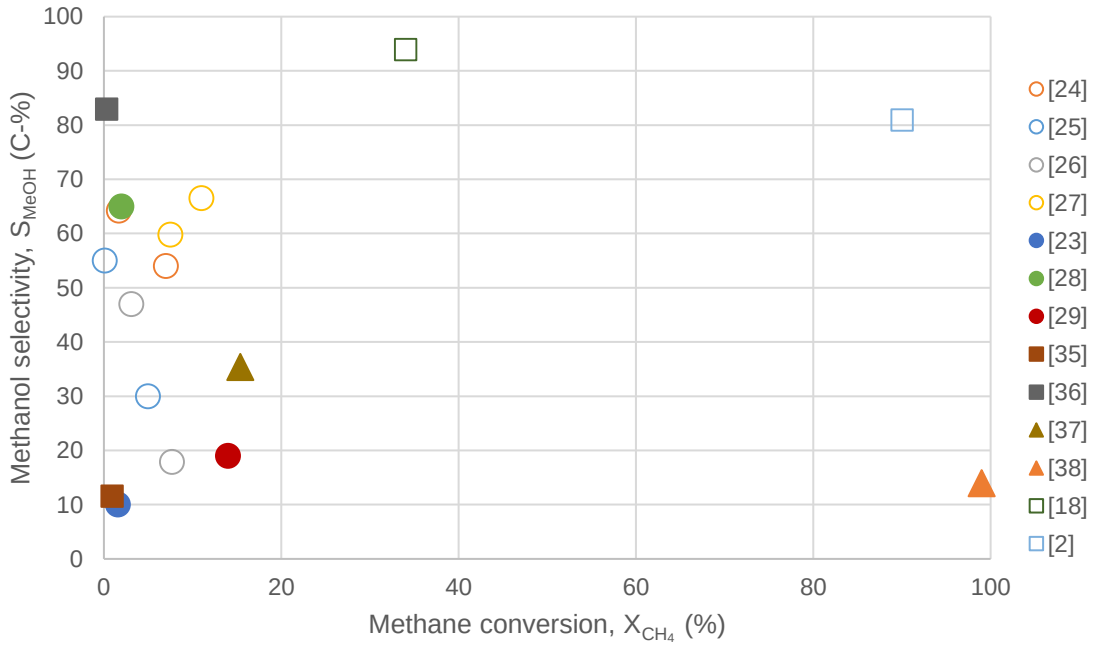

Figure 1.1: Conversion - selectivity relationship for selected direct methane to methanol processes (open circles: auto-catalytic process; closed circles: catalytic processes involving O_2; closed squares: catalytic processes involving H_2O_2; open squares: acid assisted processes to a methanol derivative; closed triangles: light and plasma catalysed processes)

Furthermore, the heterogeneously catalysed DMTM using hydrogen peroxide is industrially unattractive due to the high cost of hydrogen peroxide in relation to the selling price of the product methanol. It should be further considered that heat (an essential product in methane oxidation) cannot easily be recovered from these systems as these systems operate at temperatures lower than 100 °C. The heterogeneously catalysed step-wise DMTM processes are also industrially unattractive as it requires a heating – cooling cycle and only produces traces amount of methanol.

An ideal DMTM process from an industrial point of view should be:

- Continuous – allow the steady state conversion of large volumes of methane
- Catalytic – the use of a highly active catalyst will minimize reactor volume for a given throughput
- Heterogenous – the use of a solid catalyst eliminates the need for catalyst recovery post reaction
- Selective – methanol selectivity greater than 80 % at methane conversions greater than 10 % [46]
- Cheap – Using atmospheric oxygen as an oxidant instead of expensive oxidants like hydrogen peroxide
- Energy efficient – by carrying the reaction at elevated temperatures (>150 °C) the heat of reaction can be recovered, via e.g. steam generation.

1.7 Platinum as a catalyst for direct methane to methanol conversion

It is speculated from first principle calculations that the heterogenous catalytic conversion of methane to methanol may proceed over transition metal surfaces [47], transitional metal oxide surfaces [48] or transitional metal clusters on zeolites [49] via the reaction between methane and adsorbed oxygen atoms on the surface of the catalyst, as demonstrated in Figure 1.2 (p21) for a metal surface. Such catalytic system may possibly allow the conversion of methane to methanol using molecular oxygen as an oxidant and will be well suited for a continuous direct methane to methanol (DMTM) process.

The activation energy of this reaction was shown to be linearly dependent on the difference in adsorption energy of OH and O on the surface of the catalyst [47], [48]. As surfaces that bonds weakly to adsorbed oxygen, such as Ag [47] or PtO_2 [48], will have a lower O adsorption energy compared that of OH, and the adsorbed O atoms on these surfaces will become more reactive, decreasing the activation energy barrier for the reaction between methane and the adsorbed oxygen.

In fact, it was shown that the reaction between methane and adsorbed O on oxide surfaces such as SnO_2, PtO_2, and TiO_2 does not have any kinetic barrier [48]. Considering that platinum has the highest activity with regards to O and OH adsorption of any pure noble metal [50], it should be well suited for the conversion of methane to methanol via the mechanisms presented in Figure 1.2.

In addition to $CH_{4\,(g)} + O_{(a)} \rightarrow CH_3OH_{(a)}$ two competing side reactions may also occur on the catalyst surface, both involving vacant active sites (*) [47]:

$CH_{4\,(g)} + 2\,* \rightarrow CH_{3\,(a)} + H_{(a)}$

$CH_{4\,(g)} + O_{(a)} + * \rightarrow CH_{3\,(a)} + OH_{(a)}$

The adsorbed methyl species from these side reactions can then react further with active oxygen species leading to the formation of deep oxidation products such as CO and CO_2 [39], [47]. Thus, eliminating vacant sites on the surface of the platinum catalyst (i.e. increasing its oxygen coverage) may consequently results in an increase in the methanol selectivity in the methane oxidation. This has been demonstrated with DFT calculations for Ag surfaces [47] and Pd-Pt-(111) surfaces [51] with a monolayer of adsorbed oxygen.

Due to lateral repulsive interactions the oxygen coverage on pure Pt-(111) and Pt-(100) surfaces is not energetically favourable above 0.5 monolayer [52], [53], [50], but it can be increased with the use of a promoter. For example, the oxygen adsorption of Pd [54], [55] and Pt [55] was shown experimentally to be enhanced by the presence of a Bi promoter.

In addition to using promoters, exposing the Pt surface to high oxygen and water partial pressures would also increase its oxygen coverage. DFT calculations have shown that co-adsorption of OH groups can stabilize the adsorption of O atoms [53]. It was later shown with DFT calculations that the surfaces of Pt-(100) can indeed attain a full monolayer of oxygen coverage under high oxygen partial pressures and in the presence of steam [50]. This was however not possible on Pt-(111) surfaces [50]. Under these conditions (high steam partial pressures and in the presence of oxygen) a full monolayer coverage with hydroxyl species is obtained on Pt-(111) surfaces [50]. The calculated surface phase diagram of O and OH adsorbed on Pt-(100) and Pt-(111) surfaces under different oxygen and water partial pressures from Cilliers [50] is presented in Figure 1.3.

1.8 The role of water in direct methane to methanol conversion

Besides the possibility of saturating the catalyst surface with oxygen species as mentioned previously for a Pt catalyst, the presence of steam/water is also experimentally shown to be a very important variable in the catalytic conversion of methane to methanol.

Surface experiments in near vacuum on the conversion of methane to methanol with molecular oxygen in the presence of water have shown a massive increase in methanol selectivity and yield for an inverted $CeO_2/Cu_2O/Cu(III)$ catalyst (selectivity increased from 5% to 70% with 20 times higher yield) [56] and Ni-CeO_2 catalyst [57], due to the saturation of the active catalyst surface with OH groups and its subsequent site blocking action caused by the presence of steam [56], [57].

In continuous catalytic conversions of methane to methanol carried out in packed bed reactors, the co-feeding of steam was sometimes shown to be essential for the selective production of methanol: NiO-CeO_2/ZrO_2 catalyst produced only CO_2 without steam [29], $FePO_4$-SiO_2 catalyst produced only formaldehyde without steam [28].

The role of steam co-feeding should be investigated for any potential industrial DMTM catalyst as it can possibly offer a massive improvement in performance for very little increase in cost and complexity of a process as steam is an easily available utility on most chemical plants.

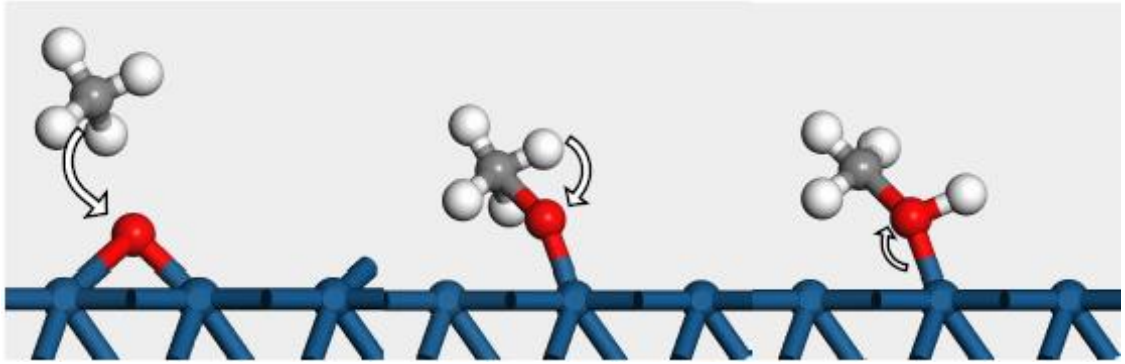

Figure 1.2: $CH_4 + O_{(a)} \rightarrow CH_3OH_{(a)}$ over a metal surface [50]

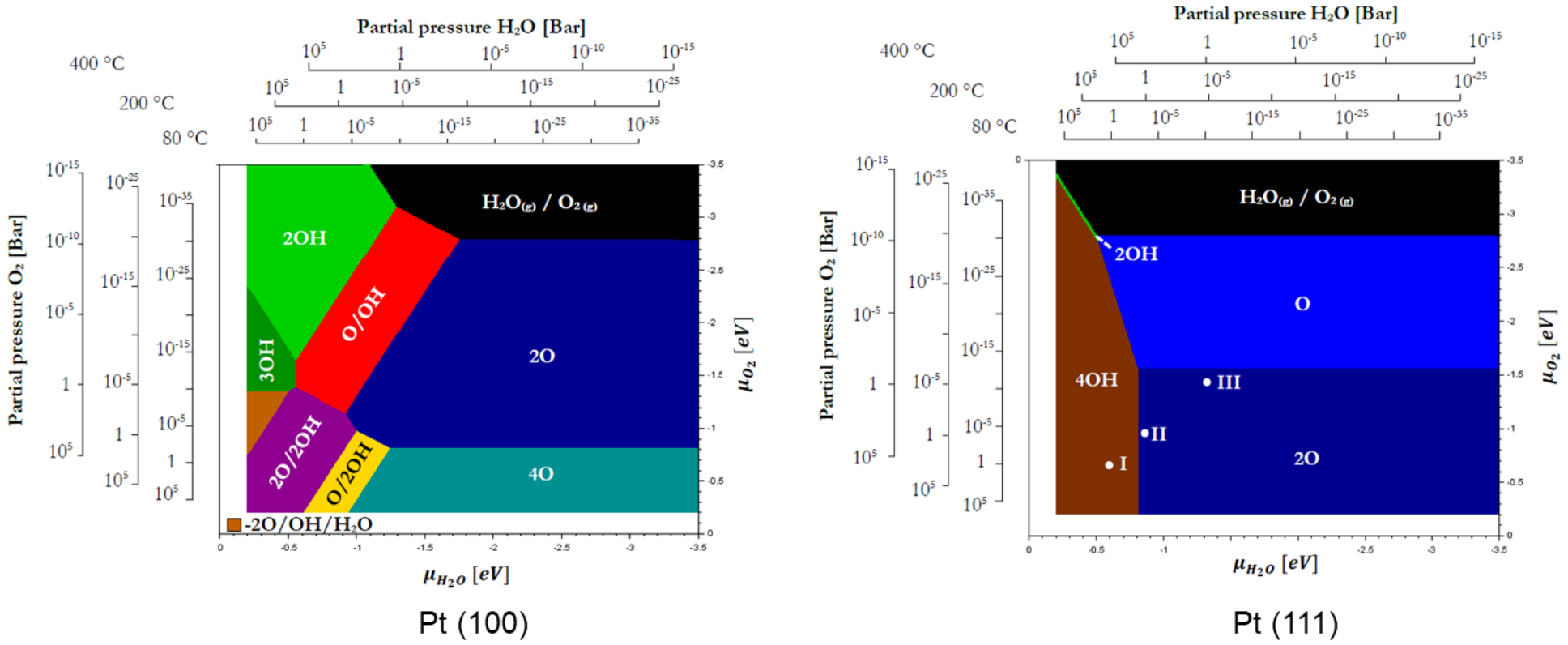

Figure 1.3: Calculated surface phase diagram for the co-adsorption of O and OH on Pt (100) and Pt (111) surfaces, reproduced from Cilliers [50]

2. Objectives

2.1 Problem statement

The conversion of methane to methanol not only renders the vast natural gas reserve easily transportable in a liquid form under ambient conditions but also allows more value to be added to natural gas as methanol is a versatile precursor to other chemical products. However, the current production method of methanol from methane via synthesis gas as an intermediate is a complex and costly two-step process. An industrially attractive single step process that can convert methane to methanol selectively using molecular oxygen as an oxidant with the possible addition of steam co-feeding can thus have far reaching economics consequences. It is speculated that platinum-based catalysts may achieve this due to its ability to adsorb oxygen as reactive surface oxygen species that can react with methane to form methanol. The selective conversion to methanol over such a catalyst should be possible through the site blocking action with the presence of steam and/or high oxygen partial pressures as well as the presence of a promoter. Thus, it is desirable to test the performance of platinum-based catalysts in the conversion of methane to methanol using molecular oxygen as an oxidant. It is also desirable to explore the effect of steam co-feeding and promoters in the catalyst for any improvement on methanol selectivity and productivity.

2.2 Scope of study

The scope of this work is to design, construct and commission a packed bed reactor system capable of evaluating the performance of platinum-based catalysts in direct methane to methanol conversion using molecular oxygen as an oxidant with provision for steam co-feeding. Proof of concept experiments are to be carried out evaluating the performance of some in-house prepared platinum-based catalysts as well as determining whether the constructed reactor system is capable of accurately evaluating the performance of these catalysts.

2.3 Hypothesis

Due to platinum's ability to adsorb molecular oxygen and generate reactive surface oxygen species, which can react with methane to produce methanol, platinum-based catalysts are anticipated to be active in the conversion of methanol to methanol. Platinum-based catalysts are also anticipated to more selectively convert of methane to methanol under conditions that causes higher oxygen coverage, such as through the presence of suitable promoters or high oxygen and steam partial pressures, via the effect of site blocking under high oxygen coverage.

2.4 Key Questions

- Is the designed and constructed packed bed reactor system capable of operating safely during the direct conversion of methane to methanol using molecular oxygen as an oxidant.
- Is the designed and constructed packed bed reactor system capable of evaluating the performance of platinum-based catalysts in the direct conversion of methane to

methanol using molecular oxygen as an oxidant with provisions for high oxygen and steam partial pressures.

- From the proof of concept experiments carried out on the performance of platinum-based catalysts for the conversion of methane to methanol using molecular oxygen as an oxidant and with provisions for high oxygen and steam partial pressures, are platinum-based catalysts suited for a potential direct conversion of methane to methanol process?

3. Flowsheet development of experimental set-up

3.1 Block diagram development

A system is to be designed and built that can be used to investigate the conversion of methane to methanol using molecular oxygen over a platinum-based catalyst with provision for the co-feeding of water in a fixed bed reactor. Reproducible results should be obtained so that the performance of these catalyst can be evaluated. This packed bed reactor system must contain the catalytic packed bed reactor itself alongside with any required upstream equipment, while a portion of the effluent from the packed bed reactor is to be sampled and analysed.

In terms of upstream units, since the gaseous reagents are supplied from gas cylinders whose pressure decreases as their contents are emptied, pressure controls are essential on the methane and oxygen entering the reactor to maintain constant inlet pressures. The required steam feed to the reactor must be generated from liquid water and thus a liquid pump and a water evaporator are also needed.

We have hypothesized that a high partial pressures of oxygen and/or water will allow the selective conversion of methane to methanol over a platinum-based catalyst through the site blocking actions of adsorbed O and OH species, it is thus necessary to control the partial pressures of the oxygen and steam in the fixed bed reactor. The partial pressures of gases in a system is given by Dalton's law of partial pressures, where the total pressure of a system is the sum of its component's partial pressures:

$$P_{total} = P_{CH_4} + P_{O_2} + P_{H_2O} + P_{inert}$$

Consequently, for any mixture of methane, oxygen and steam, the partial pressures of the individual components will be smaller than that of the total pressure. Since fluids only flow from high pressure to low pressure, we cannot directly control the partial pressures of components in the reactor by adjusting their feed pressures. The feed pressures of these gases must be greater than the total reactor pressure to allow flow.

The partial pressure of components in a system is also related to its composition and total pressure, assuming the Lewis-Randall rule holds:

$$P_{total} = y_{CH_4}P_{total} + y_{O_2}P_{total} + y_{H_2O}P_{total} + y_{inert}P_{total}$$

For a flow system this can be rewritten as:

$$P_{total} = \frac{F_{CH_4}}{F_{total}}P_{total} + \frac{F_{O_2}}{F_{total}}P_{total} + \frac{F_{H_2O}}{F_{total}}P_{total} + \frac{F_{inert}}{F_{total}}P_{total}$$

Therefore, to control the partial pressures of oxygen and steam in the packed bed reactor, we must control the flow rate of the components entering the reactor and the total pressure in the reactor. Since the flow control of water entering the reactor can be accomplished by the water pump, a flow control section is only needed for methane and oxygen entering the reactor.

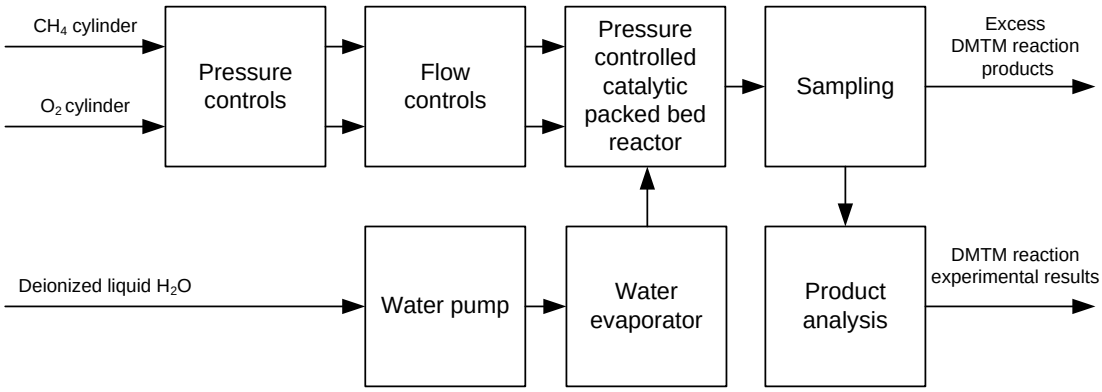

Figure 3.1: Block flow diagram of packed bed reactor system for direct methane to methanol conversion

3.2 Flowsheet development

The flowsheet for the packed bed reactor system is developed by expanding on the block flow diagram in Figure 3.1. In this section, generic symbology will be used to represent the various units. In chapter 4, the generic flowsheet developed in this section will be expanded to incorporate the physical design of the various units.

3.2.1 Pressure and flow controls

Pressure controls are needed on the methane and oxygen gases entering the packed bed reactor system to maintain steady state pressure despite being fed from depleting cylinders. Flow controls are also needed on these streams to manipulate the partial pressures of the reactants in the packed bed reactor by altering its composition. This can be done using pressure-controlled diaphragm valves as pressure indicator-controllers and the mass flow controller system described in Appendix I as flow indicator-controllers.

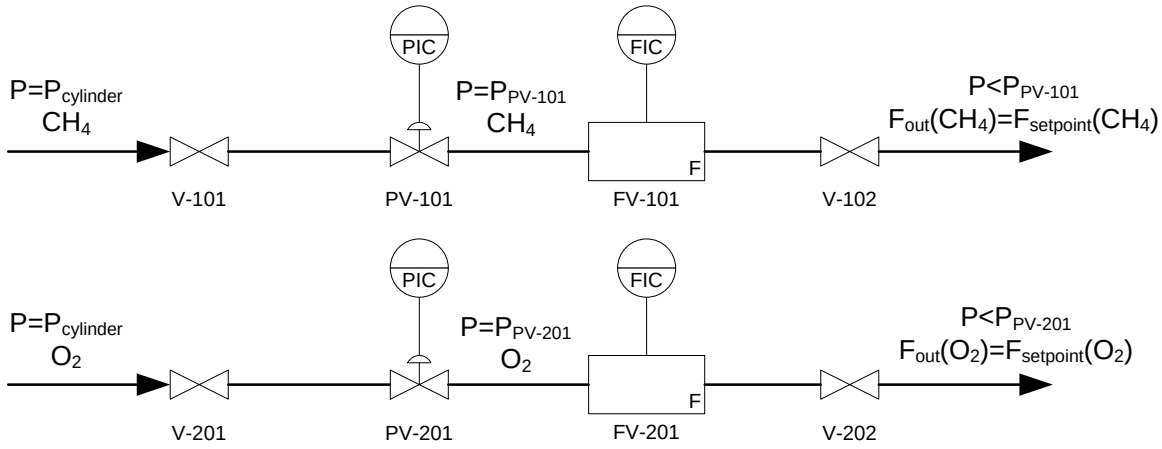

Figure 3.2: Flowsheet for pressure and flow control section

In our proposed flowsheet, a set of valves is also added at the beginning and end of this section to serve as on-off valves for the reactor system (V-101 and V-201) as well as on-off valves for the physical reactor unit (V-102 and V-202). The gases (methane and oxygen) will first be

throttled to a constant pressure by PV-101 and PV-201 and then further throttled to a constant flow by FV-101 and FV-201 at a lower pressure.

3.2.2 Water evaporator

The water evaporator section of the packed bed reactor system must be able to evaporate a flow-controlled stream of liquid water into a stream of water vapour. This is accomplished with a flow-controlled water pump and a heated vessel in which the actual evaporation takes place.

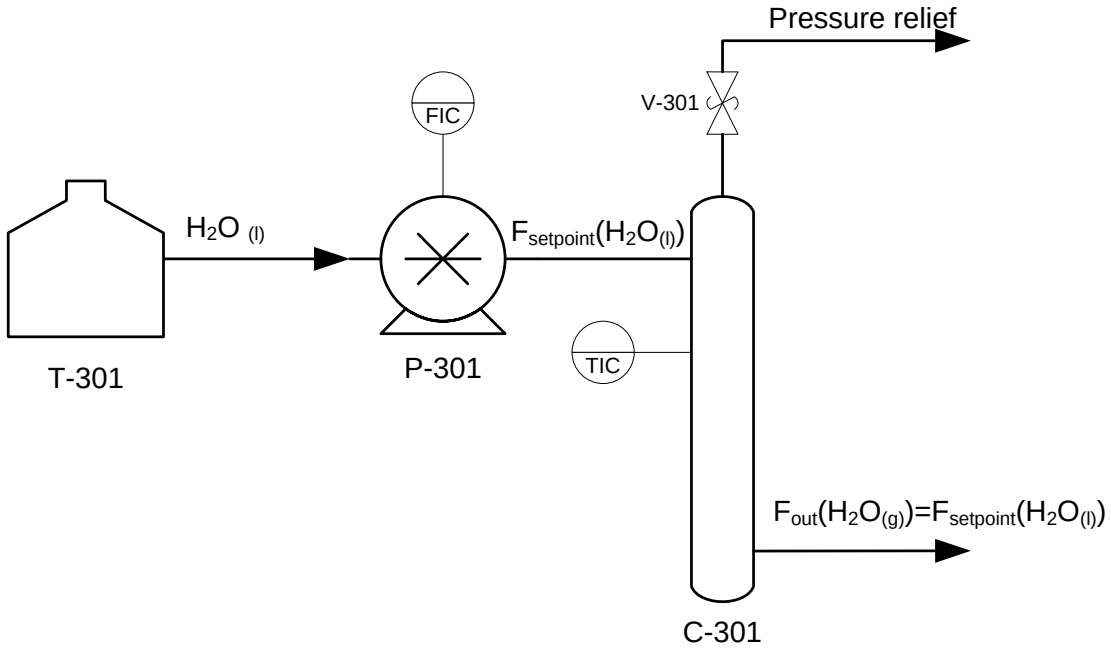

Figure 3.3: Preliminary flowsheet of water evaporator section

This is presented in flowsheet format in Figure 3.3, where liquid water from a storage device is pumped and metered into a heated vessel. It is important to note, unless indicated, that flow rates presented in this work are always on a molar basis. Hence the flow rate is presented as unchanging during evaporation, in terms of volumetric flow rate, an increase of 1600 times is expected when evaporating water at atmospheric pressure. Thus, it is vital that a relief valve (V-301) be added to the evaporator in case of uncontrollable pressure build up under unforeseeable circumstances, such as a blockage at the exit of the evaporator.

Up to this point, we have not discussed the thermodynamics of the evaporation of water, in short, for pure water to change from liquid to vapour phase at a certain pressure, it must be heated beyond its saturation temperature for this specific pressure, shown in Figure 3.4.

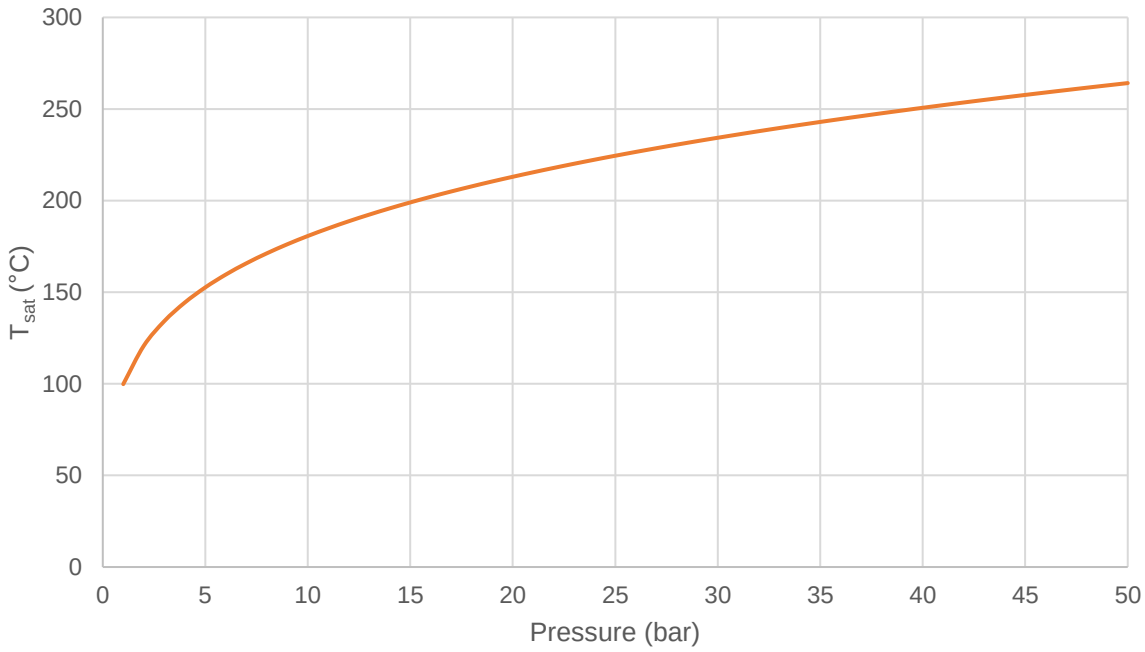

Figure 3.4: Boiling point of water at elevated pressures [11]

A limitation on the achievable water partial pressure is given by the condensation point of steam. For example, suppose we want to operate our reactor at 40 bar and 150 °C with an extreme large excess of steam to make the partial pressures of methane and oxygen insignificant compared to the steam partial pressure. We would have to heat the liquid water to above 250 °C for it to enter the vapour phase, however, immediately upon entering the colder reactor at 150 °C, it will condense back into liquid water.

Thus, to ensure the steam from the evaporator remains in the vapour phase in the reactor which may be at a lower temperature than the boiling temperature of water for the pressure the reactor is under, a make-up gas must be co-fed into the evaporator. This will essentially reduce the partial pressure of water in the evaporator for a constant total evaporator pressure (P_{steam} + $P_{make\text{-}up}$), thus lowering the saturation temperature of the water – make-up gas mixtures and preventing it from condensing, as shown in Figure 3.5. The make-up gas stream is also important to ensure smooth evaporation of the liquid water by preventing it from boiling transiently.

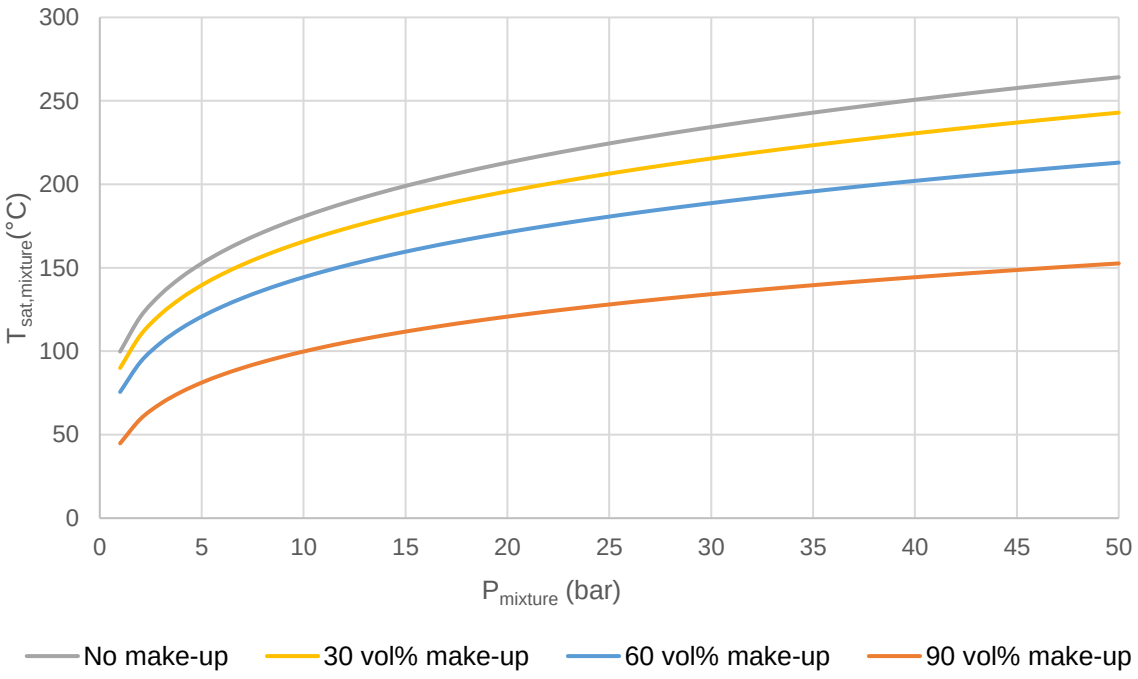

Figure 3.5: Effect of make-up gas composition on the saturation temperature of steam – make-up gas mixtures at elevated pressures

If we are to reconsider the hypothetical case of feeding steam into the reactor at 40 bars and 150°C, we can deduct from Figure 3.5 that a make-up gas fraction of just under 90 vol% is needed to bring the water partial pressure down (to just over 4 bars) in order to prevent condensation of the steam – make-up gas mixture at 150°C. In addition, if the flow of methane and oxygen in the reactor is not insignificant compared to that of the evaporator stream (makeup + steam), it will only act as extra make up gas, moving the system even further away from condensation.

Helium is chosen as the makeup gas for the evaporator, due to its inertness and availability. Since it is only available through a gas cylinder and its flow rate needs to be controlled to adjust the make-up ratio in the evaporator, a similar pressure – flow control system is added to the helium stream under the same rationale mentioned in the previous chapter for methane and oxygen.

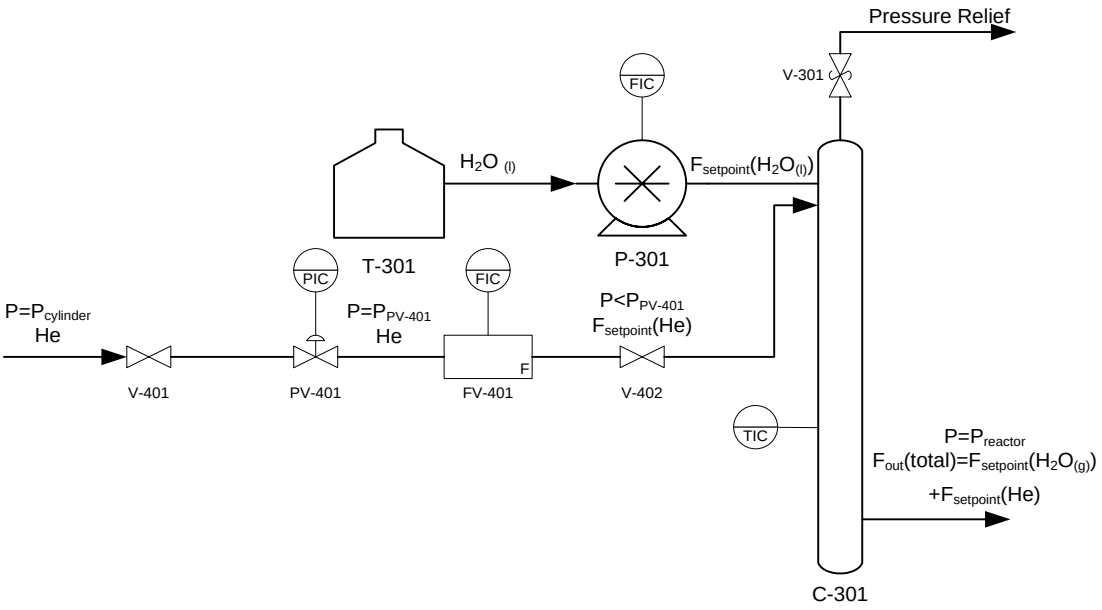

Figure 3.6: Flowsheet for water evaporator section

3.2.3 Packed bed reactor

In our catalytic reactor, different partial pressures of methane, oxygen, steam and helium will react over the surface of the solid platinum-based catalyst. The different partial pressures are achieved by controlling the total pressure of the reactor and the flow of the individual gases as discussed in the previous 2 sections. Since we are interested in the site blocking actions caused by high oxygen and steam partial pressures, the total pressure of the reactor is likely to be above ambient. However, the reactor products must be vented at ambient pressure, thus necessitating an expansion valve downstream of this pressurized reactor.

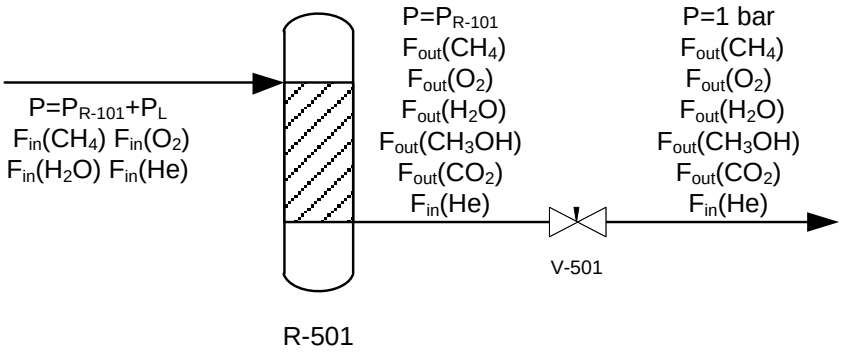

Figure 3.7: Schematic of catalytic packed bed reactor including the expansion valve

As a matter of definition, the pressure of the catalytic reactor will be considered as the pressure at the outlet of the reactor, thus the pressure of the feed streams entering the reactor will be the reactor pressure with the addition of the pressure loss over the reactor, P_L. Considering both the direct conversion of methane to methanol and the complete oxidation of methane to CO_2, we can draw up a stoichiometric table for the reactor, defining the conversions of the two reactions based on methane:

Table 3.1: Stoichiometric table for methane to methanol conversion using oxygen

	In	Change	Out
CH_4	$F_{in}(CH_4)$	$-(X_1 + X_2)\ F_{in}(CH_4)$	$(1 - X_1 - X_2)\ F_{in}(CH_4)$
O_2	$\theta F_{in}(CH_4)$	$-(0.5X_1 + 2X_2)\ F_{in}(CH_4)$	$(\theta - 0.5X_1 - 2X_2)\ F_{in}(CH_4)$
H_2O	$\omega F_{in}(CH_4)$	$+(2X_2)\ F_{in}(CH_4)$	$(\omega + 2X_2)\ F_{in}(CH_4)$
CH_3OH	0	$+X_1\ F_{in}(CH_4)$	$X_1\ F_{in}(CH_4)$
CO_2	0	$+X_2\ F_{in}(CH_4)$	$X_2\ F_{in}(CH_4)$
He	$\varphi F_{in}(CH_4)$	0	$\varphi F_{in}(CH_4)$
Total	$(1+\theta+\omega+\varphi)F_{in}(CH_4)$	$-0.5X_1\ F_{in}(CH_4)$	$(1+\theta+\omega+\varphi-0.5X_1)\ F_{in}(CH_4)$

Since the pressure lost through the reactor at steady state will be a constant, ideally, we can control the reactor pressure ($P_{R\text{-}501}$) by controlling the feed pressure to the reactor. However, for any non-zero conversion in reaction one, the total flow through the reactor will be reduced by a certain amount and subsequently the reactor exit pressure would be reduced as well. Thus, another stream of make-up gas should be added at the end of the reactor to compensate for the change in total flow. Argon gas is used as the make-up gas due to its inertness, and availability. Helium is not used again here due to its higher costs compared to argon as the consumption of this make-up gas is high to avoid flammable mixtures from forming after the reactor (discussed in Chapter 4.2.2). The make-up argon gas should not be flow controlled, as the required flow rate depends on the conversion inside the reactor and more importantly on the expansion valve.

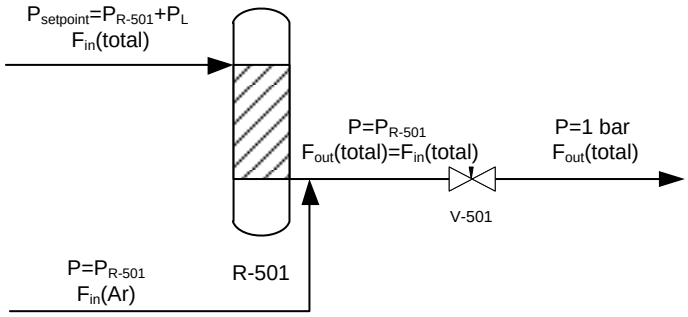

Figure 3.8: Schematic of catalytic packed bed reactor including argon make-up

An expansion valve, like any flow constrictor, will produce a flow depending on the pressure difference across the valve and its constriction/friction factor. This means:

$$F_{out}(total) = \frac{P_{R-101} - 1\,bar}{K_{expansion\ valve}}$$

where the constriction factor of the expansion valve is physically manipulated by opening/closing the valve. This leads to the dilemma where the flow through the reactor is physical set by the constriction of the expansion valve and the reactor pressure while simultaneously this total flow rate is also set by the flow controls upstream of the reactor and the addition of makeup gas to compensate for the change in flow due to conversion. In this case, an under-expanded V-501 will lead to the accumulation of reactants within the reactor,

increasing its pressure until it can no longer be fed by the feed pressure. In the case of an over-expanded V-501, reactants under pressure will exit the reactor faster than it can be fed, making it impossible to pressurize the reactor.

However, by letting the flow rate of the make-up gas float and controlling its pressure instead the reactor exit pressure can be effectively controlled by keeping the total flow rate through the expansion valve constant for any given reactor pressure. The amount of make-up gas entering the system at a set pressure will change to match the difference in the total flow allowed to exit the reactor by V-501 and the amount of product gases exiting the reactor. This set-up is represented in Figure 3.9, where PV-601 is shown to ultimately set the total pressure in the reactor. Argon gas entering the reactor system passes through a similar train of valves and controllers like all the other gaseous reagents with exception of a flow controller. Instead of being supplied directly via cylinder, argon as a commonly used gas in our laboratory is available through a centralized high-pressure supply at roughly 50 bar. As this is much lower than the 200 bar available initially from the gas cylinders for the other gases (methane, oxygen and helium) its pressure of roughly 50 bar will thus be the highest pressure attainable in our reactor.

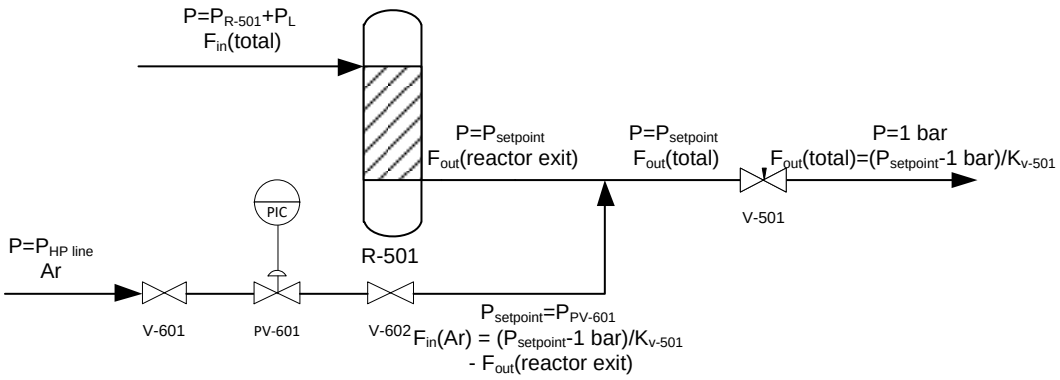

Figure 3.9: Schematics of catalytic packed bed reactor demonstrating the control of reactor pressure using the argon make-up stream

It has been argued, that an industrially attractive catalyst for direct methane to methanol conversion should be able to operate at elevated temperatures of > 150 °C to allow the recovery of the heat of reaction via steam generation. Thus, the packed bed reactor should be heated, and its temperature controlled. The temperature control is not only essential for steady state operation, and thus reproducible results, it will also directly affect the rate of reaction, and thus its conversion, via the Arrhenius relationship, where the rate constant of a chemical reaction changes exponentially with temperature:

$$k(T) = k(T_{ref})e^{\frac{E_a}{R}\left(\frac{1}{T}-\frac{1}{T_{ref}}\right)}$$

Additionally, given a complex system of reactions with different activation energies, the selectivity of the reaction network will be dependent on temperature too. Thus, temperature will be an important variable to investigate when the packed bed reactor system is used to evaluate the performance of the platinum-based catalyst. Therefore, the reactor must be temperature controlled.

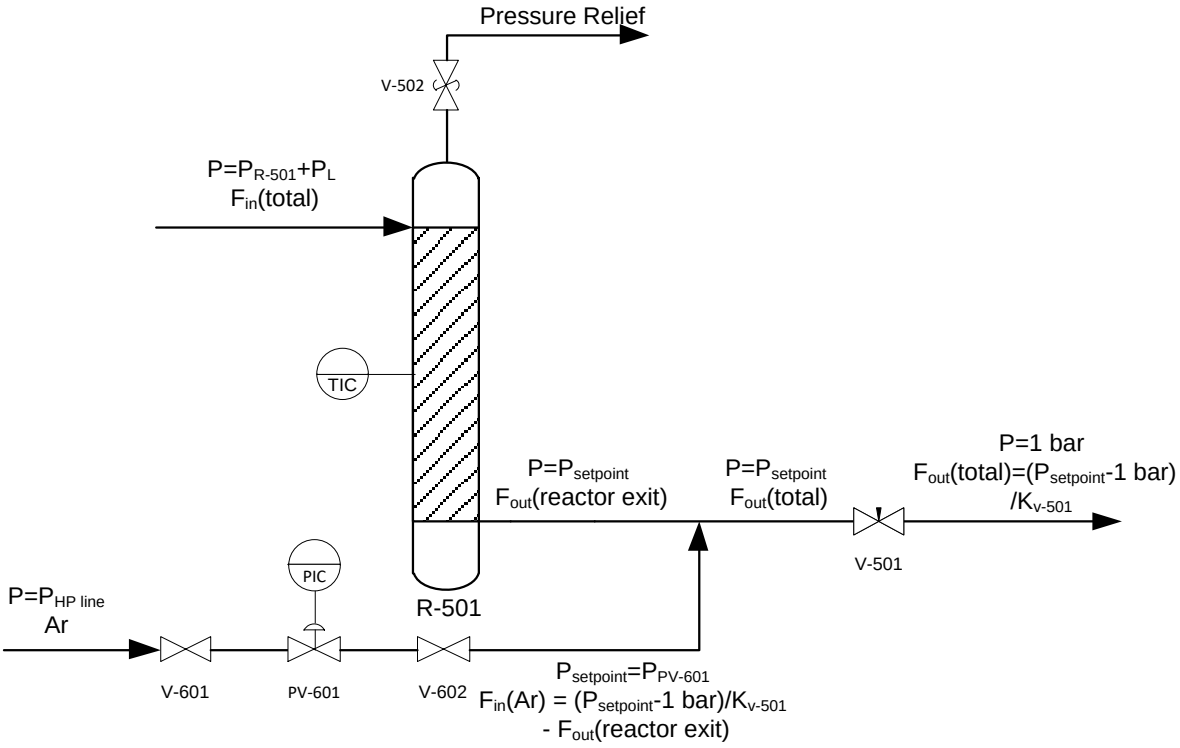

Figure 3.10: Flowsheet for catalytic packed bed reactor section

In addition to temperature control, a pressure relief valve is added to the packed bed reactor as it is a well-known fact that mixtures of methane and oxygen can be flammable under certain compositions (this will be discussed in more detail during the physical design of the reactor, R-501).

3.2.4 Sampling and product analysis

In order to evaluate the performance of the platinum-based catalysts in the direct conversions of methane to methanol, a part of the reaction products has to be sampled and analysed. The methanol selectivity enhancing effects of high oxygen and water partial pressures on the platinum-based catalysts can then be studied via these analysis results.

A gas chromatography (GC) based analysis system is almost always used for product analysis during the conversion of methane to methanol in a packed bed reactor system reviewed in the introduction of this work. In our laboratory, an Agilent 6890N gas chromatograph system is available for this project. This will be represented as one unit for now and detailed design around it will be discussed during the next design phase. For now, the sampling system consists of a valve manifold compromised of V-701 and V-801, which can selectively direct the expanded product from the reactor to either the GC for analysis or to the overhead vent lines in the reactor hood where the reactor system is placed. A flowmeter (FM-801) is added to the vent line to enable the measurement of the flow exiting the reactor system. Since all flows besides argon is controlled, this total flow measurement will allow the amount of argon flowing through the reactor system to be measured. In addition, this flowmeter can be used to verify and calibrate the various flow control elements in the reactor system.

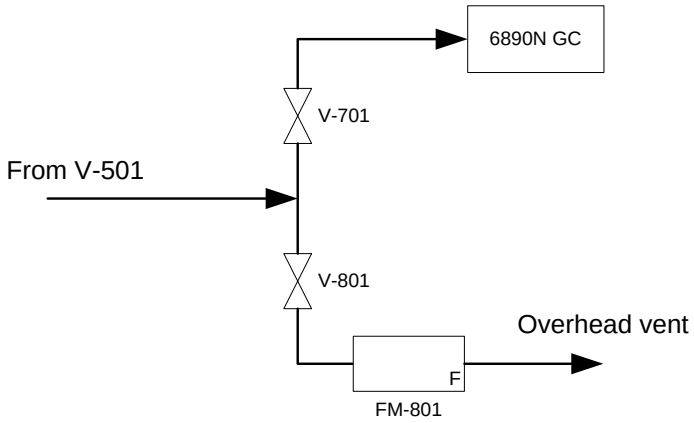

Figure 3.11: Flowsheet for sampling and product analysis section

3.2.5 Considerations applying to the entire flowsheet

By combining the flowsheets developed in the previous sections, we arrive at the flowsheet for the entire reactor system shown in Figure 3.12. A few additional units must be added when considering the entire process.

PV-102, PV-202, PV-402: Pressure control valves are added at the outlet of the gas cylinders. As discussed previously, the highest pressure we can run the reactor system is limited by the argon high pressure line at roughly 50 bar. Therefore, it would be advantageous to limit the pressure supply from the gas cylinders to this value to avoid having lines (between the cylinders and PV-X01's) at cylinder pressures of roughly 200 bar.

S-101, S-201, S-401, S-601: Filters are added at the beginning of the gas lines to filter out any solid particles that may be entrained in the gases coming from the cylinders and the high-pressure argon line. These particles may damage the sensitive valves in the mass flow controllers (FV-X01) as well as causing obstructions in the reactor system. These solid particles can also be propelled at high speeds while entrained in the gas streams, if not filtered out these particles can become hot enough to act as an ignition source or combust themselves during the high-speed impact with the inner surfaces of the lines and fittings in the reactor system.

V-302: A three-way valve is added to the outlet of the water pump, this allows the HPLC pump to be manually primed before operation (see Appendix II on reactor operation).

V-103, V-203, V-303, V-403, V-603: Non-return valves (one-way valves) are added to all the feed lines into the reactor system to prevent backflow. This is especially important for V-303, as P-301 work in pulses and back flow from the pressurized evaporator (C-301) into the pump will occur during the non-pumping phase of P-301 without this non-return valve.

S-102, V-104, S-202, V-204, S-501, V-503: As mentioned previously, mixtures of methane and oxygen can be flammable and explosive. Therefore, flame arresters must be placed in the methane, oxygen and reactor exit lines to prevent flame propagation into the exit lines and methane and oxygen feed lines. The issue of flammability will be discussed in detail during the design of R-501. A typical flame arrester consists of a flame quench element constructed from sintered metal and a non-return valve to prevent back flow during an ignition [58]. Commercial flame arrester rated for the maximum pressure of roughly 50 bar expected in our reactor could not be obtained as flame arresters were only available up to 20 bar from our supplier (Afrox).

Thus, 3 sets of flame arresters based on the working principles of commercial flame arresters have been added: a quench element consists of sintered metal filter (S-102, S-202, S-501) placed next to a standalone non-return valve (V-104, V-204, V-503).

Extra TICs: Steam in a mixture of gases must be heated to a certain temperature to prevent condensation. Oxidation products from the methane oxidation reactions such as methanol may also condense if these lines are not heated. Thus, two additional temperature control loops are added to the lines that will be carrying steam and/or reaction products to prevent condensation.

C-801, V-802: The overhead vent system for our reactor hood is not designed to handle liquid condensates (water, and oxidation products from the DMTM reaction) thus before we vent the products from the reactor system into the overhead vent, a condenser (C-801) must be added to remove condensable vapours (steam, methanol, etc) from the reactor effluent. This condensate can then be drained periodically via V-802.

The flowsheet shown in Figure 3.12 will not be the final flowsheet of the packed bed reactor system, as it will be revised after the individual units have been chosen and/or designed in the next chapter.

3.3 Flowsheet of experimental set-up

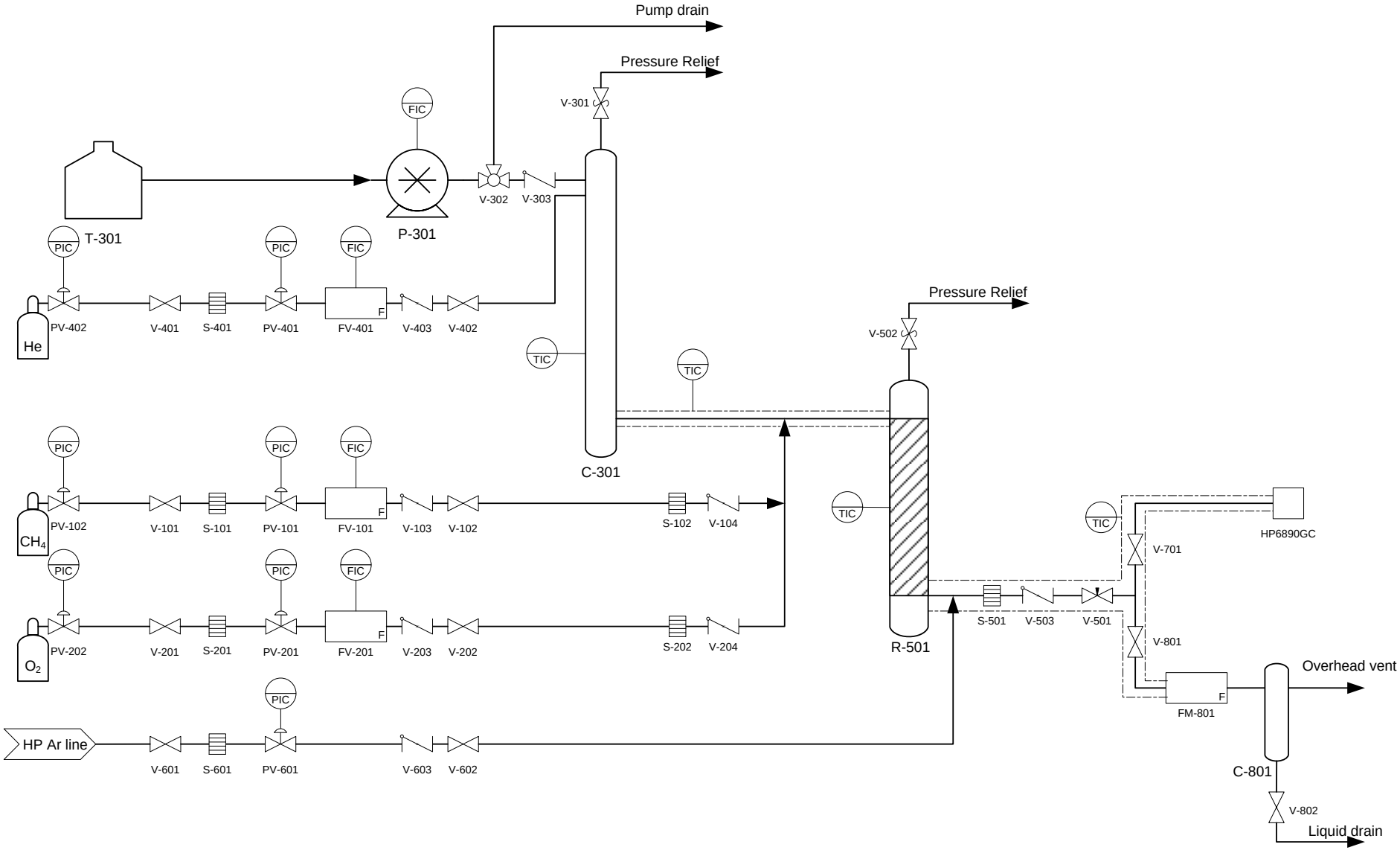

Figure 3.12: Preliminary PFD for packed bed reactor system for direct methane to methanol conversion

4. Experimental set-up

4.1 Choice of minor units

The new catalytic packed bed system for methane to methanol conversion was constructed in-house. An existing reactor stand (A6) was stripped, its chassis and some of its parts (see Appendix I) were used in our new reactor system. Most of the additional units needed as shown in Figure 3.12 was obtained from Swagelok®. The choice of these minor units is tabulated in Table 4.1.

Stainless-steel (SS316L) tubings, ⅛" (3.2 mm) OD with a wall thickness of 0.035" (0.9 mm) from Swagelok®, was used for all of the lines in the reactor system unless otherwise stated. The use of these relatively thin lines is a result of the small size of our catalytic reactor and the associated small flow rates, which will be discussed further during the detailed design of the reactor. Only the gas supply lines before the reactor system (before V-101, V-201, V-401, V-601) are ¼" (6.35 mm) in outer diameter as they already exist inside our reactor hood. The relief valves were also connected together with ¼" OD lines before being send to the overhead ventilation system.

A variety of fittings (cross and tee union, tubing reducers and expanders, nuts and ferrules), fasteners (screws, bolts, washers, brackets, etc.) and extra electrical wiring was also needed. These are not shown in Table 4.1, due to their trivial functions.

In addition to these minor units, the design of the catalytic reactor (R-501), the evaporator (C-301), the HP6890 gas chromatography system, the condenser (C-801) and the reactor system instrumentation and control will be discussed in detail in the subsections following Table 4.1.

Table 4.1: Minor units in packed bed reactor system for direct methane to methanol conversion

Unit symbol		**Manufacturer**	**Description, and stock code (where applicable)**
Water stream	T-301	Duran Schott	Schott glass bottle, 1000 ml
	P-301	Lab Alliance	Series I HPLC pump (flow range: 0.01 $ml.min^{-1}$ to 10 $ml.min^{-1}$ of liquid in 0.01 $ml.min^{-1}$ intervals)
	V-302	Swagelok	⅛" three-way valve, nylon handle, SS-41GXES2
	V-303	Swagelok	⅛" check valve, ⅓ psi cracking pressure, SS-2C-1/3
Helium stream	He cylinder	Air Products	50 litre Helium 5.0 gas cylinder, initially at 200 bar
	PV-402	Tescom	Diaphragm pressure control valve, max inlet pressure 6000 psi, max outlet pressure 1000 psi; with 2 Wika 2.5" pressure gauges attached (inlet: 0 – 25 MPa, outlet: 0 – 6000 kPa)
	V-401	Swagelok	⅛" on-off valve, nylon handle, SS-41GES2
	S-401	Swagelok	⅛" inline sintered metal filter, 7 µm pore size, SS-4TF-7
	PV-401	Air Products	Diaphragm pressure control valve, max regulated pressure 2000 psi, with 2 Wikia 2.5" 0 – 25 MPa pressure gauges attached
	FV-401	UNIT	UNIT 7000 mass flow controller, max rated flow rate 100 $ml_n.min^{-1}$ N_2[b]
	V-403	Swagelok	⅛" three-way valve, nylon handle, SS-41GXES2
	V-402	Swagelok	⅛" on-off valve, nylon handle, SS-41GES2

Methane stream	CH_4 cylinder	Air Products	50 litre Methane 3.5 gas cylinder, initially at 190 bar
	PV-102	Tescom	Diaphragm pressure control valve, max inlet pressure 6000 psi, max outlet pressure 1000 psi; with 2 Wika 2.5” pressure gauges attached (inlet: 0 – 25 MPa, outlet: 0 – 60 bar)
	V-101	Swagelok	⅛” on-off valve, nylon handle, SS-41GES2
	S-101	Swagelok	⅛” inline sintered metal filter, 7 µm pore size, SS-4TF-7
	PV-101	Tescom	Diaphragm pressure control valve, max inlet pressure 6000 psi, max outlet pressure 1000 psi; with 2 Wika 1.5” pressure gauges attached (inlet: 0 – 250 bar, outlet: 0 – 100 bar)
	FV-101	UNIT	UNIT 7000 mass flow controller, max flow $50ml_n.min^{-1}$ H_2[b]
	V-103	Swagelok	⅛” check valve, ⅓ psi cracking pressure, SS-2C-1/3
	V-102	Swagelok	⅛” on-off valve, nylon handle, SS-41GES2
	S-102	Swagelok	⅛” inline sintered metal filter, 7 µm pore size, SS-4TF-7
	V-104	Swagelok	⅛” check valve, ⅓ psi cracking pressure, SS-2C-1/3
Oxygen stream[a]	O_2 cylinder	Air Products	50 litre Medical oxygen gas cylinder, initially at 200 bar
	PV-202	Tescom	Diaphragm pressure control valve, max inlet pressure 6000 psi, max outlet pressure 1000 psi; with 2 Wika 2.5” 25 MPa pressure gauges attached
	V-201	Swagelok	⅛” on-off valve, nylon handle, SS-41GES2
	S-201	Swagelok	⅛” inline sintered metal filter, 7 µm pore size, SS-4TF-7
	PV-201	Tescom	Diaphragm pressure control valve, max inlet pressure 6000 psi, max outlet pressure 1000 psi; with 2 Wika 1.5” pressure gauges attached (inlet: 0 – 120 bar, outlet: 0 – 100 bar)
	FV-201	UNIT	UNIT 7000 mass flow controller, max rated flow rate $50ml_n.min^{-1}$ N_2[b]
	V-203	Swagelok	⅛” check valve, ⅓ psi cracking pressure, SS-2C-1/3
	V-202	Swagelok	⅛” on-off valve, nylon handle, SS-41GES2
	S-202	Swagelok	⅛” inline sintered metal filter, 7µm pore size, SS-4TF-7
	V-204	Swagelok	⅛” check valve, ⅓ psi cracking pressure, SS-2C-1/3
Argon stream	V-601	Swagelok	⅛” on-off valve, nylon handle, SS-41GES2
	S-601	Swagelok	⅛” inline sintered metal filter, 7 µm pore size, SS-4TF-7
	PV-601	Tescom	Diaphragm pressure control valve, max inlet pressure 6000 psi, max outlet pressure 1000 psi; with 2 Wika 1.5” pressure gauges attached (inlet: 0 – 130 bar, outlet: 0 – 100 bar)
	V-603	Swagelok	⅛” check valve, ⅓ psi cracking pressure, SS-2C-1/3
	V-602	Swagelok	⅛” on-off valve, nylon handle, SS-41GES2
Post reactor	S-501	Swagelok	⅛” inline sintered metal filter, 7 µm pore size, SS-4TF-7
	V-503	Swagelok	⅛” check valve, ⅓ psi cracking pressure, SS-2C-1/3
	V-501	Swagelok	⅛” needle valve, stainless-steel metal handle, SS-ORS2-SH
	V-701	Swagelok	⅛” on-off valve, nylon handle, SS-41GES2
	V-801	Swagelok	⅛” on-off valve, nylon handle, SS-41GES2
	FM-801	Hirschmann EM Techcolor	50 ml burette/bubble flow meter

Relief Valves	V-301	Swagelok	¼" proportional pressure relief valves, set to open at 50 bar, SS-4R3A
	V-502	Swagelok	¼" proportional pressure relief valves, set to open at 50 bar, SS-4R3A

a: All fittings on this line is rated for oxygen service, i.e. no combustible lubricant and seal materials are used

b: See appendix I on the calibration of mass flow controllers flow rate ranges for the actual gas used in our reactor system instead of the rated gas

4.2 Packed bed reactor – R-501

4.2.1 Requirement for quartz liner

Past studies on direct methane to methanol conversion usually used a quartz lined reactor [24], [25], [26], [1], [28], [30], [59], [44], as metals, typically used as material of construction for reactors such as stainless steel and copper were found to be catalytically active in the direct conversion of methane to methanol, leading to a drastic reduction in methanol selectivity [1], [60]. The experiments done at atmospheric pressure used only a quartz tube as the reactor [28], [30], [59], whilst experiments done at elevated pressures use a quartz tube lined steel reactor to withstand the elevated pressures [24], [25], [26], [1].

In our direct methane to methanol conversion reactor, we are interested in the effect of high oxygen and water partial pressures and will thus be operating the reactor at elevated pressures, requiring the use of a quartz liner to separate the reactant gases and the catalyst from the stainless-steel reactor surfaces. This can be achieved by using a tight-fitting quartz insert in a stainless-steel reactor [24] or sealing the quartz tube from the reactor surface using O-rings [1]. We chose the O-ring approach to ensure a proper seal is maintained. Since we are using argon as the reactor pressure control gas and the post reaction make-up gas, we decided it was appropriate to pressurize the annular space between the quartz liner and the metal reactor surface with argon gas. This argon gas will only mix with the reactor effluent at the end of the quartz liner. This way the quartz liner will only be exposed to a pressure difference equivalent to the pressure drop of the catalyst bed inside the quartz liner, irrespective of the total reactor pressure. This updated reactor schematic is illustrated in Figure 4.1. The symbology of the temperature control loop for the reactor is also updated in Figure 4.1 to reflect the operation of the Gefran temperature controllers (see Appendix I).

4.2.2 Flammability of methane-oxygen mixtures

The flammable nature of methane and oxygen mixtures poses a serious safety problem if not addressed properly, as 1 kg of methane and oxygen mixture in stoichiometric ratio for complete combustion (33 vol.% methane) will releases 10 MJ of energy during combustion, equivalent to the energy released during the detonation of 2.4 kg of TNT [11].

Combustions are rapid exothermic radical chain reaction between oxygen and a combustible material such as methane gas. A fuel, oxygen and a source of ignition is required to start the combustion reaction. Once started, a combustion reaction requires heat, fuel and oxygen to be sustained. This is commonly referred as the fire triangle.

The combustion of a methane-oxygen mixture can only happen if the composition of methane and oxygen is within a certain range, known as the flammability limits. Figure 4.2 illustrates the upper and lower flammability limits of methane (UFL and LFL) mixed with pure oxygen

in terms of volumetric percentage of methane at different temperatures and pressures, given by correlations provided in Zabetakis [61]. It is noted that while temperature does not have much of an effect on the flammability limits, elevated pressures does significantly increase the upper flammability limit of methane in oxygen. At 50 bar, even a 95 vol.% methane, 5 vol.% oxygen mixture is flammable.

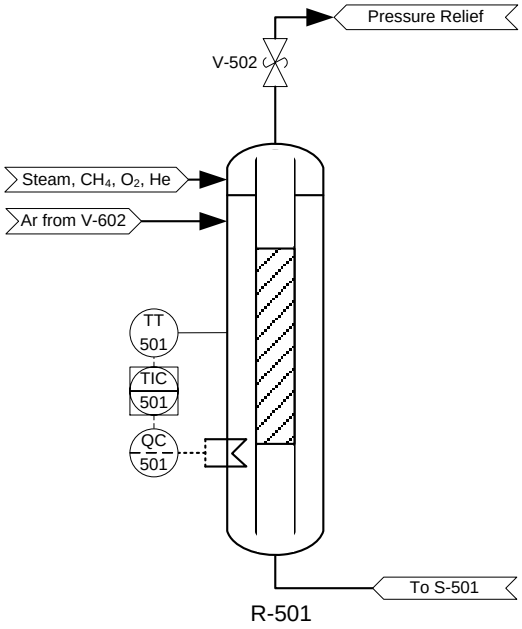

Figure 4.1: Schematic of R-501 showing catalyst bed inside reactor quartz liner

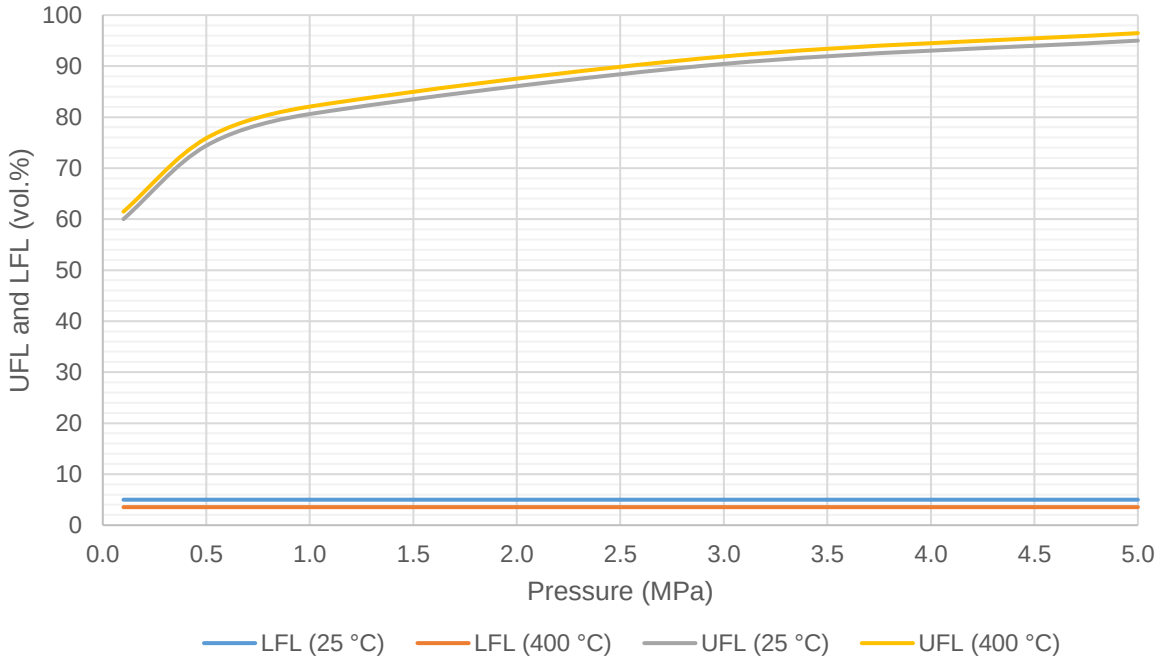

Figure 4.2: Methane-oxygen mixture flammability limits at elevated temperatures and pressures

The flammability limits can be derived from the adiabatic temperature of the combustion reaction [62], where any mixture of methane and oxygen with an adiabatic combustion

temperature above 1500 K will be within the flammability limits [62]. Consequently, the presence of inerts, such as helium, steam and argon in our reactor will lower the adiabatic combustion temperature of the methane-oxygen-inert mixtures. Thus, it will also lower the flammability range (decreasing the upper flammability limit and increasing the lower flammability limit) of these methane-oxygen-inert mixtures, compared to that of pure methane and oxygen.

In our direct methane to methanol conversion reactor, the requirement to manipulate the partial pressure of the reactants does not always give us the freedom to stay out of these flammability limits. Thus, a worst-case scenario approach is used in the designing of this reactor: assuming we must pass a stoichiometric mixture of methane and oxygen for combustion (33 vol.% methane, reminder oxygen) through the reactor whilst some arbitrary source of ignition is present, and the methane-oxygen mixture ignites.

Assuming also that the inlet and outlet of the reactor is somehow blocked, essentially turning the reactor into an explosive device, the maximum pressure rise can be estimated [61] as:

$$\frac{P_{m_f}}{P_i} = \frac{n_i T_a}{n_f T_i}$$

Where P_{m_f} and P_i is the maximum pressure obtainable after combustion and the pressure of the initial mixture, n_i and n_f is the moles of gases before and after combustion (the same in the case of the combustion between methane and oxygen), T_a and T_i is the adiabatic temperature of combustion (3000 K for a stoichiometric methane-oxygen mixture [62]) and the temperature of the initial mixture. The maximum pressure obtainable will thus occur at the highest reactor pressure (50 bar) and lowest initial reactor temperature (ambient).

$$P_{m_f} = P_i \frac{T_a}{T_i} = 50\ bar \times \frac{3000\ K}{298\ K} = 503\ bar$$

The fixed bed reactors in our laboratory is mostly constructed using imperial units sized seamless stainless-steel tubing from Swagelok®. These tubing are pressure rated according to their sizes, with thinner inner diameter tubings able to withstand higher pressures. This pressure rating degrades with temperature and is reduced to 76 % of their rated pressure at their maximum rated temperature of 537 °C [63]. However, evident from Table 4.2, the decrease in maximum pressure obtainable outweighs the tubings' strength reduction at elevated temperatures.

Table 4.2: Pressure ratings needed to withstand maximum pressure obtainable during the stoichiometric combustion of methane and oxygen in a closed vessel at different temperatures

Temperature (°C)	P_{rated} degradation factor of tubing [63]	P_{rated} required for tubing (bar)
25	1	503
93	0.96	427
204	0.85	370
315	0.79	323
426	0.76	282

For our worst-case scenario, the tubing should have a maximum rated pressure of 503 bar. This rated pressure is only available in tubings with an outer diameter of ¼" (6.35 mm) or smaller [63]. It should be noted the above analysis grossly overestimates maximum pressure obtainable during combustion as:

- The reactor is extremely unlikely to be closed (have both inlet and outlet blocked)
- Pressure relief valve (V-502) is added to the reactor
- Any presence of inerts will lower the adiabatic combustion temperature from 3000 K and thus the maximum pressure obtainable
- Any deviation from the stoichiometric ratio of methane and oxygen (1:2 by volume) will lower the adiabatic combustion temperature from 3000 K and thus the maximum pressure obtainable
- A source of ignition is unlikely to be present in our reactor
- In case ¼" diameter tubings are used together with a quartz liner with a thickness of 1mm, very little energy will be released during combustion due to its small size as shown in Table 4.3. Furthermore, the shattering of the quartz tube will also absorb energy from the combustion reaction.

Table 4.3: Energy released during the combustion of a stoichiometric mixture of methane and oxygen at 50 bar inside 1 mm quartz lined ¼" stainless steel tubing available from Swagelok®

Tube Thickness (inch)	Pressure rating at T < 93°C [63] (bar)	Tube internal diameter [63] (mm)	Quartz liner internal diameter (mm)	Energy released during combustion (kJ/m_{tubing})
0.028	276	4.93	2.93	3.5
0.035	352	4.57	2.57	2.7
0.049	517	3.86	1.86	1.4
0.065	703	3.05	1.05	0.5

Conventional ¼" stainless steel tubing from Swagelok® was conservatively chosen as the material of construction for the outer shell of R-501 based on its high-pressure ratings and its small internal volume. The problem with flammability of methane and oxygen mixture upstream of the reactor is eliminated by mixing methane and oxygen only at the reactor inlet. Downstream of the reactor a large amount of argon make-up gas (approximately 90 vol.% argon in reactor effluent) can be added to dilute the reactor effluent, preventing it from becoming flammable. At a volume fraction of at least 50 % argon [64] can prevent a stoichiometric mixture of methane and air from becoming flammable (90 % total inert volume fraction, Ar and N_2), while a volume fraction of CO_2 [65] or N_2 [61] of at least 80 % can prevent a mixture of methane and pure oxygen from becoming flammable. It should be noted that these experiments were carried out under atmospheric pressure. The flammability problem outside of the reactor is further mitigated using the sintered metal filter – non-return valve flame arresters (S-102, V-104, S-202, V-204, S-501, V-502).

4.2.3 Main body of reactor

The quartz liner needed for the reactor was sourced from Friedrich & Dimmock, Inc. and constructed out of Suprasil 310 quartz. To improve temperature control inside the reactor, the thermocouple (TT-501) of TIC-501 is placed inside the reactor quartz liner and requires a quartz sheath to isolate the reactant gases from the thermocouple's metal surface. For the thermocouple quartz sheath, the smallest tube available from Friedrich & Dimmock, Inc. was used, with an outer diameter of 2 mm and an inner diameter of 1 mm.

The reactor quartz liner needs to have an inner diameter greater than 2 mm to accommodate the quartz sheathed thermocouple and an outer diameter that fits inside the inner diameter of one of the ¼" stainless steel reactor shell from Table 4.3. The only size that meet this criterion available from Friedrich & Dimmock, Inc. is a quartz tube with an outer diameter of 4 mm and an inner diameter of 2.4 mm.

Limited by the outer diameter of the reactor quartz liner, only ¼" tubings with a wall thickness of 0.028" or a wall thickness of 0.035" can work as the reactor. A wall thickness of 0.028" is preferred over a wall thickness of 0.035" as the low clearance (0.29 mm) between the quartz liner and the reactor shell in the latter case often caused the breakage of the quartz tube when the reactor shell is subjected to slight bending forces during installation. This arrangement is shown to scale in Figure 4.3.

With the reactor diameters set, one can approximate the length of the catalyst bed required to obtain a space velocity range agreeable with space velocities used in literature for methane oxidation. In the experiment carried out by Kwon et al. [33] on methane oxidation at 260 °C and ambient pressure using a Rh-ZrO_2 catalyst, the authors used a space velocity of 60 $\frac{ml_{n_{CH_4}}}{g_{cat}.min}$. The Rh-$ZrO_2$ catalyst used by Kwon et al. should be comparable to performance as a platinum-based catalyst since they are all platinum group noble metals. We would like to be able to change this space velocity by at least an order of magnitude in each direction from 6 $\frac{ml_{n_{CH_4}}}{g_{cat}.min}$ to 600 $\frac{ml_{n_{CH_4}}}{g_{cat}.min}$.

As our methane flow controller (FV-101) has a flow range of 0.4 $ml_n.min^{-1}$ to 39.4 $ml_n.min^{-1}$, the catalyst mass must be approximately 65 mg to meet the required methane space velocity range with our methane flow controller. Using a conservative bulk catalyst bed density of 0.5 $g.ml^{-1}$ (1 $g.ml^{-1}$ catalyst particles packed with 50 % voidage), the catalyst bed will have a volume of 0.13 ml to meet the required space velocity range. In reality, our methane space velocity range will be lower as the catalyst bed will denser than the assumed 0.5 $g.ml^{-1}$. This is done deliberately as the space velocity can be increased by diluting the catalyst with inert particles or packing less catalyst particles in the reactor, whereas there are no methods of decreasing the space velocity besides changing the methane flow controller.

Since the diameter of the catalyst packing is already determined, the length of the catalyst packing must be 57.5 mm to have a volume of 0.13 ml. This length was rounded off to 60 mm. 10 mm is added to each end of the catalyst packing to accommodate a set of glass wool plugs which keeps the catalyst packing in place, making the packed section 80 mm in length. 60 mm of packing free space is added to each end of the 80 mm packing zone, making the overall reactor shell 200 mm in length. Three sets of the aluminium cubic blocks (50 mm sides) are

placed around the reactor shell for heating and structure support of the reactor (these blocks are bolted via brackets to the reactor system stand). The overall length of the heating block is only 150 mm as oppose to 200 mm of the reactor shell due to how Swagelok® compression fitting works as shown in Figure 4.5. As 15 mm of tubing is enclosed in each Swagelok® fitting, the straight section of the reactor shell is only 170 mm, leaving only 10 mm of space on each end that is not covered inside the aluminium heating block, shown in Figure 4.4.

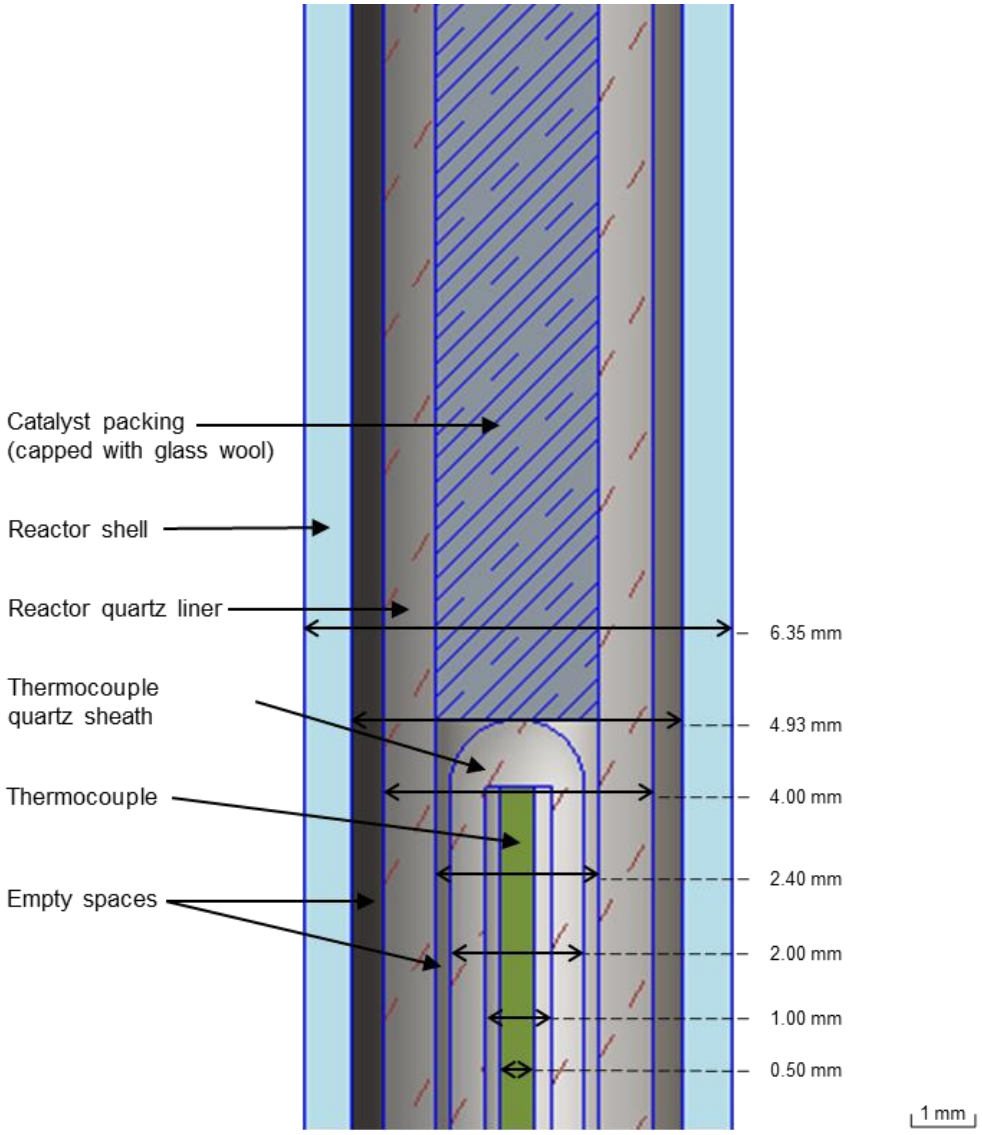

Figure 4.3: Cross section view showing the arrangement of steel shell, quartz liner, thermocouple quartz sheath and thermocouple (0.5 mm in diameter) inside R-501 at the end of the catalyst bed

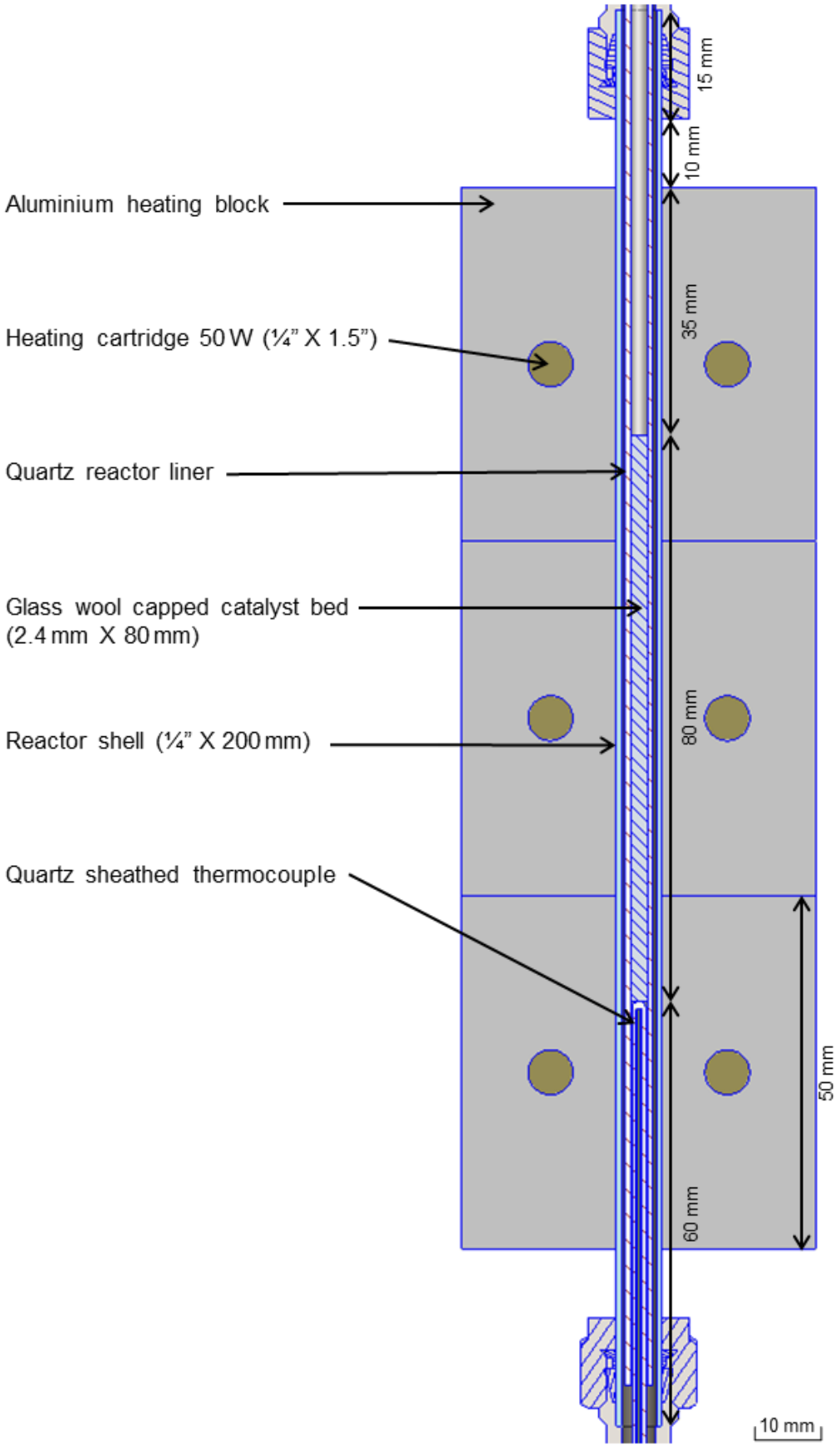

Figure 4.4: Cross section view showing the main body of R-501

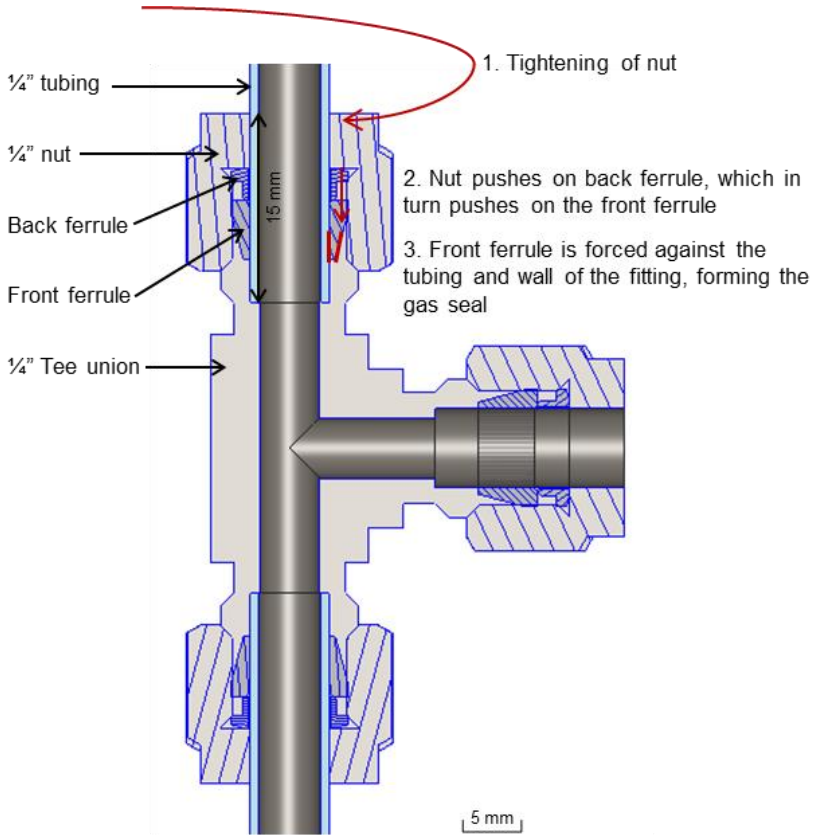

Figure 4.5: Illustration on the working principles of Swagelok® tube fittings

The external temperature of the reactor along the aluminium heating block is measured once at a reactor set point temperature of 200 °C. This was done during the autocatalytic conversion of methane to methanol (no reaction is expected at this temperature, i.e. no heat released by reaction) with a silicon carbide packed reactor quartz liner and shown in Figure 4.6. This was done by pulling a spare 0.5 mm diameter thermocouple down the gap between the aluminium heating block and the reactor and recording the temperature at 1 cm intervals. Overall, the temperature profile is deemed acceptable as the temperature variation across most of the aluminium heating block covered part of the reactor (beside 1 cm on either ends) is within 15 °C.

The external temperature along 67 % of the location reserved for the catalyst bed (4 cm out of 6 cm) is isothermal at 210 °C with the top 0.5 cm and the bottom 1.5 cm of the reserved zone at a slightly lower temperature of 200 °C. The maximal deviation from the isothermal zone at 210 °C is -8 °C at the bottom of the zone reserved for the catalyst bed. It should be noted that the external reactor temperature may not be reflective of the reactor temperature inside the reactor quartz liner due to the presence of the reactor quartz liner and the argon gas flowing outside of the quartz liner. The internal temperature profile in the reactor is impossible to measure with conventional thermocouples due to the lack of clearances.

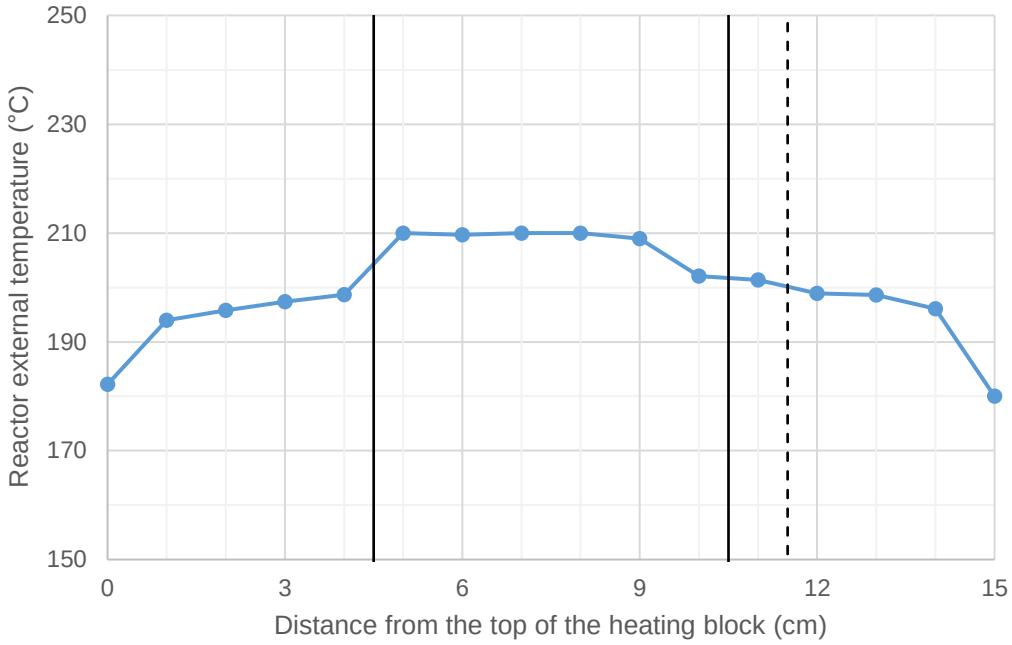

Figure 4.6: External reactor temperature profile along the aluminium heating block at a temperature set point of 200 °C, solid vertical lines indicate location reserved for the catalyst bed, control thermocouple placed inside the reactor at the dashed vertical line

4.2.4 Estimation of pressure drop inside reactor quartz liner

The pressure drop, ΔP, inside the reactor quartz liner must be estimated first as the quartz liner is required to hold against this pressure drop. For this case study the gas mixture passing through the reactor quartz liner is assumed to be pure oxygen at 300 °C and 30 bar. Oxygen was chosen as the case study gas as it has the highest viscosity, μ (3.37×10^{-5} Pa.s [66]) and density, ρ (20 $kg.m^{-3}$ assuming ideal gas) out of all the gases flowing inside the reactor quartz liner (methane, helium and steam) at 300 °C and 30 bar.

The flow rates considered in this analysis ranges from 13 $ml_n.min^{-1}$ (all flow controllers set to 5 %, no steam co-fed) to 1500 $ml_n.min^{-1}$ (all flow controllers set to 99.9 % resulting in 260 $ml_n.min^{-1}$ of gases along with 1240 $ml_n.min^{-1}$ of steam from 1ml.min^{-1} of liquid water).

The Reynold number and superficial fluid velocity, u, over the top cylindrical section of the quartz liner and the annular bottom section of the quartz liner over a range of flow rates between the minimum and maximum flow rates possible is plotted in Figure 4.7. The flow is laminar in this region as the Reynold number is significantly lower than 2300, the criteria for incompressible laminar flow of inside a closed conduit [66]. The compressibility of the gas flow in the reactor quartz liner is deemed negligible as its superficial velocity is minuscule compared to the speed of sound. The pressure drop in the top cylindrical section of the quartz liner and the annular bottom section was calculated using the Hagen-Poiseuille equation, which is applicable to incompressible laminar flow [66], where L and D are length and equivalent diameter of the section under consideration:

$$\Delta P = 32\frac{\mu u L}{D^2} \quad where\ D = 4\frac{cross-sectional\ area\ of\ flow}{wetted\ perimeter}\ for\ the\ annular\ section$$

The calculated pressure drop across these 2 sections using the data in Figure 4.7 is deemed insignificant (< 5 mbar at the maximum flow rate).

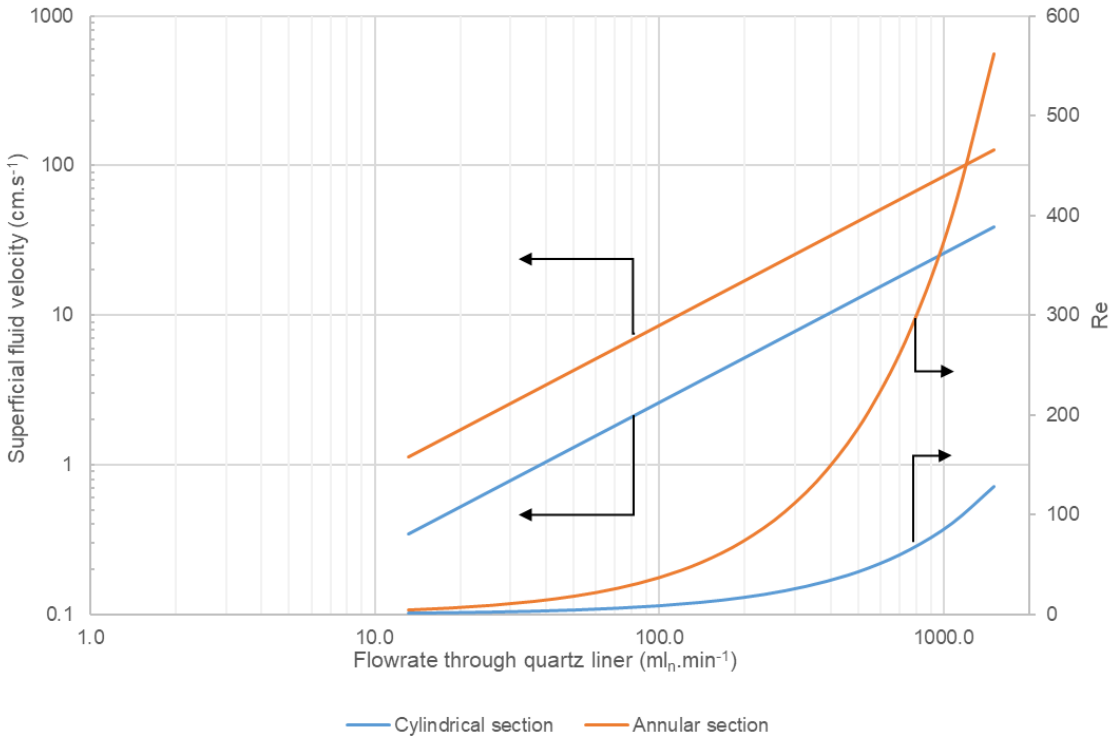

Figure 4.7: Superficial fluid velocity (u) and Reynold's number over the non-packed sections of the reactor quartz liner with a feed of oxygen at 300 °C and 30 bar

Although the pressure drop inside the unpacked sections of the reactor quartz liner is negligible, the pressure drop inside the catalyst packing can be significant and is highly dependent on the particle size of the catalyst, d_p, indicated in Figure 4.8. These pressure drops were calculated using the Ergun equation [67]:

$$\frac{\Delta P}{L} = \frac{150\mu(1-\varepsilon)^2 u}{\epsilon^3 d_p^2} + \frac{1.75(1-\varepsilon)\rho u^2}{\varepsilon^3 d_p}$$

A packing voidage, ε, of 0.5 is assumed for this analysis while all the other conditions remain constant from the previous analysis in Figure 4.7. Defining a maximum acceptable pressure drop to be 2 bar, catalyst particles with sizes between 100 µm to 50 µm can be used throughout the flow rate range without causing excessive pressure drop (see Figure 4.8). At lower flow rates particles with sizes down to 25 µm can be used below 500 $ml_n.min^{-1}$, down to 10 µm used below 100 $ml_n.min^{-1}$ and down to 5 µm used below 20 $ml_n.min^{-1}$ without causing excess pressure drop.

In addition, particles greater than 160 µm in diameter should not be used in the reactor to minimize wall effects by keeping $d_{rctr}/d_{particle} < 15$ [68].

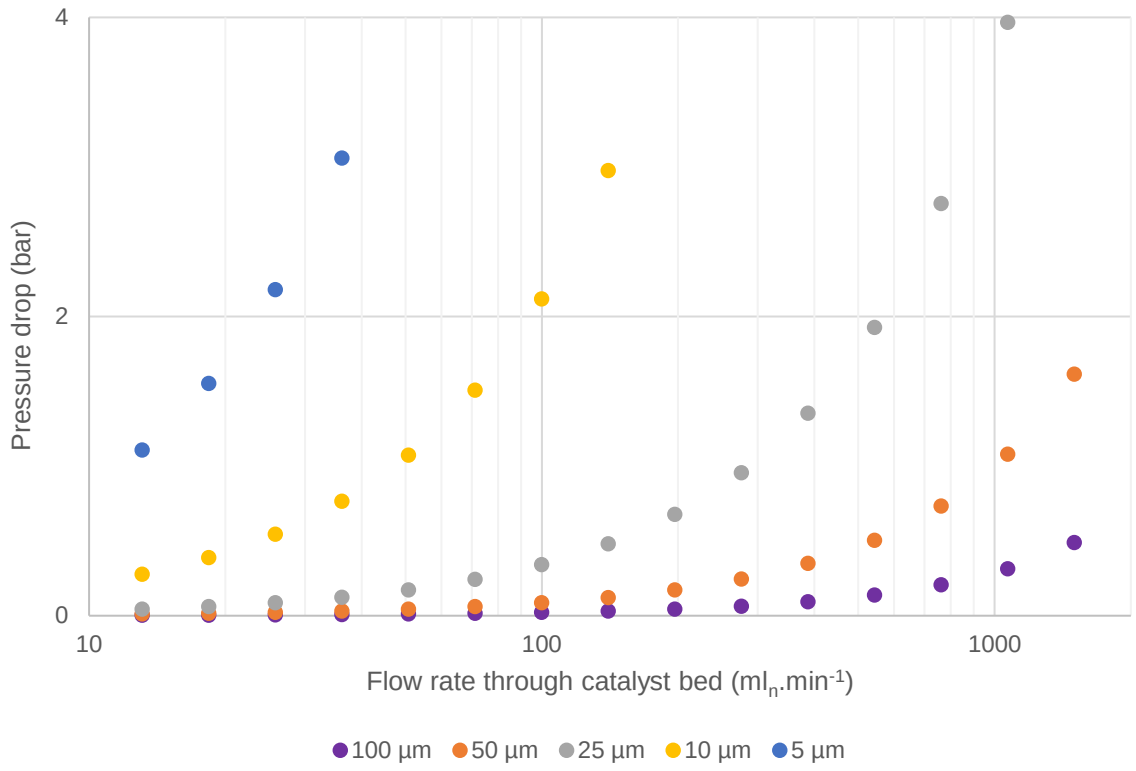

Figure 4.8: Pressure drop over packed section of the reactor quartz liner with a feed of oxygen at 300 °C and 30 bar, assuming spherical particles and a packing voidage of 0.5

4.2.5 Estimation of axial dispersion inside reactor quartz liner

The superficial fluid velocity inside the reactor quartz liner can be slow at low flow rates evident from Figure 4.7. The axial dispersion inside the catalyst bed should be estimated to determine the deviation from plug flow caused by diffusion. For this case study, the gas under consideration is still pure oxygen at 300 °C and 30 bar.

The dispersion number $\frac{D}{uL}$ can be calculated from the product of the packed bed dispersion number, $\frac{D\varepsilon}{ud_p}$ and the packed bed geometric factor, $\left(\frac{d_p}{L\varepsilon}\right)$ [69]:

$$\frac{D}{uL} = \left(\frac{D\varepsilon}{ud_p}\right)\left(\frac{d_p}{L\varepsilon}\right)$$

When the dispersion number is less than 0.01, the deviation from plug flow caused by diffusion is negligible [69]. A dispersion number less than 0.01 means the bed length should be more than:

$$L > 100\left(\frac{D\varepsilon}{ud_p}\right)\left(\frac{d_p}{\varepsilon}\right)$$

The packed bed dispersion number, $\frac{D\varepsilon}{ud_p}$, is correlated to the particle Reynold's number, Re_p shown in Figure 4.9 for a Schmidt number of 0.2 (the Schmidt number of methane in oxygen at 300 °C and 30 bar is 0.16).

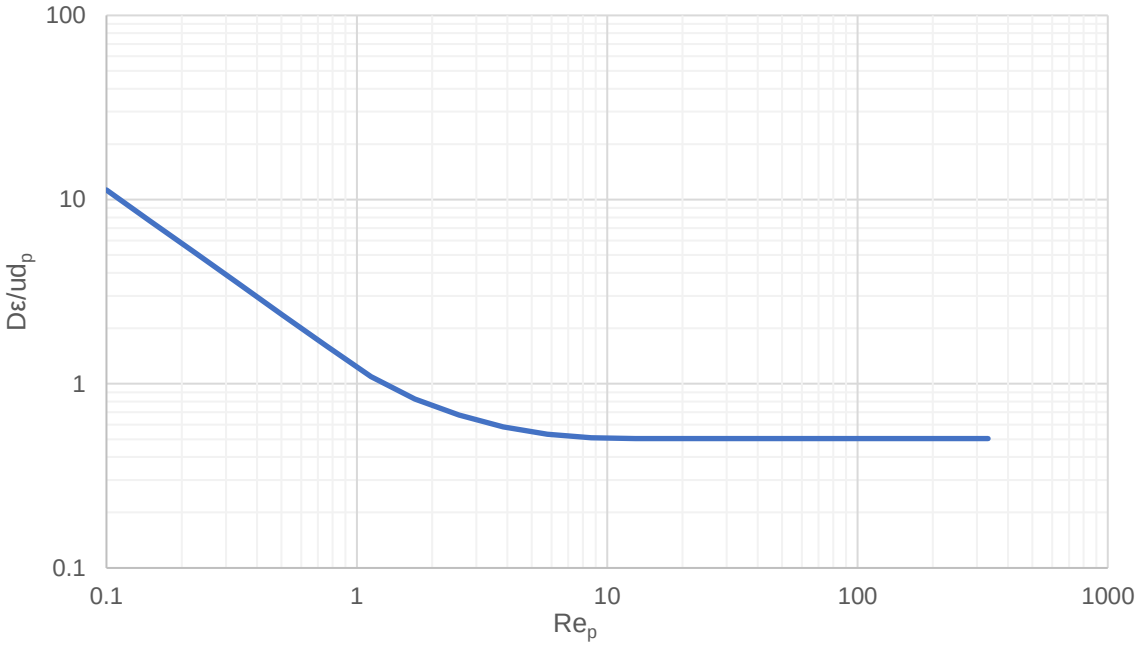

Figure 4.9: Correlation between particle Reynold's number to packed bed dispersion number, reproduced from Levenspiel (1999) for gases with a Schmidt number of 0.2 [69]

Using Figure 4.9 and different particle sizes of the catalyst, we can calculate the minimal length of the catalyst bed needed to keep the dispersion number below 0.01 (see Table 4.4) at different flow rates through the reactor quartz liner. As the required bed length is always less than the designed bed length of 60 mm, there should be no deviation from plug flow throughout the flow rates possible in the reactor system caused by dispersion.

Table 4.4: Estimated dispersion number inside catalyst bed for different particle sizes and total flow rates with a feed of infinitesimal amount of methane in pure oxygen at 300 °C and 30 bar, assuming spherical particles and a packing voidage of 0.5

Total flow rate ($ml_n.min^{-1}$)	Minimal bed length (mm) for $\frac{D}{uL} < 0.01$				
	100 µm	50 µm	25 µm	10 µm	5 µm
13	58	57	55	53	52
18	42	41	40	39	38
26	30	29	29	28	27
36	22	21	21	20	20
51	17	15	15	14	14
71	14	11	11	10	10
100	13	9	8	8	7
140	11	7	6	5	5
197	11	6	4	4	4
276	10	6	4	3	3
387	10	5	3	2	2
543	10	5	3	2	1
762	10	5	3	1	1
1069	10	5	3	1	1
1500	10	5	3	1	1

4.2.6 Reactor top section

The purpose of the top section of the reactor are the mixing of the reactant gases prior to entering the reactor main body as well as holding the O-ring seal to isolate the reactant gases inside the reactor quartz liner and the argon make-up gas in the annular space outside of the reactor quartz liner.

Fluorocarbon O-ring sourced from RS components® is used to seal the reactor quartz liner due to its high temperature tolerance (250 °C). Since the reactor quartz liner is 4 mm in diameter, O-ring with a slightly smaller inner diameter of 3.68 mm and a cross sectional diameter of 1.73 mm is used. The grove in which the O-ring sits is dependent only on the O-ring's cross-sectional diameter [70], for an O-ring with a cross-sectional diameter of 1.73 mm, the ideal grove size is 2.5 mm in width and 1.2 mm in depth [70].

The grove for the O-ring in our reactor is made from a standard ¼" tubing cross union from Swagelok® by expanding the bore for one of the ¼" tubing from 6.35 mm to 7 mm and pulling the ¼" tubing out from the end of the fitting by 2.4 mm, forming a grove 2.4 mm in width and 1.5 mm in depth. The modified end of the cross union is placed at the top and connected to a small piece of ¼" tubing 30 mm in length, the tightening of the top nut of this cross union drives this small tubing down which in turn pushes down into the O-ring grove, reducing its width and tightening the O-ring seal as shown in Figure 4.10. The bottom end of the cross union is connected to the reactor body. The two branching ends of the cross union is aligned with the front-back axis of the reactor, with the argon make up gas entering at the back side and a 2.5" 0 – 100 bar pressure gauge connected to the front side. This pressure gauge provides an easily accessible reading of the pressure in the annular space between the reactor shell and quartz liner, and thus the pressure at the end of the catalyst packing.

The reactor quartz liner is extended up until the end of the small ¼" tubing 30 mm in length (these short tubings with nuts and ferrules fitted on both ends are also known as port connectors), making the reactor quartz liner 250 mm in overall length. This is done so the reactor main body, end section, the first cross union of the top end and the 30 mm long port connector can be constructed as one unit at a workbench and install into the reactor system stand as one unit. This subassembly is shown in Figure 4.11.

It is noted from Figure 4.10 there is a gap between the port connector and the outer surface of the O-ring grove at the top end of the O-ring, this may impact the performance of the O-ring seal. Therefore, the O-ring seal was tested by replacing the quartz liner in the reactor with a quartz liner that is sealed at the bottom end. By closing the exit of the reactor (V-501) and opening the reactor feed side to the atmosphere, we can pressurize the annular space around the quartz liner under the O-ring seal whilst the top of the O-ring seal (as well as the inside of the quartz tube) is exposed to the atmosphere. During this test the O-ring seal was found to seal against 12 bar of pressure at its maximum rated temperature of 250 °C for 24 h. This should be fit for use in our reactor system, considering the O-ring is only exposed to a pressure difference equal to the pressure lost across the catalyst bed.

The reactor feed mixer was originally another cross union connected to the top of the subassembly in Figure 4.11. The top of this cross union was connected to the reactor pressure relief valve (V-502 set to open at 50 bar) while the branching ends of the cross union was placed in line with the left-right axis of the reactor. Methane enters the cross union from the left while oxygen, steam and helium enters from the right. Later it was discovered that the

heated line containing oxygen and steam under high pressures was extremely corrosive to the stainless-steel tubing carrying them and led to the formation of cracks in the tubing.

Thus, a tee union was used in conjunction with a cross union to separate the oxygen feed from the evaporator feed (steam and make-up helium). This setup is illustrated in Figure 4.12 alongside with the open arrangement of the aluminium heating blocks.

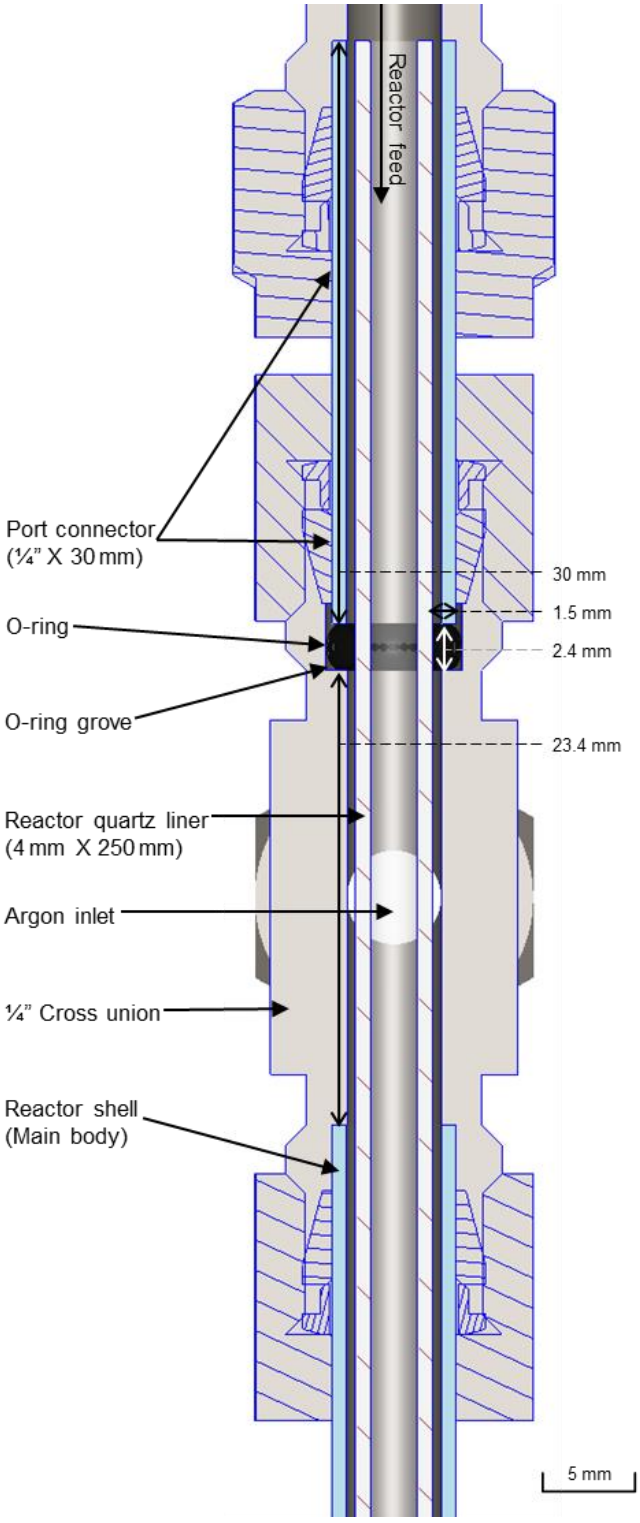

Figure 4.10: Cross section view of reactor top section showing the first cross union and O-ring seal

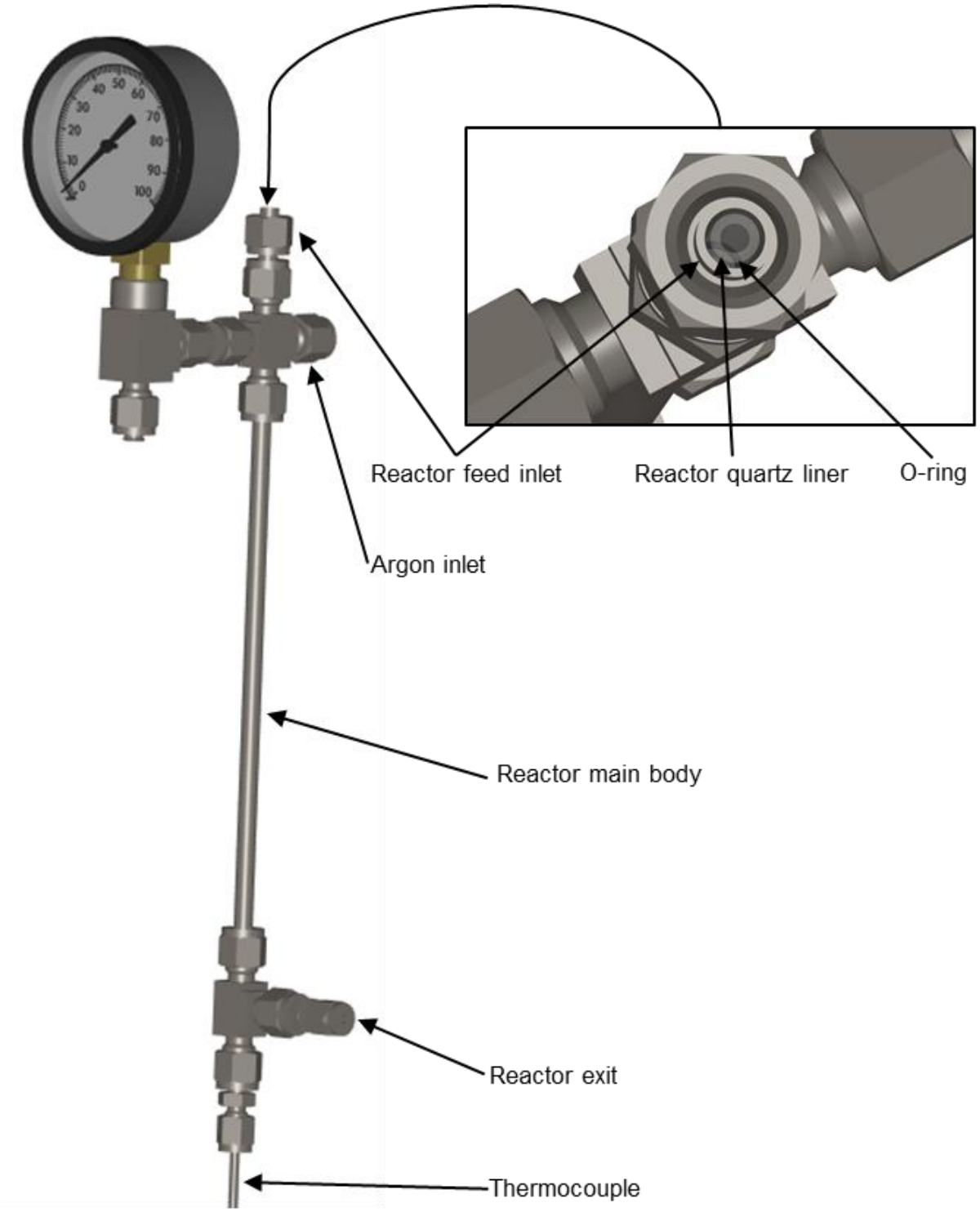

Figure 4.11: 3D model of removeable subassembly of R-501

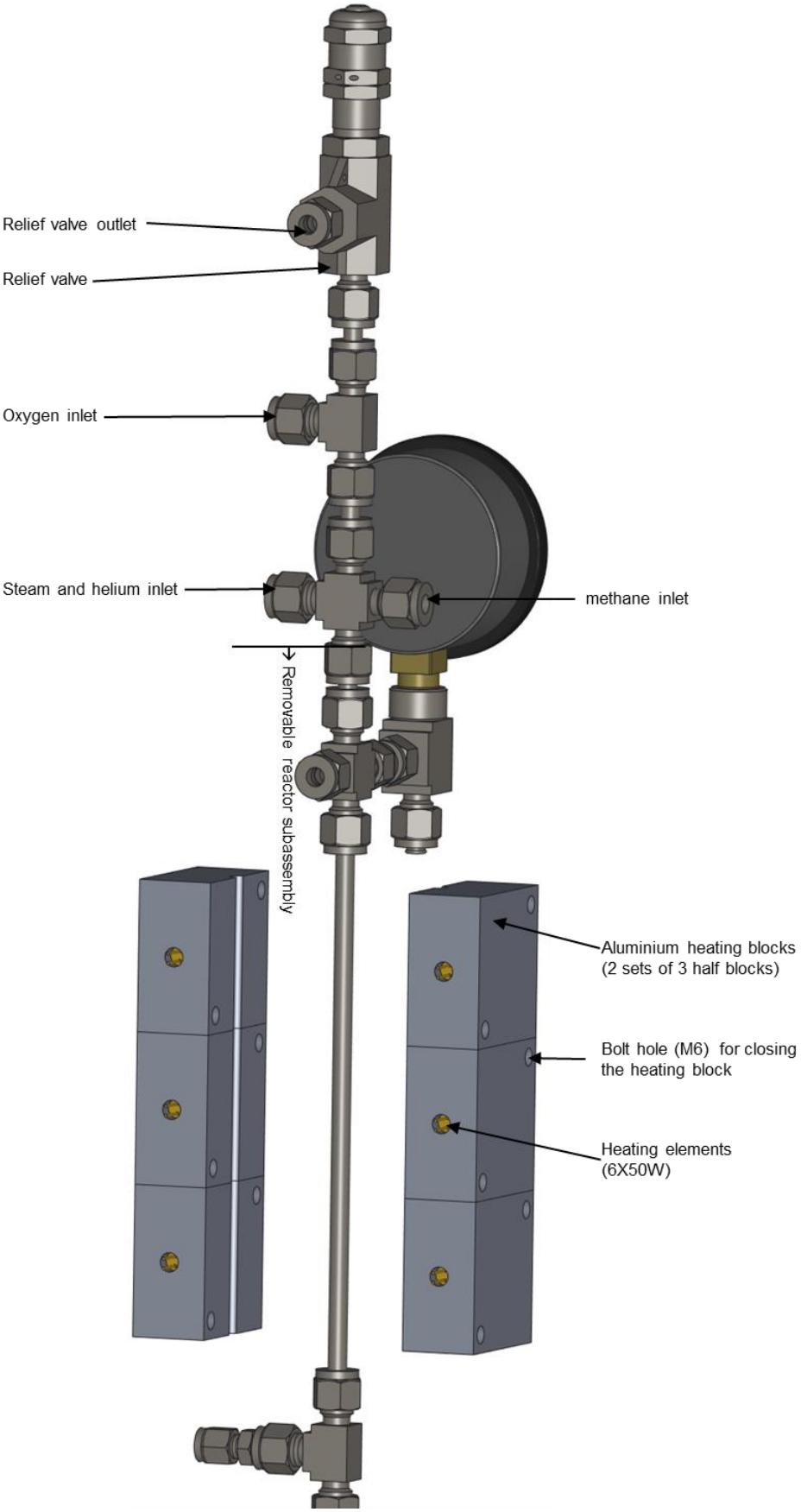

Figure 4.12: 3D model of R-501 with annotation for reactor top section and heating block arrangement (reactor bottom section partial omitted)

4.2.7 Reactor bottom section

The main purpose of the bottom section of the reactor is to pressure seal the thermocouple. In most packed bed reactors in our laboratory, this is either done using a movable thermocouple (1.5 mm in diameter) inside a stainless-steel thermowell welded into the reactor or using a fixed thermocouple (1.5 mm in diameter) fitted into the reactor through a standard 1/16" Swagelok® tube fitting. These techniques cannot work in our reactor due to the small size of the reactor and the thermocouple (2.4 mm and 0.5 mm respectively in diameter) and the need for a quartz sheath over the thermocouple.

To achieve pressure seal of the thermocouple, the thin thermocouple (0.5 mm in diameter) is placed inside a ⅛" stainless steel tubing and fitted to the bottom of the reactor via a tee union using Swagelok® tube fittings, shown in Figure 4.14. The pressure seal is formed at the far end of this ⅛" tubing using solder over the phosphoric acid treated stainless steel surfaces of the tubing and thermocouple. Since a solder seal is temperature sensitive it is moved as far away from the hot reactor as possible by using a long thermocouple (500 mm in length). The thermocouple must extend out of the ⅛" stainless steel tubing for 107 mm to reach the bottom of the catalyst packing. The top 100 mm of the exposed thermocouple under the catalyst bed is quartz sheathed, while the last 7 mm is left exposed due to the lack of clearance inside the ¼" to ⅛" reducer. Since the thermocouple is 500 mm in length overall, the length of the ⅛" stainless steel cover for the thermocouple outside of the reactor is therefore 393 mm. The stainless-steel cover for the thermocouple is fixed to the thermocouple body mechanically with locking nuts and welded reinforcing bars shown in Figure 4.13, which allows the solder joint to not be subjected to mechanical stress.

It would be ideal if the reactor quartz liner can extend all the way to the branching point of the tee union, however during the construction of the reactor, it was extremely difficult to extend this liner past the ferrule at the end of the reactor main body and it often led to breakage of the quartz liner at this point. Thus, it was decided that the reactor quartz liner should end here, 6mm short from the end of the reactor stainless steel shell.

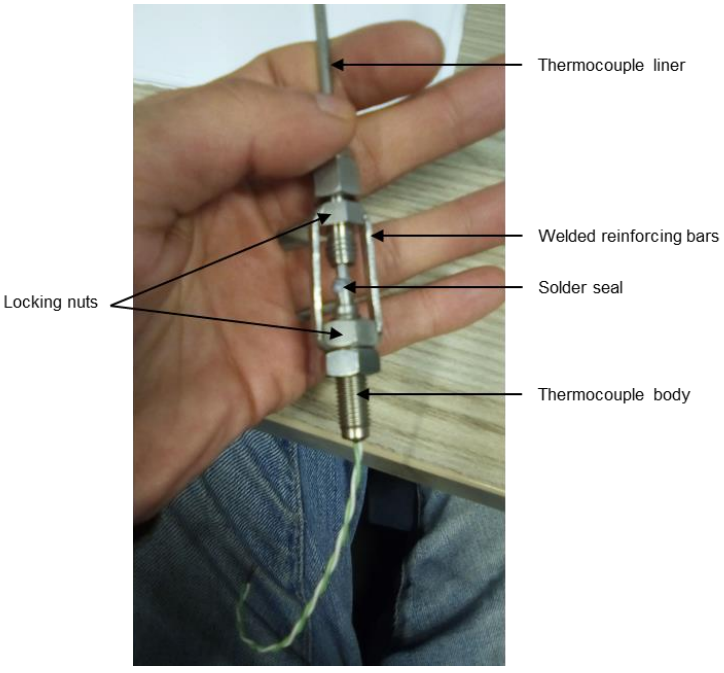

Figure 4.13: Mechanical reinforcement for fixing thermocouple body to its stainless-steel liner

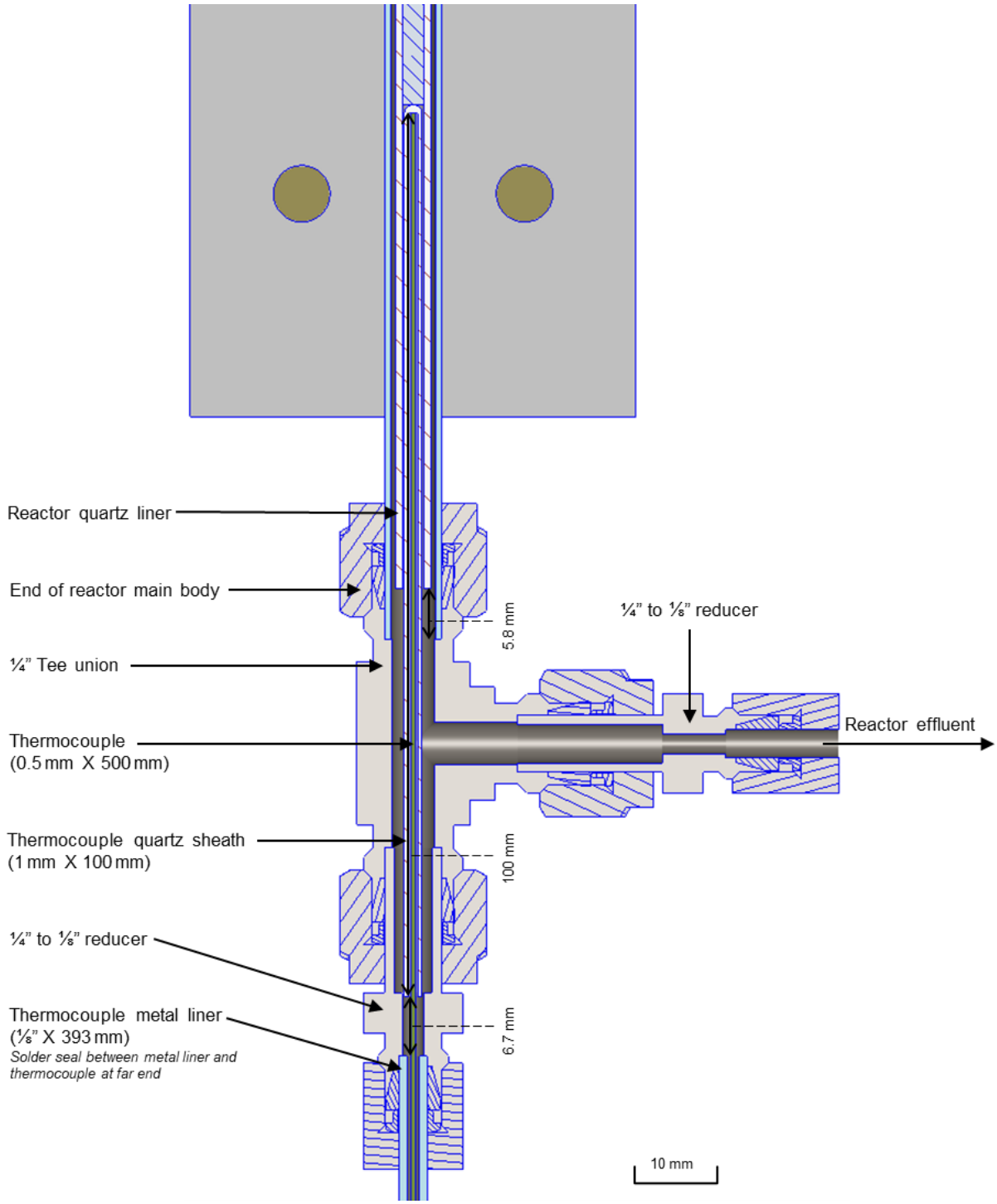

Figure 4.14: Cross section view of reactor bottom section

4.2.8 Overview of packed bed reactor

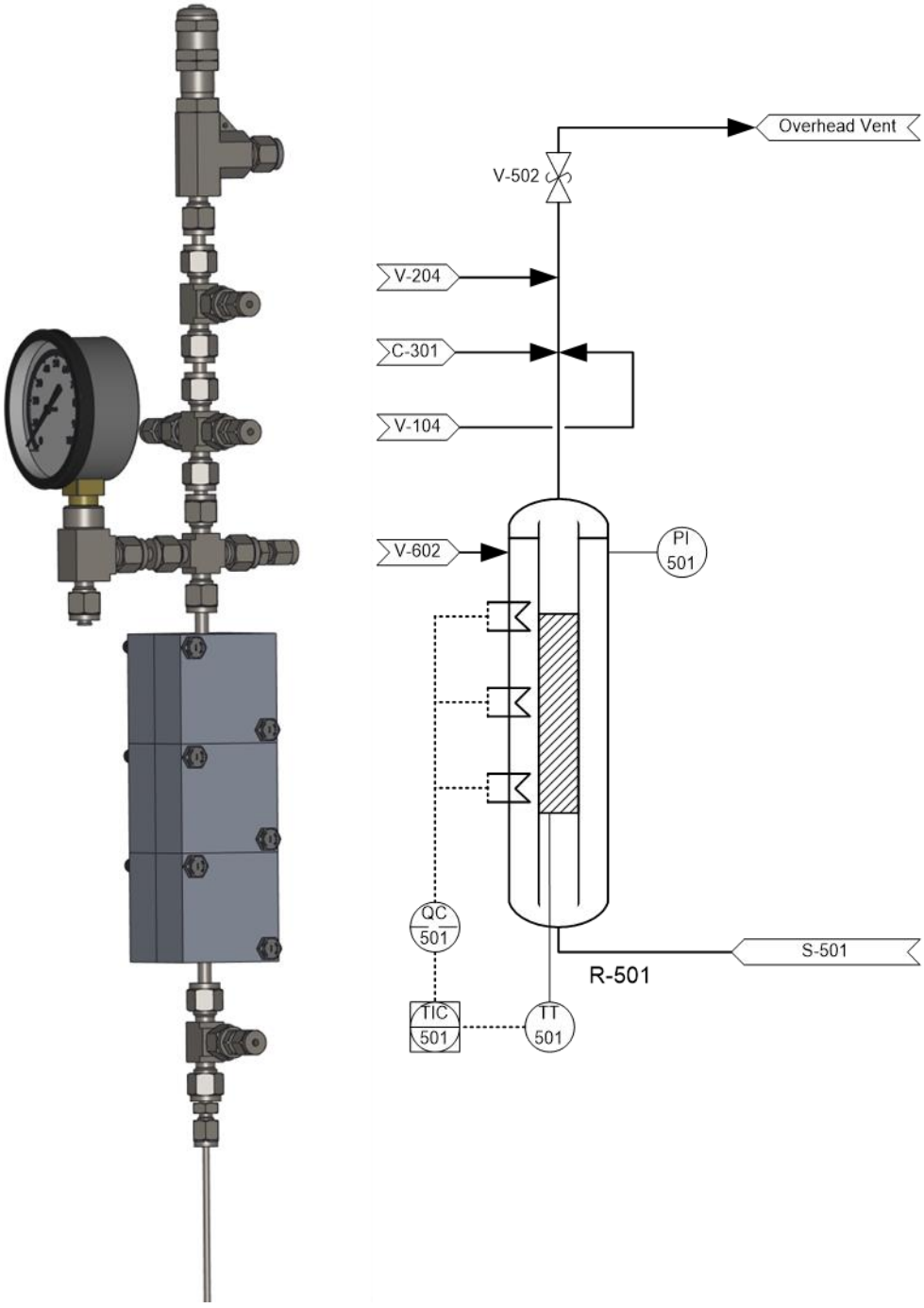

Figure 4.15: 3D model and revised schematic of catalytic packed bed reactor

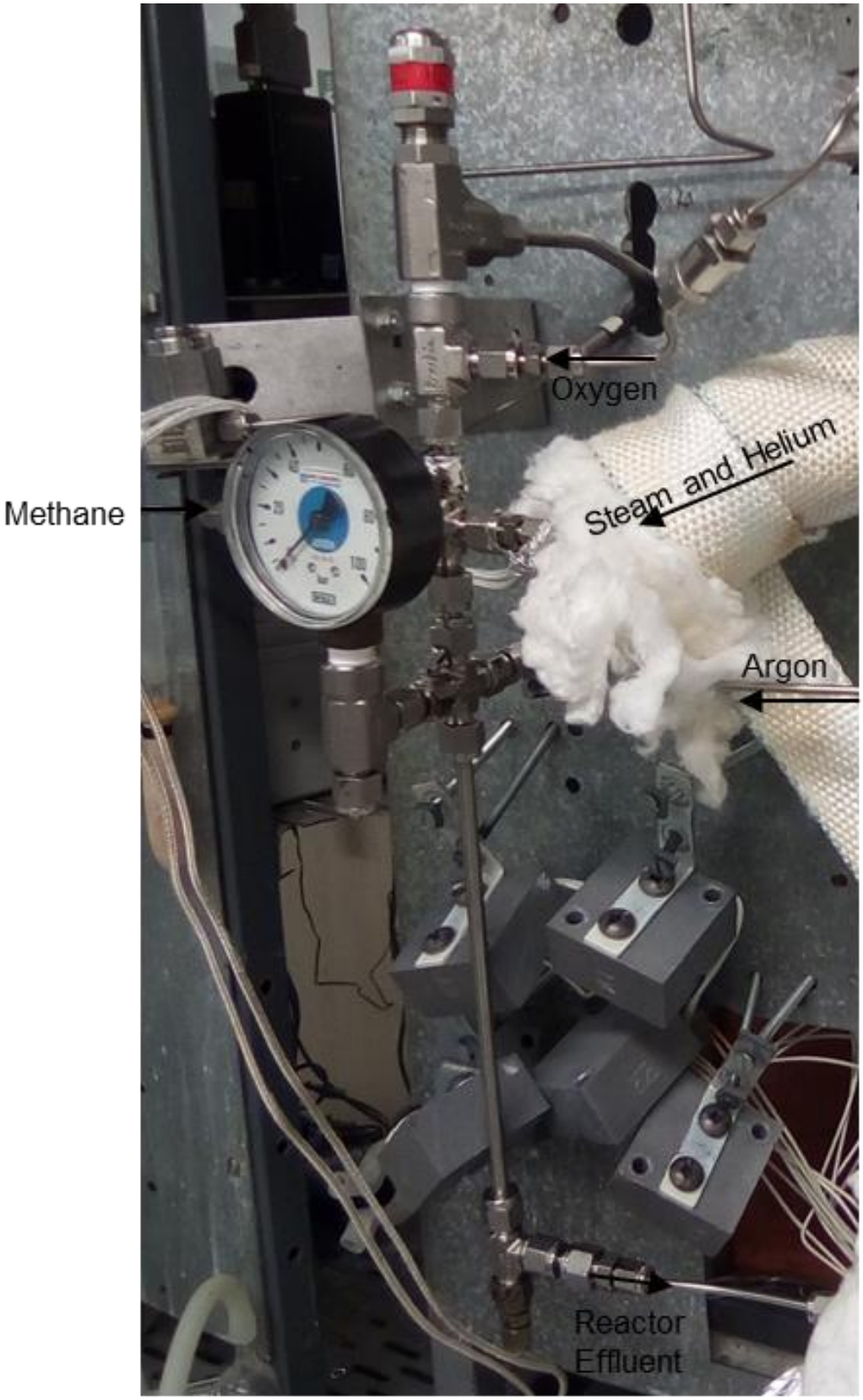

Figure 4.16: Photograph of the catalytic reactor with the aluminium heating blocks detached

Table 4.5: List of materials for removeable subassembly of the catalytic packed bed reactor and its heating block, these components are subjected to wear and tear during reactor changes

Name	Dimension	Supplier	Catalogue Code	Quantity
Clear Suprasil 310 quartz tubing	OD 4 mm, ID 2.4 mm, L 250 mm	Friedrich & Dimmock, Inc.	HS 02408	1
	OD 2 mm, ID 1 mm, L 100 mm		HS 01205	1
Fluorocarbon Elastomer O-Ring	OD 7.14 mm, ID 3.68 mm	RS - Components	128-990	1
Stainless-steel probe K type thermocouple	OD 0.5 mm, L 500 mm		444-1269	1
50 W, 220 V Cartridge heater	OD ¼", L 1.5"		860-6814	6
SS316L Tee union	Connects ¼" tubings	Swagelok	SS-400-3	1
	Connects ¼" tubing to ¼" male NPT		SS-400-3-4TFT	1
SS316L Cross union	Connects ¼" tubings (¼" bore drilled out to 7 mm on one end)		SS-400-4	1
SS316L Reducers	Connects ⅛" tubing to		SS-200-R-4	3
SS316L Plug	Blocks ¼" fitting		SS-400-P	1
SS316L Tubing	OD ¼", WT 0.028", L 35 mm		SS-T4-S-028-6ME	1
	OD ¼", WT 0.028", L 30 mm			1
	OD ¼", WT 0.028", L 200 mm			1
	OD ⅛", WT 0.035", L 393 mm		SS-T2-S-035-6ME	1
SS316L Nut, Front Ferrule and Back Ferrule	For ¼" OD tubing		SS-402-1 SS-403-1 SS-404-1	9
	For ⅛" OD tubing		SS-202-1 SS-203-1 SS-204-1	3
Analogue Pressure gauge (1 - 100 bar)	¼" male NPT thread	Salvaged from old reactor stand		1
Fasteners (Bolt, Nut and 2 split washers)	M6	Local hardware store		6
Machined aluminium block	50 mm X 50 mm X 25 mm blocks with correct holes and half holes bored out	Non-Ferrous Metals		6

4.3 Water evaporator (C-301)

4.3.1 Evaporator main body

The water evaporator (C-301) is built using stainless-steel tubing ¼" in outer diameter with a wall thickness of 0.028" as the catalytic packed bed reactor. The length of the evaporator is slightly shorter than the reactor main body at 150 mm instead of 200 mm. The evaporator is packed with silicon carbide (SiC) packing with an average diameter of 600 µm.

The smooth evaporation of water inside the evaporator is important for the steady-state operation of the reactor as the water pump (P-301) is a positive displacement pump and thus the liquid water flow into the evaporator will be pulsed in nature. Thus, it is desirable to have a buffer zone with liquid water present at the top of the evaporator. This is achieved by not heating the top of the evaporator, allowing the evaporation of water to take place in the middle of the packing in the evaporator. Instead of using aluminium heating blocks as in the reactor, the evaporator is wrapped in multiple layers of heavy-duty aluminium foil and then covered with nichrome heating wires, controlled by one of the Gefran PID controllers from the existing temperature control box. The thermocouple of this control loop is placed 50 mm from the bottom of the evaporator. Figure 4.17 illustrates the cross section of the evaporator main body.

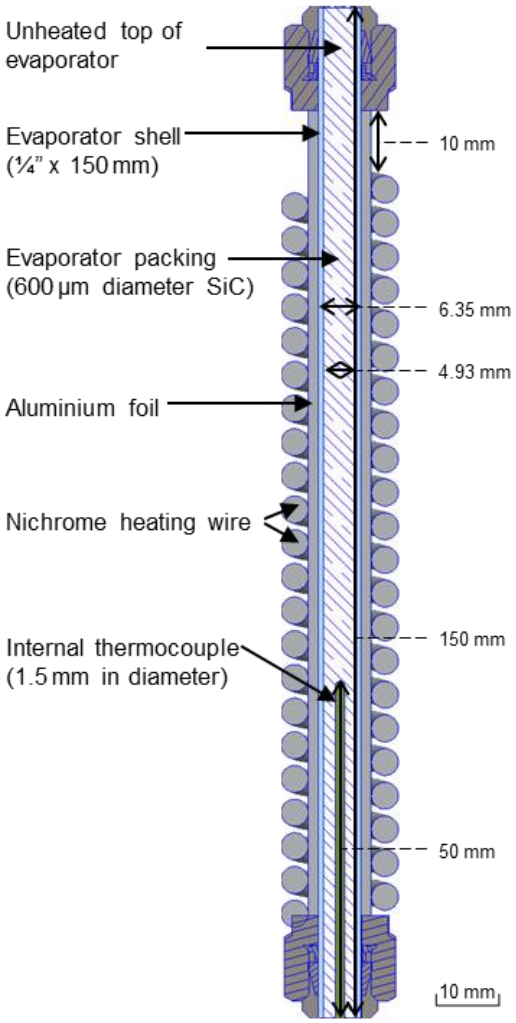

Figure 4.17: Cross section view of evaporator main body

4.3.2 Evaporator top section

The top section of the evaporator is built similarly to the top section of the reactor using a ¼" cross union. Helium make-up gas enters the left side of the cross union through a 60 mm ¼" port connector. The port connector is anchored to the reactor stand with a bracket, identical that used at the bottom of the evaporator. These two brackets secure the entire evaporator assembly to the reactor stand. A 0 - 100 bar pressure gauge and a relief valve (V-301) set to 50 bar is connected to the right side of the cross-union via a tee union (see Figure 4.18). Liquid water is fed to the top of the cross union via a ¼" to ⅛" reducer through ⅛" tubing. The bore of the reducer was expanded to 4 mm in order to extend the feed tube of water 60 mm past the reducer to make contact with the top of the evaporator packing. This set-up allows the liquid water to be swept into the packing by the helium gas flowing around it when it exits the water feed tube, preventing a poorly mixed biphasic mixture that would otherwise exist in the ¼" cross union if the water feed tube was not extended.

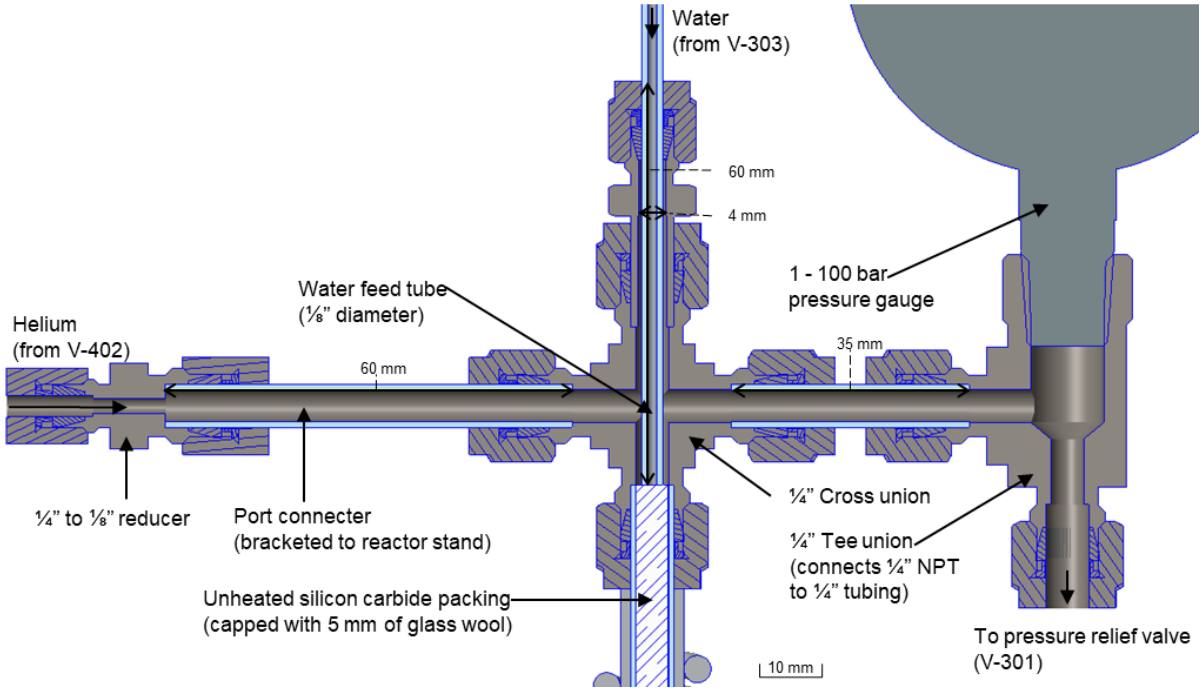

Figure 4.18: Cross section view of evaporator top section

4.3.3 Evaporator bottom section

The main purpose of the evaporator bottom section is identical to that of the reactor end section, i.e. providing a pressure seal for the internal thermocouple inside the evaporator. Since no reaction takes place in the evaporator, a stainless-steel thermocouple can be inserted directly in the evaporator. This was done by fixing a thermocouple 1.5 mm in diameter through a standard 1/16" Swagelok® tube fitting, attached to the bottom of the evaporator through a tee union (packed with glass wool to hold the silicon carbide packing in place) as shown in Figure 4.19. The evaporator effluent (steam and helium) exits through the side of the tee union via a port connector before being reduced to 1/8" tubing. This port connector is anchored to the reactor stand with brackets to provide structural support for the evaporator. The aluminium foil and heating wire cover of the evaporator main body is present around the entire end section of the evaporator but is omitted in Figure 4.19 for clarity.

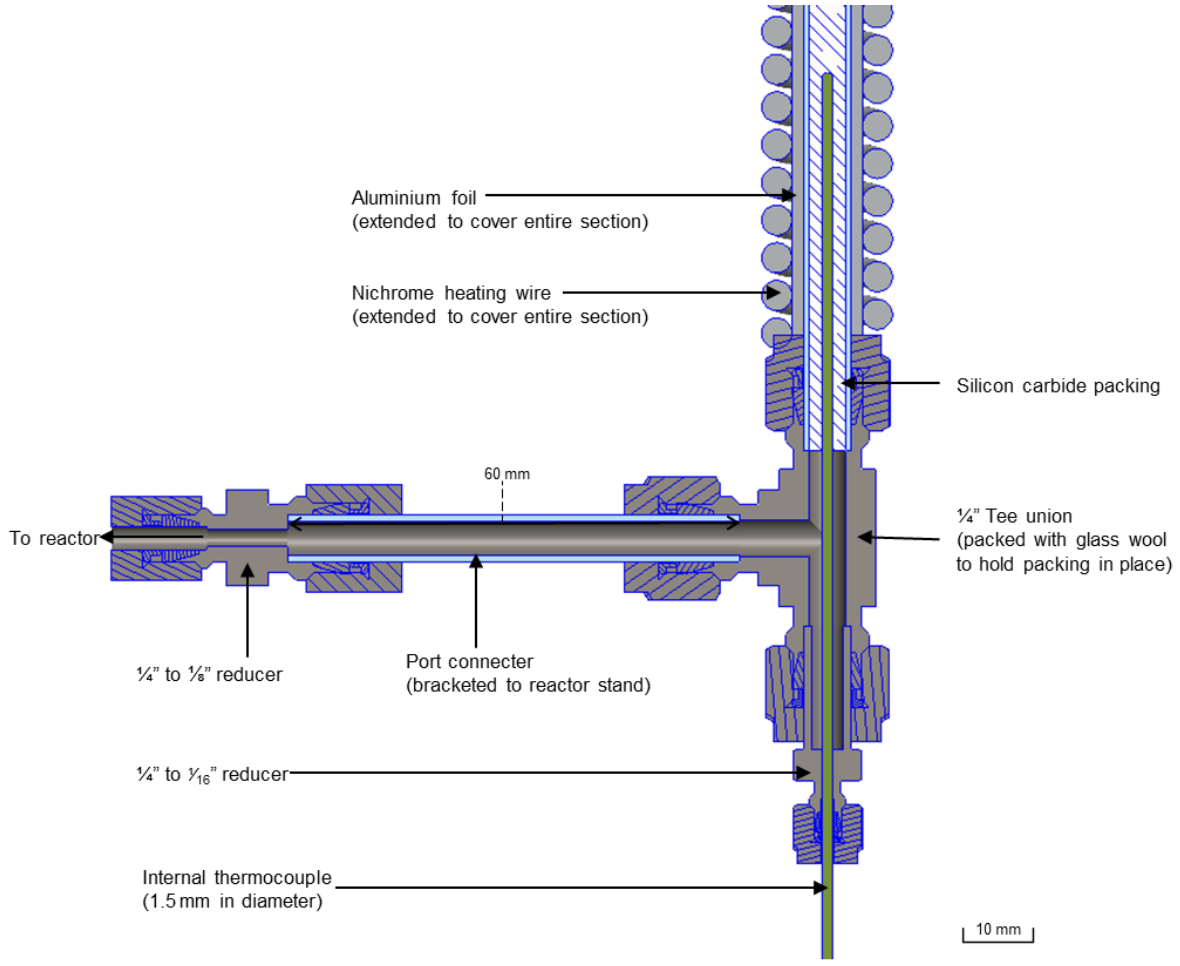

Figure 4.19: Cross section view of evaporator bottom section, foil and heating wire from evaporator main body extends to cover the tee union, port connector and ¼" to ⅛" reducer

4.3.4 Overview of water evaporator

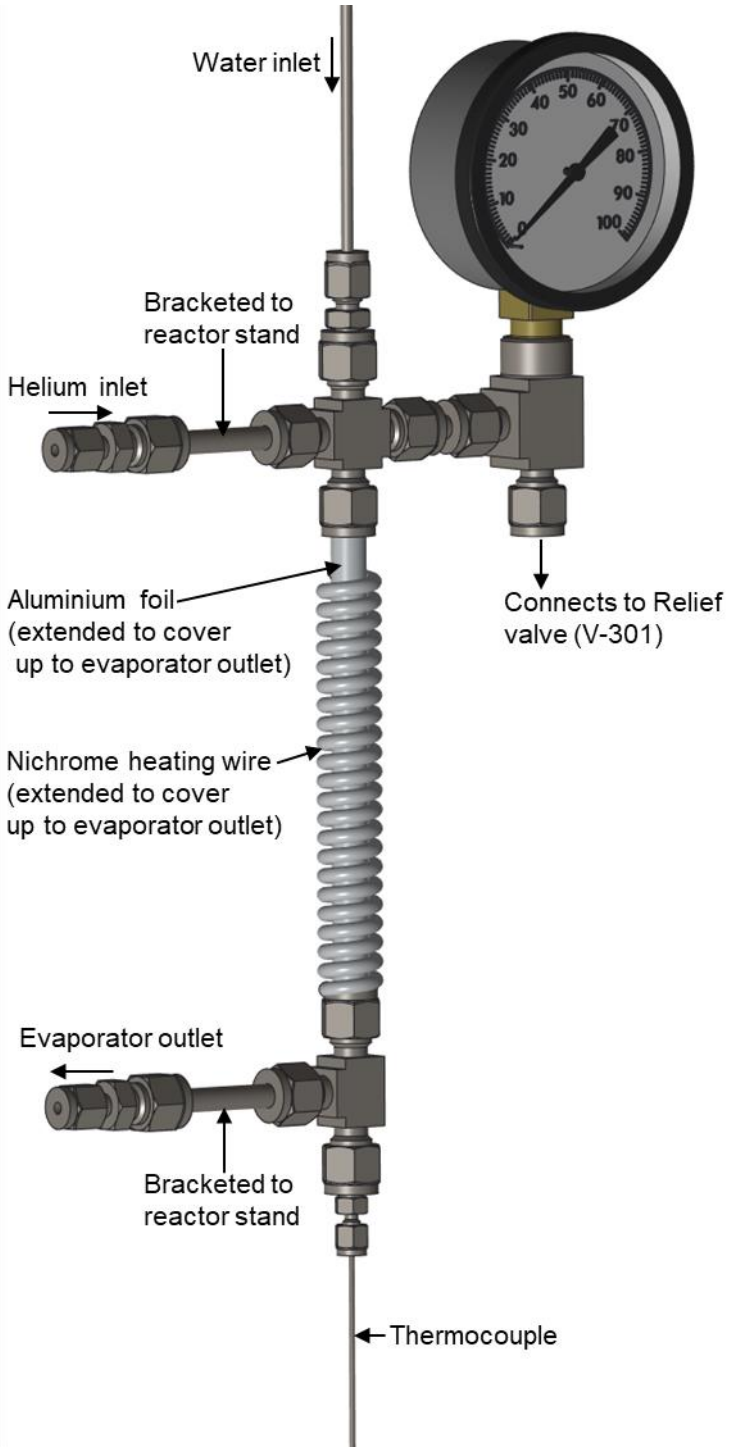

Figure 4.20: 3D model of water evaporator

Figure 4.21: Photograph of water evaporator with insulation in place

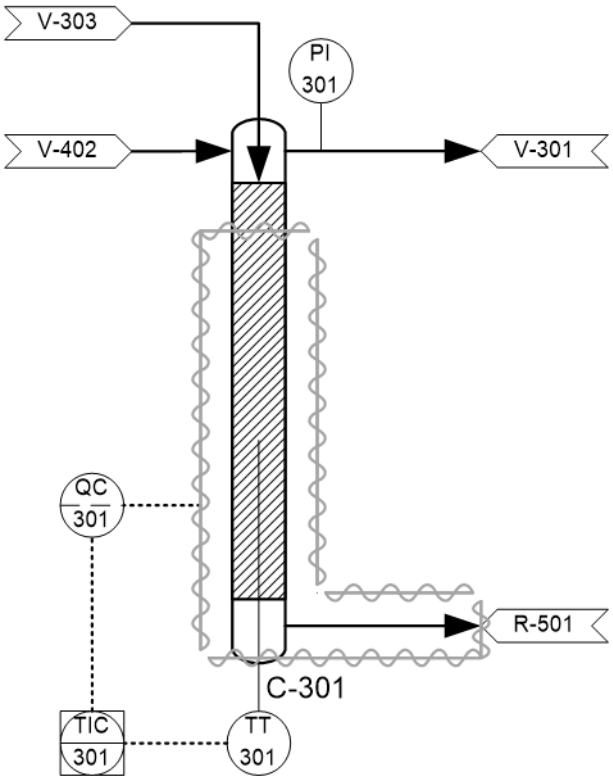

Figure 4.22: Revised schematic of water evaporator, grey lines indicate heating wire

4.4 Gas Chromatograph system

4.4.1 Gas chromatography column and detector

The gas chromatograph (Agilent 6890N) must accurately analysis the product from the direct methane to methanol reactor system to quantify the performance of our platinum-based catalysts in the direct methane to methanol conversion reaction. A gas chromatograph system operates via the separation of a complex mixture of gases through a gas chromatography column coated or packed with a stationary phase. The mixture of gas to be separated is introduced into this column via a carrier gas, which forms the mobile phase of the column. Since different compounds will have different affinity to the stationary phase in the column, they will be retained by the stationary phase to a varying degree and exit the column at different times. Lastly, the separated compounds in the starting mixture is quantified in a detector at the end of the column.

The two detectors present in our gas chromatograph system are the thermal conductivity detector (TCD) and the flame ionization detector (FID), their typical performance and usage is tabulated in Table 4.6.

Table 4.6: Summary of thermal conductivity detector and flame ionization detector [71]

Type	Mechanism of detection	Detectable sample types	Detection limits	Linear dynamic range [a]
Thermal conductivity detector	Measures changes in heat conduction between the sample gas and a reference gas	Universal detector: can detect any sample that is different from the reference gas used	10 ppm	30 dB to 40 dB
Flame ionization detector	Measures current from pyrolysis of samples in a hydrogen flame	Hydrocarbons	10 ppb	60 dB to 70 dB

a. The range where the detector responds linearly to change in sample quantity:

$$\frac{Maximum\ qunatity\ to\ have\ linear\ response}{Minimum\ detectable\ quantity} = 10^{0.1 \times linear\ range\ in\ dB}$$

Three types gas chromatography set-ups are prominent from past experimental set-up on direct methane to methanol conversion in flow reactor system: dual GC, single GC, and GCMS.

The GCMS system used by Pappas et al. [32], Le et al. [31] and Dyballa et al. [30] uses a mass spectrometer (MS) as a detector, which can both quantify and identify (statistically by matching fragmentation patterns with a database) products from their reactors. This analysis technique is not available to us as our 6890N GC does not have a MS detector.

The dual GC system used by Foulds et al. [26], Gesser et al. [27], Zhang et al. [1] and Parfenov et al. [59] uses two separate GC columns and detectors for product analysis where the permanent gases are separated in one GC column while the condensable products are separated

in another GC column. These systems use TCD detectors which is lacking in linear response range to analyse products at low yields (see Table 4.6).

This inherent problem in dynamic range of the TCD can be solved by the single GC system used by Burch et al. [25] where all the carbon containing products is analysed using a single GC with an FID by adding a methanizer. This technique both simplifies analysis by avoiding the two-phase analysis of the reaction product as well as increasing sensitivity by using an FID instead of a TCD. Thus, a single GC-FID system with a methanizer was chosen as our product analysis set-up.

A single HP-PLOT Q PT capillary column with a polystyrene-divinylbenzene stationary phase (0.32 mm diameter, 30 m length, 20 µm stationary phase film thickness) from Agilent Technologies® was purchased and used as the column in our GC. A single HP-PLOT Q PT column was shown to separate carbon monoxide, carbon dioxide, methane, methanol and an array of simple carbon compounds [72].

The FID detector is already built into the GC whilst the methanizer had to be added in. The methanizer was first built according to instructions provided in Maduskar et al. [73]. Maduskar et al. [73] demonstrated the feasibility of an oxidizer – methanizer system in GC-FID analysis where carbon containing analytes separated in a GC column is first oxidized to CO_2 over a palladium catalyst and then reduced to methane over a nickel catalyst before entering the FID. Such system was shown to allow the calibration free analysis of all carbon containing analytes in a GC-FID, whereas a FID only system displayed no response to carbon dioxide and very little response to 2-methylfuran; the addition of a oxidizer – methanizer system before the FID enabled all analytes tested to be picked up by the FID with the same response as methane, within experimental error [73].

However, our constructed methanizer was not able to generate reproducible results as claimed by Maduskar et al. [73] and a commercially available oxidizer-methanizer was purchased from Activated Research Company® and installed in our GC instead as a replacement for the existing TCD. This oxidizer-methanizer system is named the Polyarc™ reactor and is an integrated microreactor system developed from the oxidizer-methanizer system from Maduskar et al. [73]. The Polyarc™ reactor is designed to enable calibration free analysis of all carbon containing compounds via a FID by first oxidizing the organic samples eluting out of a GC column with air to carbon dioxide and then reducing the carbon dioxide with hydrogen to methane before passing it onto the FID [74]. The Polyarc™ reactor was found to perform as designed and will be discussed in the section on gas chromatography method development.

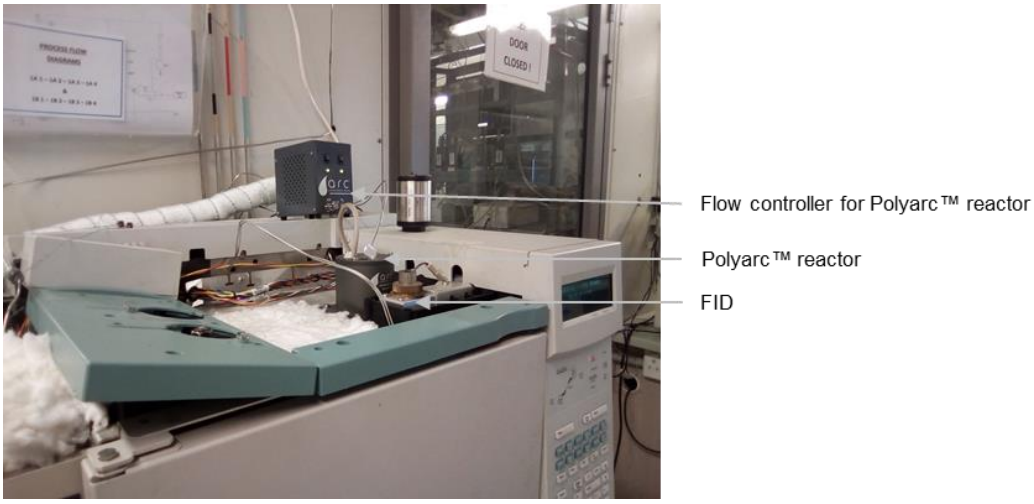

Figure 4.23: Polyarc™ reactor from activated research company installed in the Agilent 6890N GC

4.4.2 Product sampling

Initially, after the Polyarc™ reactor was installed in the GC, products from the direct methane to methanol reactor system was sampled and introduced into the GC using a gas syringe. However, the results from these analyses included many unidentified peaks. It was later realized that due to the addition of the Polyarc™ reactor the carbon containing compounds in air (CO_2 and organic contaminants) was being picked up by the GC-FID. Small amounts of air somehow entered the GC-FID system either during the sampling of the reactor products, the transfer of the sample from the reactor hood to the analysis room next door or during the offline injection into the GC itself. Thus, the GC was moved to outside of the reactor hood and permanently connected to the reactor system to enable online sampling.

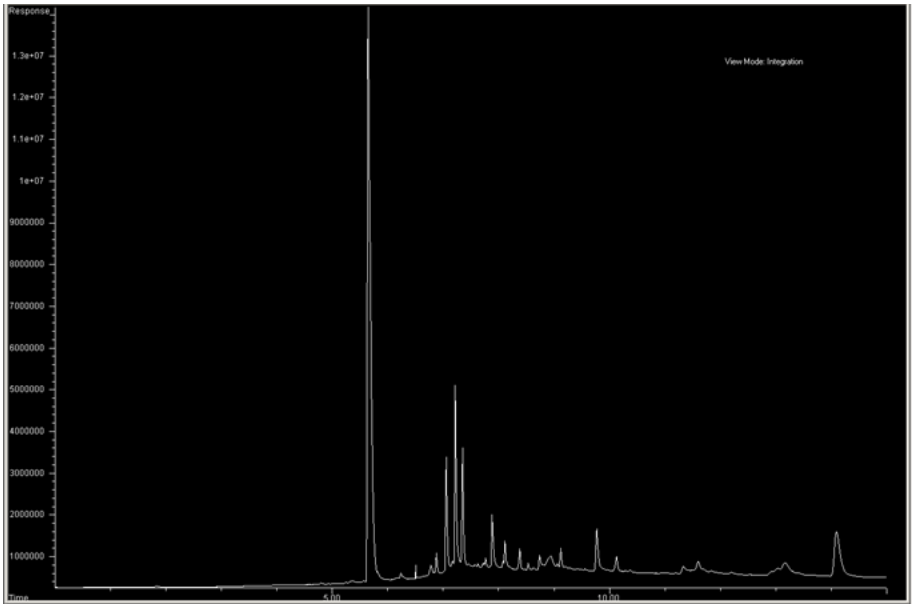

Figure 4.24: Test chromatogram of an air injection in the GC-FID system equipped with Polyarc™ reactor, showing the various detectable contaminants present in air

A 6-way pneumatically actuated sampling valve from Vici ® already present on the HP6890N GC was used to enable online sampling. Its principle of operation is shown in Figure 4.25. In the default position of the valve (sampling loop filling), effluent from the reactor system is

routed through an 1ml sampling loop wound from 1/16" stainless-steel tubing before vented into the overhead vent and the carrier gas of the GC column is routed directly into the GC column. In order to introduce a sample into the GC, the pneumatically controlled 6-way valve is switched to the other position (sample loop emptying), now the carrier gas is able to flush the reactor effluent still present in the sample loop into the GC column while the reactor effluent is directly routed to the overhead vent.

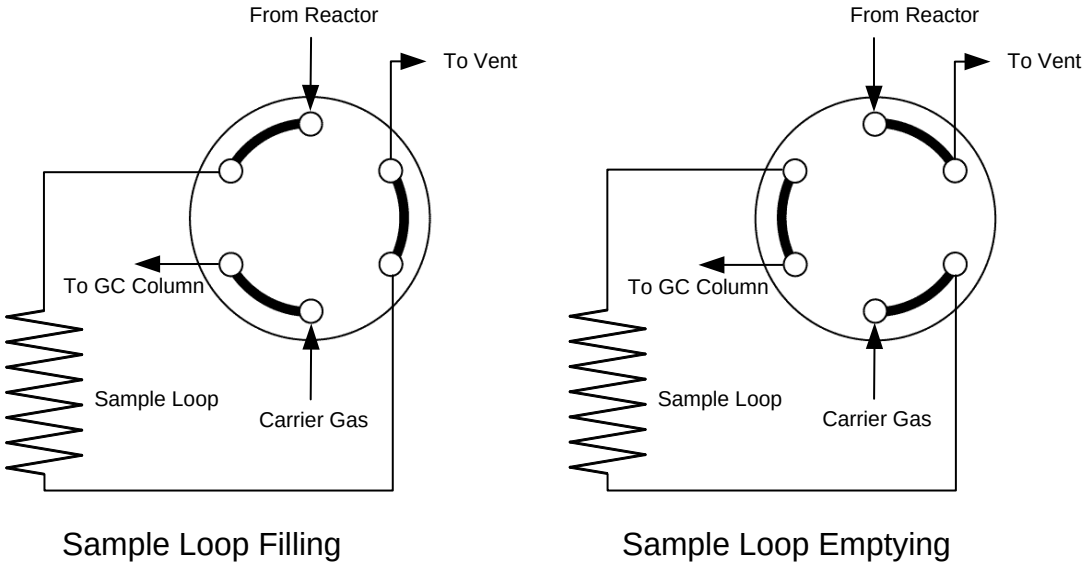

Figure 4.25: Working principle of a 6-way sampling valve in online sampling

During the operation of the reactor system, this sampling valve is left in the sample loop filling position. To take a sample, the valve is switched to the emptying position for 6 seconds at the beginning of the analysis to introduce the sample into the column before being switched back to the filling position.

With online sampling, the reactor effluent is routed through the sampling valve instead of the bubble flow meter (FM-801), thus the liquid product condenser (C-801) is also moved from after the bubble flow meter to after the vent outlet of the 6-way sampling valve instead and renamed to C-701 (see Figure 4.26). The 6-way sampling valve (V-702) together with the sampling loop is fixed into an aluminium block and heated to 100 °C though the Aux 2 heating channel on the HP6890N GC, indicated in Figure 4.26 as TIC-701. As with all heated parts, the aluminium block is insulated with a layer of ceramic fibre.

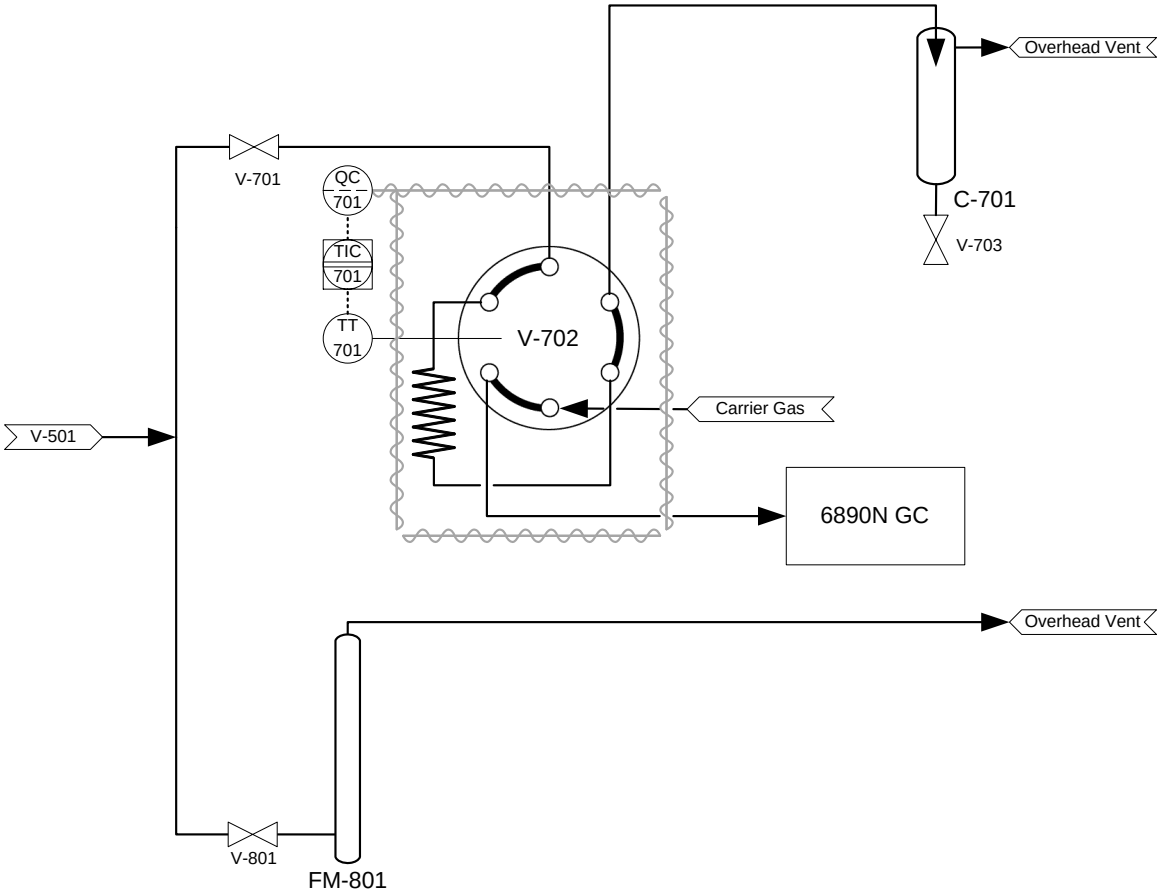

Figure 4.26: Revised flowsheet of sampling and product analysis section, V-702 in sample loop filling position

4.4.3 Gas chromatography method development

A GC method is developed for the HP6890N GC-Polyarc™ reactor-FID system to work with our direct methane to methanol conversion reactor system. This section will go through the various parameters needed during an GC analysis.

4.4.3.1 Valves

The sampling valve V-702 was left in the sample loop filing position by default and switched to the sample loop emptying position at the start of the GC run. It is switched back to the sample loop filling position 6 seconds after the run has started.

4.4.3.2 Inlet split ratio

The HP6890N GC is equipped with a split injector liner, allowing the injected sample to be diluted before entering the column. This is an important parameter as it indirectly controls the amount of sample injected into the column (the amount injected into the injector is fixed by the volume of the sample loop at 1 ml). As shown in Table 4.6, a FID has a linear dynamic range of 6 to 7 orders of magnitude, and the noise floor of our FID is seen to be approximately 1000 signal units; the split ratio of the injector should be set so the signal from the highest peak is less than 10^9 units (1000×10^6). This achieved using a split ratio of 10:1.

The inlet of the GC is also heated to 100 °C to prevent condensation.

4.4.3.3 *Column carrier gas*

A GC column is essentially a separation column, given a fixed column length the degree of separation depends on the number of theoretical plates and hence the height equivalent of the theoretical plates (HETP). This height equivalent of the theoretical plate can be determined from a Golay plot depending on the carrier gas used and the linear velocity of the carrier gas through the column [75]. While nitrogen, helium and hydrogen can be used as the carrier gas with the available instrument gas supplies in our laboratory, hydrogen appears to be the best carrier gas as it enables a relatively short height equivalent of theoretical plate over a large linear velocity range for the carrier gas (see Figure 4.27). Thus, hydrogen was chosen as our carrier gas and used in constant flow mode with a relatively fast carrier gas flow rate of $3ml_n/min$, giving an initial linear velocity of 60 $cm.s^{-1}$ in our capillary column.

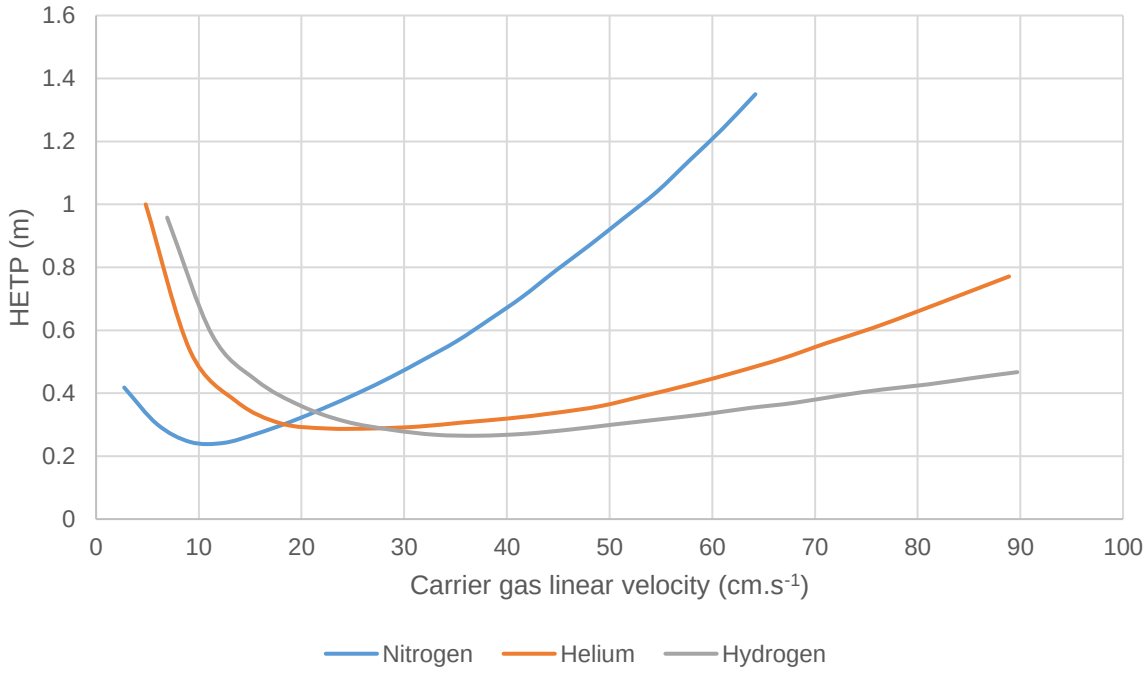

Figure 4.27: Golay plot for a typically capillary GC column [75].

4.4.3.4 *Column temperature program and peak identifications*

In the application note of the HP-PLOT Q PT GC column by Zou (2013), a mixture containing CO, methane, CO_2 and methanol was separated in the column over 18 minutes with the following temperature program in the GC column oven:

32 °C for 5 min

32 °C to 70 °C at 30 $°C.min^{-1}$

70 °C for 5 min

70 °C to 160 °C at 10 $°C.min^{-1}$

With the above temperature program, the author was able to elute the gases (CO, methane, CO_2) out of the column at a retention time of roughly 2.5 min while methanol was eluted out of the column at roughly 15 min. In order to shorten the analysis time, we intend to develop a different temperature program for the GC column oven. The initial temperature was increased from

32 °C to 40 °C due to the hot ambient temperatures in summer in Cape Town, where the temperature frequently exceeds 30 °C. A calibration gas mixture of CO, CH_4 and CO_2 was cleanly separated at 40 °C in just under 2 min (see Figure 4.28). The gases were identified through their peak area ratio as the volume ratio in the calibration gas is known, this will be discussed later during the section on the Polyarc™ reactor.

Beside CO, CH_4 and CO_2, C-1 oxygenates such as methanol, formaldehyde and formic acid can also be produced in the direct conversion of methane to methanol. The CO, CH_4 and CO_2 calibration gas is bubbled through a liquid mixture containing methanol, formaldehyde and formic acid to form a test gas mixture to be separated at an oven temperature of 200 °C. Four peaks were detected in under 2 min. The first peak is assumed to be the unseparated calibration gas (see Figure 4.29), while the next three peaks were identified by injecting the pure liquids, which will be discussed later.

Combining the information from Figure 4.28 and Figure 4.29, the GC column oven was set on a temperature program starting at 40 °C for 2 min to separate CO, CH_4 and CO_2, the oven temperature is then ramped up to 200 °C at a rate of 40 °C.min^{-1} for the separation of the liquids. This produced 6 peaks in under 5 min, shown in Figure 4.30. The single gas peak in Figure 4.29 is separated into three peaks, CO, CH_4 and CO_2.

Later, it was realized that either the fast ramp rate of 40 °C.min^{-1} or the high final column oven temperature of 200 °C was causing excessively column bleed evident by a rising baseline during every run. Hence, the ramp rate was reduced to 20 °C.min^{-1} and the final temperature was reduced to 180 °C. The 6 compounds in the calibration mixture can still be fully separated but the analysis time was increased to 10 min (see Figure 4.31). The computer and software used to control the GC was also changed from EZChrome™ on Windows 98 to the relatively new Agilent Chemstation™ on Windows XP to allow export of chromatogram data via USB drives.

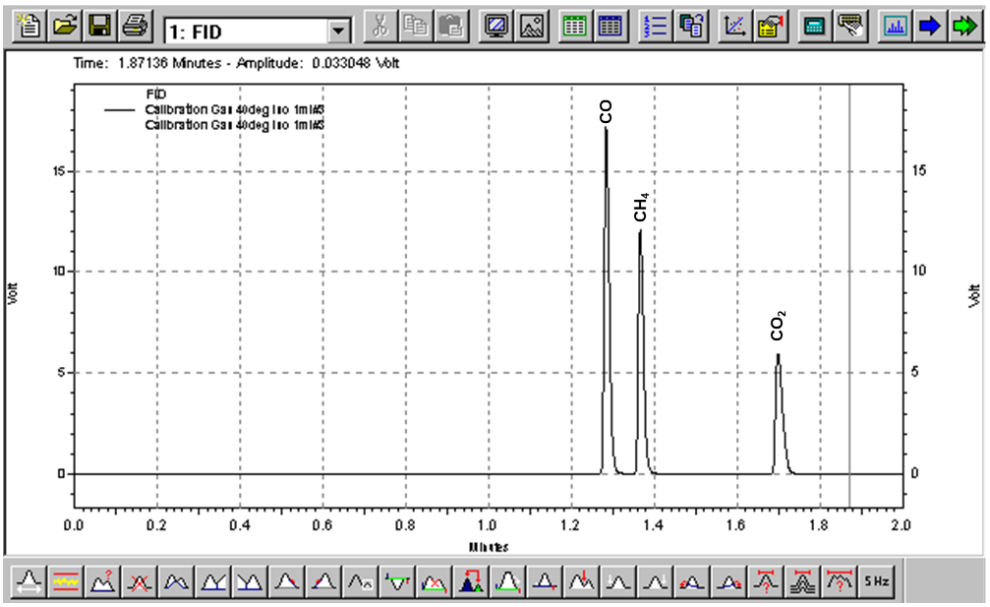

Figure 4.28: Test chromatogram of calibration gas (CO, CH_4 and CO_2), offline injection, separation at 40 °C, carrier gas H_2, constant flow 3 $ml_n.min^{-1}$, Agilent 6890N GC operated with EZChrome™

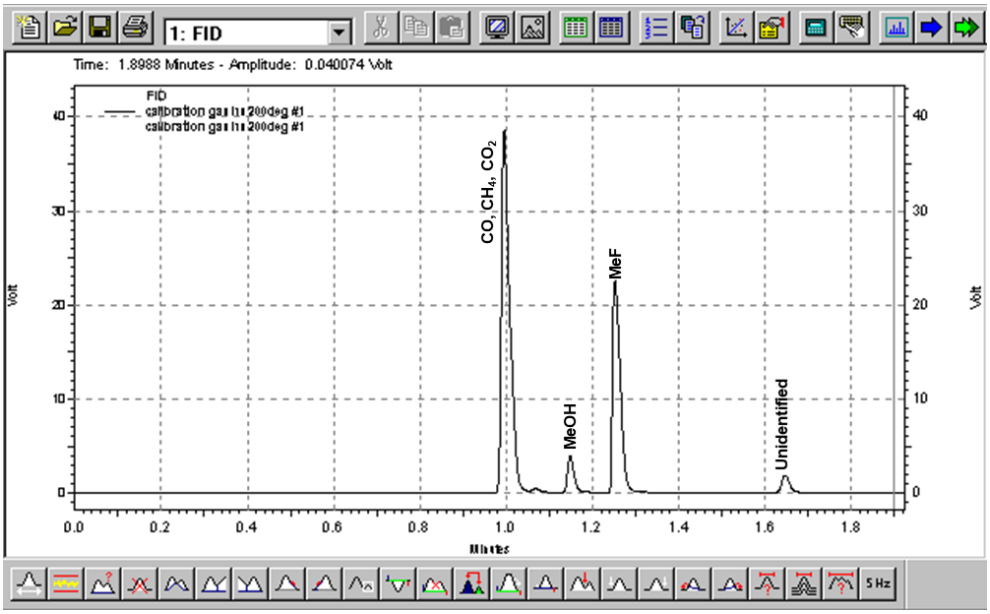

Figure 4.29: Test chromatogram of calibration gas mixture (CO, CH_4 and CO_2 bubbled through methanol, formaldehyde and formic acid), offline injection, separation at 200 °C, carrier gas H_2, constant flow 3 $ml_n.min^{-1}$, Agilent 6890N GC operated with EZChrome™

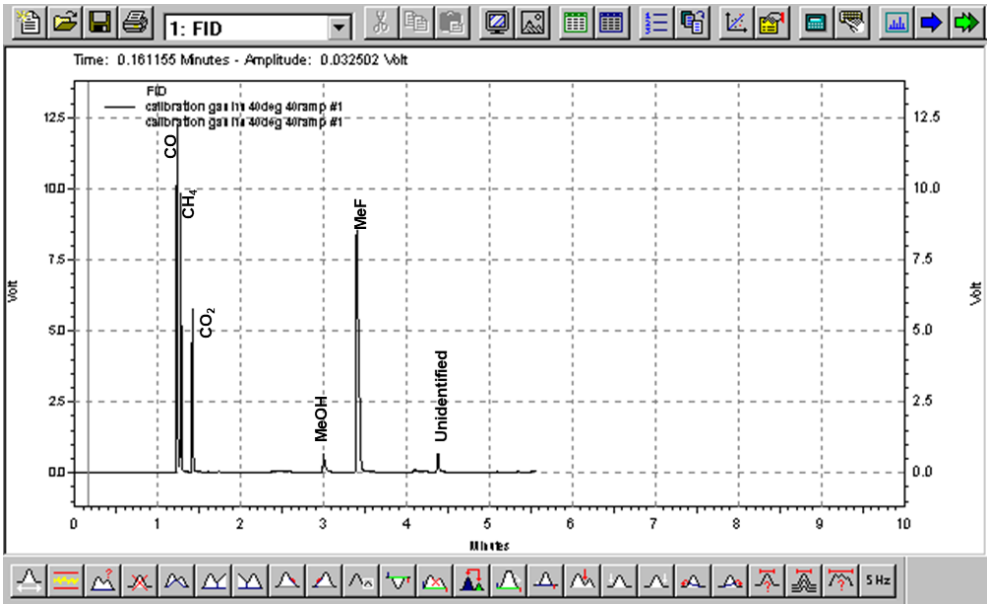

Figure 4.30: Test chromatogram of calibration gas (CO, CH_4 and CO_2 bubbled through methanol, formaldehyde and formic acid), offline injection, separation starting at 40 °C for 2 min followed by 40 °C.min^{-1} ramp to 200 °C, carrier gas H_2, constant flow 3 $ml_n.min^{-1}$, Agilent 6890N GC operated with EZChrome™

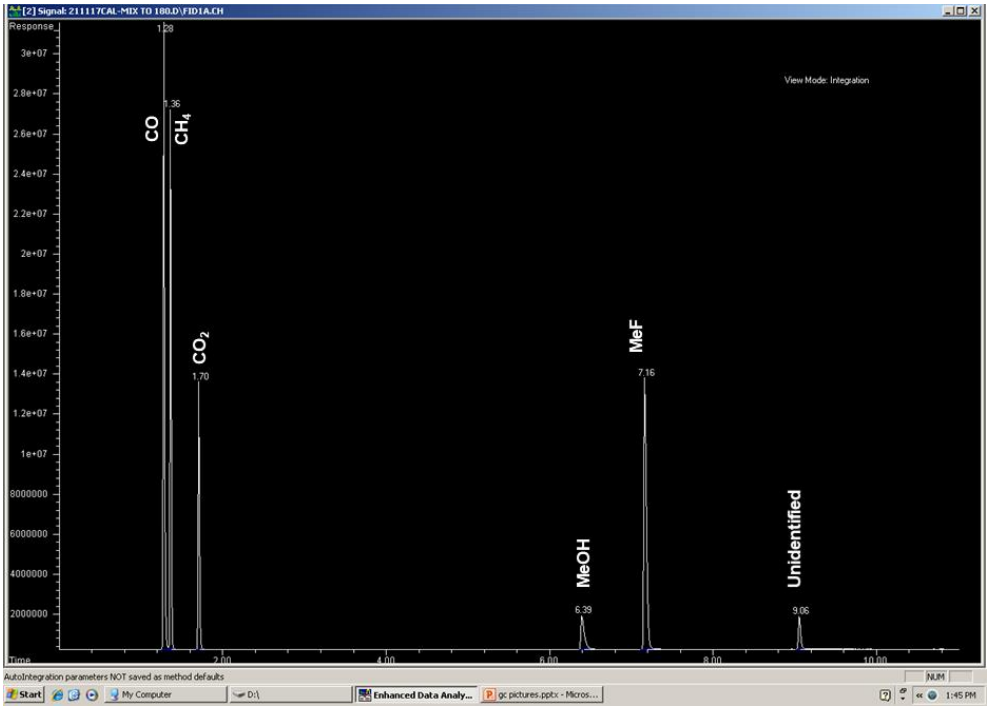

Figure 4.31: Test chromatogram of calibration gas (CO, CH_4 and CO_2 bubbled through methanol, formaldehyde and formic acid), offline injection, separation starting at 40 °C for 2 min followed by 20 °C.min^{-1} ramp to 180 °C, carrier gas H_2, constant flow 3 ml_n.min^{-1}, Agilent 6890N GC operated with Agilent Chemstation™

The retention times of the liquids were then identified by injecting the pure liquids with the final temperature program. Methanol's retention time was identified as 6.9 min by evaporating methanol in the reactor system with a calibration gas of CO_2 and ethane as the evaporator make-up gas through online injection (see Figure 4.32). Ethane's retention time was identified as 3.1 min and CO_2 at 2.1 min. The methanol was then spiked by adding in some formic acid and an extra peak at 7.8 min was detected (see Figure 4.33). This was identified as methyl formate formed in the spontaneous reaction between formic acid and methanol.

Formaldehyde with 13 % methanol (added as stabilizer) was injected next through offline injection to produce the chromatogram in Figure 4.34. The major peak at centred at 5.4 min was identified as formaldehyde, the stabilizer methanol identified at 7.0 min and an unknown compound with a retention time of 9.8 min was detected as well. Formic acid was identified last with offline injection and found to have a retention time of 10.9 min (see Figure 4.34). The same unknown compound with the retention time of 9.8 min was detected too alongside a new unidentified compound with a retention time of 12.2 min. The retention times of all the identified compounds are tabulated in Table 4.7. A sample chromatogram from the autocatalytic conversion of methane to methanol is shown in Figure 4.36 along with the peak identifications.

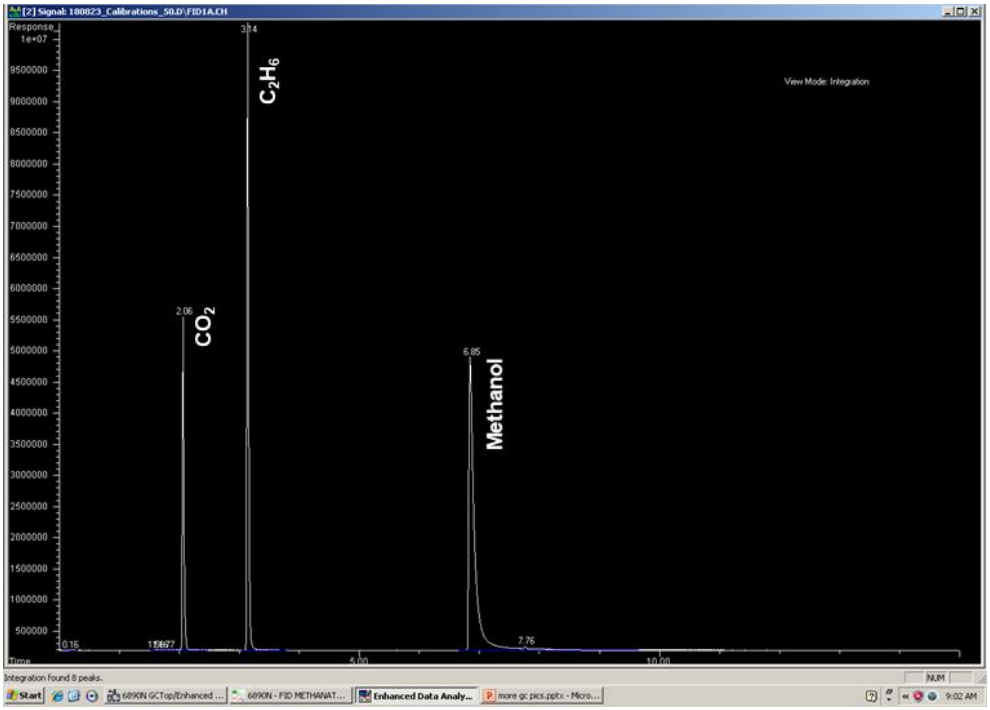

Figure 4.32: Test chromatogram of online injection of CO_2, C_2H_6 and methanol, separation starting at 40 °C for 2 min followed by 20 °C.min^{-1} ramp to 180 °C, carrier gas H_2, constant flow 3ml$_n$.min^{-1}, Agilent 6890N GC operated with Agilent Chemstation™

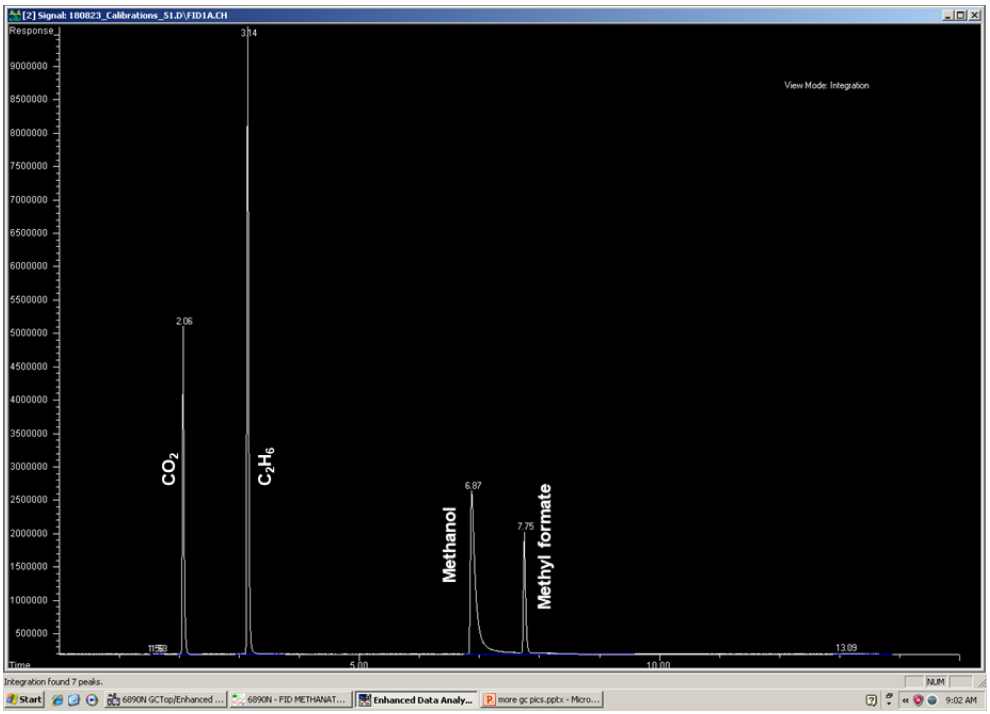

Figure 4.33: Test chromatogram of online injection of CO_2, C_2H_6 and methanol spike with formic acid, separation starting at 40 °C for 2 min followed by 20 °C.min^{-1} ramp to 180 °C, carrier gas H_2, constant flow 3ml$_n$.min^{-1}, Agilent 6890N GC operated with Agilent Chemstation™

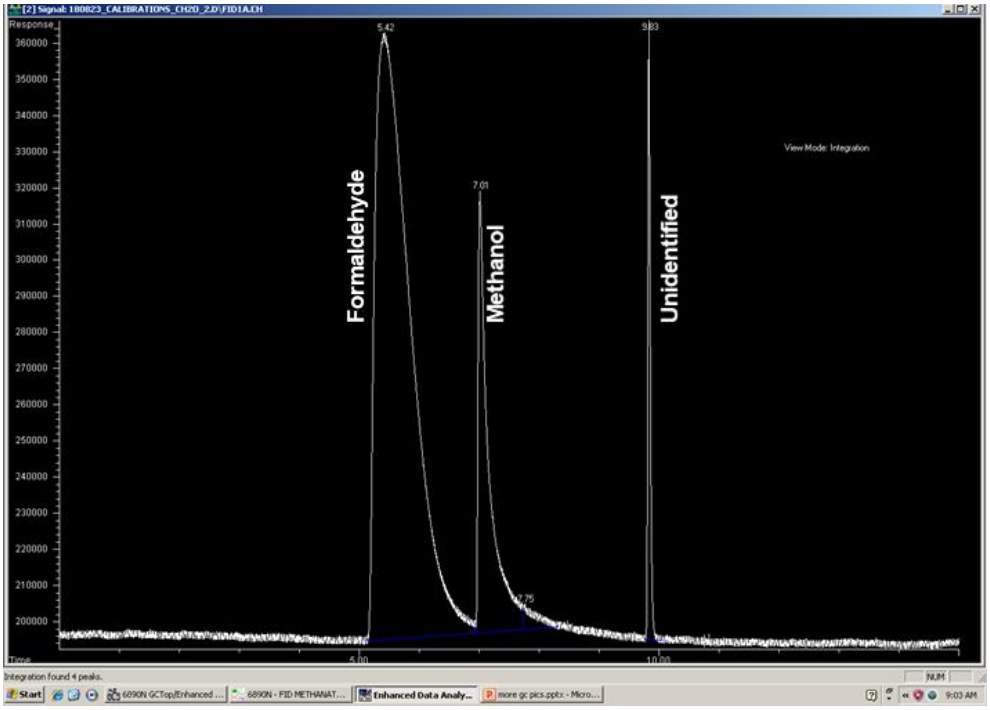

Figure 4.34: Test chromatogram of offline injection of formaldehyde with 13% methanol, separation starting at 40 °C for 2 min followed by 20 °C.min^{-1} ramp to 180 °C, carrier gas H_2, constant flow 3ml$_n$.min^{-1}, Agilent 6890N GC operated with Agilent Chemstation™

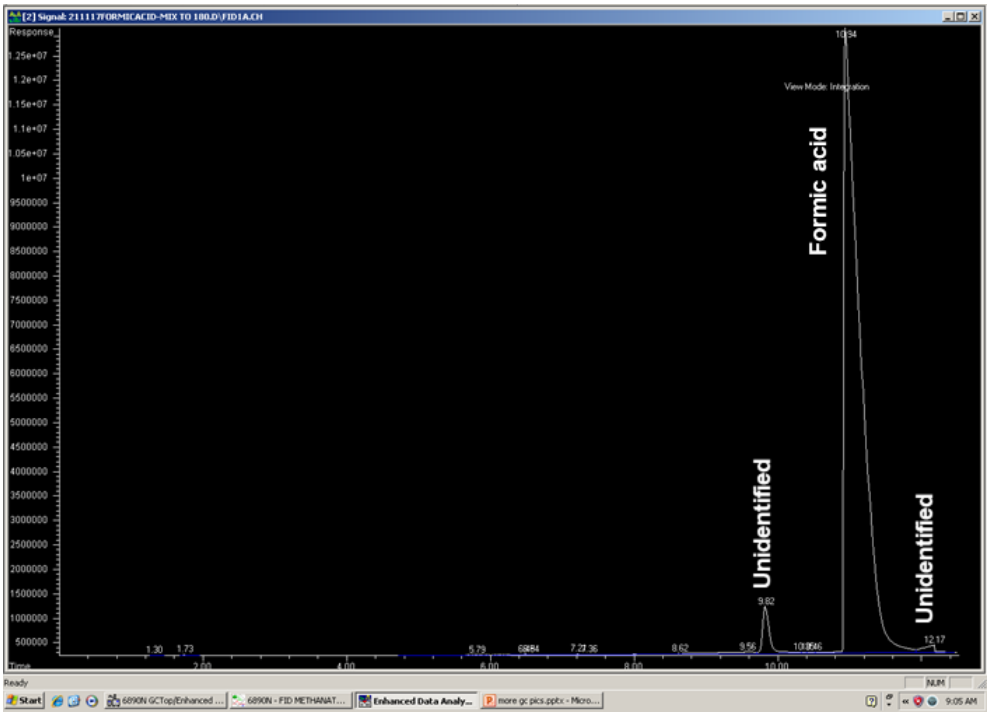

Figure 4.35: Test chromatogram of offline injection of formic acid, separation starting at 40 °C for 2 min followed by 20 °C.min^{-1} ramp to 180 °C, carrier gas H_2, constant flow 3ml$_n$.min^{-1}, Agilent 6890N GC operated with Agilent Chemstation™

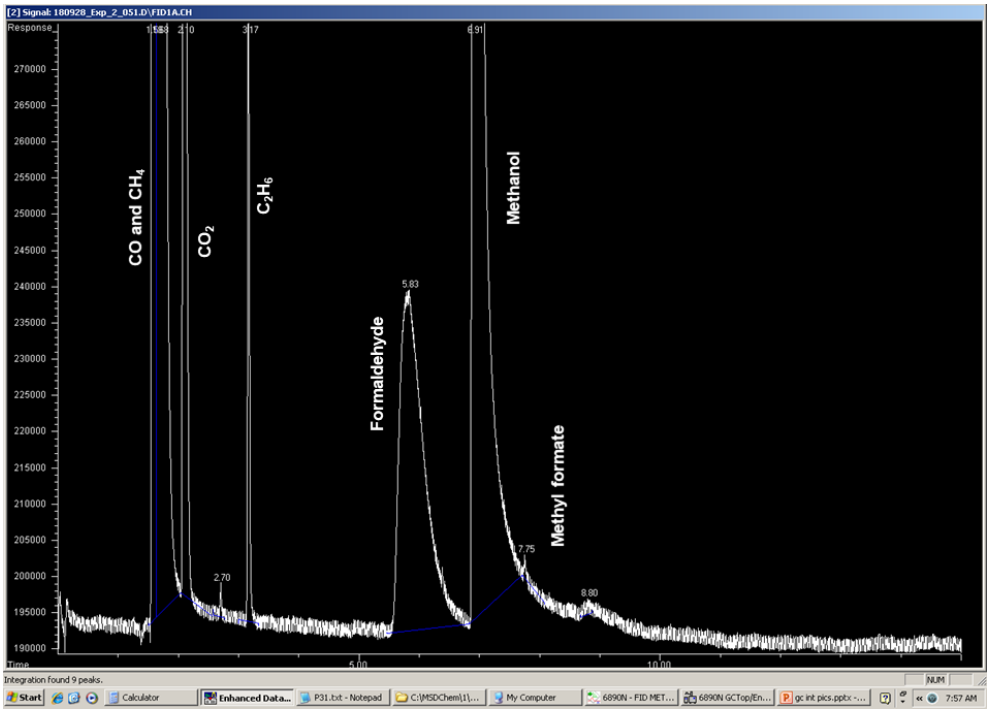

Figure 4.36: Chromatogram from the online injection of product gas from the autocatalytic conversion of methane to methanol with a feed of 39 $ml_n.min^{-1}$ CH_4, 3.9 $ml_n.min^{-1}$ O_2 and 5.7 $ml_n.min^{-1}$ N_2, at 505 °C and 40 bar, separation starting at 40 °C for 2 min followed by 20 $°C.min^{-1}$ ramp to 180 °C, carrier gas H_2, constant flow $3ml_n.min^{-1}$, Agilent 6890N GC operated with Agilent Chemstation™

Table 4.7: Retention time table of all identified compound, separation starting at 40 °C for 2 min followed by 20 $°C.min^{-1}$ ramp to 180 °C, carrier gas H_2, constant flow 3 $ml_n.min^{-1}$

Compound	**Retention time (min)**
CO	~1.6
CH_4	~1.7
CO_2	~2.1
C_2H_6	~3.2
Formaldehyde	~5.4 (board standard peak of 2 min, retention time defined as between 5 and 6 min)
Methanol	~6.9
Methyl formate	~7.8
Formic acid	~10.9

4.4.3.5 Polyarc™ reactor and flame ionization detector (FID)

The Polyarc™ reactor and the flame ionization detector were configured according to the instructions provided in the installation manual of the Polyarc™ reactor [76]. The Polyarc™ reactor is supplied with 2.5 $ml_n.min^{-1}$ of air and 35 $ml_n.min^{-1}$ of H_2 through its own dedicated

flow controller. The heating connection of the Polyarc™ reactor is connected to the heating channel of the back detector of the GC. According to the manual of the Polyarc™ reactor, the temperature set point of the back detector must be set at 293 °C. This is not the actual temperature of the Polyarc™ reactor as it have a temperature readout offset (-4 °C readout at room temperature). This is likely due to the use of a different type of temperature transducer in the Polyarc™ reactor as opposed to the Pt 100 RTD (a platinum wire with 100 Ω of resistance at 0 °C) used in the GC.

The flow rates through the flame ionization detector are also set according to the Polyarc™ reactor's manual at 1.5 $ml_n.min^{-1}$ of H_2 (as most of the H_2 is now supplied through the Polyarc™ reactor), 350 $ml_n.min^{-1}$ of air and 20 $ml_n.min^{-1}$ of N_2 make-up gas. The temperature of the flame ionization detector is set to 250 °C.

The Polyarc™ reactor can convert all carbon containing compound to methane before entering the FID. Thus, the FID will respond equally to all carbon containing compounds. This is tested three times during this study with calibrated gas mixtures containing compounds where the FID alone will not respond equally.

The first gas mixture did show enhanced response to CO (+ 6 %) and reduced response to CO_2 (- 5 %). In the second mixture, the FID showed a - 2 % response to methanol. Whereas in the third mixture the CO_2 responded equally with ethane, leading to the same carbon ratio in the gas mixture and peak area ratio detected in the chromatogram (see Table 4.8).

These experiments were carried out over a time of 9 month, indicating the Polyarc™ reactor can indeed allow the FID to respond equally (within an error of 5 %) to all tested carbon containing compounds over long periods of time.

Table 4.8: Calibration results for various gas mixture using the Polyarc™ reactor, FID alone will show reduced to no response for greyed out compounds

Date	**Gas mixture**	**Volume ratio in gas mixture**	**Carbon ratio in gas mixture**	**Peak area ratio of gas mixture**
2017/11/27	CO/CH_4/CO_2	1.29:1.00:0.65[a]	1.29:1.00:0.65	1.37:1.00:0.62
2018/03/19	CH_4/MeOH	1.00:7.14[b]	1.00:7.14	1.00:6.99
2018/08/23	CO_2/C_2H_6	1.02:1.00[a]	0.51:1.00	0.50:1.00

a. Certified volume ratio from gas supplier
b. Made during methanol stability test, see chapter 5.1

The Polyarc™ reactor introduces extra pressure drop in the GC and the installation manual recommend an increase of around 20 % in the column flow rate's set point. Therefore, the column flow rate set point is changed from 3 $ml_n.min^{-1}$ to 3.5 $ml_n.min^{-1}$.

The catalyst in Polyarc™ reactor can be reactivated through the procedure listed below. This is recommended on a quarterly basis.

1. Turn off air flow to Polyarc™ reactor
2. Set back detector temperature to 350 °C, and the GC oven to 250 °C
3. Wait for 2 h (minimum)
4. Set the back detector temperature back to 293 °C

5. Wait for 30 min after the back detector temperature reached 293 °C
6. Turn on the air flow to the Polyarc™ reactor and wait for another 2 h

4.4.4 GC method summary

Table 4.9: Summary of GC method developed for product analysis

Gas sampling valve:			
	Loop volume	1	ml
	Load time	0.01	min
	Inject time	0.11	min
	Heater	Aux 2	
	Heater temp	100	°C
Front Inlet:			
	Mode	Split	
	Temperature	100	°C
	Split ratio	10:1	
Column:			
	Column	Agilent 19091P Q04P-PLOTQ-PT	
	Length	30	m
	Diameter	320	µm
	Film thickness	20	µm
	Carrier gas	H_2	
	Flow rate	3.5	$ml_{n}.min^{-1}$
Oven:			
	Initial temp	40	°C
	Initial time	2	min
	Ramp rate	20	$°C.min^{-1}$
	Ramp time	7	min
	Final temp	180	°C
	Final time	6	min
	Run time	15	min
FID:			
	Temperature	250	°C
	H_2 flow rate	1.5	$ml_{n}.min^{-1}$
	Air flow rate	350	$ml_{n}.min^{-1}$
	Make-up gas	N_2	
	Make-up flow rate	20	$ml_{n}.min^{-1}$
Polyarc™ reactor:			
	Heater	Back-detector	
	Heater temp	293	°C
	H_2 flow rate	35	$ml_{n}.min^{-1}$
	Air flow rate	2.5	$ml_{n}.min^{-1}$

The above GC method produces the retention times tabulated in Table 4.10. Unidentified compounds encountered as reaction products from the reactor during this study is also included.

Table 4.10: Retention times of all compounds encountered during this study using the GC method described Table 4.9 (unidentified compounds in liquid standards are not included[a])

Approximate retention time (min)	**Peak identification**
1.6	CO
1.7	CH_4
2.1	CO_2
2.7	Unknown[b]
3.2	C_2H_6
5.5	Formaldehyde[c]
6.9	Methanol
7.8	Methyl formate
9.2	Unknown[d]
10.9	Formic acid
14.1	Unknown

a: Likely to be impurities/contaminants in the standards
b: Possibility ethene
c: Board peak width of roughly 1 min
d: Possibly methyl hydroperoxide

The chromatograms are integrated using the method in Table 4.11 to obtain the peak area for the different compounds (identified by their retention times).

Table 4.11: Integration parameter for GC chromatograms

Event:		**Comment:**
Area reject	0	For the detection of minor peaks
Min peak width	0.1 min	To avoid baseline noise to be detected as peaks
Threshold	12.5	Found to detect peaks corresponding to an area percent of roughly 0.001 %
Integrator off	< 1 min	To avoid false peaks introduced through sampling valve actuation to be detected
Baseline all valleys off	5 min	To hold the baseline during the board formaldehyde and methanol peak
Baseline all valleys on	7.7 min	

4.4.5 Evaluation of experimental results

To quantify the performance of a catalyst in the conversion of methane to methanol, the following performance indicator must be calculated: methane conversion, product yields, product selectivities and catalyst activity. They can be calculated as follows using the integrated results from the GC chromatogram of the reactor products:

Products yield:

Since all the carbon fed to the reactor is in the form of methane any detected compound, p, is a product from the conversion of methane. Assuming no carbon deposition occurs in the reactor and equal response to all carbon containing compounds from the FID via the use of the Polyarc™ reactor. The peak area percentage for any compound, p, will be their yield in C-%, Y_p, the percentage of carbon atoms in the feed methane that ended up in their respective products.

$$Y_p(C-\%) = \frac{Peak\ area\ of\ p}{Total\ peak\ area} \times 100\ (C-\%)$$

This allows for the methane conversion to be calculated:

Methane conversion:

The fraction of methane fed converted in the catalytic reactor, symbolized by X_{CH_4}, is defined as:

$$X_{CH_4} = \frac{F_{in_{CH_4}}\left(\frac{mol}{h}\right) - F_{out_{CH_4}}(\frac{mol}{h})}{F_{in_{CH_4}}\left(\frac{mol}{h}\right)}$$

Note the equivalence between mol/h and C-mol/h for CH_4:

$$X_{CH_4} = \frac{F_{in_{CH_4}}\left(\frac{C-mol}{h}\right) - F_{out_{CH_4}}(\frac{C-mol}{h})}{F_{in_{CH_4}}\left(\frac{C-mol}{h}\right)}$$

Since the only carbon containing compound fed is methane and assuming no carbon deposition occur in the system, as well as all carbon leaving the system have been detected with equal response in the FID. $F_{in_{CH_4}}\left(\frac{C-mol}{h}\right)$ will be equal to the sum of all detected compounds leaving the system in C-mol/h, $\sum F_{out}\left(\frac{C-mol}{h}\right)$:

$$X_{CH_4} = \frac{\sum F_{out_i}\left(\frac{C-mol}{h}\right) - F_{out_{CH_4}}(\frac{C-mol}{h})}{\sum F_{out_i}\left(\frac{C-mol}{h}\right)} = \frac{\sum F_{out_{products}}\left(\frac{C-mol}{h}\right)}{\sum F_{out}\left(\frac{C-mol}{h}\right)}$$

Since the yield for any product is defined as:

$$Y_p(C-\%) = \frac{F_{out_p}\left(\frac{C-mol}{h}\right)}{\sum F_{out}\left(\frac{C-mol}{h}\right)} \times 100\ (C-\%)$$

The methane conversion can be calculated as the sum of all the yields in C-%:

$$X_{CH_4} = \frac{\sum F_{out_{products}} \left(\frac{C-mol}{h}\right)}{\sum F_{out} \left(\frac{C-mol}{h}\right)} = \frac{\sum Y_p(C-\%)}{100(C-\%)}$$

Products selectivity:

The selectivity of a product, p, indicates how selective a reaction is to the product, p. It is symbolized by S_p and is defined as (in C-%) the fraction of carbon in methane converted that ended up in the product, p, as opposed to other products. It is simply the quotient between the yield of the product and the methane conversion:

$$S_p(C-\%) = \frac{Y_p(C-\%)}{X_{CH_4}}$$

Catalyst activity:

The catalyst activity is defined as how fast the catalyst can carry out a reaction, is characterized by the turn-over frequency (TOF) of a catalyst.

$$TOF(h^{-1}) = \frac{number\ of\ methane\ molecules\ converted\ per\ hour}{number\ of\ active\ sites\ on\ the\ catalyst} = \frac{F_{in_{CH_4}} \left(\frac{mol}{h}\right) - F_{out_{CH_4}} (\frac{mol}{h})}{number\ of\ active\ sites\ on\ the\ catalyst}$$

Assuming an average size of 4 nm for the active platinum nano-particles on the supported platinum-based catalyst particles, approximately 25 % of the atoms in the nano-particle will be on the surface of the particle and considered as an active. Thus, the number of active sites can be calculated from the catalyst mass, molar mass of platinum and the Pt metal loading:

$$TOF(h^{-1}) = \frac{M_{w_{Pt}} (\frac{g}{mol}) \times \left[F_{in_{CH_4}} \left(\frac{mol}{h}\right) - F_{out_{CH_4}} (\frac{mol}{h})\right]}{0.25\ \times \left(\frac{\%\ metal\ loading}{100\%}\right) \times m_{catalyst}(g)}$$

It must be noted that the above definition of turnover frequency is integral in nature over the entire reactor, this definition is certainly true for mixed reactors where the conditions are the same throughout the reactor. It is not true for our packed bed plug flow reactor where the number of methane molecules converted varies over the length of the reactor depending on the rate law of the reaction. Thus, the above definition of turnover frequency should only be used at small conversions of methane where the concentration variation of reactants over the entire length of the reactor is small.

In addition to conversion, yields, selectivities and catalyst activity, the carbon mass balance and catalyst deactivation can be inferred from the results obtained via the product analysis GC system:

Carbon mass balance:

Assuming no carbon deposition occurs in the reactor system and the FID respond equally to all carbon containing compounds, the flow rate of methane entering the reactor, $F_{in_{CH_4}} \left(\frac{C-mol}{h}\right)$, will be equal to the sum of all flow rates of carbon containing compounds leaving the system

in C-mol.h^{-1}, $\sum F_{out}\left(\frac{C-mol}{h}\right)$. The carbon mass balance in the reactor system will hold if $\sum F_{out}\left(\frac{C-mol}{h}\right)$ is equal to $F_{in_{CH_4}}\left(\frac{C-mol}{h}\right)$.

The sum of all flow rates of carbon containing compounds leaving the system, $\sum F_{out_i}\left(\frac{C-mol}{h}\right)$, is directly proportional to the total peak area via a constant representing the amount of reactor effluent injected into the GC injector, the dilution of the quartz lined reactor effluent with argon at the end of the reactor, the dilution of the GC injector, and the response factor of the GC:

$$\sum F_{out_i}\left(\frac{C-mol}{h}\right) = K_{injection\ volume} \cdot K_{dilution\ GC} \cdot K_{dilution\ Ar} \cdot K_{response\ factor}\left(\frac{C-mol}{signal.min.h}\right) . Total\ peak\ area\ (signal.min)$$

The injection volume is kept constant via the constant actuation time of the sampling valve and the constant temperature the sample loop. The inlet dilution ratio is kept constant via a constant injector split ratio. Although the flow rate of argon will change as it is used as a pressure control makeup gas, but since the quartz lined reactor's effluent is highly diluted in argon (by a factor of around 10). The overall dilution ratio of argon to quartz lined reactor effluent should remain constant provided the pressure on the different sides of the expansion valve (V-501) stays constant.

Thus, for a series of samples taken under the same reactor pressure, expansion valve setting and methane feed flow rate, the total peak area of those samples should stay constant. This will infer that carbon mass balance holds true for the reactor system over the times these samples are taken. This is especially true if the total peak area of these samples remains constant over a range of conversions, indicating the carbon molar flow rate out of the reactor system is constant regardless of conversion. However, if the total peak area does not stay constant, it does not necessarily mean the carbon mass balance does not hold true. As the variation in total peak area could be the result of variation in e.g. the injection volume, the methane feed flow rate or the argon dilution ratio, etc, beside the variation in the carbon molar flow rate out of the reactor.

Catalyst deactivation:

In addition, since our reactor system is continuous in nature, the deactivation of the catalyst in the reactor can be determined by observing how the catalyst's performance indicators (conversion, activity and selectivities) changes during an experiment. This can either be done by looking at how the catalyst's performance indicator changes during steady state reactor condition with increasing time on stream, or by testing the catalyst in the reactor with a temperature program where the reactor temperature is increased and then decreased. If the catalyst performance is inferior (lower conversion, poorer selectivities etc.) during the decreasing part of the temperature program, compared to the increasing part of the temperature program at the same temperature. It will imply that the catalyst has been subjected to deactivation.

4.5 Product condenser (C-701)

The product condenser (C-701) is a simple design based on a 150 ml stainless steel sample bottle shown in Figure 4.37. The reactor effluent from the GC sampling valve enters the sample bottle through a ⅛" dip tube extended all the way to the bottom of the sample bottle. Once the

gas exits the dip tube, the cold metal wall of the sample bottle will allow the liquid in the gas to condense and collect at the bottom of the sample bottle. This liquid is periodically drained via V-703. The gas then exits the sample bottle via the annular spaces around the dip tube into the branching end of a tee union, before being vented to the overhead vent in the reactor hood.

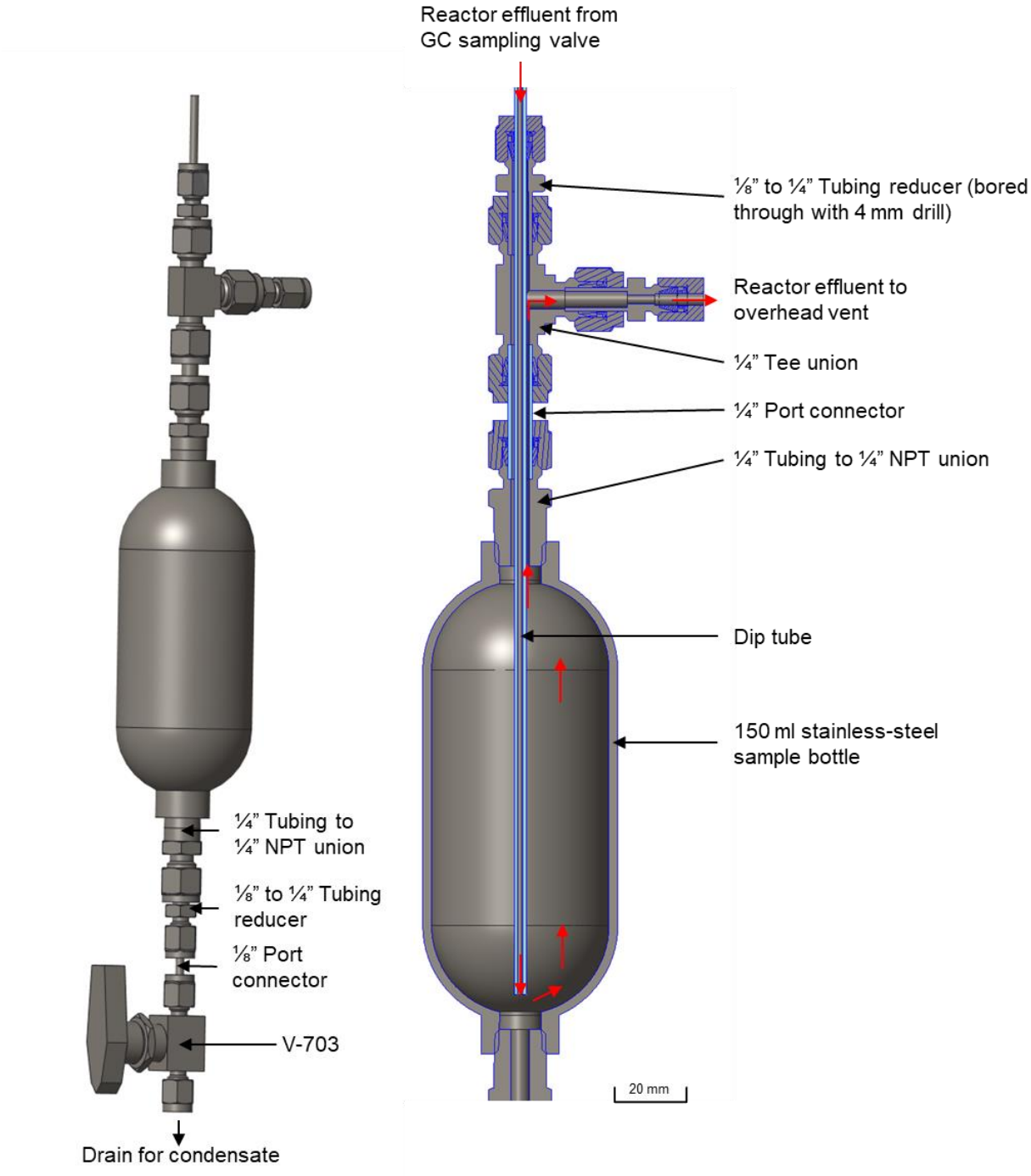

Figure 4.37: 3D model (not to scale) and cross-sectional view of product condenser

4.6 Reactor system instrumentation and control

With the packed bed reactor system for direct methane to methanol conversion fully designed, we can revise the preliminary flowsheet of the reactor system in Figure 3.12 to arrive at the flowsheet in Figure 4.42. The symbology for minor units such as the pressure control valves, mass flow controllers, needle valves, water pump and product condenser have been changed to reflect their actual principles of operation. The instrumentation and controls for the reactor system is also fully annotated in Figure 4.42.

4.6.1 Pressure

The pressure in the reactor system is controlled by the various pressure control valves (PV's). The pressure downstream of these valves are adjusted by manually adjusting the valve while observing the pressure gauge (PI's) immediately downstream of the valve. The cylinder pressure controllers (PV-x02) are adjusted to obtain a pressure of around 50 bar on PI-x04 and are not changed during the operation of the reactor system. The reactor pressure is adjusted with PV-601 while observing PI-602 and PI-501 (both gauges should give the same reading). The feed pressure of helium, methane and oxygen are adjusted with PV-101, PV-201 and PV-401 whilst observing PI-102, PI-202 and PI-402 respectfully. These feed pressures should be adjusted to be slightly higher (< 5 bar) than the reactor pressure to create a small pressure difference across the mass flow controllers.

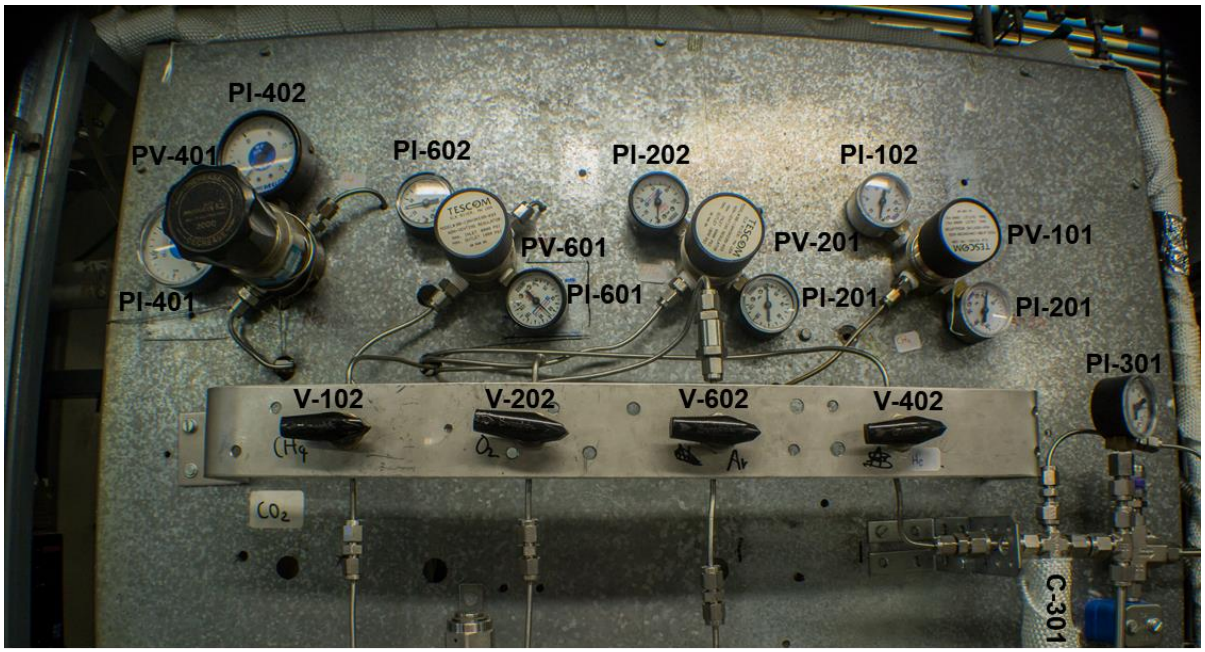

Figure 4.38: Pressure control valves and indicators, accessible on front panel of reactor system, PI-501 is attached to the removable reactor assembly and is not shown

The pressure drop across the catalyst bed can be measured from the difference in pressure between PI-301 and PI-602 (or PI-501), assuming the pressure drop in the evaporator (C-301) and in the lines between the evaporator and the reactor is negligible. This is a reasonable assumption as the packing in the evaporator (diameter 600 µm) is much greater than the catalyst particles in the reactor (diameter < 160 µm to avoid wall effects in the reactor).

4.6.2 Reactant (and inert) flow rates

The flow rate of methane, oxygen and helium through the reactor system is adjusted with the control modules (FIC-101, FIC-201 and FIC-401) for their respective mass flow controllers (FC's). The calibration and operation of the control modules are discussed in the Appendix I. The flow control for the water pump (FIC-301) is located locally on the water pump.

Figure 4.39: Flow control modules and indicators for methane, oxygen and helium, accessible from front platform of reactor system

Figure 4.40: Flow controller and indicator for water, accessible on bottom front panel of reactor system

4.6.3 Temperatures

The temperature control for the reactor (TIC-501) and evaporator (TIC-301) have already been discussed in their respectful section. The aluminium foil – nichrome heating wire heating scheme used in the evaporator is also applied to the intermediate temperature control loops to prevent condensation (2 TICs on the lines in Figure 3.12). The heating loop between the evaporator and reactor (TIC-302) is extended to cover the top of the reactor. The thermocouple of this control loop is placed at the top of the reactor assembly where the O-ring is placed to ensure the temperature here does not exceed the maximum temperature of the O-ring seal.

Two extra thermocouples are added on this line as extra temperature indicators. TT-102 is placed at the bracket holding the evaporator to the reactor stand, where the evaporator heating loop ends (TIC-301) and the steam line heating loop begins (TIC-302). This is the coldest point in the steam line and its temperature has to be checked to ensure it is higher than the saturation

temperature of the steam-helium mixture passing through the evaporator. The control thermocouple (TT-302) for the steam line heating loop (TIC-302) is located on the reactor head which has a much greater thermal mass than the bare line, thus the bare steam line will be heated to a higher temperature than its setpoint on TIC-302. Another measuring thermocouple TT-103 is placed on the steam line itself, to ensure the steam line is not overheated.

TT-101 is added as an extra temperature measuring thermocouple at the top of the evaporator packing, the temperature here must be checked to ensure it is less than the saturation temperature of the steam-helium mixture in the evaporator. This is done to ensure liquid water is present at the top of the evaporator, as discussed previously.

The post reactor heating loop in Figure 3.12 is split into 3 different heating loops in the revised reactor system flowsheet (Figure 4.42). The first post-reactor heating loop, TIC-502 is responsible for heating the pressurized reactor effluent before the reactor expansion valve (V-501). The control thermocouple (TT-502) for this heating loop is placed on the fitting with the biggest thermal mass (S-501). TT-104 is added as a measuring thermocouple at the end of the reactor to ensure this section of the line is not overheated, identical to principle as TT-103 mentioned previously. A new heating loop (TIC-801) is added from the reactor expansion valve (V-501) to the vent/GC manifold (V-701 and V-801). Another heating loop (TIC-702) is added to the relatively long line from the vent/GC manifold to the 6-way sampling valve (V-702). These two new heating loops are usually heated to a temperature set-point of 100 °C. The mixture in these 2 heating loops are at ambient pressures and highly diluted in argon, making condensation less of an issue than in the pressurized parts of the reactor. For example, a dilution ratio of 9:1 with argon after the reactor means the maximum water partial pressure in the depressurized part of the reactor is only 0.1 bar. This 9:1 mixture of argon and water will only condense at 45 °C.

TIC-801 and TIC-502 are built in the exact same fashion as the 4 TICs (301, 501, 302, 702) in the existing temperature control box, using the flow diagram discussed in Appendix I. The two new temperature control unit are placed inside its own box and placed on top of the temperature readout controller TI-10x (see Figure 4.41)

In addition, all heated parts of the reactor system are insulated in a layer of ceramic fibre roughly 2 cm thick to prevent heat loss. The ceramic fibre insulation is held in place by wrapping them in a layer of fibreglass webbing. The measuring thermocouples (TT-10x) are all wired to the 12-way thermocouple readout device (see Appendix I).

During the operation of the reactor, the measured temperatures at TI-10x were monitored and some selected temperature measurements from the reactor system are listed in Table 4.12. As intended, the top of the evaporator is always significantly colder than the inside of the evaporator to ensure the boiling of water happens in the packing of the evaporator. The cold point on the steam line where the line is bracketed and fastened to the rig chassis can be somewhat colder than the evaporator temperature. Although the maximum difference observed was only 15 °C, this temperature reading should be checked regularly during experiments with water co-feeding to ensure it does not fall below the condensation temperature of the steam. The steam line and the line leaving the reactor is generally warmer than the control point of heating zones. This is as expected since their control points (O-ring seal on top on reactor and S-501 on the reactor effluent line, respectively) have higher thermal mass than the steam line and the line exiting the reactor. Their temperature is not considerable hotter than their control

points, with the biggest temperature difference observed at around 30 °C (except in the third column in Table 4.12, where the hot 250 °C reactor caused the line leaving the reactor to be heated to 264 °C).

Table 4.12: Selected temperature measurements from the reactor system for methane to methanol conversion

Heating zone	**Temperature measurement point**	**Location of thermocouple**	**Temperature readings (°C)**				
TIC-301	TIC-301	Inside of evaporator	150	120	150	200	100
	TI-101	Top of evaporator	55	43	54	60	41
	TI-102	Cold point on steam line, where steam line is fastened to rig chassis	140	126	135	203	102
TIC-302	TI-103	On steam line	158	148	153	228	117
	TIC-302	O-ring seal on top on reactor	150	120	150	200	100
TIC-501	TIC-501	Inside of reactor	150	100	250	200	100
TIC-502	TI-104	Bottom of reactor	158	146	264	201	99
	TIC-502	S-501 on the reactor effluent line	150	120	150	200	100
TIC-801	TIC-801	V-801 on vent line	100	120	150	150	100
TIC-701	TIC-701	On 6-way GC sampling valve	100	100	100	100	100
TIC-702	TIC-702	On the reactor effluent line going to the GC	100	150	150	135	100

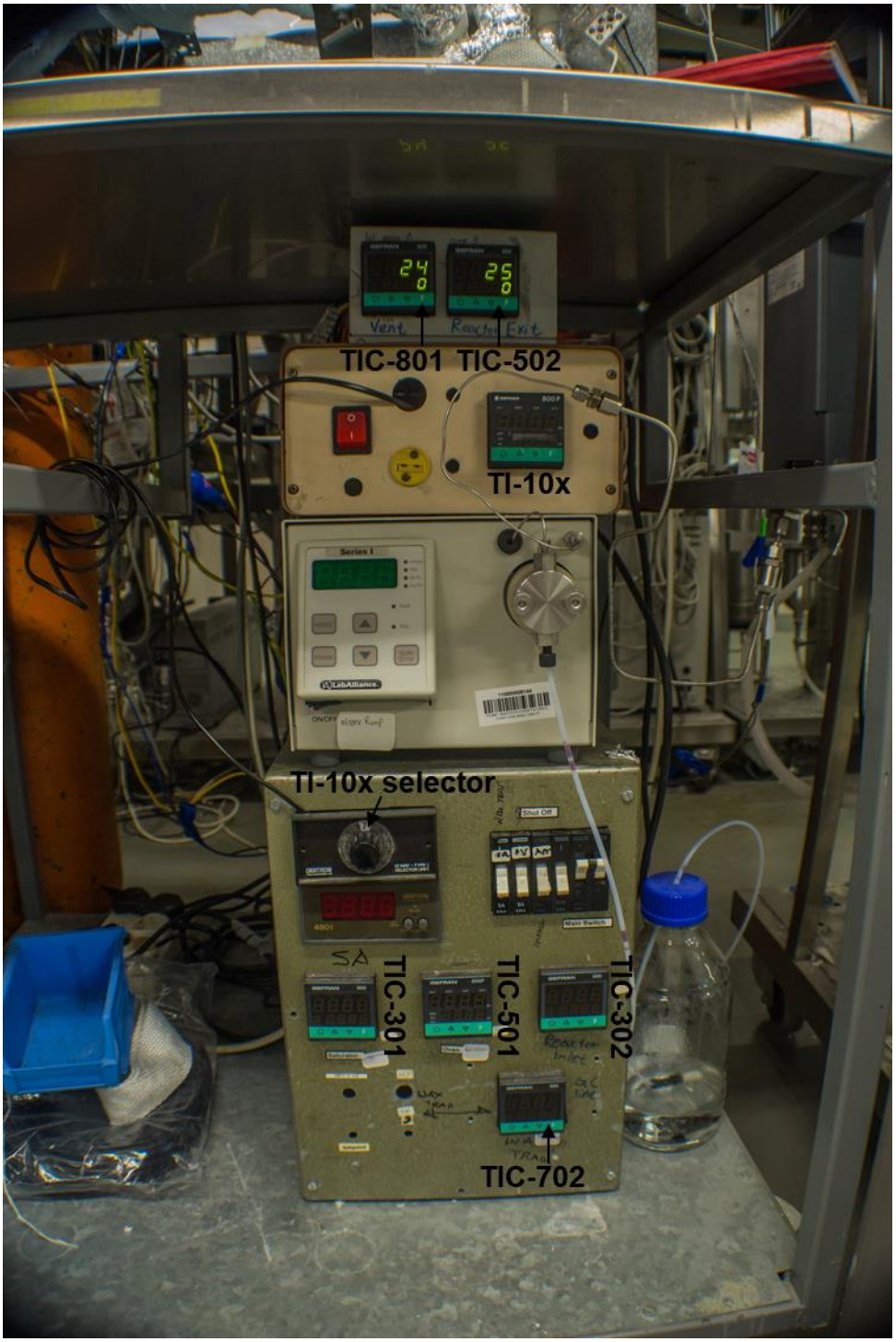

Figure 4.41: Temperature controllers and indicators, accessible on bottom front panel of reactor system

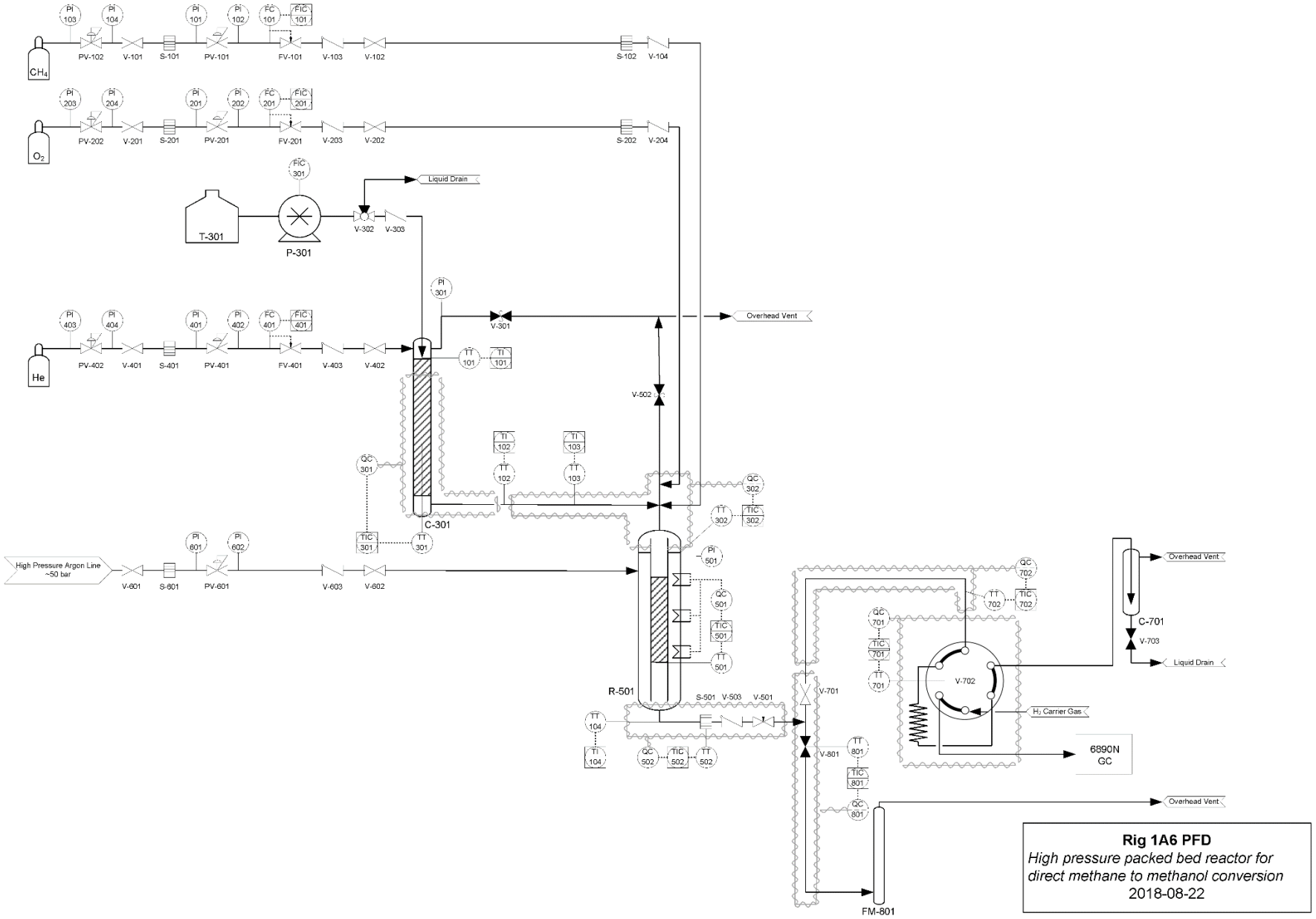

Figure 4.42: Revised flowsheet with instrumentation and control for packed bed reactor system for direct methane to methanol conversion, blacked out valves are normally closed, grey indicates heating wire

4.7 Reactor system safety

4.7.1 Chemical safety

Beside the hazard involving the flammability of methane and oxygen mixtures, no other hazardous chemicals are involved in the packed bed reactor system for methane to methanol conversion. By containing the reactants inside the reactor system, all chemical hazards besides the flammability of methane and oxygen mixtures can be mitigated. This containment is achieved by leak testing the reactor system before operation (see Appendix II on reactor operation).

The measures taken to prevent unintentional combustion/explosion inside the reactor system due to the presence of methane and oxygen have been discussed during the design of the packed bed reactor, to summarize it includes:

- Isolate reactant gases before entering the reactor to prevent mixing
- Using oxygen rated fittings and valves for the oxygen line
- The small size of the quartz lined reactor minimizes the energy released during combustion
- The small diameter stainless steel shell around the reactor is mechanically strong due to its high wall thickness to inner diameter ratio
- Pressure relief valve is added to the reactor head
- The reactor effluent is highly diluted in argon upon exiting the reactor
- The maximal flow rate of methane into the reactor is $39 ml_n.min^{-1}$, its complete combustion can only generate 26 W of heat

4.7.2 Mechanical safety

The reactor system for direct methane to methanol conversion does not have any moving parts in the main reactor and will not pose any hazards due to mechanical movements.

The reactor system is under pressure during most of its operation and can pose a risk to the operator. Though this is minimal as the pressure during the operation of the reactor system (< 50 bar) is far less than the rated pressures of the fittings and tubings used in the reactor system and this pressurized volume is minimal at 50 ml (see Appendix II on how the volume was calculated).

Great care must be taken to ensure no work is done on the reactor system (disconnecting or connecting fittings, bending and stressing the lines etc) when the reactor system is pressurized and connected to the gas supply to avoid an unwanted release of pressurized gas. However, even if such action is mistakenly carried out all lines feeding into the reactor system has an inner diameter of 1.5 mm, limiting the amount of pressurized gases that can escape the reactor system.

4.7.3 Electrical safety

Electricity is the greatest hazard in the reactor system for direct methane to methanol conversion, as live 220 V AC is used in the heating of the reactor system. Various measures must be strictly adhered to, to avoid any potential electrical faults and/or accidents.

The entire reactor system is electrically connected to the reactor stand, this must be grounded at multiple points as a fail-safe measure and checked often. Currently the reactor system is grounded through the main temperature control box, the water pump, the temperature indicator and the auxiliary temperature control box, i.e. all units shown in Figure 4.43. To check for the ground connection, measure the resistance between any exposed metal part of the reactor to the earth pin of a mains plug, it must be zero. This ensures the earth leakage breaker for the reactor system (1PH6) on the distribution board at the west end of the reactor hood will trip if an electrically live wire contacts the metal surface of the reactor due to faulty insulation. This happens often as the insulations on the heating wires are subjected to both thermal stress during heating and mechanical stress during reactor changes.

The second kind of electrical fault that may possibly happen in the reactor system heating circuits is a short circuit. This happens most often with the six heating cartridges of the reactor heating blocks as the wire terminals of these heating elements are subjected to bending stresses during reactor changes and when insulating ceramic fibre blankets are wrapped around the reactor heating blocks. During a short circuit, the over current circuit breakers in the temperature control box as well as the distribution board will trip. A detailed troubleshooting guide for repairing these electrical faults as well as any other faults that can be experienced in the reactor system can be found in the Appendix II.

In addition, a feed (methane and oxygen) shutoff fail-safe circuit (see Figure 4.43) is added to the reactor system to allow emergency shut down of methane and oxygen feed to the reactor system and reactor system heating. This is a generic reset-set latch circuit built around a pair of transistors (Q1 and Q2) operating a normally open relay (RL1). The circuit is powered by an 18 V DC switched mode power supply (SMPS) from an old laptop charger that is always on.

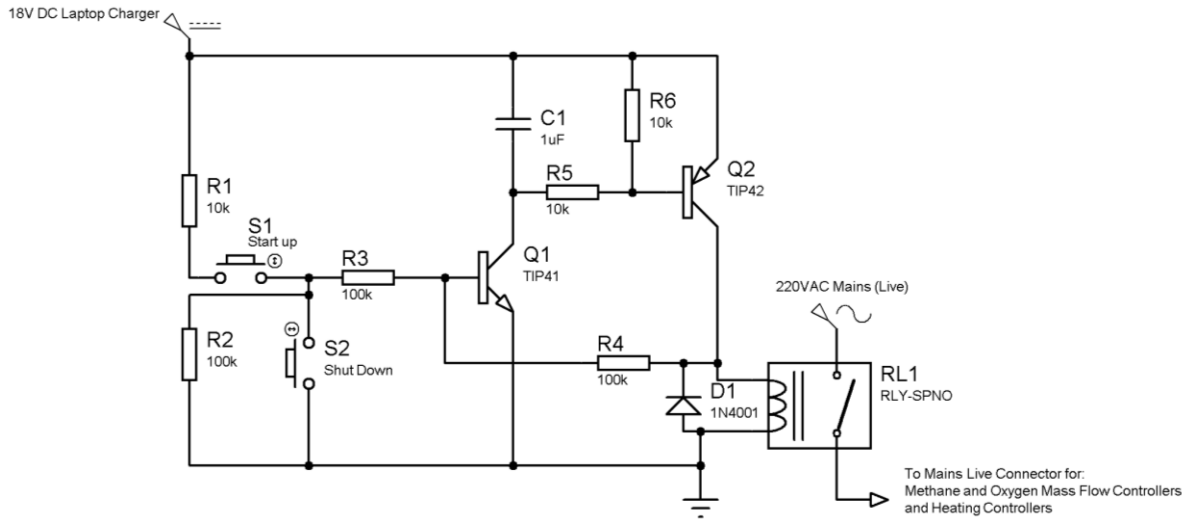

Figure 4.43: Schematics of fail-safe circuit

The relay in its open state will not provide power to the mass flow controllers for methane and oxygen (thus shutting off the flow as these are fail shut valves) as well as all heating controllers besides the GC line (TIC-702) and the vent manifold (TIC-801). During the start-up of the reactor system, S1 is momentarily pressed, turning on the NPN transistor Q1 by creating a

positive voltage at the gate (relative to its emitter) of Q1 via R1 and R3. With Q1 turned on, a current can flow through it via R6 and R5, generating a negative voltage at the gate (relative to its emitter) of the PNP transistor (Q2) turning it on. With Q2 turned on, a current can now flow through it and the relay, energizing the methane and oxygen mass flow controllers and the heating controllers in the reactor system; simultaneously, a feedback resistor (R4) generates a positive voltage at the gate of Q1, keeping it turned on. This is the set-cycle of the fail-safe circuit.

During an electrical fault in the reactor system, or when the emergency shut-off switch (S2) is momentarily pressed; the feedback cycle through R4 will be broken, resetting the fail-safe circuit to its initial state. This de-energizes the relay (RL1), turning off power to the mass flow controllers for methane and oxygen as well as the heating controllers of the reactor system.

5. Exploratory Experimental Results

In order to commission the packed bed reactor system for catalyst testing in the conversion of methane to methanol, a number of exploratory experiments were carried out on the reactor system. The main purpose of these experiments is to diagnose any potential problems with the reactor system in addition to investigate the conversion of methane to methanol under high oxygen and water partial pressures as we postulated in the introduction of this dissertation.

Four sets of experiments were carried out to commission the packed bed reactor system: methanol stability tests, autocatalytic conversion of methane to methanol, as well as catalytic conversion of methane to methanol over two different platinum-based catalysts, Pt_3Mo and Pt_3Bi.

Several unknown compounds were detected during these experiments, at this stage they will be identified via their retention times on the GC chromatogram, as RT-x (x is the retention time of the unknown compound) using the method described during the development of the GC method. Potential methods for identifying them will be discussed in the recommendation section of this dissertation.

The method for calculating the conversion, yield and selectivities in this section is described at the end of the section on the gas chromatography system in Chapter 4.

5.1 Methanol stability tests

The stability of our expected product, methanol, is tested first in the reactor system. This is done by purging a fixed ratio of methane and methanol gas through the empty reactor (no catalyst and no packing) at different temperatures and pressures with continuous sampling.

The methanol flow rate through the system is set at 0.05 $ml.min^{-1}$ (liquid) at P-301. This flow rate was confirmed by measuring the mass flow out of T-301 using an analytical scale to be 0.0503 $ml.min^{-1}$. A helium make-up of 16.6 $ml_n.min^{-1}$ is send through the evaporator alongside the methanol. Methane was used as an internal reference in this experiment at a flow rate of 3.9 $ml_n.min^{-1}$. Assuming no reaction takes place the exit yield of methanol should be 87.7 % with the remainder being methane since only carbon containing compounds can be picked up on the GC-oxidizer-methanizer-FID system used for product analysis. The yield of methanol as well as any produced products in this experiment is normalized with respect to the expected methanol yield of 87.7 %.

The reactor and evaporator temperatures and pressures used in this experiment is shown in Table 5.1. All other temperature set points of the system is set to avoid condensation (200 °C for steam line and reactor exit, 150 °C for vent manifold and GC line). The entire experiment was conducted as a series with continuous sampling.

Table 5.1: Pressure and temperature set points during the experiment on methanol stability

Pressure (bar)	$T_{boil\ MeOH}$ (°C)	$T_{reactor}$ (°C)	$T_{evapourator}$ (°C)
1	52	100	100
10	121	150	150
20	148	200	200
30	166	250	250
30	166	300	250
30	166	350	250
30	166	400	250
30	166	450	250

During the first 2 conditions in Table 5.1, the normalized methanol yield was stable at 100 % after 2 h indicating no conversion of methanol took place (see Figure 5.1). 1 h of lag was observed between the start of methanol flow until its normalized yield reached 100 %. Afterwards the normalized yield of methanol increased beyond 100 %. A normalized yield greater than 100 % is possible if more methanol was evaporated in the evaporator than liquid methanol fed during the initial unsteady state of the reactor system. Some methanol was decomposed to formaldehyde at 150 °C and 10 bar, but its yield is not significant at ppm levels.

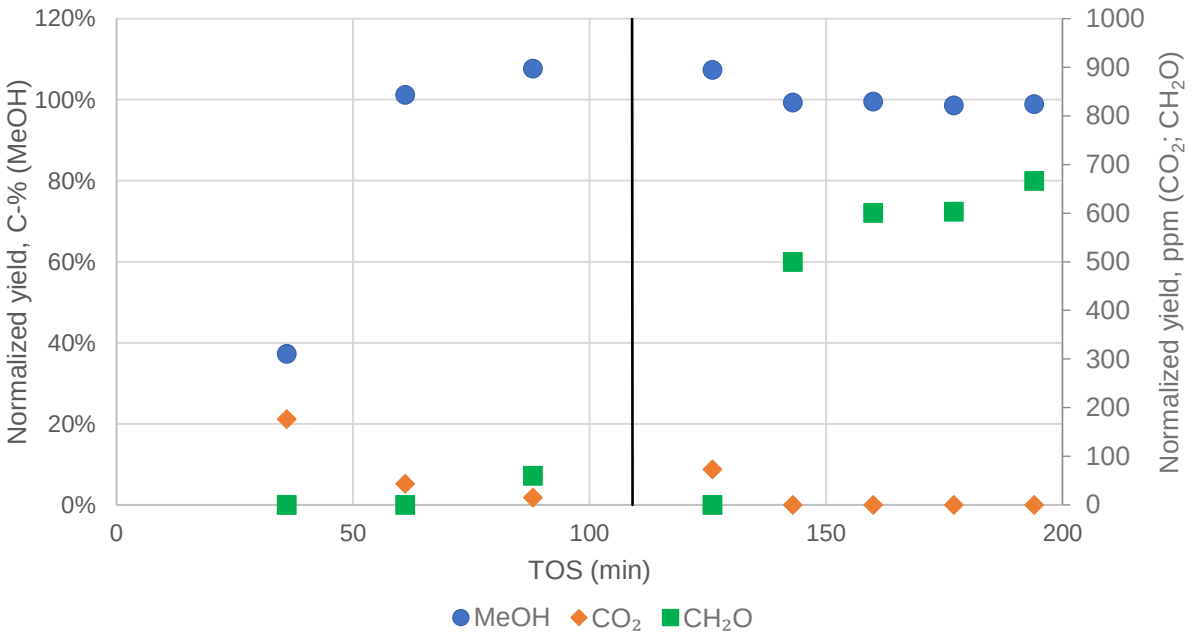

Figure 5.1: Methanol stability test starting at 100 °C and 1 bar, solid vertical line indicates where temperature is increased to 150 °C and pressure to 10 bar

The methanol stability experiment was started again at 200 °C and 20 bar, also taking around 2 h to reach steady state conditions (see Figure 5.2). Trace amounts of formaldehyde were also observed as some of the methanol decomposed. However, at the higher pressures and

temperatures of this experiment, the normalized methanol yield is slightly less than 100 %, and this cannot be explained by the trace amounts of formaldehyde formed. Since the flow rate of methanol was verified through mass balance on the methanol tank, the flow rate of methane, our internal reference may have slightly increased at higher pressures due to changes in the mass flow controller's calibration curve at higher pressures.

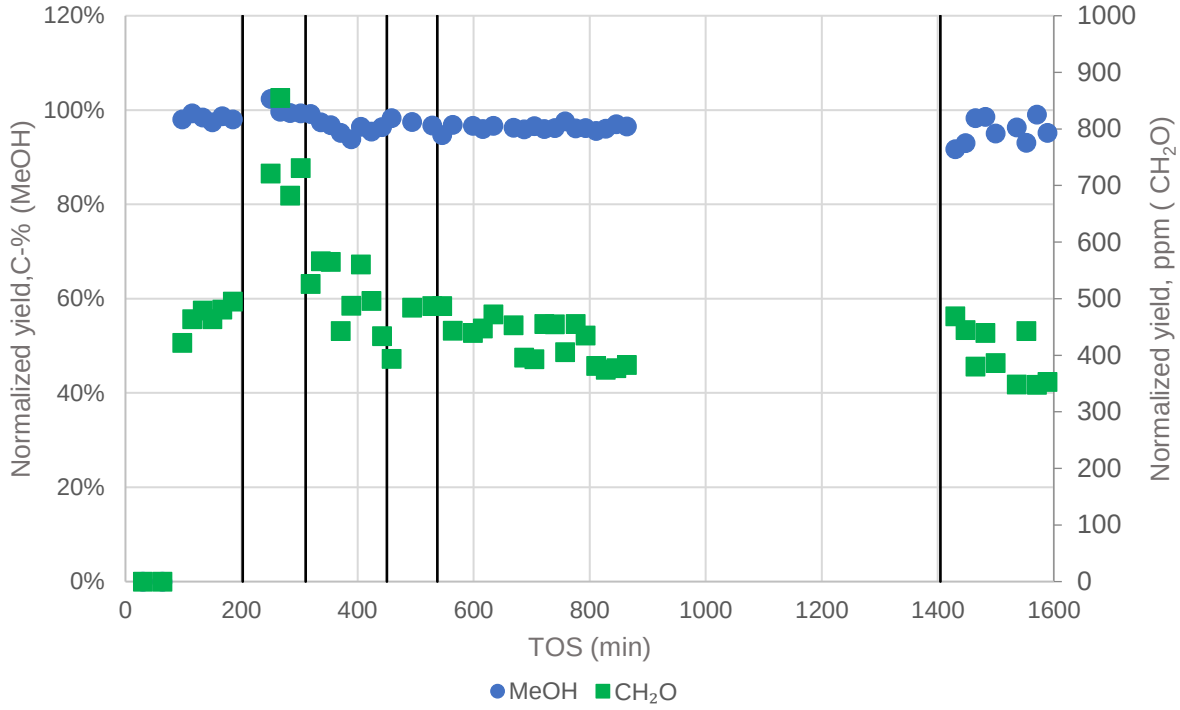

Figure 5.2: Methanol stability test starting at 200 °C and 20 bar, first solid vertical line: pressure increased to 30 bar and temperature to 250 °C; subsequent solid vertical lines: increase of 50 °C in temperature

The total peak area plot of the experiment in Figure 5.2 is shown in Figure 5.3. The total peak area is seen to increase in the beginning of the experiment, due to the increase in carbon molar flow rate through the reactor as the methanol begins to evaporate. When the pressure is increased to 30 bar at the first vertical line, the total area decreased as more argon make-up gas enters due to the increased pressure difference across the post reactor expansion valve (V-501). The decreased total peak area is the result of increase in argon dilution factor discussed in Chapter 4.4.5.

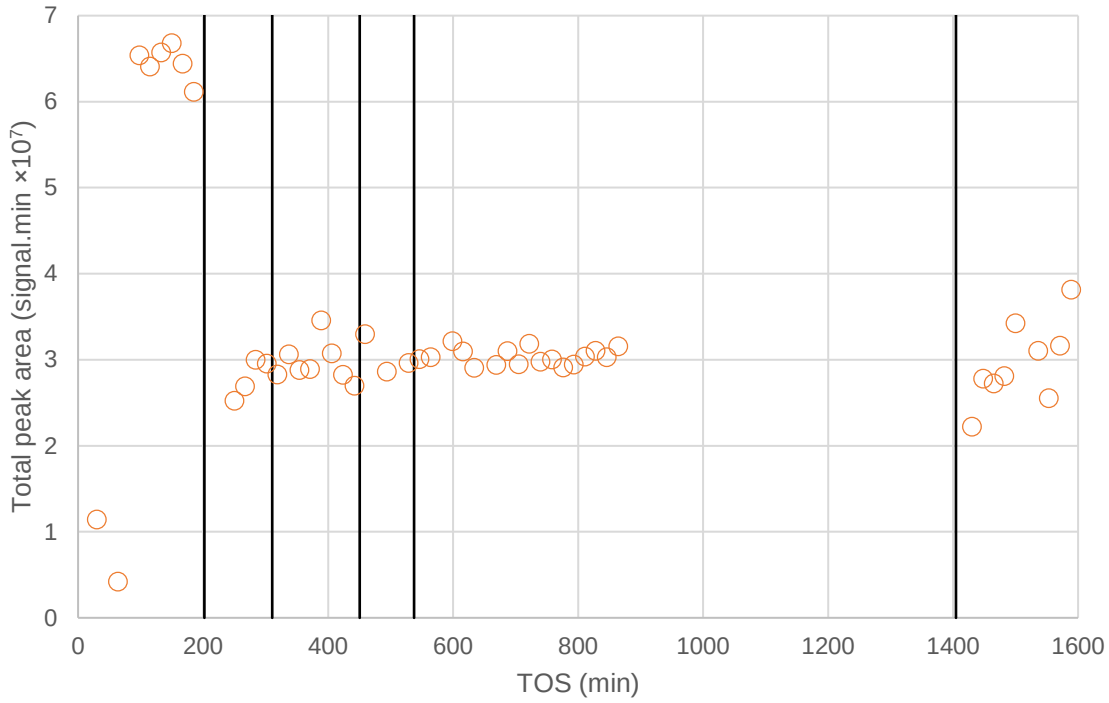

Figure 5.3: Total peak area plot for experiment in Figure 5.2, solid vertical lines represent the same condition changes as in figure 5.2； starting at 200 °C and 20 bar, first solid vertical line: pressure increased to 30 bar and temperature to 250 °C; subsequent solid vertical lines: increase of 50 °C in temperature

The steady state operation of the reactor system can be assessed by statistically testing whether the total peak area is significantly related to time on stream. This is done by doing a student's t-test to determine the P-value for the significance of the null hypothesis (total peak area is irrelated to time on stream) in the slope of the regression line between total peak area and time on stream. If the null hypothesis holds true, then we can infer the molar flow rate of carbon out of the reactor during the experiment is constant.

Using a confidence level of 95 %, a P-value of < 0.05 indicates the total peak area and the time on stream is significantly related. If this slope is negative, i.e. the total peak area decreases with time on stream, it indicates can indicate the carbon molar flow rate leaving the reactor system is decreasing. This could mean either organic residue is being driven out of the reactor system, the flow of methane into the reactor is decreasing, methane is carbonizing over the catalyst or a leak is developing in the reactor system. A decreasing total peak area can an increase in argon dilution ratio (due to pressure drifts or accidental adjustment of the expansion valve). A significant increase in total peak area, i.e. a positive slope of total peak area vs time on stream either means the methane flow rate is increasing or the argon dilution ratio is decreasing.

A P-value of > 0.05 indicates the total peak area is not significantly related to the time on stream and the scatter in the total peak area is random. This scatter is likely due to the sampling valves actuation leading to different amounts of reactor effluent being injected or scattering of the methane flow rate coming into the reactor. By analysing the total peak area between 200 min and 1600 min in Figure 5.3, during which the methanol stability experiment was carried out at 30 bar, a P-value of 0.99 was obtained. This indicates the total peak area, thus the carbon molar flow rate out of the reactor system during this part of the experiment is constant. This is expected as the carbon molar flow into the reactor system is constant.

5.2 Autocatalytic conversion of methane to methanol

5.2.1 Experiment 1

Before any catalytic experiments, the autocatalytic conversion of methane to methanol is attempted in our reactor system with an unloaded reactor quartz liner (no catalyst nor packing). These experiments are done with a reactant feed of 28 $ml_n.min^{-1}$ CH_4, 2.8 $ml_n.min^{-1}$ O_2 and 8.3 $ml_n.min^{-1}$ He at 35 bar and 400 °C. This feed composition was chosen in accordance with the past experiments on the autocatalytic conversion of methane to methanol where excess methane and high pressures were essential to the formation of methanol.

This experiment was carried out on the day of the methanol stability experiment discussed previously. The yield vs time on stream plot of this experiment is shown in Figure 5.4. Initially methanol, formaldehyde, methyl formate and CO_2 was observed in the reactor products. However, the yield of all products was seen to decrease during the first 500 min of the experiment before reaching a steady state conversion of 0.01 % to CO_2.

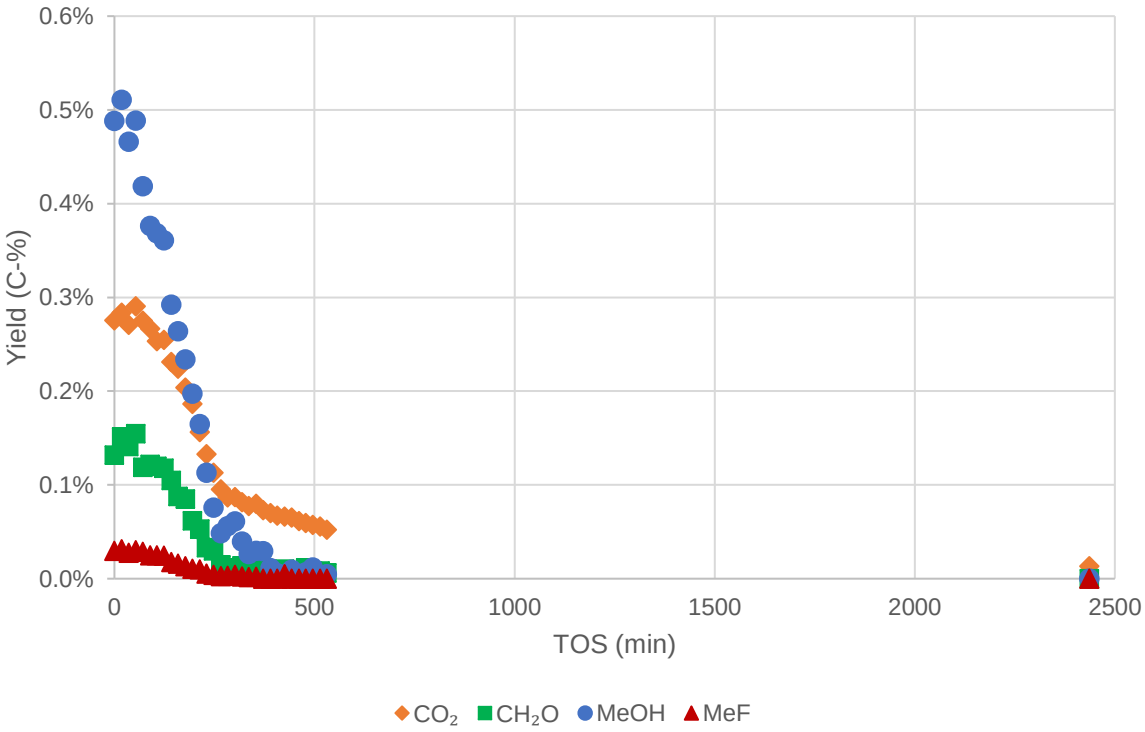

Figure 5.4: Yield vs time on stream plot for autocatalytic conversion of methane to methanol at 35 bar and 400 °C, with a feed of 28 $ml_n.min^{-1}$ CH_4, 2.8 $ml_n.min^{-1}$ O_2 and 8.3 $ml_n.min^{-1}$ He

The decrease in product yield was due to residual methanol adsorbed on the walls of the lines in the reactor system during the methanol stability experiment carried out prior to this experiment. This can be ascertained by looking at plot of the total peak area vs time on stream in Figure 5.5, which significantly decreased during the experiment with a P-value of 0.02 for the null hypothesis (total peak area is not related to time on stream). The decrease in total peak area indicates a decrease in the molar flow rate of carbon out of the reactor system as the residue methanol is being driven out.

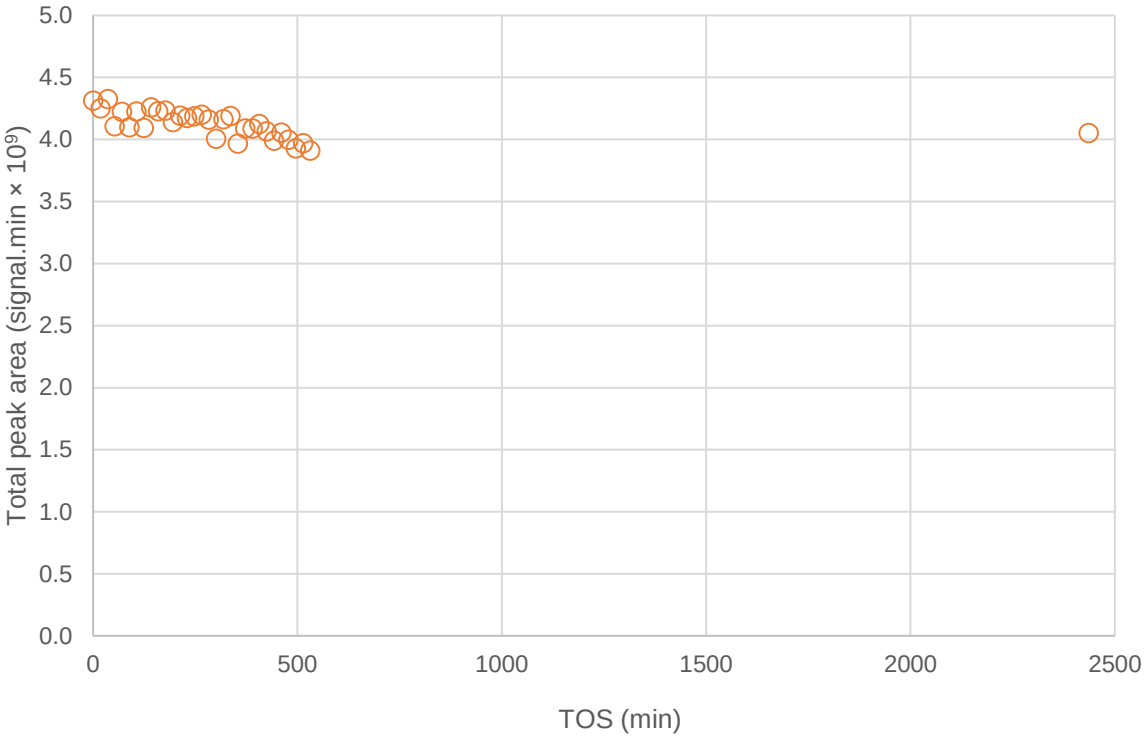

Figure 5.5: Total peak area vs time on stream plot for autocatalytic conversion of methane to methanol at 35 bar and 400 °C, with a feed of 28 $ml_n.min^{-1}$ CH_4, 2.8 $ml_n.min^{-1}$ O_2 and 8.3 $ml_n.min^{-1}$ He

5.2.2 Experiment 2

The autocatalytic conversion of methane to methane was attempted again after the reactor had been thoroughly purged of any methanol. The same reactant feed was used (28 $ml_n.min^{-1}$ CH_4, 2.8 $ml_n.min^{-1}$ O_2 and 8.3 $ml_n.min^{-1}$ He) while the pressure was increased to 40 bar. A temperature range from 570 °C to 390 °C was investigated in intervals of 30 °C. The reactor was held at each temperature for 3 h and approximately 10 samples were taken at each temperature. The total peak area vs time on stream plot of this experiment is shown in Figure 5.6 indicates all the methanol residual from the previous experiment has left the reactor system as the total peak area was not significantly related to the time on stream (P-value for null hypothesis is 0.09), i.e. the molar flow rate of carbon out of the reactor system is constant.

The conversion and selectivities plot for this experiment was determined from the average conversion and selectivities of the last three samples at each condition and shown in Figure 5.7. No methanol was observed in this experiment with CO_2 being observed as the major product along with some CO, ethane and formaldehyde at higher temperatures. The error bars presented in Figure 5.7 as well as all subsequent plots were calculated as 2 times the standard deviation of the data points at that temperature. This represents a 95 % confidence interval assuming the data is normally distributed.

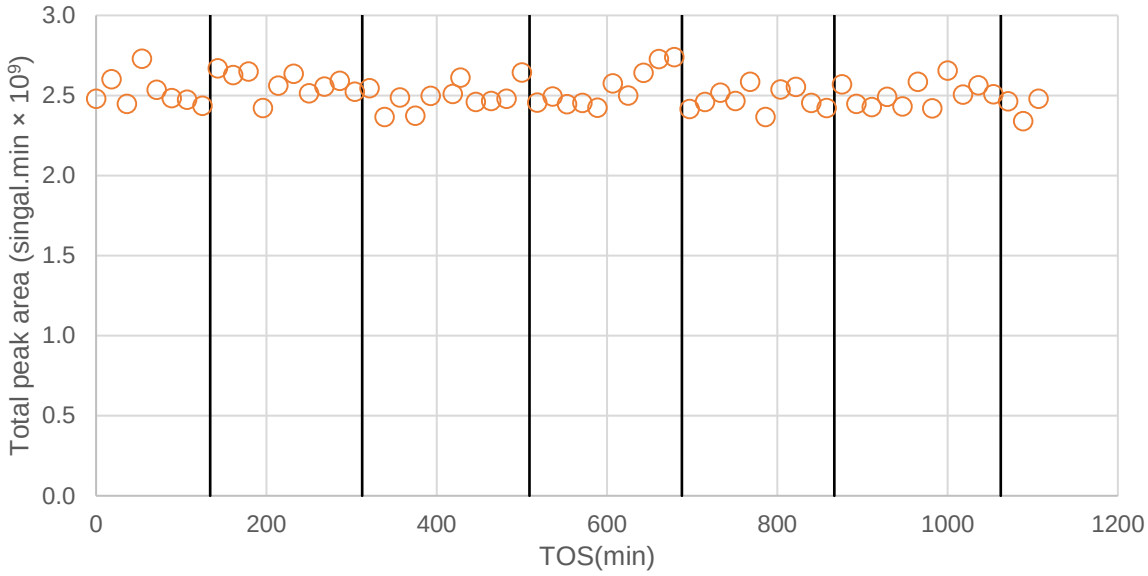

Figure 5.6: Total peak area vs time on stream plot for autocatalytic conversion of methane to methanol starting at 40 bar and 570 °C, with a feed of 28 $ml_n.min^{-1}$ CH_4, 2.8 $ml_n.min^{-1}$ O_2 and 8.3 $ml_n.min^{-1}$ He; solid vertical lines indicate a temperature decrease of 30 °C

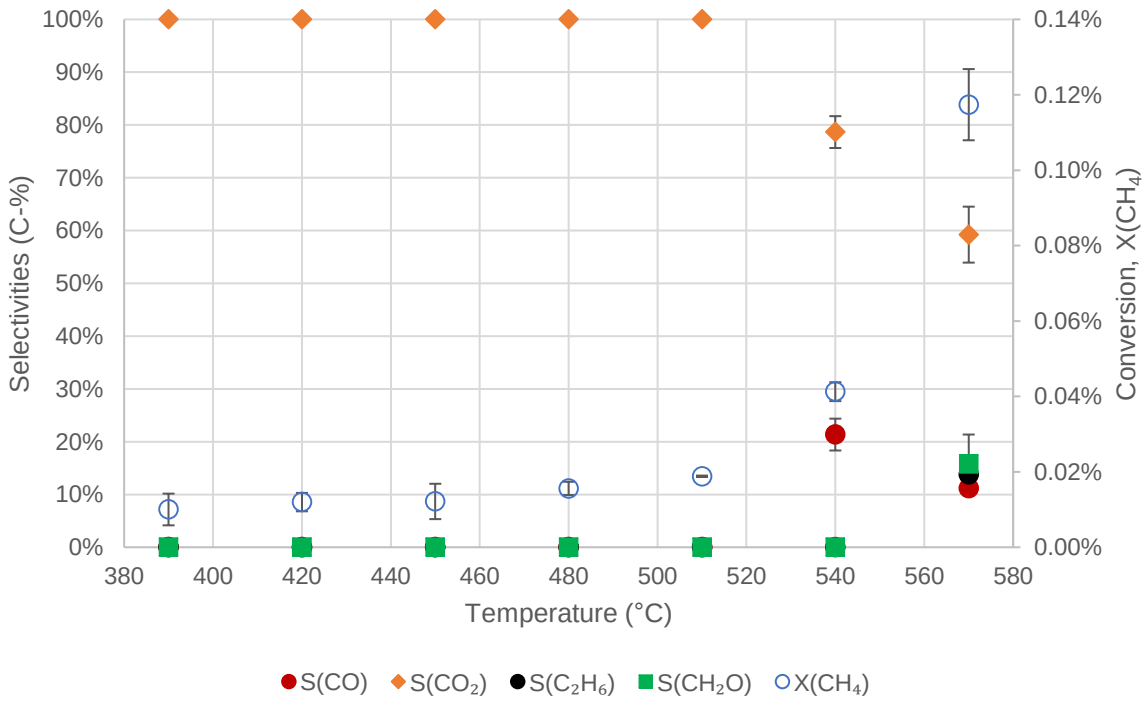

Figure 5.7: Temperature vs conversion and selectivities plot for autocatalytic conversion of methane to methanol at 40 bar with a feed of 28 $ml_n.min^{-1}$ CH_4, 2.8 $ml_n.min^{-1}$ O_2 and 8.3 $ml_n.min^{-1}$ He

Compared to the autocatalytic experiment carried out by Zhang et al. [1] in an empty quartz reactor, the conversion obtained in our reactor is extremely low. At a pressure of 40 bar and a temperature of 450 °C Zhang et al. [1] obtained a methane conversion of 12.5 % with a feed of 100 $ml_n.min^{-1}$ CH_4, 10 $ml_n.min^{-1}$ O_2 and 10 $ml_n.min^{-1}$ N_2 (a reactor productivity of 97

$\frac{mol_{CH4\ converted}}{min.m^3_{rctr\ volume}}$). While we only obtained a conversion of 0.01 % at the same temperature and pressure. Although the gas space velocity in our experiment was twice as fast as that used in Zhang et al. [40], at 0.04 s^{-1} as oppose to 0.02 s^{-1}, it cannot explain the 1000-fold decrease in conversion. Later, it was discovered that the quartz liner in our reactor had been broken during this experiment. The broken quartz liner led to a highly diluted reactor feed in argon and the contact of the reactant gases with the metal wall of the reactor shell. Therefore, at the end of any experiment where the conversion appeared very low, the reactor should be disassembled to check whether the quartz liner is still intact.

5.2.3 Experiment 3

At the end of this study, the autocatalytic conversion of methane to methanol was attempted again using a feed of 39 $ml_n.min^{-1}$ CH_4, 3.9 $ml_n.min^{-1}$ O_2 and 5.7 $ml_n.min^{-1}$ of N_2 under a total pressure of 40 bar. N_2 was used instead of helium as the helium cylinder have been depleted down to 35 bar, too low to allow the reaction to be carried out at 40 bar (see Appendix I for calibration curve). The experiment was started at 545 °C and carried out with a temperature program where the temperature is decreased in steps of 10 °C at 0.5 °C.min^{-1} and held at each new temperature for 4 h. Instead of using an empty reactor, the reactor was packed with 300 µm silicon carbide particles for this experiment. The time on stream vs conversion and selectivities plot for this experiment is shown in Figure 5.8. An identified minor product (selectivity < 0.1 C-%) was formed at higher temperatures and has a retention time of 2.7 min was detected, which is likely to be ethene. The oxygen conversion was calculated assuming RT 2.7 is ethene and no hydrogen is produced in the reactor, i.e. all hydrogen atoms from the feed is either part of the detected carbon compounds or is oxidized to water.

Compared to the previous experiment much greater conversion was achieved in this experiment despite of the slightly higher space velocity (0.06 s^{-1} compared to 0.04 s^{-1} in the previous experiment), as the quartz reactor liner was intact throughout the experiment. A maximum methane conversion of around 5 % was reached at 485 °C, with higher temperatures unable to increase the conversion any further. Assuming a packing voidage of 0.5, the reactor productivity in this experiment at 5 % methane conversion is 282 $\frac{mol_{CH4\ converted}}{min.m^3_{rctr\ volume}}$, comparable in orders of magnitude to the 97 $\frac{mol_{CH4\ converted}}{min.m^3_{rctr\ volume}}$ obtained by Zhang et al. [1]. The difference in productivity is likely due to the temperature sensitivity of the radical autocatalytic reaction, especially considering both Zhang et al. [1] and our reactor does not have a perfect isothermal temperature profile.

The temperature vs conversion and selectivities of this experiment is presented in Figure 5.9. Instead of using only the last three data points as in the previous experiment, all the data points from each temperature is used to calculate the conversion, selectivities and error bar in Figure 5.9. This meant to 8 samples taken for each temperature (out of the 10 data points taken, the 2 data point at the start and end of a temperature step is discarded). The methanol selectivity peaked at around 30 % at a methane conversion of 1.5 % before falling off at higher temperatures and conversions in favour of CO. Interestingly, at very low conversions (T < 450 °C), formaldehyde was observed as the major product. At higher temperatures (> 500 °C), small amounts of ethane and possibility ethene (RT 2.7) is formed, both showed increase in selectivity as temperature increased reaching a selectivity of 0.2 C-% RT 2.7 and

2 C-% ethane at 545 °C. Small amounts of methyl formate is detected throughout the experiment, with a maximum selectivity of 0.7 C-%.

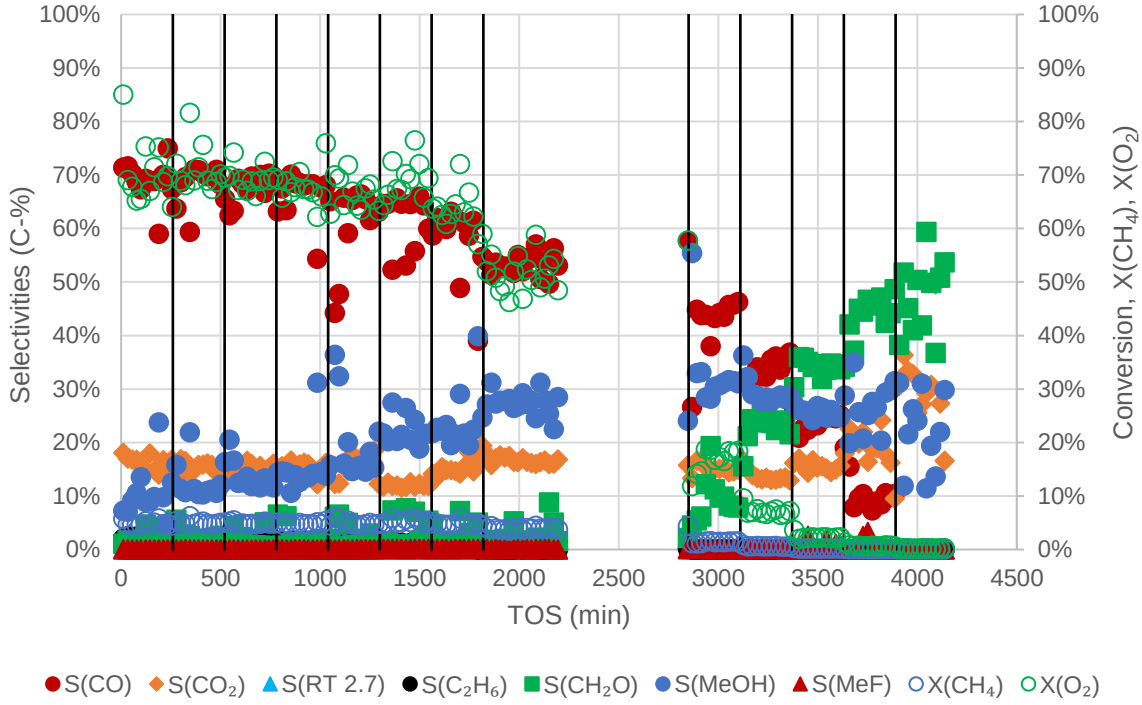

Figure 5.8: Time on stream vs conversion and selectivities plot for autocatalytic conversion of methane to methanol at 40 bar with a feed of 39 $ml_n.min^{-1}$ CH_4, 3.9 $ml_n.min^{-1}$ O_2 and 5.7 $ml_n.min^{-1}$ N_2, starting at 545 °C; solid vertical line indicate temperature decrease of 10 °C, down to 425 °C

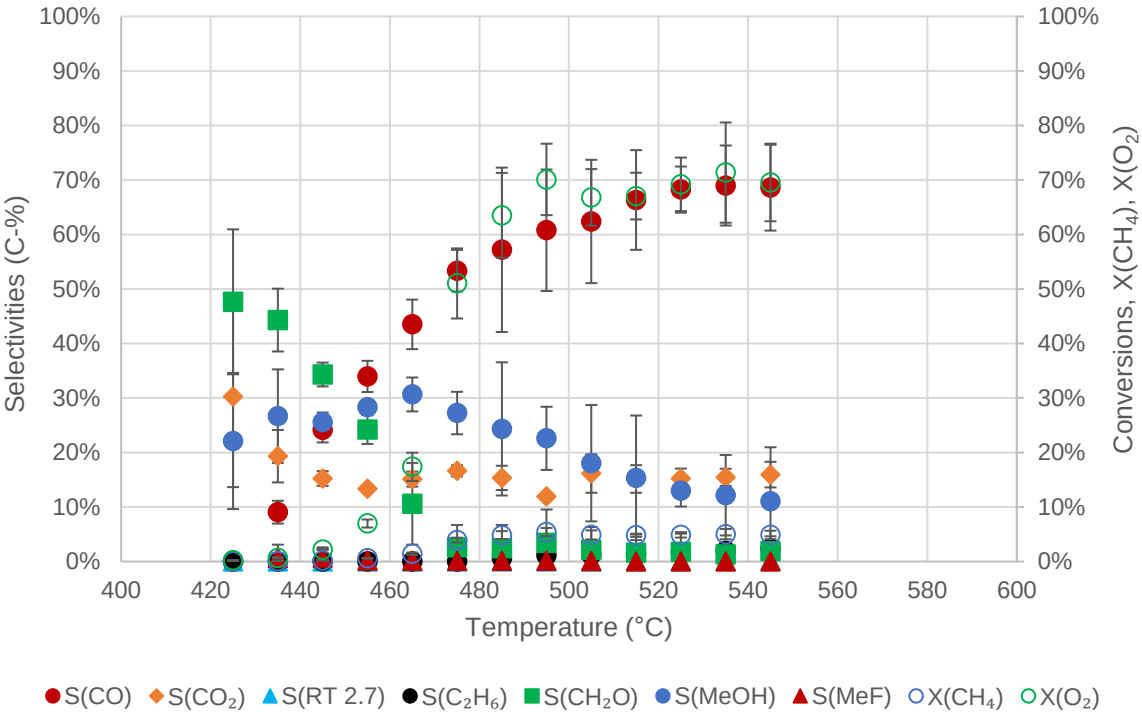

Figure 5.9: Temperature vs conversion and selectivities plot for autocatalytic conversion of methane to methanol at 40 bar with a feed of 39 $ml_n.min^{-1}$ CH_4, 3.9 $ml_n.min^{-1}$ O_2 and 5.7 $ml_n.min^{-1}$ N_2

However, large scatter in the data is observed during this experiment, evident from Figure 5.8 and the error bars in Figure 5.9. Similar scattering is observed in the total peak area shown in Figure 5.10. The total peak area is seen to continuously increase for the first 1500 min of the experiment, nullifying the null hypothesis of the irrelevance between total peak area and time on stream. The total peak area remained relatively stable between 1500 min and 3000 min before decreasing and settling again after 3500 min.

This is either a temperature effect, as large scatter in the total peak area was also observed in the methanol stability tests at temperatures higher than 400 °C. Since we do not anticipate carrying out catalytic methane to methanol conversion at such high temperatures, the reactor temperature profile was only measured at 200 °C. It is likely that the reactor temperature profile is not as uniform at temperatures > 400 °C as it is at 200 °C. Any fluctuation in temperature will translate to fluctuations in conversions and selectivities as the autocatalytic reaction is highly sensitive to temperature.

However, this does not explain the slow increase and then decrease in total peak area throughout the experiment as temperature starts to decrease, nor does it explain why the previous autocatalytic experiment showed consistent total peak areas despite of the use of high temperatures (see Figure 5.6). The methane flow controller was set to 99 % of its maximum flow during this experiment as opposed to 71 % in the previous experiment. The combination of the high set point and high pressure during the experiment may lead to the methane flow rate to drift and/or scatter during the experiment, explaining the changes in total peak area due to the changes in carbon molar flow rate into the reactor. Moreover, the changes in total peak area may possibly be caused by the 6-way sampling valve, as it started to malfunction soon after this experiment and had to be replaced.

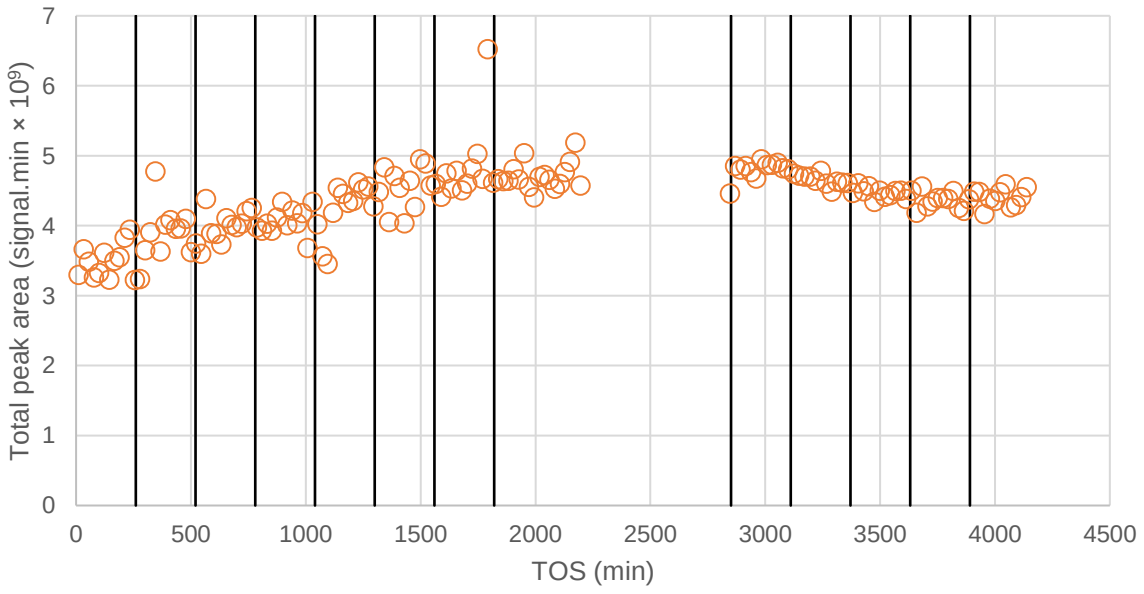

Figure 5.10: Total peak area vs time on stream plot for autocatalytic conversion of methane to methanol starting at 40 bar and 545 °C, with a feed of 39 $ml_n.min^{-1}$ CH_4, 3.9 $ml_n.min^{-1}$ O_2 and 8.3 $ml_n.min^{-1}$ He; solid vertical lines indicate a temperature decrease of 10 °C

5.2.4 Summary of autocatalytic conversion of methane to methanol

Although the autocatalytic conversion of methane to methanol is not of prime interest, the three autocatalytic experiments carried out does show that the reactor system is able to measure conversion and selectivities during the conversion of methane to methanol with oxygen as an oxidant. The total peak area can be used to infer carbon mass balance as expected in experiment 1. However, it is not a great way of confirming the mass balance as a lot of other factors can influence it, evident from the variation in total peak area during experiment 3. Experiment 2 shows the importance of dissembling the reactor as a method of diagnosing low conversions, since the quartz reactor liner is rather fragile and may break inside the reactor.

In terms of conversion and selectivity, experiment 3 shows a maximum methane conversion of 5 % and a maximum methanol selectivity of 30 C-%, with methanol selectivity falling off at increasing conversions/temperature. The maximum yield of methanol occurred at 495 °C with a methane conversion of 5.4 % and a methanol selectivity of 22.6 C-%, leading to a methanol yield of 1.2 C-%. This is still too low for the 10 % methane conversion and 80 C-% methanol selectivity required for an industrially relevant direct methane to methanol conversion process. It should be noted however, since the methane is fed in large excess. The maximum conversion of methane to methanol in experiment 3 is only 20 %, and the 5 % methane conversion we obtained represent 25 % of the maximum methane conversion achievable.

As discussed in the introduction, it is difficult to control the autocatalytic conversion of methane to methanol and hence its yield remains low. The next two series of experiment will investigate whether the conversion of methane to methanol can be improved using platinum-based catalysts with and without the co-feeding of water, over two different promoted platinum catalysts, Pt_3Mo and Pt_3Bi.

5.3 Catalytic conversion of methane to methanol over Pt_3Mo catalyst

The first catalyst tested in the packed bed reactor for methane to methanol conversion was an in-house prepared Pt_3Mo catalyst. This catalyst was prepared by impregnating Pt_3Mo nanoparticles on titanium oxide support with a Pt_3Mo loading of 1 wt.%. The titanium oxide support has a particle size of 100 nm and is too small to be used in the packed bed reactor. Therefore, the catalyst was mixed with silicon carbide particles with a diameter of 300 µm roughly 1:1 by volume.

However, at the time this experiment was started we did not have any spare quartz reactor liner tube on hand. It was decided to carry out 2 exploratory experiment using only the stainless-steel reactor shell. The middle 8 cm of the stainless-steel reactor shell was packed with the silicon carbide diluted catalyst particles containing approximately 500 mg of catalyst particles. Since no quartz liner is used, the argon make-up stream is moved to connect with the reactor effluent instead, identical to the preliminary flowsheet of the reactor shown in Figure 3.12.

5.3.1 Experiment 4

The first experiment was done using a feed of 3.4 $ml_n.min^{-1}$ CH_4, 35 $ml_n.min^{-1}$ O_2 and 8.3 $ml_n.min^{-1}$ He, under a total pressure of 32.5 bar. The resulting fed mixture would have

partial pressures of 2.4 bar CH_4, 24.4 bar O_2 and 5.8 bar He, with oxygen partial pressure being the highest. The experiment was carried out over a temperature range of 150 °C to 400 °C. The conversion and selectivities plot for this experiment is shown in Figure 5.11. The methane was fully converted at 400 °C, however the major product observed was CO_2. Additionally, since no quartz reactor liner was used, we cannot eliminate the possibilities that the metal reactor surface was catalytically active in this experiment. The selectivities for minor products such as CO and methanol was seen to decrease with increasing temperature and conversion, while the selectivity for formaldehyde peaked at around 200 °C to 250 °C (no formaldehyde was formed at 150 °C). Another minor product with a retention time of 9.2 min was detected but not identified. The number of samples taken at each temperature is much smaller in this experiment at less than 3 (can be read in Figure 5.12) since we had not started with automatic sampling yet.

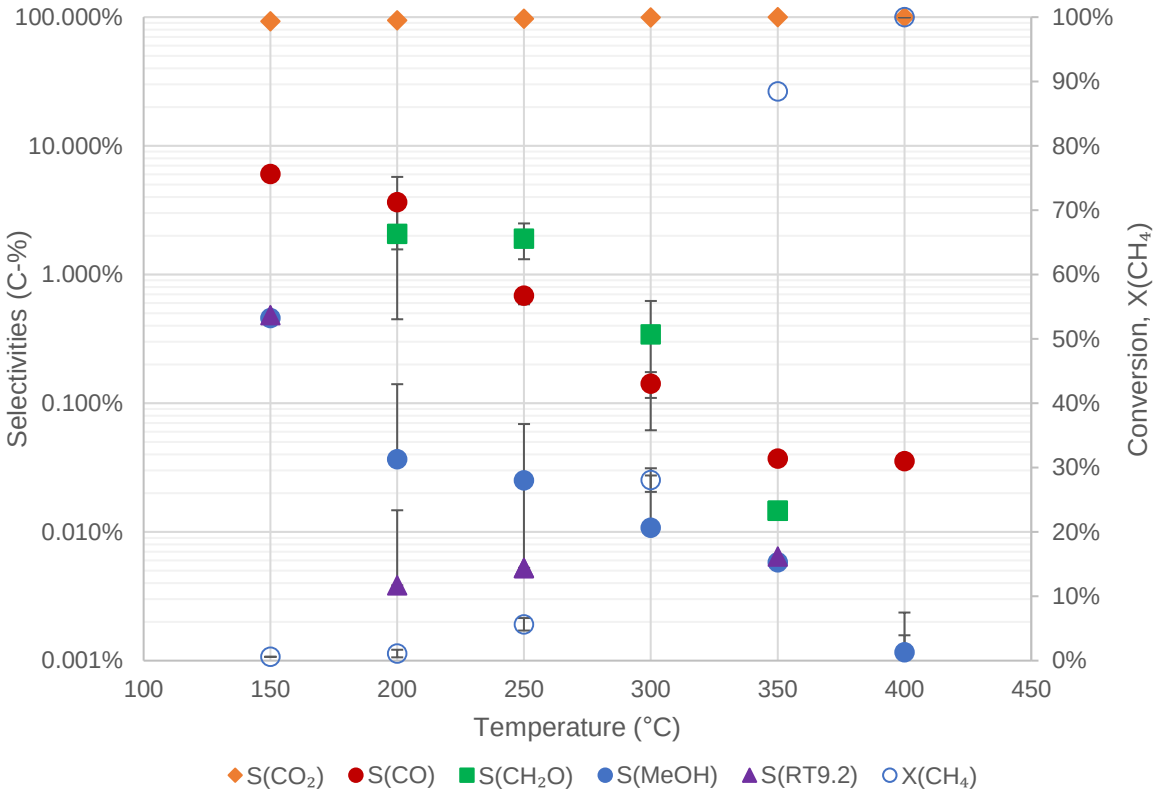

Figure 5.11: Temperature vs conversion and selectivities plot for conversion of methane to methanol over Pt_3Mo catalyst with a feed of 3.4 $ml_n.min^{-1}$ CH_4, 35 $ml_n.min^{-1}$ O_2 and 8.3 $ml_n.min^{-1}$ He at 32.5 bar without using reactor quartz liner

The measured conversion of methane can be verified by looking at the total peak area vs time on stream plot for this experiment (see Figure 5.12). The total peak area was not related to the time on stream with a P-value of 0.07 supporting the null hypothesis. Throughout the experiment, the total peak area varied less than 5 % from its mean value. As this experiment spans over the entire conversion range for methane, we can also establish the carbon mass balance is within 5 %, due to how the total peak area is reflective of the carbon molar flow rate out of the reactor system.

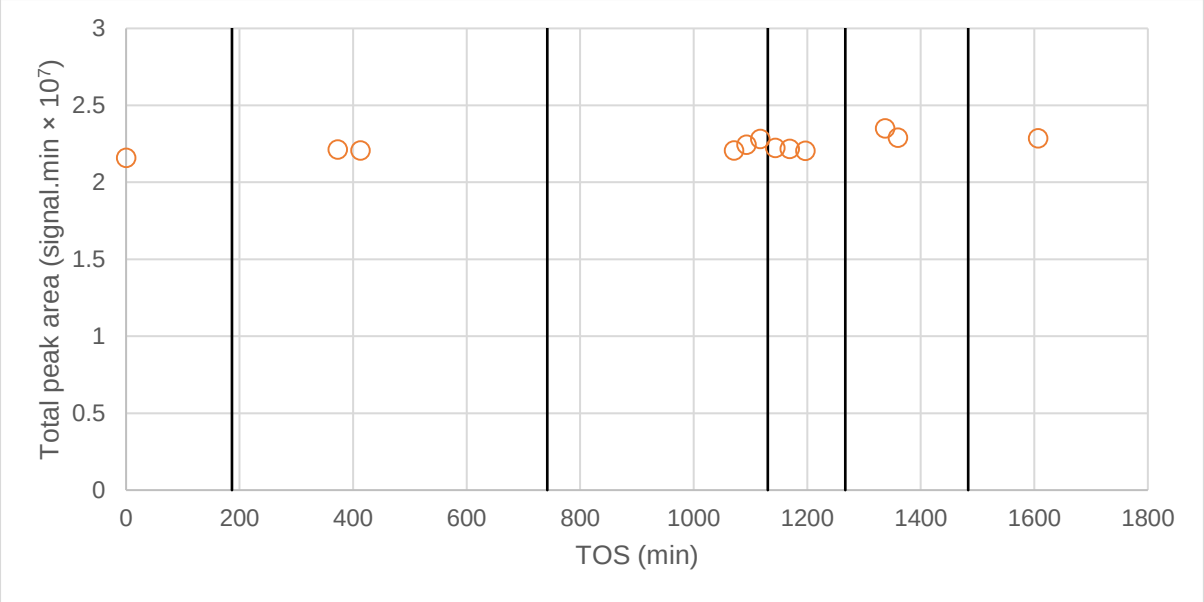

Figure 5.12: Total peak area vs time on stream plot for the experiment shown in Figure 5.11, starting at 150 °C, vertical line indicate temperature changes; 1st line: 200 °C, 2nd line 250 °C, 3rd line: 300 °C, 4th line: 400 °C, 5th line: 350 °C

5.3.2 Experiment 5

The second experiment was done using a feed of 4.5 $ml_n.min^{-1}$ CH_4, 6.5 $ml_n.min^{-1}$ O_2 and 35 $ml_n.min^{-1}$ He, under a total pressure of 16.5 bar. The resulting fed mixture would have partial pressures of 1.6 bar CH_4, 2.3 bar O_2 and 12.6 bar He, with methane and oxygen partial pressure being roughly similar. The experiment was carried out over a temperature range of 260 °C to 360 °C. The major product observed was CO_2 and the only minor product observed was ethane, with its selectivity decreasing with increasing temperature and conversion (see Figure 5.13) but still remaining in the sub 0.1 % range. The maximum conversion of methane to CO_2 under this experiment's condition is 72 % due to oxygen being a limiting reagent. The maximum measured conversion in this experiment was 76 %, the discrepancy is likely due to errors in the mass flow controllers. The reactor quartz liner was not used in this experiment, and the metal reactor surface can possibility be catalytically active in this experiment.

Similar to experiment 1, the measured conversion of methane can be verified by looking at the total peak area vs time on stream plot for this experiment (see Figure 5.14). The total peak area showed some scatter at temperatures higher than 320 °C (time on stream past 500 min) and showed a slight increase throughout the experiment. The null hypothesis for the irrelevance between total peak area and time on stream only holds before time on stream of 500 min (T < 320 °C) with a P-value of 0.28.

Throughout the entire experiment, the total peak area varied less than 18 % from its mean value. As this experiment spans over a large conversion range for methane, we can also establish the carbon mass balance is within 18 %. At temperature below 320 °C and time on stream under 500 min, the total peak area only varied 4 % from its mean value, indicating the mass balance for carbon was more accurate at temperatures below 320 °C and methane conversion below 30 %.

Although, no reactor quartz liner was used in the first two experiments and hence the catalytic performance of the Pt_3Mo catalyst cannot be isolated from the catalytic effects of the stainless-steel reactor wall. The two experiments do show the reactor system is capable of measuring conversion in the conversion of methane to methanol reaction as well as selectivities data down to 0.001 %. The conversion data obtained in these two experiments are also supported by the carbon mass balance obtained from observing the total peak area throughout the experiment. The number of samples taken at each temperature can be read from Figure 5.14.

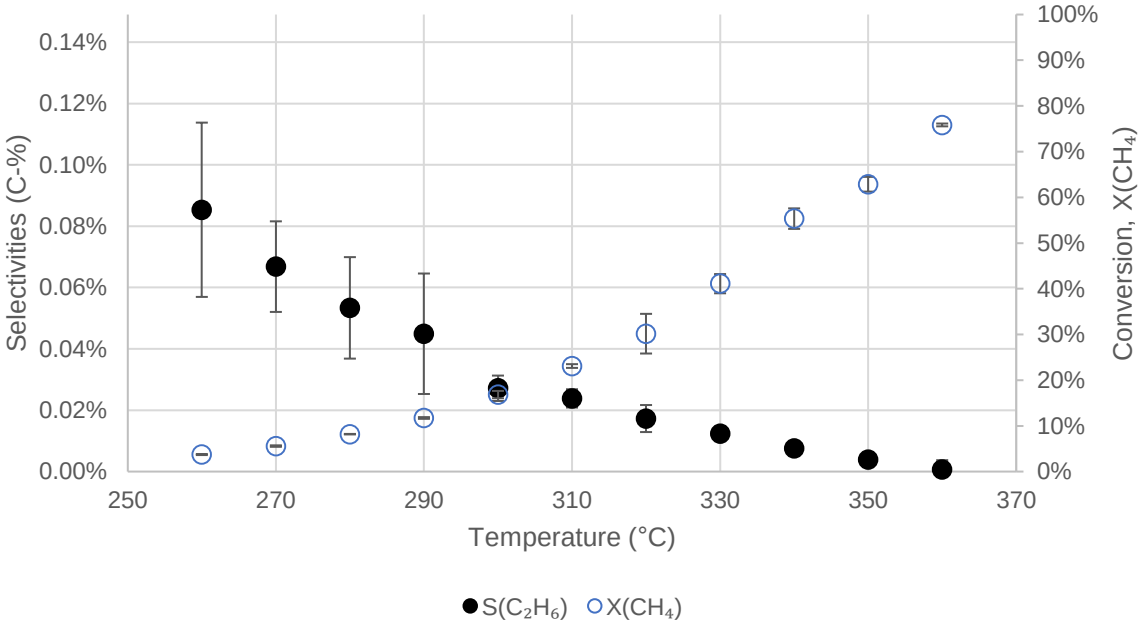

Figure 5.13: Temperature vs conversion and selectivities plot for conversion of methane to methanol over Pt_3Mo catalyst with a feed of 4.5 $ml_n.min^{-1}$ CH_4, 6.5 $ml_n.min^{-1}$ O_2 and 35 $ml_n.min^{-1}$ He at 16.5 bar without using reactor quartz liner (selectivity of the only other product, CO_2, is omitted)

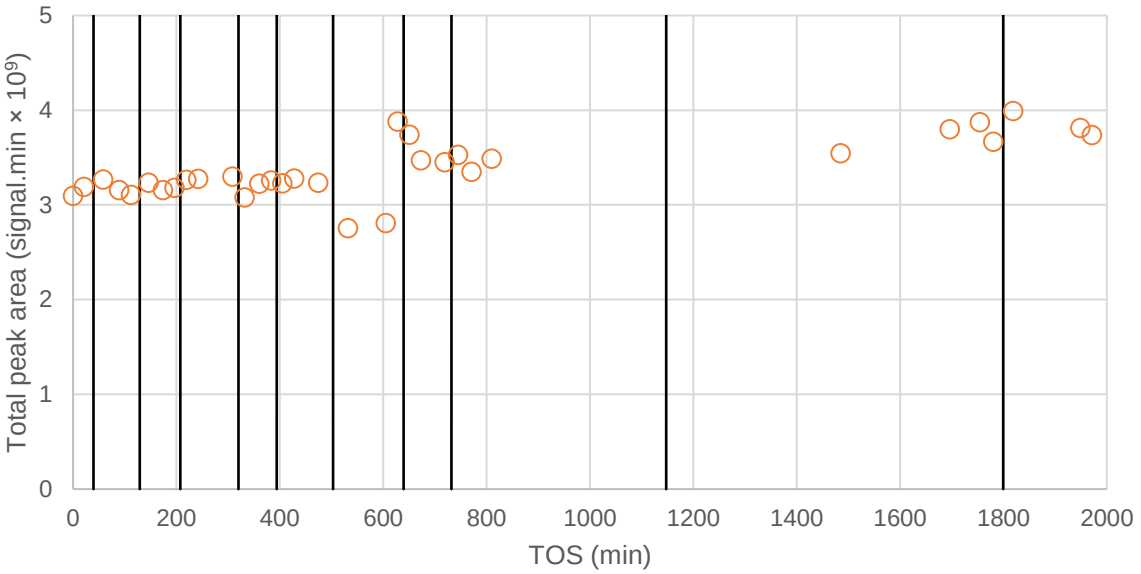

Figure 5.14: Total peak area vs time on stream plot for the experiment shown in Figure 5.13, starting at 260 °C, vertical lines indicate temperature increase of 10 °C, up to 360 °C

5.3.3 Experiment 6

After the first 2 experiments were complete, more reactor quartz tubes were obtained, and the subsequent experiments were carried out with the reactor quartz liner in place as intended. The same Pt_3Mo catalyst diluted in 100 µm diameter silicon carbide was packed in the middle 8 cm of the reactor quartz liner. Due to the small diameter of the reactor quartz liner (2.4 mm compared to 4.9 mm for the reactor shell), only approximately 100 mg of active catalyst particles were packed in the reactor (excluding silicon carbide mixed with the catalyst in a rough ratio of 1:1 by volume). Experiment 3 was done using a feed of 4.5 $ml_n.min^{-1}$ CH_4, 5 $ml_n.min^{-1}$ O_2, 34 $ml_n.min^{-1}$ He and 25 $ml_n.min^{-1}$ of $H_2O_{(g)}$, under a total pressure of 20 bar. No oxygen was fed in the beginning of the experiment, with it only switched on half way through the experiment. The resulting mixture would have partial pressures given in Table 5.2 inside the reactor if it remains in the gas phase.

Table 5.2: Partial pressures of reactor feed gas in experiment 6

Gases	Reactor Partial Pressure (bar)	
	No O_2 fed	O_2 fed
He	10.7	10.3
O_2	0	0.7
CH_4	1.4	1.4
H_2O	7.9	7.6

The experiment was carried out at temperatures less than 200 °C and with no oxygen fed initially. The initial temperature was at 100 °C, before being decreased to 50 °C. The oxygen flow was switched on whilst the reactor was at 50 °C and the temperature subsequently increased to 200 °C in steps of 25 °C. The conversion and selectivities vs time on stream plot of this experiment is shown in Figure 5.15. Below 175 °C, the major product was the unidentified compound with a retention time of 9.2 min, while above 175 °C the major product was CO_2. The overall conversion fluctuated around 0.1 % and did not respond to temperature, i.e. no increase in conversion with increase in temperature. A minor product with a retention time of 14.1 min was observed in a small number of the samples. Using a conversion of 0.1 % and assuming 25 % of the atoms in the Pt_3Mo catalyst is on the surface and considered as an active site, the turn over frequency of the catalyst is estimated as 8.2 h^{-1}. This is comparable to the 5.6 h^{-1} obtained by Al-Shihri et al. [35] using ZSM-5 catalyst and hydrogen peroxide as the oxidant at 50 °C.

It is noted that under the feed conditions and total pressure for this experiment. The water partial pressure in the reactor was 7.9 bar with no oxygen fed and 7.6 bar with oxygen fed, corresponding to a condensation temperature of 171 °C and 169 °C respectively. Therefore, below the temperature was increased to 175 °C the steam fed into the reactor would have condensed, leading to a triphasic mixture in the reactor. This introduced a mass transfer limitation for the reaction as the gaseous reactant would have to diffuse through liquid water before reaching the active catalyst surface. This transport limitation could explain the low conversion and how it did not change with increasing temperature. The conversion of methane

before oxygen was fed could possibly be caused by the minor amounts of oxygen dissolved in the deionized water fed. After the reactor was heated significantly over the condensation point of water at 200 °C the selectivity of RT 9.2 dropped significantly, ending at 0 % with all product observed being CO_2.

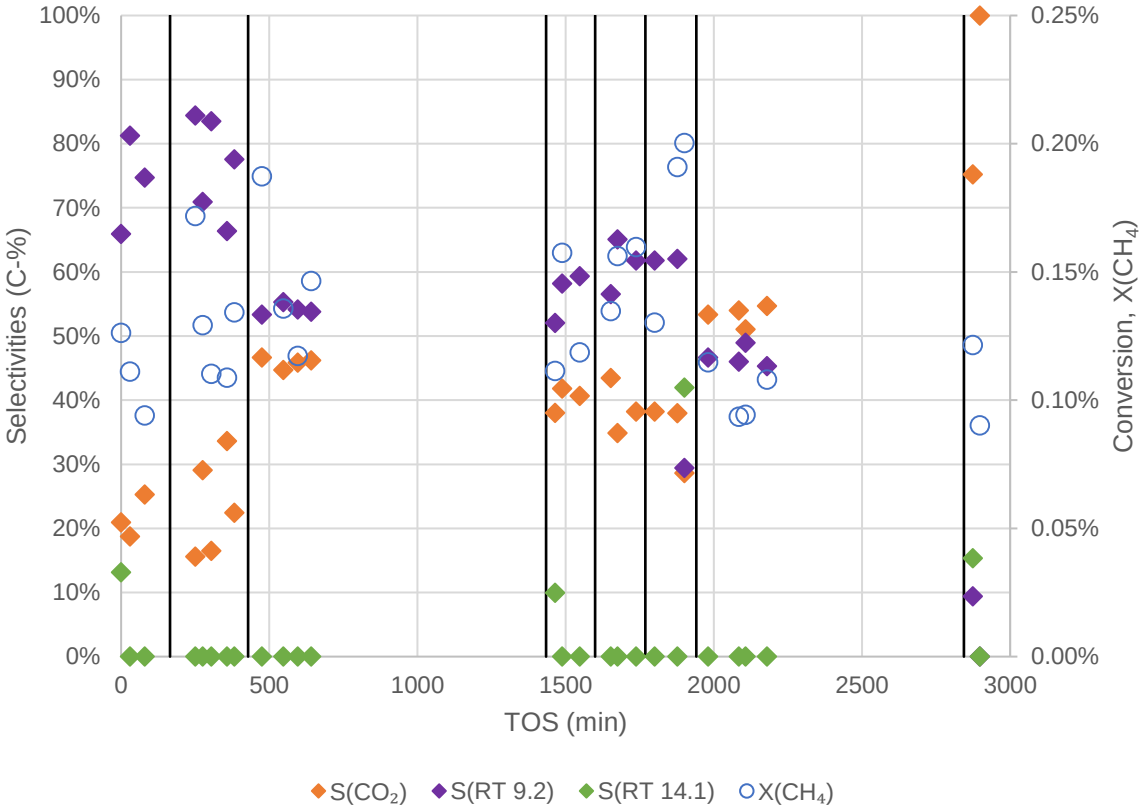

Figure 5.15: Time on stream vs conversion and selectivities plot for conversion of methane to methanol over Pt_3Mo catalyst starting with a feed of 4.5 $ml_n.min^{-1}$ CH_4, 34 $ml_n.min^{-1}$ He and 25 $ml_n.min^{-1}$ of $H_2O_{(g)}$ at 20 bar and 100 °C, solid vertical line indicates condition changes, first line: temperature decreased to 50 °C; second line: 5 $ml_n.min^{-1}$ O_2 added to the feed; third line: temperature increased to 100 °C; subsequent lines indicate a temperature increase of 25 °C (125 °C, 150 °C, 175 °C, 200 °C)

The total peak area for this experiment (see Figure 5.16) was independent on the time on stream with a P-value of 0.47 supporting the null hypothesis. However, a large scatter was observed in the total peak area. The total peak area in Figure 5.16 fluctuated 50 % relative to the mean total peak area of 7×10^8 signal.min. This scatter is most likely due to the erratic flow behaviours of the triphasic mixture in the reactor caused by the condensing steam which altered the total flow rate through the reactor as it condenses and reevaporates uncontrollably. The variation in the total flow rate through the reactor acts as a variable dilution ratio and hence caused the total peak area to scatter.

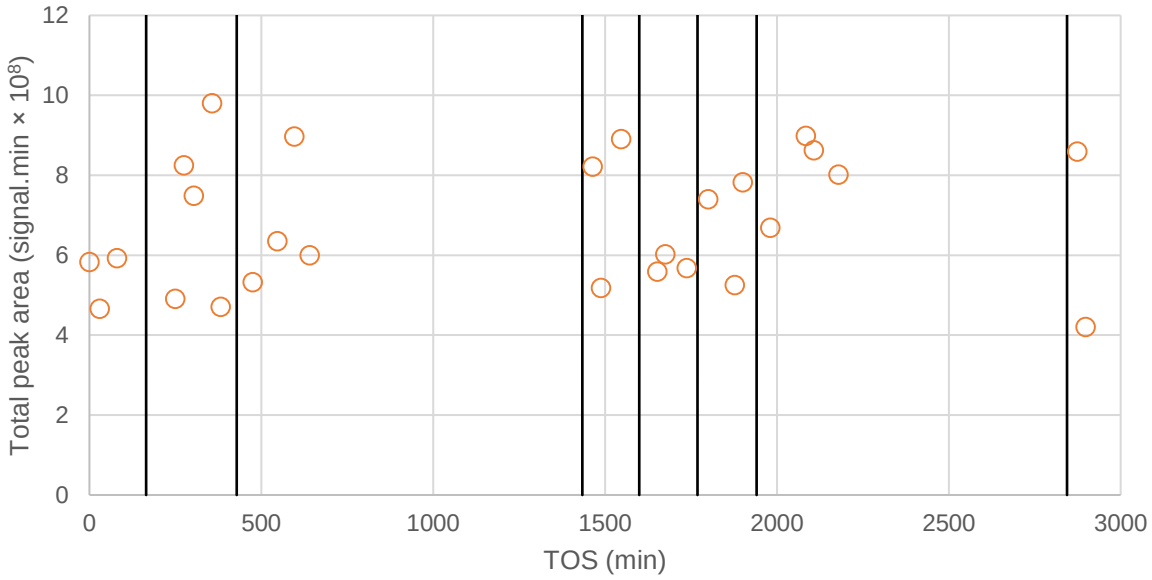

Figure 5.16: Total peak area vs time on stream plot for the experiment shown in Figure 5.15, vertical line indicates the same condition changes described in Figure 5.15

5.3.4 Experiment 7

A second experiment was carried out over the same Pt_3Mo catalyst inside the reactor quartz liner using a fed 4.5 $ml_n.min^{-1}$ CH_4, 5 $ml_n.min^{-1}$ O_2, 34 $ml_n.min^{-1}$ He and 50 $ml_n.min^{-1}$ of $H_2O_{(g)}$, under a total pressure of 25 bar. Compared to experiment 6, the steam flow rate was doubled and the total reactor pressure increased by 5 bar. Contrary to the previous experiment, the oxygen flow was on initially in experiment 7 and switched off half way through the experiment. The reactor feed partial pressures are tabulated in Table 5.3.

Table 5.3: Partial pressures of reactor feed gas in experiment 7

Gases	Reactor Partial Pressure (bar)	
	O_2 fed	No O_2 fed
He	9.3	9.6
O_2	0.6	0
CH_4	1.2	1.3
H_2O	13.8	14.2

Experiment 7 was carried out at higher temperatures than experiment 6 at 150 °C – 300 °C. The condensation temperature of the steam in the experiment would be 196 °C and 195 °C, with and without O_2 fed respectively. The conversion-selectivities plot for experiment 7 is shown in Figure 5.17. In terms of selectivities, the same trend was observed as in experiment 6. Below the condensation temperature of steam of 195 °C, the unidentified compound with the retention time of 9.2 min was the major product while above the condensation temperature CO_2 was the major product. The unidentified compound with a retention time of 14.1 min were observed in some of the samples.

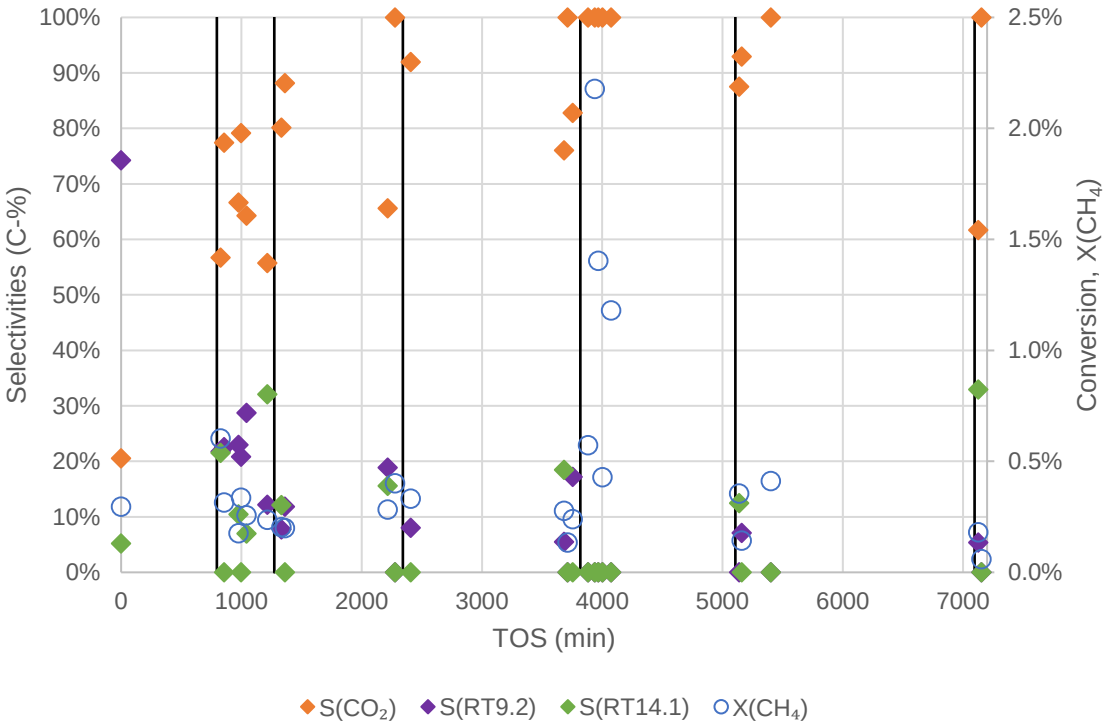

Figure 5.17: Time on stream vs conversion and selectivities plot for conversion of methane to methanol over Pt_3Mo catalyst starting with a feed of 4.5 $ml_n.min^{-1}$ CH_4, 5 $ml_n.min^{-1}$ O_2, 34 $ml_n.min^{-1}$ He and 50 $ml_n.min^{-1}$ of $H_2O_{(g)}$ at 25 bar and 150 °C, solid vertical lines indicate condition changes, first line: temperature increased to 250 °C; second line: temperature increased to 275 °C; third line: temperature increased to 300 °C; 4th line: oxygen flow turned off; 5th line: temperature decreased to 275 °C; 6th line: temperature decreased to 250 °C

The conversion remained low during experiment 7, with most conversions remaining in the approximate 0.25 % range and did not increase significantly at higher temperatures. Assuming the conversion is constant at 0.25 % and 25 % of the Pt_3Mo is on the surface and considered active, the estimated TOF for this experiment is 20.5 h^{-1}. In terms of total peak area, we would expect it to be more consistent in this experiment than in experiment 6 as most of the experiment was carried out at temperatures where steam will not condense in the reactor. However, the total peak area still varied 93 % from its mean value of 0.7×10^8 signal.min throughout the experiment (see Figure 5.18) although its variation is not dependent on the time on stream with a P-value of 0.32 supporting the null hypothesis. If this variation in total peak area is indicative of variation in the carbon molar flow rate through the reactor, then the conversion data obtained may not be relied upon, as the carbon molar flow rate fed to the reactor was constant throughout the experiment.

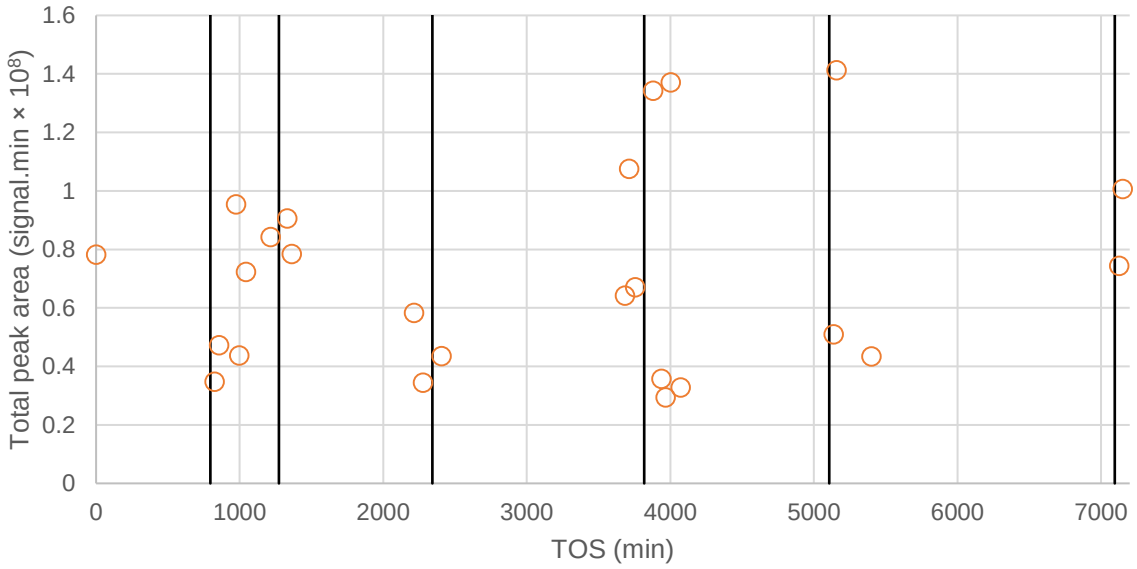

Figure 5.18: Total peak area vs time on stream plot for the experiment shown in Figure 5.17, vertical line indicates the same condition changes described in Figure 5.17

5.3.5 Summary of Pt-Mo experiments

The four exploratory experiments carried out with the Pt_3Mo catalyst have shown that using the Pt_3Mo catalyst in the packed bed methane to methanol conversion reactor was unable to selectively convert methane to methanol.

However, the first two experiments carried out without the reactor quartz liner have showed the reactor system is able to measure the conversion and selectivities in the conversion of methane to methanol via methane partial oxidation over the entire conversion range. Due to the use of the Polyarc™ reactor in our GC, the total peak area from each GC analysis can be used to ascertain steady state carbon molar flow rate through the reactor and hence confirm the carbon mass balance in these two experiments.

In the first two experiments, CO_2 was observed as the major product. In the first experiment carried out under high oxygen partial pressure of 24 bar, CO, formaldehyde, methanol and an unidentified compound with a retention time of 9.2 minutes were observed as minor products. In the second experiment under a much lower oxygen partial pressure of 2.3 bar, only ethane was observed as the minor product.

Since no reactor quartz liner is used, the performance of the Pt_3Mo catalyst in these two experiments cannot be isolated from the stainless-steel reactor shell, which can be catalytical active in methane partial oxidation reactions [23], hence the TOF of the catalyst was not calculated for these two experiments. However, the change in the selectivity of the minor products is significant and can indicate a change in reaction mechanisms over the catalyst surface. As under high oxygen partial pressures oxygenated minor products were detected while under low oxygen partial pressures only ethane was detected as a minor product from the oxidative coupling of methane.

The last two experiments were carried out with steam co-feeding and with the reactor quartz liner in place. The conversions obtained from these two experiments were both very low at < 1 % and did not respond to changes in temperature. The TOF of the catalyst was estimated

in these two experiments to be 8.2 h^{-1} and 20.5 h^{-1} respectively. Furthermore, large scatter in the total peak area were also observed in these two experiments.

The third experiment was mostly carried out at temperature where the steam fed into the reactor would have condensed into liquid water. The resulting triphasic mixture in the packed bed reactor will have erratic flow patterns and the gaseous reactants may be mass transfer limited if it must diffuse through liquid water to reach the catalyst surface. This is a possible reason for the low conversion. In this experiment, major product observed was an unidentified compound with a retention time of 9.2 min. One possible candidate for this compound may be methane hydroperoxide, a major product observed in the triphasic conversion of methane to methanol using methane, oxygen and aqueous hydrogen peroxide over an Au-Pd catalyst [34]. Another possibility is ethanol, observed as a major product during the conversion of methane to methanol with oxygen as the oxidant and water co-feeding over $NiO\text{-}CeO_2/ZrO_2$ [29]. However, this is not likely as the retention time of pure ethanol was determined on our GC to be 8.6 min.

In the fourth experiment, higher temperatures were used to prevent water condensation and the selectivity of the catalyst changed in favour of CO_2. Although the conversion was still very low and did not respond to changes in temperature. The change in selectivity could either be a result of the lack of liquid water, as liquid water can possibly extract hydrophilic reaction product/intermediate (unidentified compound, RT 9.2) or due to the change in temperature needed to prevent condensation.

This highlights one of the unforeseeable issues with our hypothesised scenario of using high oxygen and water partial pressures to increase the selectivity in the conversion of methane to methanol over platinum-based catalysts. As the water partial pressure is thermodynamically linked to the reaction temperature, with higher water partial pressures in the reactor requiring the use of higher temperatures to prevent condensation. Taken the condensation of water into account, we can redraw the phase diagram of Pt (111) and (100) surfaces presented in Figure 1.3 (see Figure 5.19). In Figure 5.19, the limit of water and oxygen partial pressures is added to the phase diagram. The oxygen partial pressures are limited to the maximum reactor pressure of 50 bar, whilst the water partial pressure is limited to its condensation pressure (0.5 bar at 80 °C, 15.3 bar at 200 °C) and the maximum reactor pressure of 50 bar (at 400 °C beyond the critical point of water). Evident from Figure 5.19, the regions where the Pt surfaces are fully covered with oxygen species are much smaller and are limited to lower temperatures of < 200 °C. As the computational model used to derive Figure 1.3 may not be fully accurate and the catalyst used in the four above mentioned experiments used Pt_3Mo alloy catalyst instead of pure platinum. In reality we may not be able to achieve full oxygen species coverage under the conditions of the four above mentioned experiments. Thus, leading to the formation of deep oxidation products instead of methanol.

Another unexplained phenomenon in the last two experiments conducted using Pt_3Mo catalyst is the large scattering in total peak area, which should stay constant as the molar flow rate of carbon fed is constant through the entire experiment. The scattering in the total peak area for experiment 6 can be explained by the erratic flow patterns in the reactor due to the triphasic mixture present in the reactor due to steam condensation. In experiment 7, the temperature was high enough to prevent condensation, however the same large scatter in total peak area was observed. The reason for this scattering was found during the disassembly of the reactor at the

end of these experiments. During the last two experiments, the initial catalyst bed containing a 1:1 mixture by volume of fine catalyst particles (100 nm in diameter) and silicon carbide dilutant (300 µm in diameter) have separated into collapsed sections of compacted fine catalyst particles, void spaces and silicon carbide (see Figure 5.20). This non-uniform catalyst bed means the flow pattern in the reactor will deviate extremely from ideal plug flow. The resulting erratic flow pattern is likely the result of the scattering in the total peak area as well as the low conversions obtained in experiment 6 and 7, due to dead volumes, channelling and the bypassing of the compacted sections of consolidated fine catalyst particles.

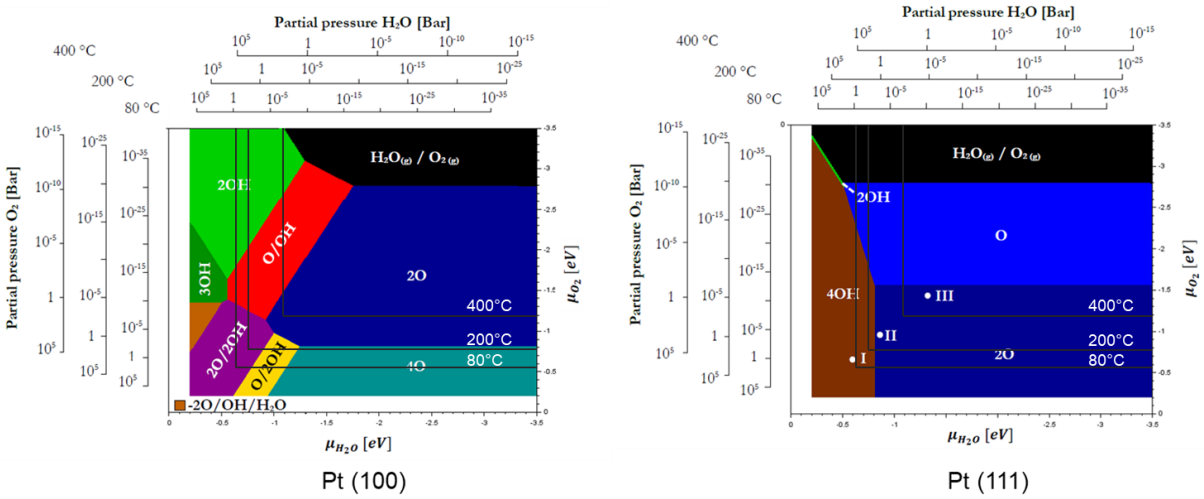

Figure 5.19: Phase diagram of Pt (100) and Pt (111) surfaces in the co-adsorption of oxygen and steam, regions to the left and below the solid lines are impossible to achieve for the given temperature, modified from Cilliers (2017)

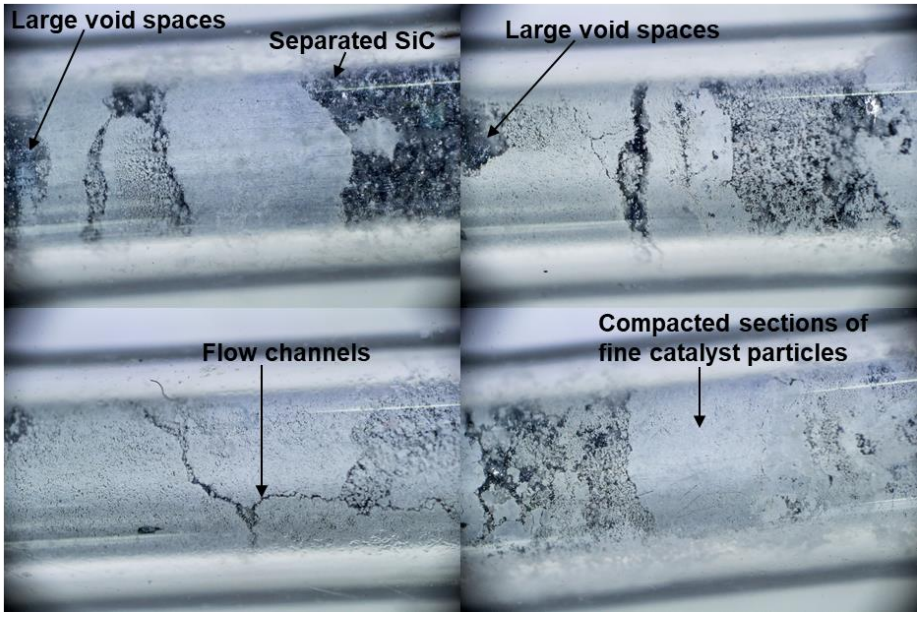

Figure 5.20: Macro photographs of reactor quartz liner showing the catalyst bed after experiment 3 and 4 with Pt-Mo catalyst

5.4 Catalytic conversion of methane to methanol over Pt_3Bi catalyst

The next platinum-based catalyst tested in the packed bed reactor for methane to methanol conversion was an in housed prepared Pt_3Bi catalyst. This catalyst was prepared by impregnating Pt_3Bi nanoparticles on titanium oxide support with a Pt_3Bi loading of 1 wt.%. Evident from the experiment on Pt_3Mo catalyst, we cannot use the catalyst particles directly in the reactor as they sizes are too small. Therefore, the Pt_3Bi catalyst particles are first pressed into a pellet under a hydraulic press with 3 ton-force and then crushed and screened to obtain the fraction between 106 µm to 36 µm. This size fraction was used as it keeps the pressure drop in the reactor less than 2 bar for all flow rates possible (see Figure 4.8). 436 mg of the screened Pt-Bi catalyst pellets are packed in the middle 6 cm of the reactor quartz liner. A macro photograph of the reactor quartz liner was taken (see Figure 5.21) before it is loaded into the reactor.

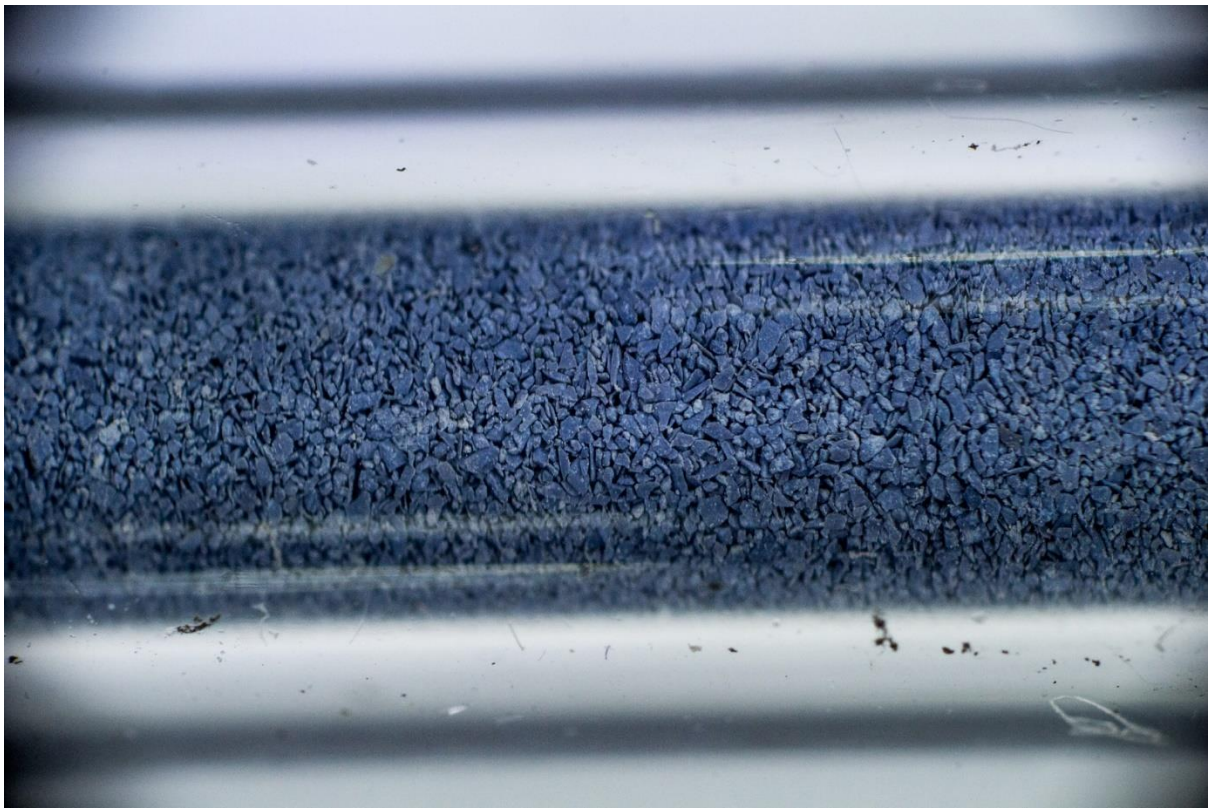

Figure 5.21: Macro photograph of screened Pt_3Bi catalyst pellets inside reactor quartz liner prior to reaction

5.4.1 Experiment 8

The first experiment conducted using the Pt_3Bi catalyst was carried out under high oxygen partial pressure between 100 °C and 300 °C. The space velocity of methane is reduced by a factor of 5 at 300 °C and the temperature progressively lowered to 100 °C for the second leg of the experiment. The reactor was fed with a mixture of 21.4 $ml_n.min^{-1}$ He, 55.4 $ml_n.min^{-1}$ O_2 and 3.9 $ml_n.min^{-1}$ of CH_4, the CH_4 flow rate was reduced to 0.8 $ml_n.min^{-1}$ for the second leg of the experiment. The reactor total pressure was kept at 40 bar throughout the entire experiment. The resulting reactor partial pressures is tabulated in Table 5.4.

Table 5.4: Reactor partial pressure in experiment 8

Reactor Partial Pressures (bar)	4 $ml_{n}.min^{-1}$ CH_4	0.8 $ml_{n}.min^{-1}$ CH_4
He	10.6	11.1
O_2	27.4	28.5
CH_4	2.0	0.4

The time on stream vs conversion and selectivities plot of this experiment is shown in Figure 5.22. CO_2 was observed as the major product alongside with CO, ethane, methanol, methyl formate and the unidentified compound RT 9.2. The scattering in conversion at 300 °C was due to the change in methane flow rate. However, it appears that steady state was not reached during the 3 h each temperature was held at. The conversion decreased at each temperature and increased during temperature ramp ups before falling again during the isothermal phase of the temperature program. Methanol was formed in the beginning of the experiment at 100 °C with a selectivity of around 30 % but decreased to < 5 % when the temperature was increased to 140 °C.

During the second leg of the experiment, no increase in conversion was noted after the decrease in space velocity (6^{th} vertical line in Figure 5.22). Furthermore, on the decreasing temperature program the conversion of methane dropped to 0 % at 190 °C, whereas it remained active throughout the increasing temperature program. This is indicative of deactivation of the catalyst, which is possibility caused by phase changes in the catalyst due to high oxygen partial pressure.

Since steady state is not reached in this experiment due to catalyst deactivation, the temperature vs conversion and selectivity graph is not plotted, nor is the TOF calculated.

The total peak area from this experiment is also analysed and is shown in Figure 5.23. Beside the data points from 300 °C where the methane flow rate was changed, the total peak area is independent from the time on stream for both legs of the experiment (P-value for null hypothesis is 0.16 and 0.14 respectivefully). The maximum deviation in total peak area to its mean value for any data point is 20 % for the first leg of the experiment when the temperature is increasing and 10 % for the second leg of the experiment when the temperature is decreasing.

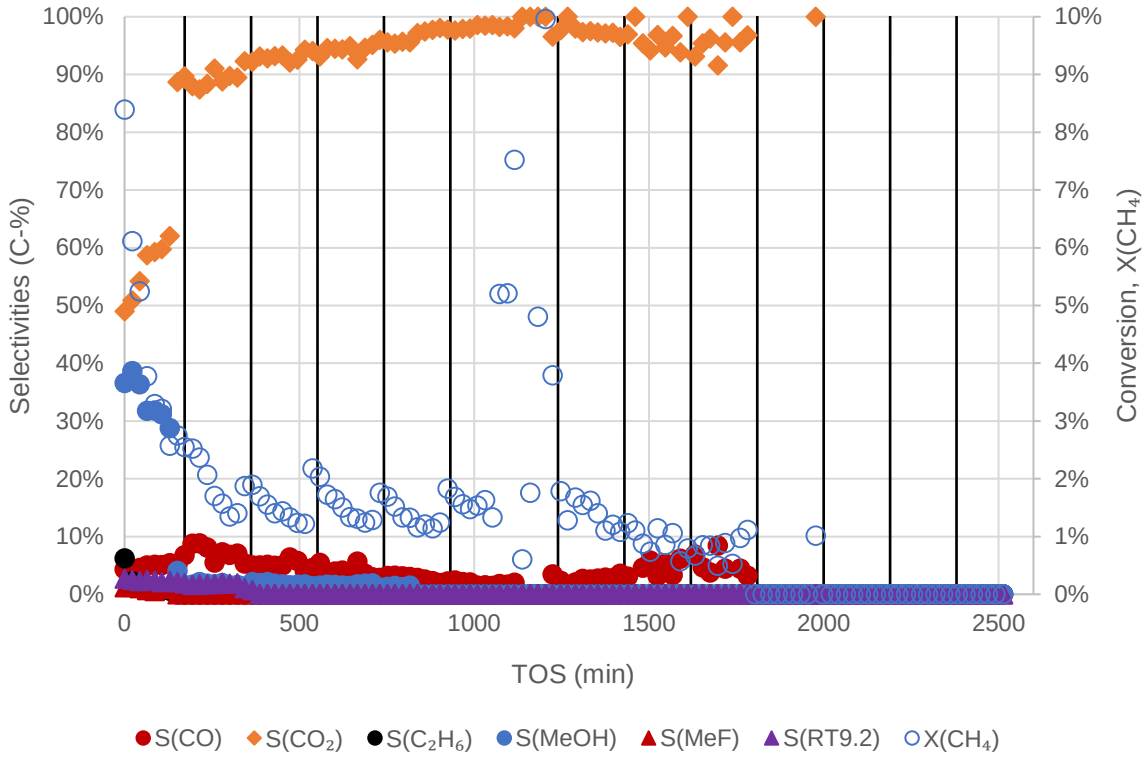

Figure 5.22: Time on stream vs conversion and selectivities plot for conversion of methane to methanol over Pt_3Bi catalyst starting with a feed of 3.9 $ml_n.min^{-1}$ CH_4, 55.4 $ml_n.min^{-1}$ O_2 and 21.4 $ml_n.min^{-1}$ He at 40 bar and 100 °C, solid vertical lines indicate temperature changes. First 5 lines: temperature increase of 40 °C, up to 300 °C, CH_4 flow decreased to 0.8 $ml_n.min^{-1}$ between 5th and 6th line, 6th line: temperature decreased to 280 °C, subsequent lines: temperature decrease of 30 °C down to 100 °C

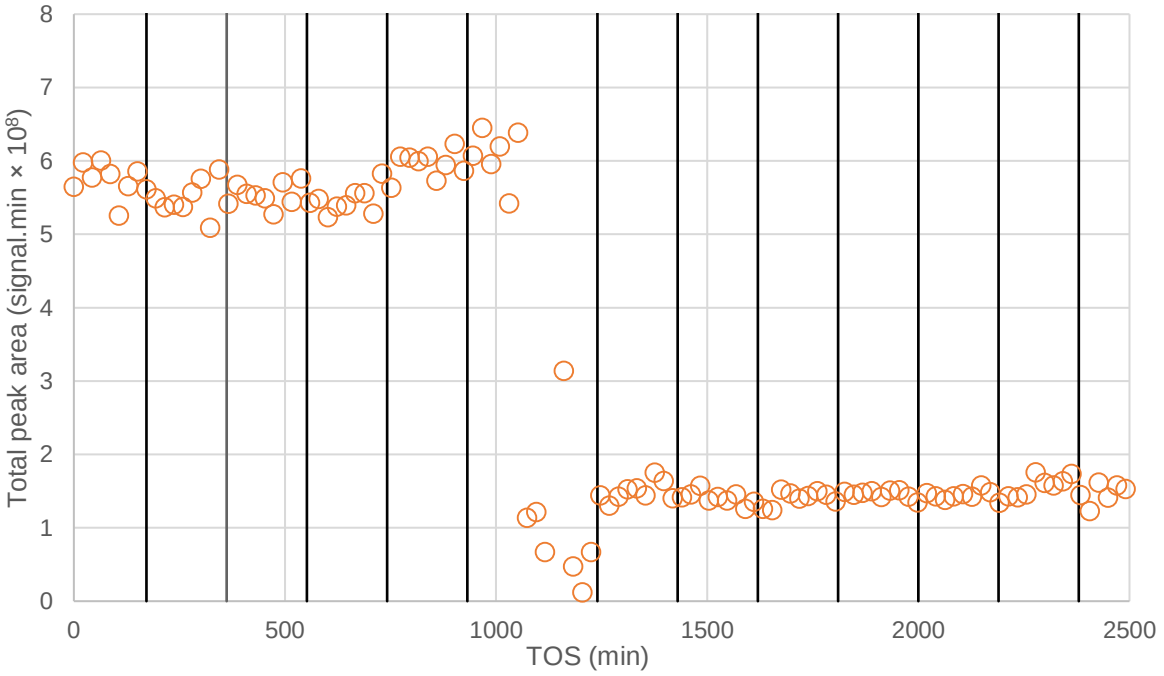

Figure 5.23: Total peak area vs time on stream plot for experiment 8, solid vertical lines indicate the same condition changes as Figure 5.22

5.4.2 Experiment 9

As experiment 8 concluded with the Pt_3Bi deactivated, possibly due to high oxygen partial pressure. A new experiment was carried out on the same catalyst with the intent of reactivating it using steam co-feeding and lower oxygen partial pressure. The experiment was carried out using 83.1 $ml_n.min^{-1}$ He, 55.4 $ml_n.min^{-1}$ O_2, 2 $ml_n.min^{-1}$ of CH_4 and 12.4 $ml_n.min^{-1}$ of $H_2O_{(g)}$ under a total pressure of 10 bar. Under this condition, the feed to the reactor have partial pressures of 5.4 bar He, 3.6 bar O_2, 0.1 bar CH_4, and 0.8 bar H_2O. The total pressure and high He flow was chosen to lower the partial pressure of water below 1 bar, preventing it from condensing at 100 °C. The experiment was started at 100 °C and uses an increasing-decreasing temperature program up to 400 °C and back to 100 °C. The temperature changes were carried out in 100 °C intervals, where the reactor will be held at 100 °C for 5 h 20 min before being increased to 200 °C at 1 $°C.min^{-1}$ and held at 200 °C for 5 h 20 min, and so forth.

During the experiment, the catalyst appeared to be reactivated at above 300 °C, however, throughout the experiment CO_2 was the only observed product. The methane conversion vs time on stream plot for this experiment is shown in Figure 5.24. The maximum methane conversion of around 3.5 % was obtained at 400 °C, assuming 25 % of the Pt_3Bi atoms are on the surface of the catalyst, the TOF of the catalyst is estimated as 149 h^{-1} at 400 °C. Using the data points in the isothermal regions of the experiment, the conversion vs temperature plot for this experiment is made and shown in Figure 5.25. It should be noted that on the decreasing temperature program of the experiment, the measured conversion is slightly but significantly lower than the conversion on the increasing temperature program at the same temperature. This is still indicative of the catalyst deactivating.

The total peak area during this experiment is plotted in Figure 5.26. The null hypothesis holds with a P-value of 0.08, indicating the scattering of the total peak area is random. The maximum deviation in total peak area is 28 % from its mean value, however 95 % of the data is within 14 % of the mean value of the total peak area.

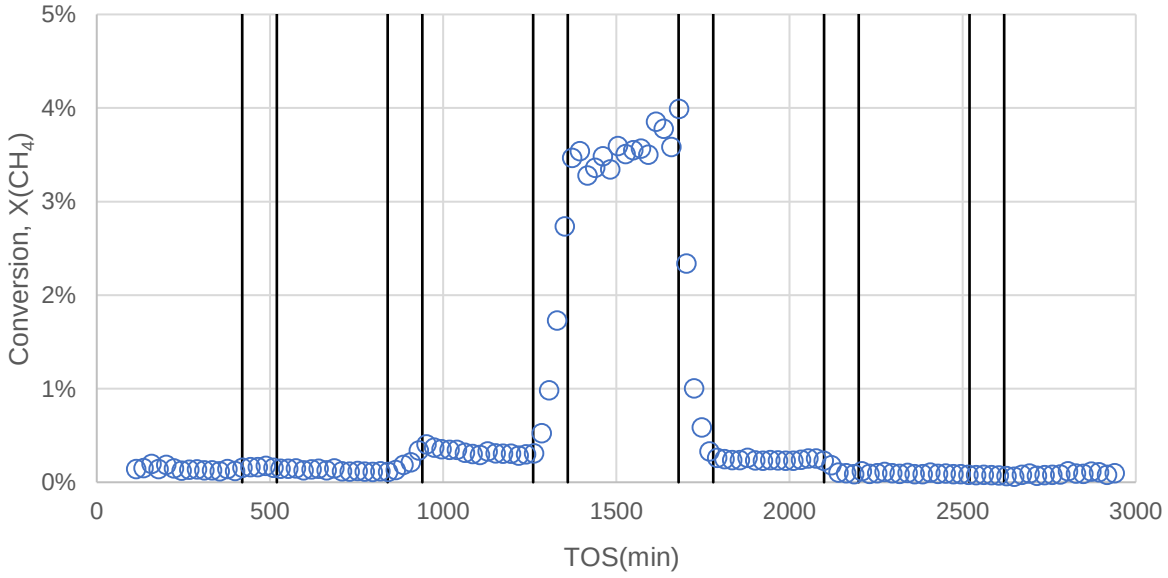

Figure 5.24: Time on stream vs conversion plot for conversion of methane to CO_2 over Pt_3Bi catalyst starting with a feed of 2 $ml_n.min^{-1}$ CH_4, 55.4 $ml_n.min^{-1}$ O_2, 12.4 $ml_n.min^{-1}$ $H_2O_{(g)}$, and 83.1 $ml_n.min^{-1}$ He at 10 bar and 100 °C, solid vertical lines indicate temperature changes; alternating lines shows the start and end of a 1 $°C.min^{-1}$ temperature change between isothermal regions at 100 °C, 200 °C, 300 °C, 400 °C, 300 °C, 200 °C, and 100 °C

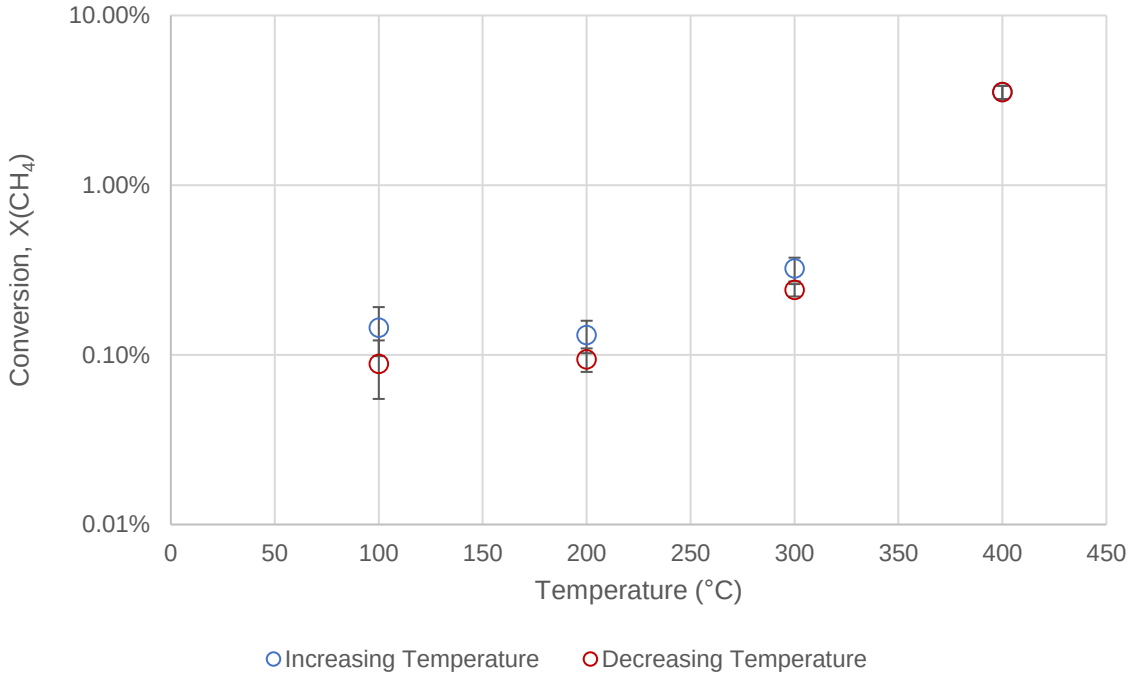

Figure 5.25: Conversion vs temperature plot for experiment 9

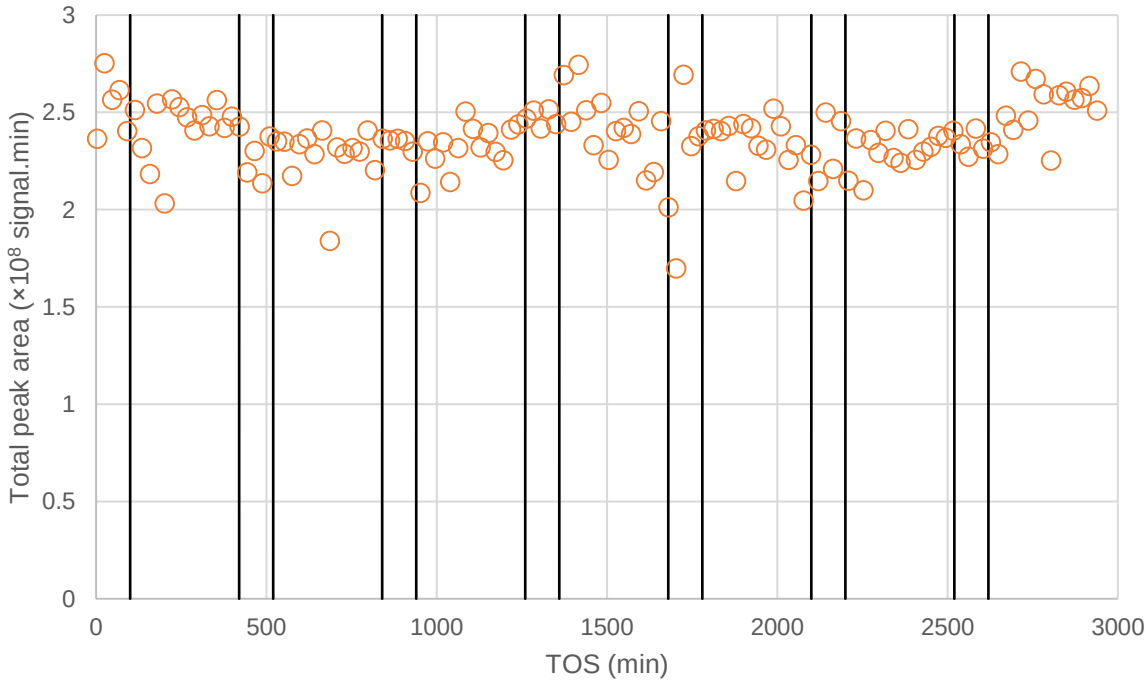

Figure 5.26: Total peak area vs time on stream plot for experiment 9, solid vertical lines indicate the same condition changes as Figure 5.24

5.4.3 Summary of Pt_3Bi experiments

In the two experiments carried out with Pt_3Bi catalysts, no methanol was consistently formed during the attempted conversion of methane to methanol using molecular oxygen with and without water co-feeding. In both experiment the Pt_3Bi catalyst showed signs of deactivation within a relatively short time span of hours.

At the end of the experiment, the reactor was disassembled, and the catalyst bed inspected. A macro photograph of the catalyst bed in Figure 5.27 shows that it is indistinguishable from the catalyst before the experiment. The total peak area in the experiments carried out using the pelletized and screened Pt-Bi catalysts were also more consistent than previous experiments carried out using the mixed silicon carbide – fine particles Pt_3Mo catalysts. This is especially true considering automatic sampling via GC sequences is used with the Pt_3Bi experiments, generating much more data points during the experiments (we were unaware of automatic sampling during the experiments on the Pt_3Mo catalyst). The use of a temperature program has also allowed the experiment to be carried out on a continuous basis without human intervention for condition changes.

Therefore, pelletized and screened catalyst particles should be used for any further experiments instead of using the mixture of silicon carbide and fine catalyst particles as in the case with the Pt_3Mo catalyst experiments. The use of automatic sampling via GC sequencing and reactor temperature programs is also highly recommended instead of manually changing conditions and starting GC runs.

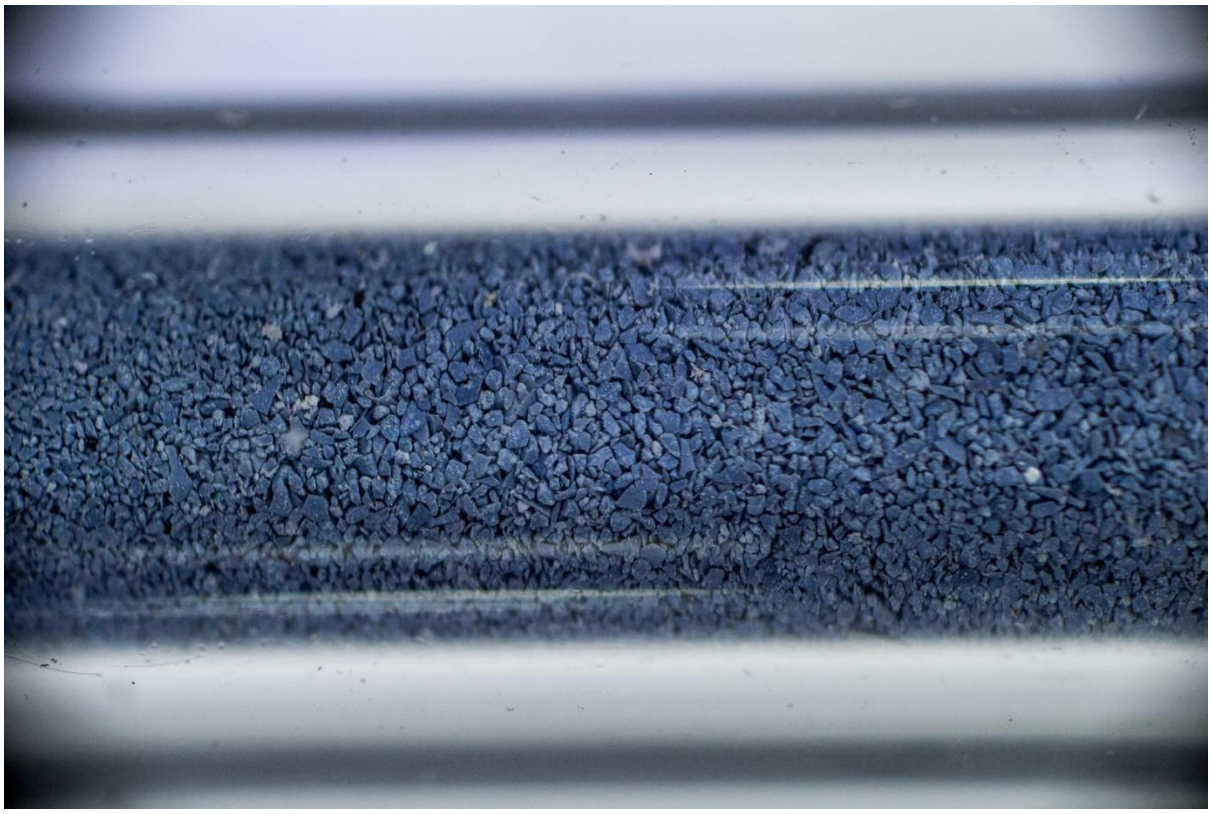

Figure 5.27: Macro photograph of screened Pt_3Bi catalyst pellets inside reactor quartz liner after experiment 8 and 9

6. Conclusion and Recommendations

The exploratory experiments on the conversion of methane to methanol is concluded after the autocatalytic experiments and the two-experiment series using Pt_3Mo and Pt_3Bi catalysts.

Methanol was not selectively formed under either of the catalysts under the experiment conditions used, which usually involved high oxygen and/or steam partial pressure over the catalyst. CO_2 was the major product for both catalysts if the reaction is carried out in the gas phase. An unidentified compound denoted as RT 9.2 was formed as a major product during the reaction of methane with oxygen and steam under conditions where the steam is condensed into liquid water, however the conversion during these experiments are very low at around 0.1 %.

In the autocatalytic experiment carried out in the attempt of converting methane to methanol using oxygen did produce methanol as a major product alongside CO. However, the methane conversion remains low at roughly 5 % as a methane to oxygen volume feed ratio of 10:1 is used, making oxygen the limiting reagent. None of the exploratory experiments on methane to methanol conversion have attained a selectivity of methanol greater than 80 % at a methane conversion greater than 10 %, the benchmark for an industrially relevant methane to methanol conversion process given by Kondratenko et al. [46].

Although we were unable to selectively convert methane to methanol, the performance of the designed packed bed reactor system for the conversion of methane to methanol appear to meet its requirement.

The reactor system can continuously measure the conversion and selectivities during the autocatalytic and catalytic conversions of methane to methanol using molecular oxygen with and without the co-feeding of water. The reactor system is also able to do this safely despite the dangers involving methane and oxygen mixtures, through the use of very little reactor volume and post reactor argon dilution. Care should be taken to only use catalyst in the right size range of between 20 µm to 160 µm inside the reactor and conditions should be set to prevent steam condensation if steam is co-fed in the reaction.

During steady state conditions, the measured conversions and selectivities is reproducible over different samples within experimental error, evident from most of the time on stream vs conversion and selectivities plot in Chapter 5. The use of the Polyarc™ reactor in our GC-FID also allows the "one-pot" analysis of all carbon containing compounds with high sensitivity and equal responses. This allows us to use the total peak area throughout an experiment to infer the carbon molar flow rate out of the reactor system hence inferring the carbon mass balance for a constant carbon molar feed flow rate into the reactor system. The increased sensitivity of the FID compared to a TCD allows all carbon containing products produced with yields > 0.001 C-% to be quantified. The obtained productivity for the autocatalytic reaction 282 $\frac{mol_{CH4\ converted}}{min.m^3_{rctr\ volume}}$ at 485 °C and 40 bar, is comparable in orders of magnitude to the 97 $\frac{mol_{CH4\ converted}}{min.m^3_{rctr\ volume}}$ obtained by Zhang et al. [1] at 450 °C and 40 bar. The turnover frequency of the Pt-based catalysts is estimated at 8.2 h^{-1} and 20.5 h^{-1} for Pt_3Mo catalyst throughout experiment 6 and 7, 149 h^{-1} for Pt_3Bi catalyst at 400 °C in experiment 9. These turnover frequencies are comparable to in orders of magnitude to the turn over frequency of 36 h^{-1} for

homogenous Pt catalyst used in the acid assist conversion of methane to methanol by Periana et al. [2].

There is still room for improvement in the packed bed reactor system. Instead of analysing the total peak area for each of the sample taken to infer the carbon mass balance. An internal reference gas such as propane can be added post reaction to the reactor effluent. Propane is a suitable reference gas as it is not expected to be formed in any of the experiments on the conversion of methane to methanol carried out by us so far. By using a set flow rate of this internal reference gas, the exit flow rate of all carbon containing compounds can be calculated and the absolute carbon mass balance established. Furthermore, it may be beneficial to expand on the current GC set up of the experimental system to incorporate a secondary TCD detector. This will allow us to establish the hydrogen and oxygen mass balance on top of the carbon mass balance.

Product identification is still something that must be worked on. In the absence of a dedicated online GC-MS, our GC-FID system can only quantify and separate the reaction products but not identify them, for example, the identity of the major product RT 9.2 formed during the triphasic reaction between methane, oxygen and liquid water over Pt_3Mo catalyst is of great interest. It is recommended that for future experiments, the reactor effluent should be bubbled through some water to capture any oxygenated products formed in the reactor. This liquid can then be taken for GC-MS analysis elsewhere to identify any dissolved reaction products in it.

In terms of the catalysts tested, Pt_3Mo showed some interesting results with the selective formation of RT 9.2 under triphasic conditions but all experiments on Pt_3Mo were either carried out without the reactor quartz liner or using a structurally unsound catalyst bed shown in Figure 5.20. The Pt_3Bi catalyst appears to be deactivating throughout the two experiments carried out over it. Pure platinum catalyst must be tested on top of the promoted platinum catalyst, as without a base case performance of pure platinum catalysts, we cannot determine whether the promotor added to platinum indeed acts as a catalyst promoter. Beside testing pure platinum catalysts, other noble metals such as Ag, Au and Pd should also be tested in the conversion of methane to methanol as Fratesi et al. [47] argued for the selective formation of methane over Ag under high oxygen coverage while AuPd catalysts have already been used by Rahim et al. [34] in the conversion of methane to methanol using hydrogen peroxide. Our hypothesis of using high oxygen and water partial pressures to saturate the catalyst surface with adsorbed oxygen species to improve methane to methanol selectivity should be tested over these noble metal catalysts.

The new catalysts should also be highly loaded in active metal content as the space velocity is limited in our reactor system (most catalytic experiments were carried out with the methane mass flow controller set to 5 %) and high conversions were never obtained when using the reactor quartz liner throughout all the catalytic exploratory experiments using the 1 wt.% active metal catalysts. The increase in active metal content will effectively reduce the space velocity of methane in our reactor per unit mass of active metal as more active metal can be loaded into the reactor volume. This should allow for higher conversions to be achieved in the reactor, as no methane conversions greater than 10 % were achieved in the catalytic exploratory experiments (beside experiment 4 and 5 carried out without the reactor quartz liner).

In conclusion, although the exploratory experiments conducted in this dissertation was unable to selectively convert methane to methanol. The packed bed reactor system designed for the

catalytic conversion of methane to methanol under high pressures and with the provision for co-feeding steam can be safely used to screen and test other catalysts in the selective conversion of methane to methanol. The reactor system can produce reproducible conversions and selectivities data at steady state reactor conditions. The following recommendations should be considered before conducting any further work:

- The catalyst particles should be pelletized, crushed and screened to the right size range (20 µm to 100 µm) before being used in the reactor.
- The catalyst particles should be highly loaded to achieve a larger conversion range by reducing the space velocity per unit active catalyst mass, smaller mass flow controllers can be added in parallel with the existing mass flow controllers to achieve the same thing.
- The reactor should be running with automatic sampling via GC sequences and reactor temperature programs, preferably an increasing then decreasing temperature program should be used. This allows for continuous monitoring of the catalyst and reactor performance. It can also determine catalyst deactivation by comparing catalyst performance between the part of the experiment that is increasing in temperature and the part that is decreasing in temperature at the same temperature.
- An internal reference gas such as propane should be used so an absolute carbon mass balance can be determined for each of the GC sample taken, by allowing the exit flow rate of all reactor products to be calculated.
- A TCD can be added as part of our GC system to determine hydrogen and oxygen mass balance by quantifying any hydrogen, oxygen and water in the reactor effluent.
- The reactor products should be bubbled through a water column to dissolve any unidentified reaction products, so they can be identified via GC-MS elsewhere.
- Pure noble metal catalysts should be tested before promoted catalysts to obtain a base case performance for each of the noble metals before promoted catalysts are tested. These pure noble metal catalysts should include Pt, Ag, Au, and Pd.

7. References

[1] Q. Zhang, D. He, J. Li, B. Xu, Y. Liang and Q. Zhu, "Comparatively high yield methanol production from gas phase partial oxidation of methane," *Applied Catalysis A: General,* no. 224, pp. 201-207, 2002.

[2] R. A. Periana, D. J. Taube, S. Gamble, H. Taube, T. Satoh and H. Fujii, "Platinum Catalysts for the High-Yield Oxidation of Methane to a Methanol Derivative," *Science,* vol. 280, pp. 560-564, 1998.

[3] World Energy Council, "World Energy Resources 2016," World Energy Council 2016, London, 2016.

[4] BP, "Statistical Review of World Energy 2018," 2018.

[5] R. Weijermars, "Value chain analysis of the natural gas industry - Lessons from the US regulatory success and opportunities for Europe," *Journal of Natural Gas Science and Engineering,* no. 2, pp. 86-104, 2010.

[6] Q. Zhang, D. He and Q. Zhu, "Recent Progress in Direct Partial Oxidation of Methane to Methanol," *Journal of Natural Gas Chemistry,* no. 12, pp. 81-89, 2003.

[7] Institute of Shipping Economics and Logistics, "ISL Shipping Statistics and Market Review (SSMR) Volume 60," ISL Institute of Shipping Economics and Logistics, Bremen, 2016.

[8] V. Arutyunov, Direct methane to methanol - Foundations and prospects of the process, Oxford: Elsevier, 2014.

[9] B. Boyd, "Methanol Industry Presentation," 2012. [Online]. Available: http://www.petroleum-economist.com/pdf/BradBoyd.pdf. [Accessed 22 04 2015].

[10] S. J. Blanksby and G. B. Ellison, "Bond dissociation energies of organic molecules," *American Chemical Society,* 2002.

[11] S. I. Sandler, Chemical, Biochemical and Engineering Thermodynamics, 4th ed., John Wiley & Sons, 2006.

[12] J. R. Rostrup-Nielsen, "Syngas in perspective," *Catalysis Today,* no. 71, pp. 243-247, 2002.

[13] BP, "BP Statistical Review of World Energy 2016," 2016.

[14] R. A. Periana, D. J. Taube, E. R. Evitt, D. G. Löffler, P. R.Wentrcek, G. Voss and T. Masuda, "A Mercury-Catalyzed, High-Yield System for the Oxidation of Methane to Methanol," *Science, New Series,* vol. 259, no. 5093, pp. 340-343, 1993.

[15] C. Jones, D. Taube, V. R. Ziatdinov, R. A. Periana, R. J. Nielsen, J. Oxgaard and W. A. Goddard, "Selective oxidation of methane to methanol catalyzed with homogenous cationic gold," *Angewandte Chemie,* no. 116, pp. 4726-4729, 2004.

[16] B. G. Hashiguchi, M. M. Konnick, S. M. Bischof, S. J. Gustafson, D. Devarajan, N. Gunsalus, D. H. Ess and R. A. Periana, "Main-Group Compounds Selectively Oxidize Mixtures of Methane, Ethane, and Propane to Alcohol Esters," *Science,* vol. 343, no. 6176, pp. 1232-1237, 2014.

[17] R. Palkovits, M. Antonietti, P. Kuhn, A. Thomas and F. Schüth, "Solid Catalysts for the Selective Low-Temperature Oxidation of methane to methanol," *Angewandte Chemie,* no. 48, pp. 6909-6912, 2009.

[18] M. Soorholtz, R. J. White, T. Zimmermann, M.-M. Titirici, M. Antonietti, R. Palkovits and F. Schüth, "Direct methane oxidation over Pt-modified nitrogen-doped carbons," *Chemical Communications,* no. 49, pp. 240-242, 2013.

[19] D. M. Newitt and A. E. Haffner, "The Formation of Methyl Alcohol and Formaldehyde in the Slow Combustion of Methane at High Pressures," *Proceedings of the Royal Society of London. Series A, Containing Papers of a Mathematical and Physical Character,* vol. 134, no. 825, pp. 591-604, 1932.

[20] V. S. Arutyunov, V. M. Rudakov, V. I. Savchenko, E. V. Sheverdenkin, O. G. Sheverdenkina and A. Y. Zheltyakov, "Partial Alkane Oxidation Kinetics at High Pressures: Methane Oxidation in Stainless Steel and Quartz Reactors," *Theoretical Foundations of Chemical Engineering,* vol. 36, no. 5, pp. 472-476, 2002.

[21] V. Arutyunov, V. Vedeneev, S. Klimovetskaya, V. Leonov and L. Pavlii, "Influence of pressure on the formation of products of partial oxidation of methane," *Theoretical Foundations of Chemical Engineering,* vol. 28, no. 6, pp. 627-632, 1994.

[22] V. Vedeneev, V. Arutyunov, V. Basevich, M. Goldenberg, M. Teitelboim and N. Krymov, "Role of pressure in homogeneous and/or catalytic oxidation of methane," *Catalysis Today,* no. 21, pp. 527-532, 1994.

[23] Q. Zhang, D. He and Q. Zhu, "Direct partial oxidation of methane to methanol - effect of reactor materials and catalyst," *Preprints of Papers- American Chemical Society, Division of Fuel Chemistry,* no. 48(2), pp. 561-562, 2003.

[24] A. S. Chellappa, S. Fuangfoo and D. S. Viswanath, "Homogeneous Oxidation of Methane to Methanol: Effect of CO_2, N_2, and H_2 at High Oxygen Conversions," *Industrial & Engineering Chemistry Research,* no. 36, pp. 1401-1409, 1997.

[25] R. Burch, G. D. Squire and S. C. Tsang, "Direct Conversion of Methane into Methanol," *Journal of the Chemical Society, Faraday Transactions 1,* no. 85(10), pp. 3561-3568, 1989.

[26] G. A. Foulds, B. F. Gray, S. A. Miller and G. S. Walker, “Homogenous gas phase oxidation of methane using oxygen as oxidant in an annular reactor,” *Industrial & Engineering Chemistry Research,* no. 32, pp. 780-787, 1993.

[27] H. Gesser, N. Hunter, L. Morton, P. Yarlagadda and D. Fung, “The direct conversion of methane to methanol by a high pressure partial oxidation reaction,” *Preprints of Papers- American Chemical Society, Division of Fuel Chemistry,* no. 32:3, pp. 255-259, 1988.

[28] G. O. Alptekin, A. M. Herring, D. L.Williamson, T. R. Ohno and R. L. McCormick, “Methane poartial oxidation by unsupported and silica supported iron phosphate catalyst,” *Journal of Catalysis,* no. 181, pp. 104-112, 1999.

[29] C. Okolie, Y. F. Belhseine, Y. Lyu, M. M. Yung, M. H. Engelhard, L. Kovarik, E. Stavitski and C. Sievers, “Conversion of methane into methanol and ethanol over nickel oxide on ceria zironia catalyst in a single reactor,” *Angewandte Chemie,* no. 56, pp. 13876-13881, 2017.

[30] M. Dyballa, D. K. Pappas, E. Borfecchia, P. Beato, U. Olsbye, K. P. Lillerud, B. Arstad and S. Svelle, “Tuning the material and catalytic properties of SUZ-4 zeolites for the conversion of methanol or methane,” *Microporous and Mesoporous Materials,* no. 265, pp. 112-122, 2018.

[31] H. V. Le, S. Parishan, A. Sagaltchik, H. Ahi, A. Trunschke, R. Schomäcker and A. Thomas, “Stepwise methane-to-methanol conversion on CuO/SBA-15,” *Chemistry – A European Journal,* 2018.

[32] D. K. Pappas, E. Borfecchia, M. Dyballa, I. A. Pankin, K. A. Lomachenko, A. Martini, M. Signorile, S. Teketel, B. Arstad, G. Berlier, C. Lamberti, S. Bordiga, U. Olsbye, K. P. Lillerud, S. Svelle and P. Beato, “Methane to Methanol: Structure−Activity Relationships for Cu-CHA,” *Journal of the American Chemical Society,* no. 139, pp. 14961-14975, 2017.

[33] Y. Kwon, T. Y. Kim, G. Kwon, J. Yi and H. Lee, “Selective activation of methane on single atom catalyst of rhodium dispersed on zirconia for direct conversion,” *Journal of the American Chemical Society,* no. 139, pp. 17694-17699, 2017.

[34] M. H. A. Rahim, M. M. Forde, R. L. Jenkins, C. Hammond, Q. He, N. Dimitratos, J. A. Lopez-Sanchez, A. F. Carley, S. H. Taylor, D. J. Willock, D. M. Murphy, C. J. Kiely and G. J. Hutchings, “Oxidation of Methane to Methanol with Hydrogen Peroxide Using Supported Gold–Palladium Alloy Nanoparticles,” *Angewandte Chemie,* no. 125, pp. 1318-1322, 2013.

[35] S. Al-Shihri, C. J. Richard, H. Al-Megren and D. Chadwick, “Insights into the direct selective oxidation of methane to methanol over ZSM-5 zeolites in aqueous hydrogen peroxide,” *Catalysis Today,* 2018. In Press, DOI: 10.1016/j.cattod.2018.03.031

[36] C. Hammond, M. M. Forde, M. H. A. Rahim, A. Thetford, Q. He, R. L. Jenkins, N. Dimitratos, J. A. Lopez-Sanchez, N. F. Dummer, D. M. Murphy, A. F. Carley, S. H. Taylor, D. J. Willock, E. E. Stangland, J. Kang, H. Hagen, C. J. Kiely and G. J. Hutchings, "Direct catalytic conversion of methane to methanol in an aqueous medium by using copper promoted Fe ZSM-5," *Angewandte Chemie,* no. 51, pp. 5129-5133, 2012.

[37] P. Chawdhury, D. Ray and C. Subrahmanyam, "Single step conversion of methane to methanol assisted by nonthermal plasma," *Fuel Processing Technology,* no. 179, pp. 32-41, 2018.

[38] K. Ohkubo and K. Hirose, "Light-Driven C-H Oxygenation of Methane into Methanol and Formic Acid by Molecular Oxygen Using a Perfluorinated Solvent," *Angewandte Chemie,* no. 57, pp. 2126-2129, 2018.

[39] K. Otsuka and Y. Wang, "Direct conversion of methane into oxygenates," *Applied Catalysis A: General,* no. 222, pp. 145-161, 2001.

[40] X. Zhang, D.-h. He, Q.-j. Zhang, Q. Ye, B.-q. Xu and Q.-m. Zhu, "Selective oxidation of methane to formaldehyde over Mo/ZrO_2 catalysts," *Applied Catalysis A: General,* no. 249, pp. 107-117, 2003.

[41] V. C. C. Wang, S. Maji, P. P. Y. Chen, H. K. Lee, S. S. F. Yu and S. I. Chan, "Alkane Oxidation: Methane Monooxygenases, Related Enzymes, and Their Biomimetics," *Chemical Reviews,* no. 117(13), pp. 8574-8621, 2017.

[42] C. Bjorck, P. Dobson and J. Pandhal, "Biotechnological conversion of methane to methanol: evaluation of progress and potential," *AIMS Bioengineering,* no. 5(1), pp. 1-38, 2018.

[43] P. Mehta, T. Ghose and S. Mishra, "Methanol biosynthesis by covalently immobilized cells of Methylosinus trichosporium: batch and continuous studies.," *Biotechnology and Bioengineering,* no. 37, pp. 551-556, 1991.

[44] R. Oord, J. E. Schmidt and B. M. Weckhuysen, "Methane-to-methanol conversion over zeolite Cu-SSZ-13, and its comparison with the selective catalytic reduction of NOx with NH_3," *Catalysis Science & Technology,* no. 8, pp. 1028-1038, 2018.

[45] P. Tomkins, M. Ranocchiari and J. A. v. Bokhoven, "Direct Conversion of Methane to Methanol under Mild Conditions over Cu-Zeolites and beyond," *Accounts of Chemical Research,* no. 50, pp. 418-425, 2017.

[46] E. V. Kondratenko, T. Peppel, D. Seeburg, V. A. Kondratenko, N. Kalevaru, A. Martin and S. Wohlrab, "Methane conversion into different hydrocarbons or oxygenates: current status and future perspectives in catalyst development and reactor operation," *Catalysis Science & Technology,* no. 7, pp. 366-381, 2017.

[47] G. Fratesi, P. Gava and S. d. Gironcoli, “Direct Methane-to-Methanol Conversion: Insight from First-Principles Calculations,” *Journal of Physical Chemistry C,* no. 111, pp. 17015-17019, 2007.

[48] L. Arnarson, P. S. Schmidt, M. Pandey, A. Bagger, K. S. Thygesen, I. E. L. Stephens and J. Rossmeisl, “Fundamental limitation of electrocatalytic methane conversion to methanol,” *Physical Chemistry Chemical Physics,* no. 20, pp. 11152-11159, 2018.

[49] M. F. Fellah and I. Onal, “C–H bond activation of methane on M- and MO-ZSM-5 (M =Ag, Au, Cu, Rh and Ru) clusters: A density functional theory study,” *Catalysis Today,* no. 171, pp. 52-59, 2011.

[50] P. L. Cilliers, “Phase diagram for the co-adsorption of O and OH on Pt(100) and Pt(111) as determined by DFT, MSc-dissertation” University of Cape Town, Cape Town, 2017.

[51] A. Dianat, N. Seriani, L. C. Ciacchi, W. Pompe, G. Cuniberti and M. Bobeth, “Dissociative Adsorption of Methane on Surface Oxide Structures of Pd-Pt Alloys,” *Journal of Physical Chemistry C,* no. 113, pp. 21097-21105, 2009.

[52] L. Qi and J. Li, “Adsorbate interactions on surface lead to a flattened Sabatier volcano plot in reduction of oxygen,” *Journal of Catalysis,* vol. 295, pp. 59-69, 2012.

[53] T. Madala, “Reaction pathways for the formation of hydrogen peroxide in fuel cells - a DFT study, MSc-dissertation,” University of Cape Town, Cape Town, 2013.

[54] M. Besson, F. Lahmer, P. Gallezot, P. Fuertes and G. Fleche, “Catalytic oxidation of glucose on bismuth promoted palladium catalyst,” *Journal of Catalysis,* no. 152, pp. 116-121, 1995.

[55] T. Mallat and A. Baiker, “Oxidation of alcohols with molecular oxygen on platinum metal catalysts in aqueous solutions,” *Catalysis Today,* no. 19, pp. 247-284, 1994.

[56] Z. Zuo, P. J. Ramírez, S. Senanayake, P. Liuc and J. A. Rodriguez, “The low temperature conversion of methane to methanol on CeOx - Cu_2O catalysts - water controlled activation of the C-H bond,” *Journal of the American Chemical Society*, no. 138(42), pp. 13810-13813, 2016.

[57] P. G. Lustemberg, R. M. Palomino, R. A. Gutiérrez, D. C. Grinter, M. Vorokhta, Z. Liu, P. J. Ramírez, V. Matolín, M. V. Ganduglia-Pirovano, S. D. Senanayake and J. A. Rodriguez, “Direct Conversion of Methane to Methanol on Ni-Ceria Surfaces: Metal−Support Interactions and Water-Enabled Catalytic Conversion by Site Blocking,” *Journal of the American Chemical Society,* no. 140, pp. 7681-7687, 2018.

[58] Afrox, “Gas Equipment - Flashback arrestors & quick release couplings,” [Online]. Available: http://www.afrox-welding.co.za/en/images/Flashback_arrestors_tcm282-29953.pdf. [Accessed 4 10 2015].

[59] M. V. Parfenov, E. V. Starokon, L. V. Pirutko and G. I. Panov, “Quasicatalytic and catalytic oxidation of methane to methanol by nitrous oxide over FeZSM-5 zeolite,” *Journal of Catalysis,* no. 318, pp. 14-21, 2014.

[60] E. H. Boomer and V. Thomas, “The oxidation of methane at high pressures: III. experiments using pure methane and principally copper as catalyst,” *Canadian Journal of Research,* vol. 15b, no. 10, pp. 414-433, 1937.

[61] M. G. Zabetakis, “Flammability Characteristics of combustible gases and vapors,” *Bulletin 627, Bureau of mines,* 1965.

[62] G. A. Melhem, “A detailed method for estimating mixture flammability limits using chemical equilibrium,” *Process Safety Progress,* vol. 16, no. 4, pp. 203-218, 1997.

[63] Swagelok®, “Tubing Data,” [Online]. Available: https://www.swagelok.com/downloads/webcatalogs/EN/MS-01-107.PDF. [Accessed 27 September 2015].

[64] S.-Y. Wu, N.-K. Lin and C.-M. Shu, “Effects of flammability characteristics of methane with three inert gases,” Wiley Online Library, 2010.

[65] X. Hu, Q. Yu, N. Sun and Q. Qin, “Experimental study of flammability limits of oxy-methane mixture and calculation based on thermal theory,” *International Journal of Hydrogen Energy,* vol. 39, no. 17, pp. 9527-9533, 2014.

[66] J. R. Welty, C. E. Wicks, R. E. Wilson and G. L. Rorrer, Fundamentals of Momentum, Heat, and Mass Transfer, John Wiley & Sons, Inc., 2008.

[67] S. Ergun, “Fluid flow through packed columns,” *Chemical Engineering Progress,* no. 48, pp. 89-94, 1952.

[68] B. Eisfeld and K. Schnitzlein, “The influence of confining walls on the pressure drop in packed beds,” *Chemical Engineering Science,* no. 56(14), p. 4321, 2001.

[69] O. Levenspiel, Chemical Reaction Engineering, 3rd ed., John Wiley & Sons, Inc., 1999.

[70] Row Inc., “Cross Section & Groove Design Data,” [Online]. Available: http://www.row-inc.com/sizes.html. [Accessed 10 October 2015].

[71] J. F. Rubinson and K. A. Rubinson, Contemporary Chemical Analysis, Michigan: Prentice Hall, 1998.

[72] Y. Zou, “Coal-to-Chemical Process Gas Analysis Using Agilent J&W HP-PLOT Q PT and HP-PLOT U PT,” Agilent Technologies, United States, 2013.

[73] S. Maduskar, A. R. Teixeira, A. D. Paulsen, C. Krumm, T. J. Mountziaris, W. Fan and P. J. Dauenhauer, “Quantitative carbon detector (QCD) for calibration-free, high-resolution characterization of complex mixtures,” *Lab on a Chip,* no. 15, pp. 440-447, 2014.

[74] C. A. Beach, C. Krumm, C. S. Spanjers, S. Maduskar, A. J. Jones and P. J. Dauenhauer, "Quantitative carbon detector for enhanced detection of molecules in foods, pharmaceuticals, cosmetics, flavors, and fuels," *Analyst,* no. 141, pp. 1627-1632, 2016.

[75] L. Sidisky, G. Baney, K. Stenerson and J. L. Desorcie, "Carrier Gas Selection for Capillary Gas Chromatography," 2011. [Online]. Available: https://www.sigmaaldrich.com/content/dam/sigma-aldrich/docs/Supelco/General_Information/1/t411126h.pdf. [Accessed 15 03 2017].

[76] Activated Research Company, "Polyarc System v2.0 Installation Manual, Agilent 7890,7820,6890 or equivalent," Activated Research Company, LLC, 2016.

[77] Strem Chemicals. Inc., "Heterogeneous Catalysts," 2017. [Online]. Available: https://www.strem.com/uploads/resources/documents/heterogeneouscatalysts.pdf. [Accessed 11 August 2017].

[78] Engineering ToolBox, "Gases - Dynamic Viscosity," 2014. [Online]. Available: https://www.engineeringtoolbox.com/gases-absolute-dynamic-viscosity-d_1888.html. [Accessed 8 11 2015].

8. Appendix I – Existing equipment

8.1 Reactor stand

The direct methane to methanol conversion reactor system is built over the existing reactor stand of rig 1A6 in reactor hood 1 of our laboratory. The reactor system chassis is built around a frame made of welded 25 mm × 25 mm square steel tubes on a movable trolley wheel base. The base, front counter and front panel is covered with 1 mm steel sheet metal fixed to the tubular steel frame using bolts or screws. The 1 mm steel sheet metal can easily be drilled through for routing of lines and mounting of fasteners. Additionally, a perforated steel sheet is bolted high in the frame at the back of the chassis for the mounting of the mass flow controllers. Isometric drawings of the front and back of this rig chassis is shown in Figure 7.11 and 7.2 with all relevant dimensions and without any attached equipment.

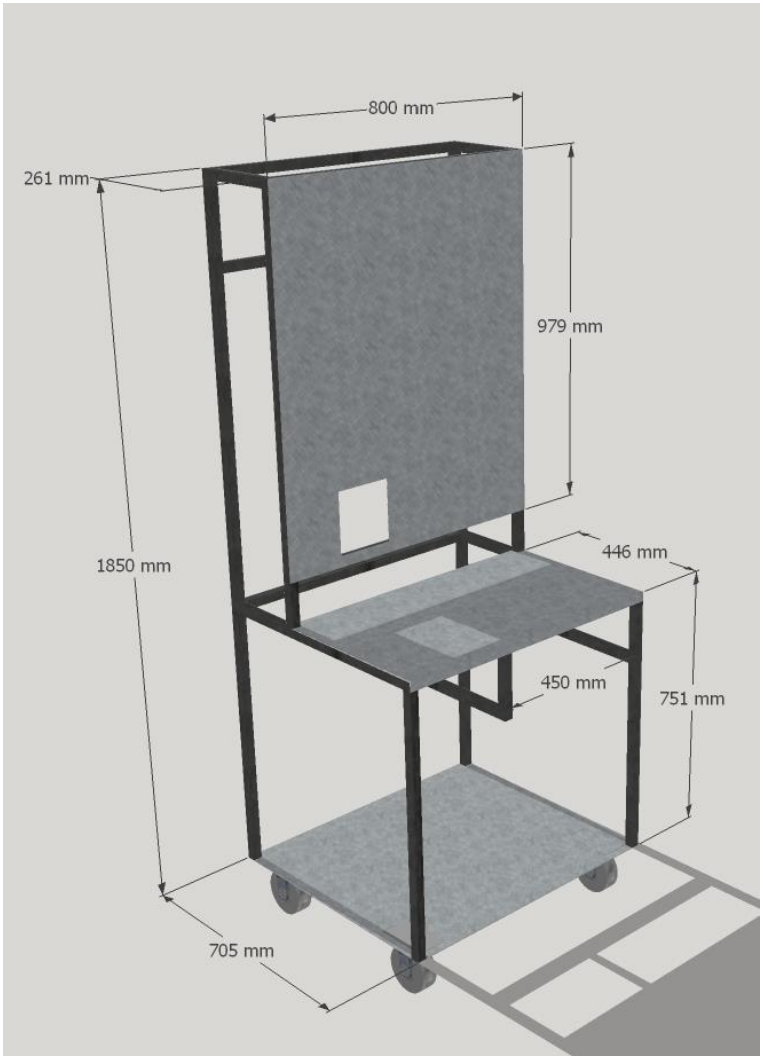

Figure 8.1 Front isometric drawing of reactor system chassis

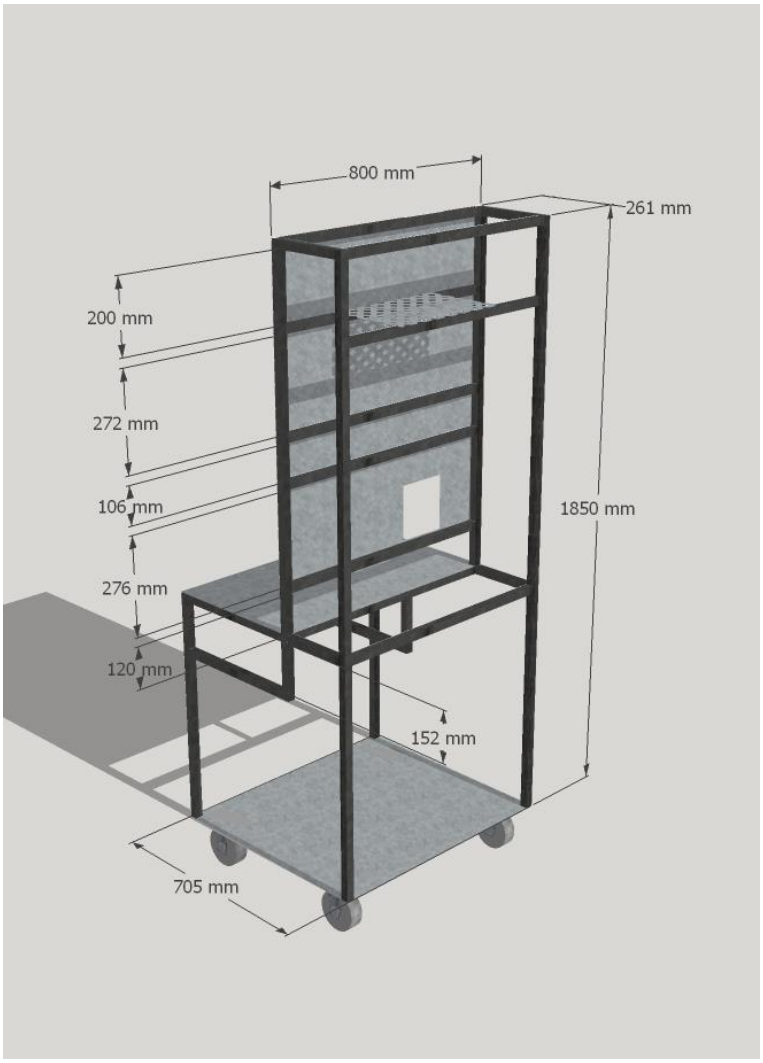

Figure 8.2: Back isometric drawing of reactor system chassis

8.2 Temperature control unit

A temperature control unit is reused in the direct methane to methanol reactor system from the existing rig 1A6. This temperature control unit contains 3 Gefran 600 PID controllers and a single Gefran 800P programmable PID controller. The 3 Gefran 600 controllers are used as the temperature indicator and controller for TIC-301, TIC-302 and TIC-702. The programmable Gefran 800P controller is used for the reactor heating blocks as the programmable controller have a ramp and hold function, enabling the reactor to operate on a temperature program.

A faulty thermocouple read out display and a 12-point positional switch is present on the temperature control unit to allow for 12 additional temperature measurements to be taken in the reactor system. The faulty thermocouple read out display is bypassed by connecting the output from the 12-point positional switch to a Gefran 800P controller, with the Gefran 800P controller acting only as an thermocouple temperature readout.

An array of 6 circuit breakers is also present on the temperature control unit. The first 2 circuit breakers are used to supply the PID controllers and thermocouple readout with power and is named the instrument power breaker. The Gefran PID controllers allow for 4 channels of closed loop temperature control. These control loops start with a voltage signal generated by the

thermocouple via the Seebeck effect proportional to the temperature of the thermocouple. This signal is processed and displayed by the Gefran controller as the present value (PV) of that temperature channel. The controller then compares this PV with the temperature set point input value and generates a square wave whose duty cycle is proportional to the difference in the temperature present value and set point value as well as the difference in the time derivative and time integral of the present value and set point (PID). The PID constants for the Gefran controllers are set to self-tuning and will continuously change to provide the best controller settings. This control signal subsequently switches the solid-state relay of its respective channel on and off, providing the heating elements of that channel with mains power in the same form as the on-off control signal. The temperature increase caused by the heating element is then picked up by its thermocouple, completing the control loop. A 5 A circuit breaker is placed on each of the heating power channel to provide over current protection. A flow diagram of the temperature control unit is shown in Figure 7.3, and the schematic of a single temperature controller PID loop is shown in Figure 7.4.

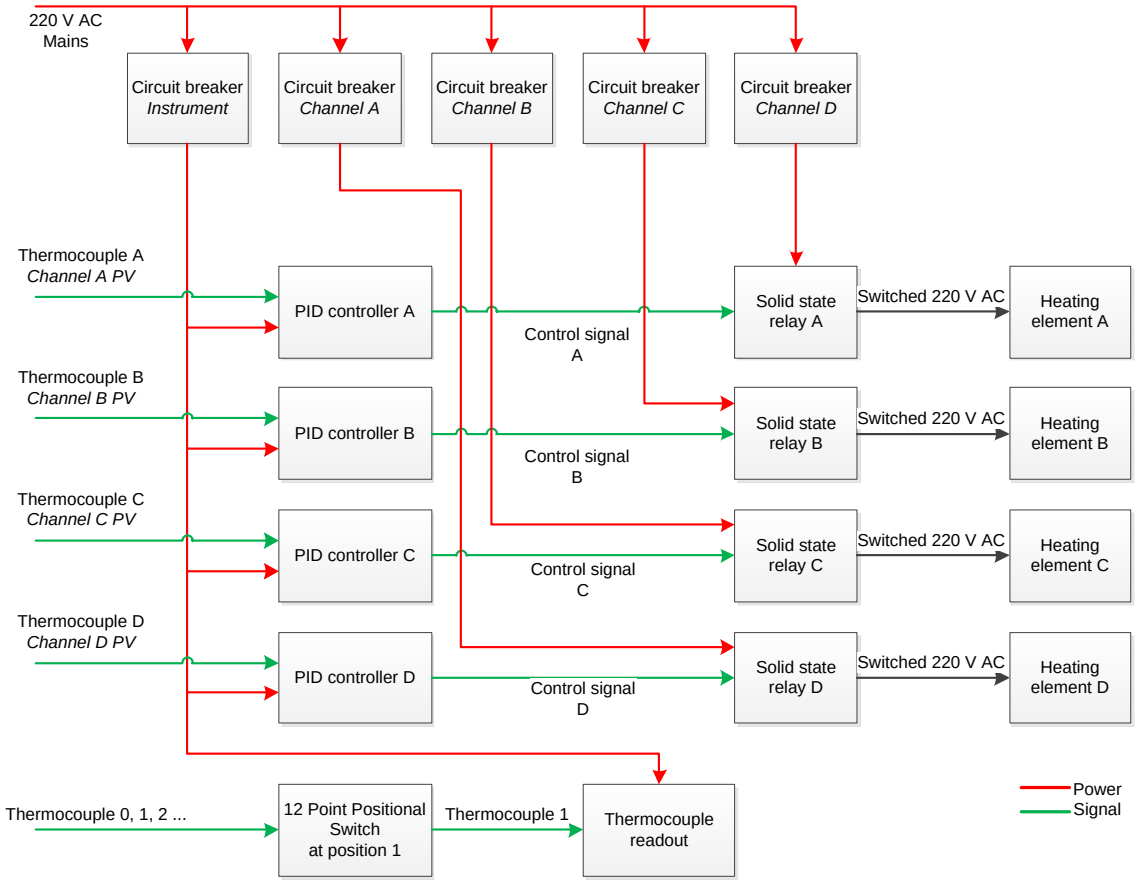

Figure 8.3: Flow diagram of temperature control unit

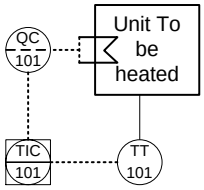

Figure 8.4: Schematic of a single Gefran PID heating loop

8.3 Mass flow controllers

A mass flow controller control unit is also present as part of the existing rig 1A6. This system consists of 2 control modules on the chassis front counter and 3 UNIT 7300 mass flow controllers (MFCs) mounted on the perforated metal plate at the back of the chassis. Each control module can throttle 2 MFCs individually to a specific flow value as a percentage of the MFC's maximum flow in set point mode as well as display the current percentage flow through the MFC in flow measurement mode. Since this is an open loop controller, an offset is usually present in the flow set point and present value. A flow diagram of the mass flow control unit is shown in Figure 7.5.

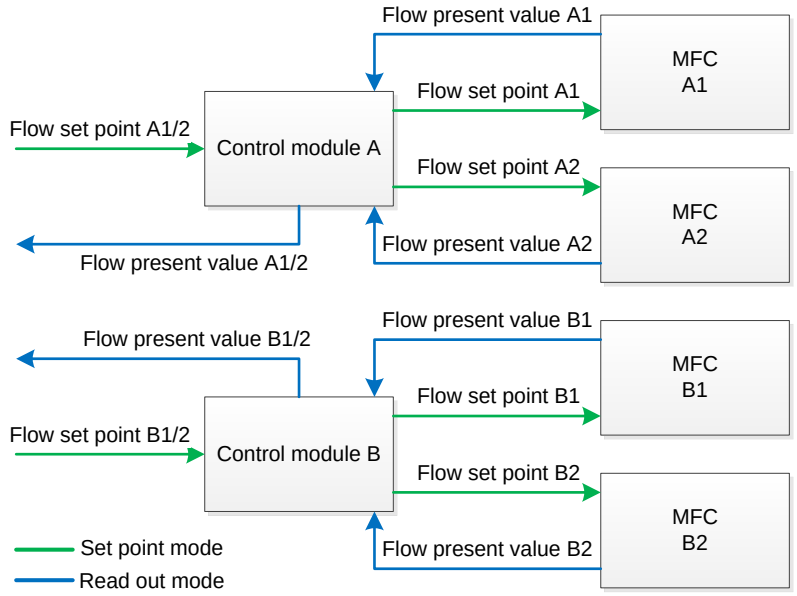

Figure 8.5: Flow diagram of mass flow controllers

The mass flow controllers are operated in voltage mode, where a 0 - 5 V signal represent the setpoint flow from 0 to 100 %. Mass flow controller A1 and A2 is used for methane and oxygen (FC-101 and FC-201) while mass flow controller B2 is used for helium (FC-401).

The mass flow controllers are calibrated for the gases flowing through them by measuring the flow rate of gases through the reactor system at the bubble flow meter (FM-801) at different set points of the mass flow controller between 0 and 100 %. The only gas flowing through the reactor system during this calibration is the gas from the mass flow controller being calibrated. At least three flow rate measurements are taken at each set point.

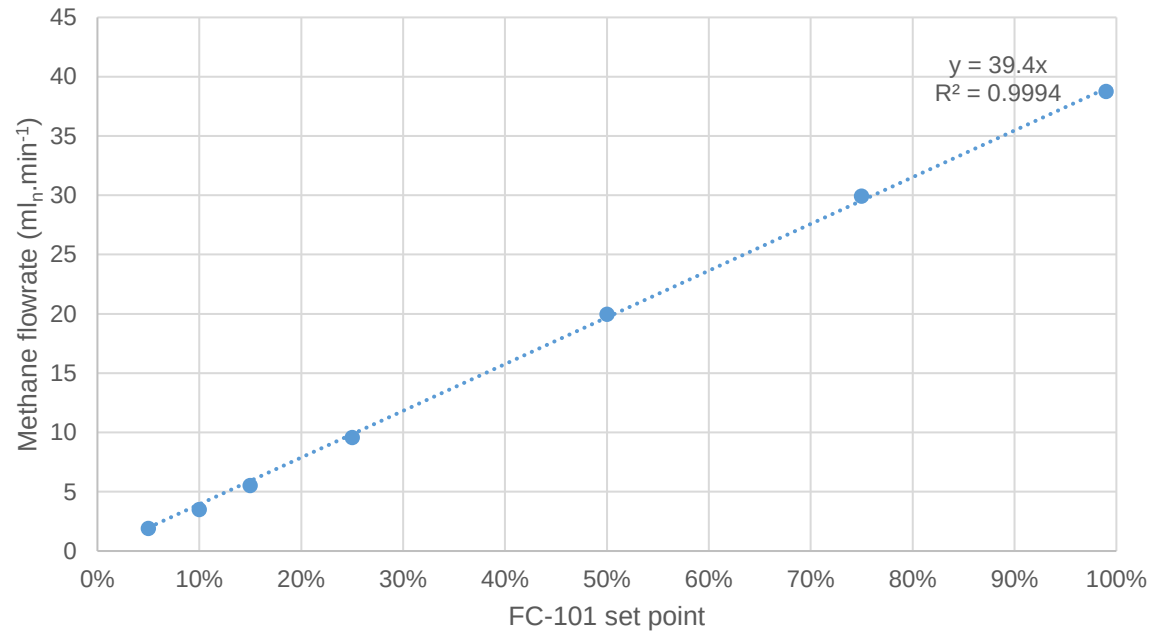

Figure 8.6: Calibration curve of mass flow controller FC-101

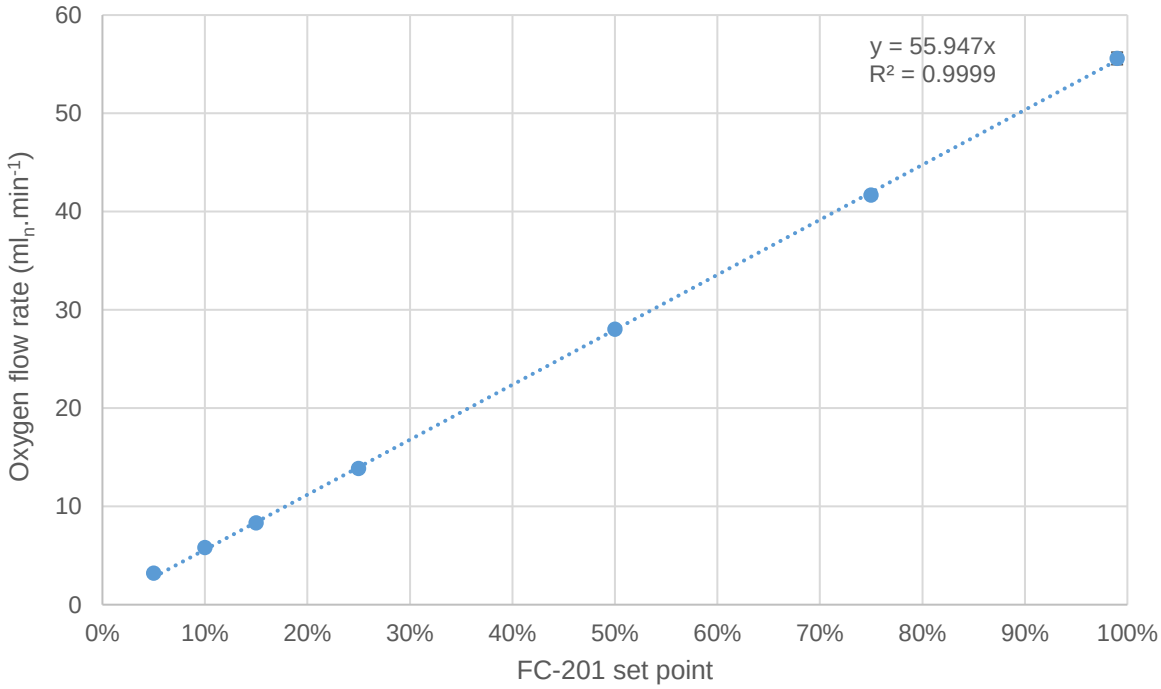

Figure 8.7: Calibration curve of mass flow controller FC-201

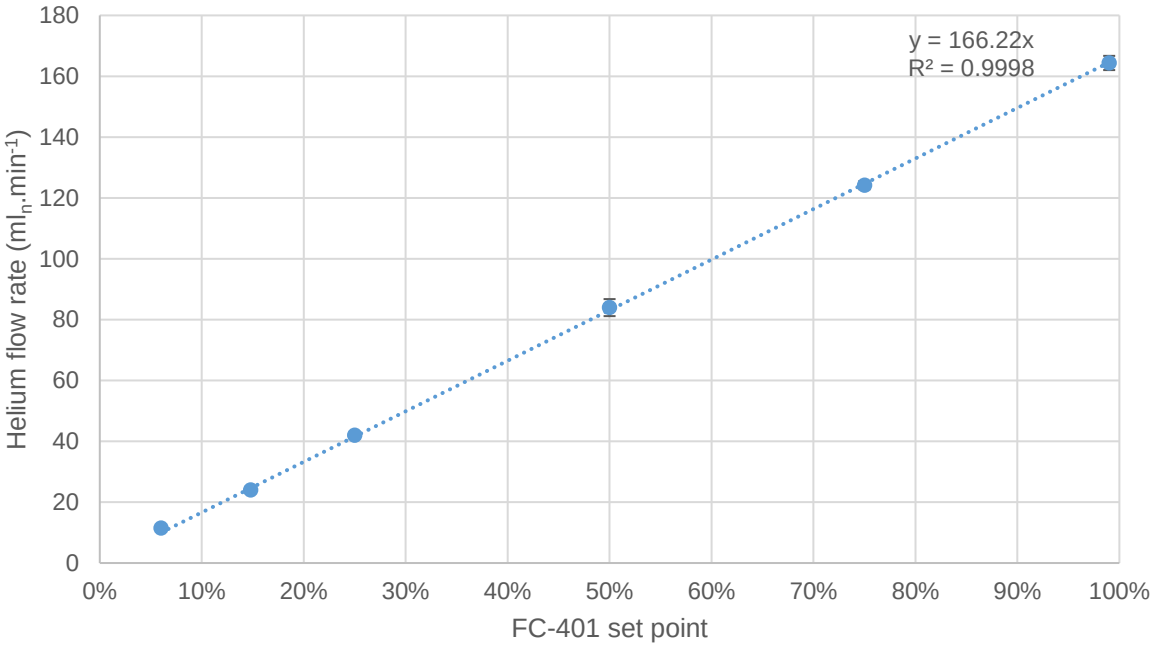

Figure 8.8: Calibration curve of mass flow controller FC-401

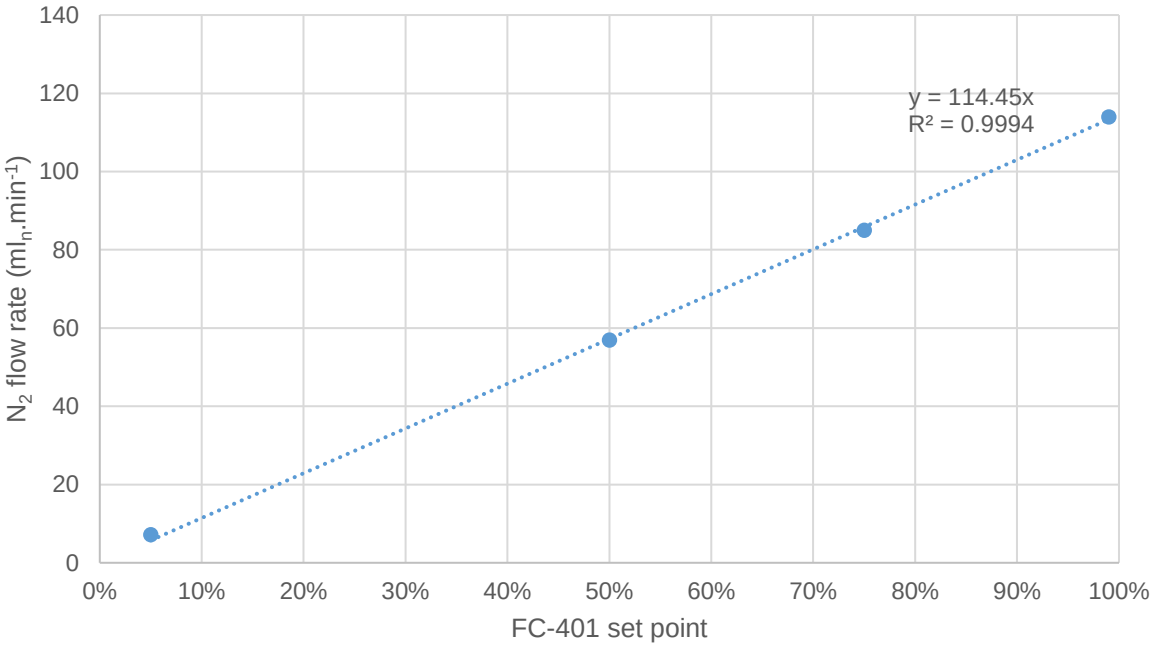

Figure 8.9: Calibration curve of mass flow controller FC-401 with N_2 instead of He

9. Appendix II – Reactor operation

9.1 Reactor leak testing

The reactor system must be leak tested after construction as well as after every time the reactor is replaced. The leak testing is first done visually by applying a soap based (Snoop™) liquid leak detector to all the fittings in the pressurized parts of the reactor system. A significant leak will manifest itself by the release of bubbles. These fittings are first tightened to stop the leak. If this fails, the fitting will be replaced. The replacement of fittings does have to be carried out on a regular basis, as the Swagelok™ compression fittings used in the reactor system deforms every time it is loosened and tightened. The compression fitting will eventually lose its ability to seal against the pressurized gases in the reactor system. It is observed that fittings in the reactor system needs to be rebuild after they are loosened and tightened approximate a dozen times.

After the all the leaks have been visually eliminated, the final leak rate of the reactor system is measured by first pressurizing the reactor system with argon gas to roughly 35 bar and then isolating the pressurized section by closing off all feed and exit valves. The rate of pressure drop is measured over a few hours and from the rate of pressure lost and reactor system volume, the volumetric leak rate can be estimated as follows:

$$\dot{L}\left(\frac{ml\ at\ 1\ bar}{min}\right) = V_{rctr}(ml) \times \frac{\Delta P}{\Delta t}\left(\frac{bar}{min}\right)$$

The reactor volume is measured by equilibrating the pressurized gas in the reactor system to a connected fixed volume vessel attached to the reactor system at ambient pressure. This was done by connecting a 150 ml gas cylinder at ambient pressure to the reactor system at 35 bar. By equilibrating the pressure between the cylinder and the reactor system, the overall system pressure decreased to 10 bar, from this observation we can calculate the volume of the reactor system:

$$P_{cylinder}V_{cylinder} + P_{rctr}V_{rctr} = P_{final}(V_{rctr} + V_{cylinder})$$

$$V_{rctr} = \frac{P_{final} - P_{cylinder}}{P_{rctr} - P_{final}}V_{cylinder}$$

$$V_{rctr} = \frac{10 - 1}{35 - 10} \times 150 = 54\,ml$$

With the reactor system's pressure determined at 54 ml, we can calculate the volumetric leak rate by observing the rate of pressure drop in the closed and pressurized reactor. For example, before the methanol stability tests mentioned later, the reactor pressure dropped from 36 bar to 23 bar over 1120 min, indicating a leak rate of 0.6$ml_n.min^{-1}$. This is significantly less than the total flow of 390 $ml_n.min^{-1}$ used in that experiment and hence the leak is negligible.

9.2 Disassembly of the reactor

1.) Ensure all the feed valves are closed

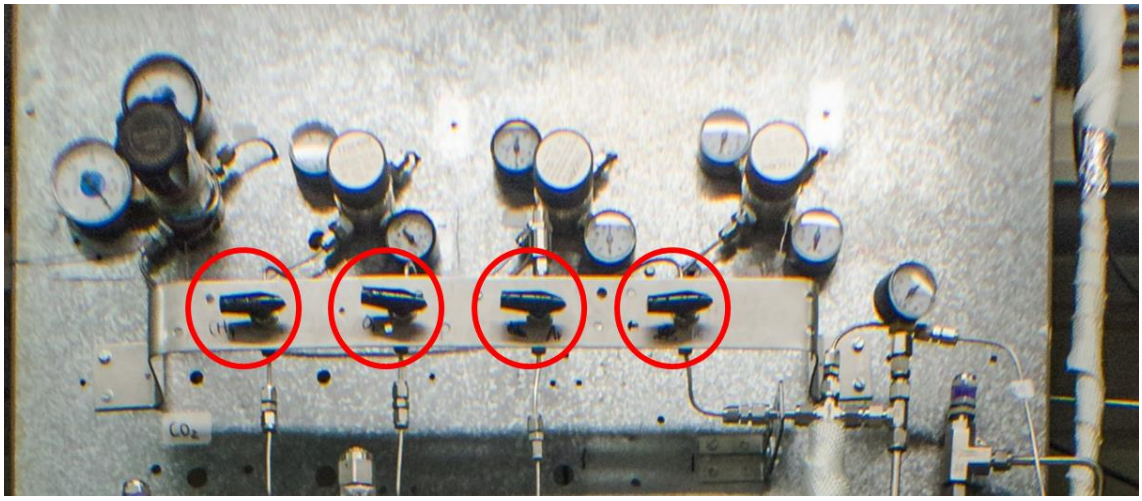

2.) turn off electrical power to the reactor system

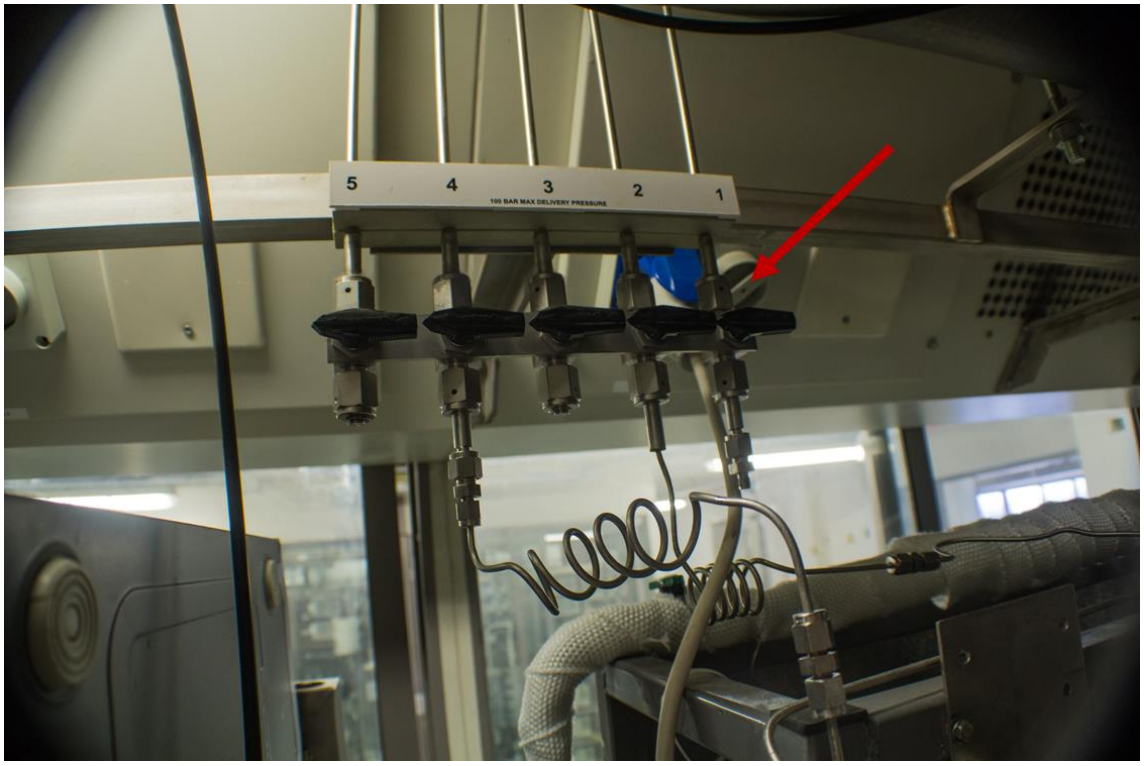

3.) Remove the ceramic fibre insulation around the reactor

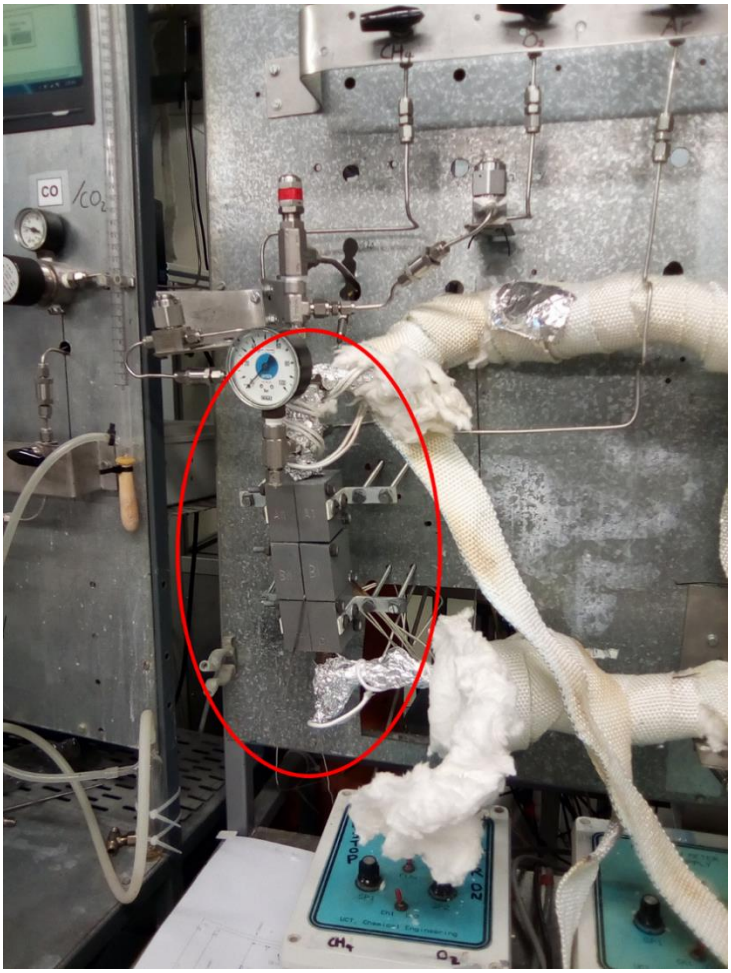

4.) Disconnect both ends of the heating wire for TIC-302 and one of the ends for the heating wire for TIC-502, as well as the reactor thermocouple (not shown)

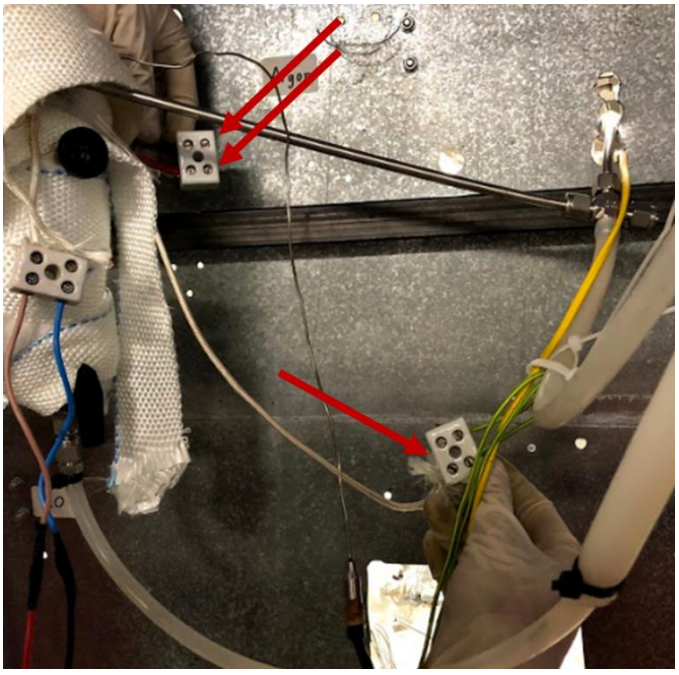

5.) Remove the heating wire, aluminium foil and aluminium heating blocks from the reactor

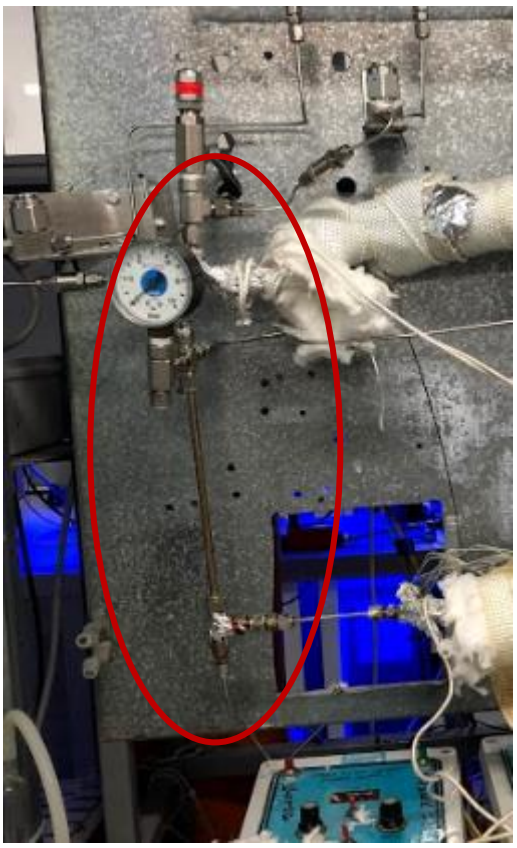

6.) Ensure the reactor is not pressurized, then remove the reactor subassembly by undoing the 3 fittings shown below

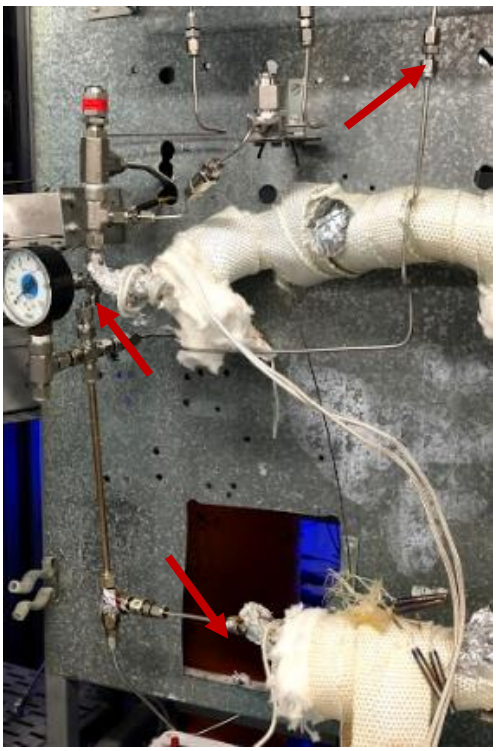

7.) Clamp down the reactor subassembly and remove the port connector holding the reactor quartz liner in place

8.) Gently pull on the exposed reactor quartz liner to remove it and its O-ring, the catalyst can be retrieved from the quartz liner for post-reaction analysis

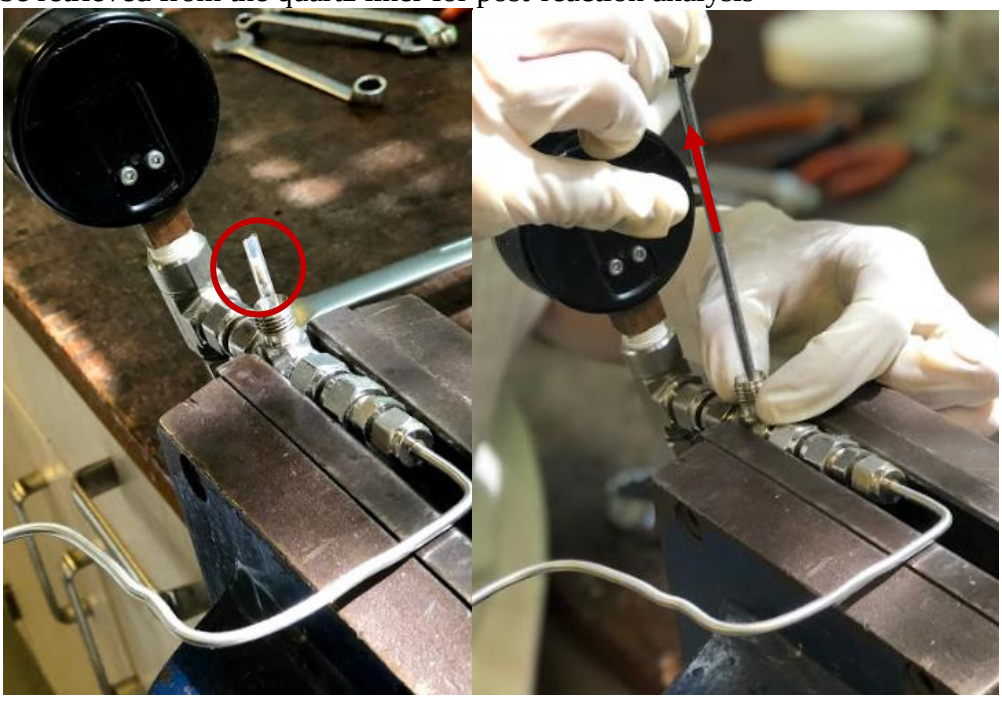

9.) Remove the stainless-steel reactor shell by undoing the two fittings below:

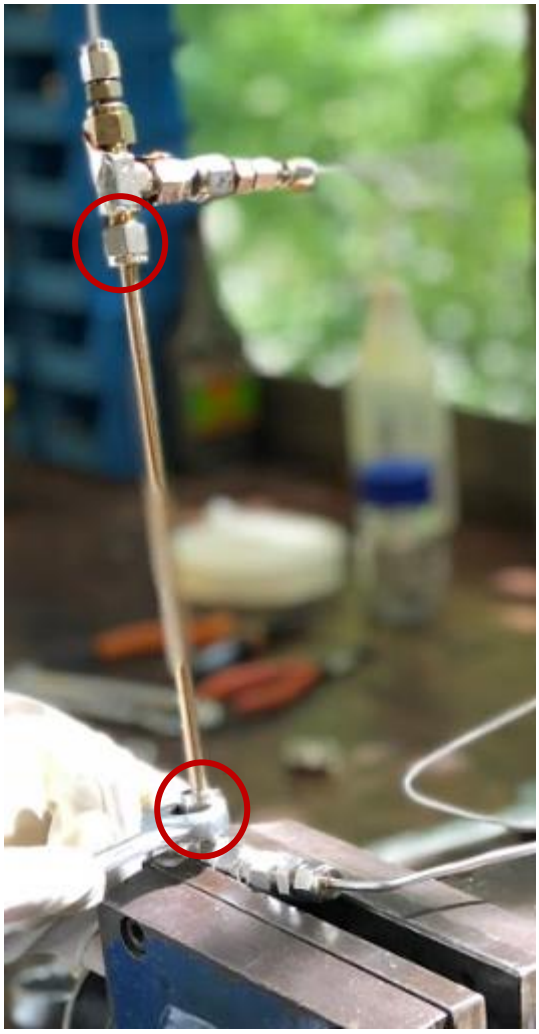

The dissembled reactor contains the following parts:

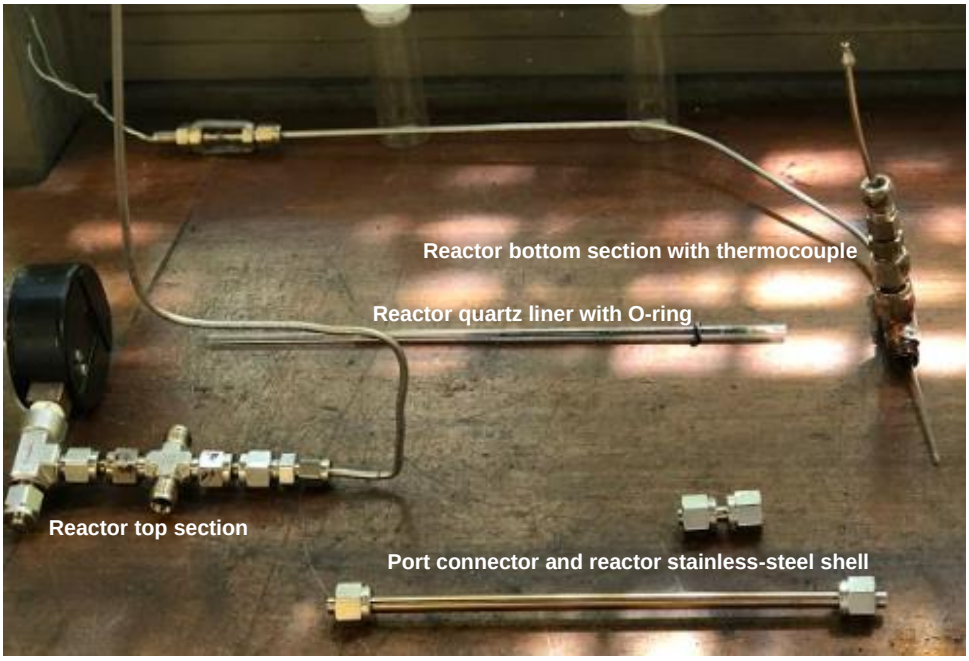

9.3 Loading of the reactor

1.) Cut 2 pieces of ¼” stainless steel tubing (0.028” WT), 200 mm and 30 mm in length, drill open the ends of the cut tube with a 4.5 mm drill bit to remove the flange formed during cutting. The quartz tube must fit freely inside these two tubes with some room to move.

2.) Add ferrules onto the tubes, for one end of the port connector, lift the tube up by 2.4 mm (measured using a calliper) before tightening the ferrule in place to create the O-ring grove.

3.) Carry out step 9 and then step 8 in the procedure for dissembling the reactor, i.e. first connect the reactor top and bottom section together then load an empty reactor quartz liner with its O-ring into the reactor. Push the O-ring down into its seat with a small metal rod

4.) Load the glass wool plug into the reactor quartz liner using an uncut piece of reactor thermocouple sheath as the ramrod, the rod can also be used as a probe to measure the length of the glass wool plug.

5.) Using a pipette tip as a funnel and the ramrod as a probe, load the desired bed length in the reactor with the catalyst before adding in another glass-wool plug. Record the mass of catalyst loaded.

6.) Tighten the port connector onto the top of the reactor, this fitting must not be over tightened as excess pressure on the O-ring will cause the reactor quartz liner to break

7.) Attach the new reactor subassembly back onto the rig, then carry out a leak test (discussed next). Once the reactor passes the leak test, carry out step 3 to 5 in the procedure for dissembling the reactor in reverse to reattach the heating and insulation parts of the reactor.

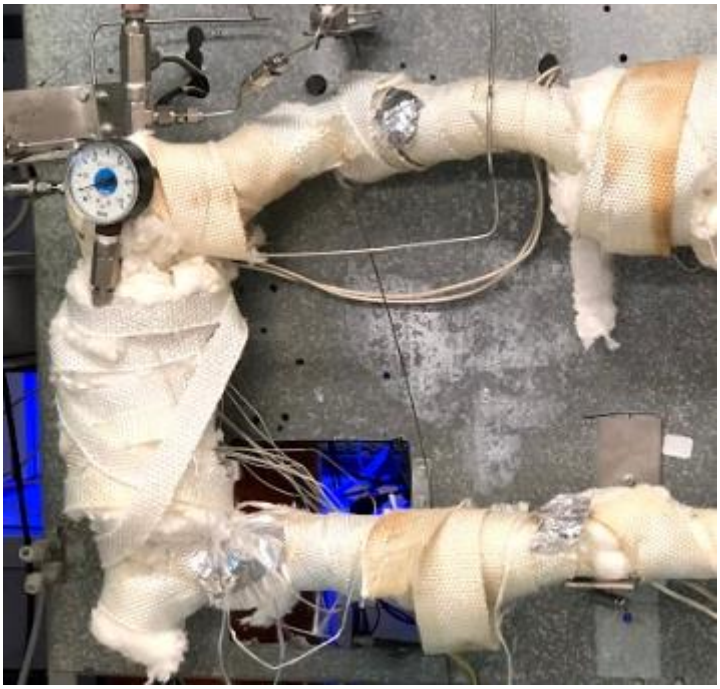

9.4 Operating the reactor system

1.) Close V-701 and open V-801 to route the reactor effluent to the bubble flow meter (FM-801) instead of the GC.
2.) Set the desired operating pressure of the reactor on the argon pressure controller (PV-601), then increase the pressure of the other gases (using PV-x01) to approximate 5 bar above the argon pressure.
3.) With the post reactor expansion valve (V-501) fully closed, pressurize the reactor with helium by opening its feed valve (V-402) and setting its flow rate to the maximum value allowed by its mass flow controller (166 $ml_n.min^{-1}$).
4.) Once the desired pressure is reached in the reactor (read from the reactor pressure gauge, PI-501), turn on the argon feed valve (V-602) and open the post reactor expansion valve (V-501) slightly (approximately 5° of a turn). Using the bubble flow meter (FM-801), adjust V-501 to obtain a total flow rate between 500 - 1500 $ml_n.min^{-1}$ through the reactor system. The total flow rate must be 10 times more than the sum of methane and oxygen's flow rate, to ensure the reactor effluent is not flammable.
5.) Enter the flow rate set point for methane and oxygen on their mass flow controller control module, then open their feed valves (V-102 and V-202). The feed valve of the gas with the higher flow rate should be opened first.
6.) Heat the reactor to the initial experiment temperature and heat all the other parts to the appropriate temperature to prevent condensation at the water partial pressures used in the experiment to be carried out.
7.) If water must be co-fed, enter the appropriate water flow rate on the water pump (P-301) and start the pump. Wait for 3 h to allow the water to fill the liquid water lines (the water flow rate used in the experiments are usually small at between 0.01 – 0.1 $ml_{liquid}.min^{-1}$).
8.) Open V-701 and close V-801 to route the reactor effluent to the GC
9.) Create a sequence on the GC software (Agilent Chemstation™) covering the length of the experiment. The interval between each sample taken is approximately 23 min.
10.) Create a sequence on the GC software (Agilent Chemstation™) covering the length of the experiment. The interval between each sample taken is approximately 23 min.
11.) Record the time and start the experiment. Record the times of any condition change made during the experiment too.

EBE Faculty: Assessment of Ethics in Research Projects (Rev2)

Any person planning to undertake research in the Faculty of Engineering and the Built Environment at the University of Cape Town is required to complete this form before collecting or analysing data. When completed it should be submitted to the supervisor (where applicable) and from there to the Head of Department. If any of the questions below have been answered YES, and the applicant is NOT a fourth year student, the Head should forward this form for approval by the Faculty EIR committee: submit to Ms Zulpha Geyer (Zulpha.Geyer@uct.ac.za; Chem Eng Building, Ph 021 650 4791).
NB: A copy of this signed form must be included with the thesis/dissertation/report when it is submitted for examination

This form must only be completed once the most recent revision EBE EiR Handbook has been read.

Name of Principal Researcher/Student: Junfeng Guo Department: Chemical Engineering

Preferred email address of the applicant: gxxjun001@myuct.ac.za

If a Student: Degree: MSc (Chemical Engineering) Supervisor: Professor Eric van Steen

If a Research Contract indicate source of funding/sponsorship: NRF

Research Project Title:
Design, construction and commissioning of a packed bed reactor system for methane to methane conversion

Overview of ethics issues in your research project:

Question 1: Is there a possibility that your research could cause harm to a third party (i.e. a person not involved in your project)?	YES	✓
Question 2: Is your research making use of human subjects as sources of data? If your answer is YES, please complete Addendum 2.	YES	✓
Question 3: Does your research involve the participation of or provision of services to communities? If your answer is YES, please complete Addendum 3.	YES	✓
Question 4: If your research is sponsored, is there any potential for conflicts of interest? If your answer is YES, please complete Addendum 4.	YES	✓

If you have answered YES to any of the above questions, please append a copy of your research proposal, as well as any interview schedules or questionnaires (Addendum 1) and please complete further addenda as appropriate. Ensure that you refer to the EiR Handbook to assist you in completing the documentation requirements for this form.

I hereby undertake to carry out my research in such a way that

- there is no apparent legal objection to the nature or the method of research; and
- the research will not compromise staff or students or the other responsibilities of the University;
- the stated objective will be achieved, and the findings will have a high degree of validity;
- limitations and alternative interpretations will be considered;
- the findings could be subject to peer review and publicly available; and
- I will comply with the conventions of copyright and avoid any practice that would constitute plagiarism.

Signed by:

	Full name and signature	Date
Principal Researcher/Student:	Junfeng Guo	2018/10/18

This application is approved by:

Supervisor (if applicable):	Professor Eric van Steen	2018/10/18
HOD (or delegated nominee): *Final authority for all assessments with NO to all questions and for all undergraduate research.*	Professor Eric van Steen	2018/10/18
Chair : Faculty EIR Committee For applicants other than undergraduate students who have answered YES to any of the above questions.		

Original ethics form from 2015 misplaced

Recompleted in 2018